ABSTRACT

KRISHNA, SHREE. Unified Constitutive Modeling for Proportional and Nonproportional Cyclic Plasticity Responses. (Under the supervision of Dr. Tasnim Hassan.)

Several features of cyclic plasticity, e.g. cyclic hardening/softening, ratcheting, relaxation, and their dependence on strain range, nonproportionality of loading, time, and temperature determine the stress-strain responses of materials under cyclic loading. Numerous efforts have been made in the past decades to characterize and model these responses. Many of these responses can be simulated reasonably by the existing constitutive models, but the same models would fail in simulating the structural responses, local stress-strain or global deformation. One of the reasons for this deficiency is that the constitutive models are not robust enough to simulate the cyclic plasticity responses when they interact with each other. This deficiency can be understood better or resolved by developing and validating constitutive models against a broad set of experimental responses and two or more of the responses interacting with each other. This dissertation develops a unified constitutive model by studying the cyclic plasticity features in an integrated manner and validating the model by simulating a broad set of proportional and nonproportional cyclic plasticity responses. The study demonstrates the drawbacks of the existing nonlinear kinematic hardening model originally developed by Chaboche and then develop and incorporate novel ideas into the model for improving its cyclic response simulations.

The Chaboche model is modified by incorporating strain-range dependent cyclic hardening/softening through the kinematic hardening rule parameters, in addition to the conventional method of using only the isotropic hardening parameters. The nonproportional loading memory parameters of Tanaka and of Benallal and Marquis are incorporated to study the influence of nonproportionality. The model is assessed by simulating hysteresis loop shape, cyclic hardening-softening, cross-effect, cyclic relaxation, subsequent cyclic softening, and finally a series of ratcheting responses under uniaxial and biaxial loading responses. Next, it is demonstrated that the hysteresis loop shape and width can be improved by incorporation of time dependence (visco-effect) and a novel modeling scheme of backstress shift. Overall, this dissertation demonstrates a methodical and systematic development of a constitutive model for simulating a broad set of low-cycle fatigue responses.

Unified Constitutive Modeling for Proportional and Nonproportional Cyclic Plasticity Responses

by
Shree Krishna

A dissertation submitted to the Graduate Faculty of
North Carolina State University
in partial fulfillment of the
requirements for the Degree of
Doctor of Philosophy

Civil Engineering

Raleigh, North Carolina

2009

APPROVED BY:

Dr. Mohammed A. Zikry	Dr. Kerry S. Havner
Dr. M. Shamimur Rahman	Dr. Murthy N. Guddati

Dr. Tasnim Hassan
Chair of Advisory Committee

DEDICATION

This dissertation is dedicated to my father Mr. Dhrub Narayan Thakur and my mother Smt. Abha Thakur for their love, care and blessings. Your son is Dr. Shree Krishna now and I still remember the story of Ramdin from grade -1 and my first dance “dighy-dinghy-do”. I hope to not let you down in my years to come and will strive to be the best.

BIOGRAPHY

Shree Krishna was born in Deoghar, a small town in Jharkhand, a state in Eastern India on 26th of September, 1981. Deoghar is a holy town of Hindus famous for 12th Jyotirlinga (deity of God Shiva). He grew up amidst temple goers and devotees turning to be true believer in God and in Lord Shiva especially. He did his secondary schooling from St. Francis School, Deoghar and went for higher secondary education to Patna Science College, Patna. He got his secondary and higher secondary degree in 1998 and 2000 respectively.

He went to Indian Institute of Technology, Kharagpur, one of the premiere institute of India and World, in 2000 and obtained a dual degree, Bachelors and Masters of Technology in the field of Ocean Engineering and Naval Architecture in 2005. Being in IIT- Kharagpur, he participated in several extra-curricular activities and learnt to handle several challenges. He did projects in Finite Element Methods and Random Vibration. During his course of studies, he developed strong research interests in Structural and Applied Mechanics. He joined the Ph.D. program in Civil Engineering- Structural Engineering and Mechanics at North Carolina State University, Raleigh in the fall of 2005. He carried out extensive research in constitutive modeling of cyclic plasticity responses of metals. His research was mostly related to cyclic plasticity and constitutive modeling of materials. He will continue his further research as a postdoctoral researcher and would try to understand the material behavior through multiscale approach. He wishes to synthesize new material and develop algorithms for modeling the materials under varied length scales and then linking them to comprehend the material behavior.

ACKNOWLEDGEMENTS

I want to give my heartfelt thanks and sincere regards to my advisor Dr. Tasnim Hassan for his meticulous guidance, continued belief in my ability, constant encouragement and sincere advice all throughout my academic research at NCSU. You are the best advisor. I enjoyed each part of the time spent with you. The effective exchange of ideas, and a well directed and regular thought process led to the completion of this research endeavor.

I would then like to thank Dr. Kerry S. Havner, my committee member, for his well-directed support and meticulous reading of my papers and dissertation. I am really thankful for your time and patience in reading my chapters and improving my writing. I wish to keep all those details in mind. I was impressed, every time I had a discussion with you. It gave me great feeling to think and know more of plasticity.

I would like to give my sincere thanks to Dr. Murthy N. Guddati, my other committee member for his valuable advice and support throughout my research. I would also like to thank my other committee members, Dr. Shamimur Rahman , Dr. Mohammed A. Zikry and Dr. Mansoor Haider for their time and advice throughout my research.

I would like to gratefully acknowledge the financial support from National Science Foundation (DMR # 0408910) and the Department of Civil, Construction and Environmental Engineering without which this research could not have been completed.

I would like to thank my parents and my brother and sister for their support and love throughout my research. You were always there beside me. Also, I would like to thank my nanaji and other family members for their support and encouragement. Finally I would like to express my thanks to my friends and members of Mann 407 i.e. Sammiuddin Syed, Vijay Subramanian, Siddharth Savadatti, Kaushal Mishra, Alok Gupta, Pratyush Sinha, Avijit Gupta, Vikas Kumar and many others. Special mention goes to Pei-Yuan Cheng for his assistance in my research.

TABLE OF CONTENTS

LIST OF TABLES

LIST OF FIGURES

CHAPTER 1
INTRODUCTION

1.1 Background and Motivation

Premature fatigue failures of structures and components are observed in nuclear power plant, chemical, offshore and other industries. One of the reasons for many fatigue failures is attributed to strain accumulation (ratcheting) at local joints or stress concentration areas initiated under extreme low-cycle loading conditions. The 1994 Northridge earthquake caused severe damage to steel structures and one of the probable reasons was indicated to be ratcheting (Castiglioni, 2005). However, ratcheting became an important research topic over the last two decades due to various fatigue failure issues of piping and pressure vessels. The primary factor that induces ratcheting is the mean stress of stress reversals. Other factors which influence ratcheting are cyclic hardening/softening, strain range effect, loading nonproportionality, rate and temperature dependence and their interactions. Most of these factors are not included in the design in a rational manner due to lack of knowledge of these factors.

Prediction of ratcheting is hence critical to estimate the fatigue life of the structure. Researchers all over the world are currently developing models to predict the ratcheting response. Accurate prediction of ratcheting is essential to prevent the failure of structures. In the past two decades significant improvement of the constitutive model development for ratcheting were made, but none of the models demonstrated success in simulating structural ratcheting response (Rahman, 2006, see References list following chapter 5). The reason for such drawback is that the models are not robust enough to capture responses under the above mentioned factors in a unified manner.

The objective of the present study is to develop a unified constitutive model to capture many of the cyclic plasticity responses, including ratcheting under various loading conditions, which can simulate a broad set of loading parameters. Past research demonstrated that the constitutive modeling of cyclic plasticity responses is quite complex. The complexity is further increased when several other effects like cyclic hardening/softening, nonproportionality and loading arbitrariness are present. Due to the interaction of temperature and stress and strain rates the modeling complexities get multiplied. Many of the present constitutive models have shown successes in simulating one set but eventually fail in simulating the other set of experiments. Hence, the model developed should be robust enough to simulate a broad range of cyclic plasticity responses. This research addresses many of these complexities and attempts to develop a robust unified constitutive model to simulate the ratcheting response under various loading scenarios.

The commercial software packages, like ANSYS, ABAQUS etc. do not have a robust constitutive model to simulate the ratcheting. Hence the prediction of the fatigue life through such analysis is not accurate. Previous research by Hassan and his coworkers have demonstrated the failure of these packages to simulate the ratcheting (Lu, 2003, Rahman, 2006). Hence, the present work also deals with the enhancement of the modeling, which can be used by others to simulate the global failure caused by local fatigue and ratcheting related failures. Also, crack tips have plastic zones and a robust unified cyclic plasticity model is required to model the fatigue cracks and therefore essential for prediction of high-cycle fatigue life as well.

The previous research by Hassan and coworkers at North Carolina State University has demonstrated that coupled modeling of cyclic plasticity (i.e. plastic modulus calculation coupled with kinematic hardening rule through the consistency condition of the yield surface) and ratcheting are robust for material level simulations of stabilized materials. The uncoupled models perform well in uniaxial conditions but fail in biaxial and other multiaxial conditions. Again, several features of cyclic plasticity (i.e. cyclic hardening and softening, strain range

effect, loading nonproportionality, time effects, and their interactions) were not incorporated in the model. One of the drawbacks of the coupled models is that the shape of yield surface is kept unchanged from the von-Mises yield surface. But it was observed by several researchers (Yoshida et al., 1978, Shriatori et al., 1979, Philips and his coworkers, 1972, 1979, 1984) that the yield surface continuously changes its shape with loading. This in a way affects the plastic increment direction; hence the estimation of plastic strain directions by the current coupled models is not representative of the actual directions. The present research makes an effort to incorporate several features of cyclic plasticity and their interactions to predict the cyclic responses accurately.

This study scrutinizes several cyclic plasticity models in order to understand their strength and weaknesses and thereby develop an improved unified constitutive model (based on Bari and Hassan's improved Chaboche model, 2002) to capture the various material responses. This model development effort focuses on several complex material behaviors like cyclic hardening/softening, strain range effect, nonproportionality, rate and temperature dependence, and their interactions. The study discusses the various features and their effect on stress-strain responses, modeling steps and an elaborate study of parameter significance and their determination.

1.2 Scope and Organization

Responses under cyclic loading, e.g. cyclic hardening/softening, ratcheting, relaxation, and their dependence on strain range, nonproportionality of loading, time, and temperature determines the stress-strain responses of materials under cyclic loading. Numerous efforts have been made in the past decades to characterize and model these responses. Many of these responses can be simulated reasonably by the existing constitutive models, but the same models would fail in simulating the structural responses, local stress-strain, or global deformation. One of the reasons for this deficiency is that the constitutive models are not robust enough to simulate the cyclic plasticity responses when they interact with each other. This deficiency can be understood better or resolved by developing and validating

constitutive models against a broad set of experimental responses and two or more of the responses interacting with each other. This dissertation develops a unified constitutive model by studying the cyclic plasticity features in an integrated manner and validating the model by simulating a broad set of proportional and nonproportional cyclic plasticity responses. The study demonstrates the drawbacks of the existing nonlinear kinematic hardening model originally developed by Chaboche and then develops and incorporates novel ideas into the model for improving its cyclic response simulations. The results of this study are presented through four chapters as stated below.

The second chapter is a journal paper published in the International Journal of Plasticity (Hassan et al., 2008) and demonstrates the influence of nonproportionality of loading history on cyclic responses. A novel set of experiments were conducted on SS304 under various uniaxial and biaxial stress-controlled nonproportional histories. The experimental responses demonstrate the influence of nonproportional loading on ratcheting responses. The Chaboche model (Chaboche 1986, 1989, 1991) was modified for simulating cyclic hardening/softening responses through the kinematic hardening rule parameters, in addition to the conventional method of using only the isotropic hardening parameters. In order to simulate nonproportional hardening, the Benallal and Marquis (Benallal and Marquis, 1987) nonproportionality parameter is added to the Chaboche model. The paper outlines the characteristics features of how kinematic hardening rule parameters represent cyclic hardening and softening, and thereby the influence of loading nonproportionality on ratcheting responses under biaxial stress-controlled loading responses. Strengths and weaknesses of the modified model in simulating a series of biaxial ratcheting responses are identified and ideas for further improving the models are presented.

The third chapter is another paper recently accepted for publication in the International Journal of Plasticity. This chapter first evaluates the modified model against a broad set of cyclic responses of SS304 under uniaxial and multiaxial cyclic loading. Two major drawbacks of the modified Chaboche model in simulating the responses were identified. One

was that the stainless steel demonstrated cyclic hardening under strain-controlled cycle, whereas cyclic softening under stress-controlled cycle. It was identified that this response depends on the strain range, and the existing models cannot describe the response. The second drawback identified was that the modified Chaboche model cannot simulate ratcheting response when loading history changes suddenly. Motivated by these findings, the model was modified further by incorporating strain-range dependent cyclic hardening/softening and nonproportional loading memory parameters of Tanaka (Tanaka 1994). The model was scrutinized against simulating hysteresis loop shape, cyclic hardening-softening, cross-effect, cyclic relaxation, subsequent cyclic softening, and finally a series of ratcheting responses under uniaxial and biaxial loading. In addition, a novel technique for simulating both the monotonic and cyclic responses with one set of model parameters is developed and validated. Finally, the strengths and weaknesses of the modified model are identified and ideas for further improving the model are presented.

The fourth chapter includes the results from my most recent work and is written in a journal paper format for submission for publication. The major drawback identified from the previous study was that the hysteresis loop shape and width were not simulated well; consequently, simulations of many of the responses were unsatisfactory. The primary reason for the deficiency was the lack of time-dependence of the model developed so far. In addition, an observation was made that the initial hysteresis loops, obtained under strain and stress-controlled cycles, match nicely when they are shifted certain amounts along the stress and strain directions. This observation was incorporated into the model through a novel modeling scheme of back stress shift. This new modeling concept improved the uniaxial ratcheting response simulation considerably. This modeling concept also gives a physical meaning to the threshold modeling concept of Chaboche (Chaboche, 1991). Next, it is demonstrated that the simulation of the hysteresis loop shape and width can be improved significantly by incorporation of time-dependence (viscous effect) into the model. The cyclic viscoplasticity model developed in the study becomes quite complex with a large number of parameters. Hence, ideas of parameter identification using genetic algorithm are discussed.

Overall, this dissertation demonstrates a methodical and systematic development of a constitutive model for simulating a broad set of low-cycle fatigue responses. However, more modification would be needed before claiming that the model would simulate structural responses acceptably. A few ideas for further improvement of the model are presented in Chapter 5, which also includes important conclusions of the study and recommendations for future research.

CHAPTER 2
Influence of Non-proportional Loading on Ratcheting Responses and Simulations by Two Recent Cyclic Plasticity Models

Abstract

Aubin and her coworkers conducted a unique set of experiments demonstrating the influence of loading nonproportionality on ratcheting responses of duplex stainless steel. In order to further explore their new observation, a set of experiments was conducted on stainless steel (SS) 304L under various biaxial stress-controlled nonproportional histories. This new set of data reiterated Aubin and her coworkers' observation and illustrated many new responses critical to model development and validation. Two recent and different classes of cyclic plasticity models, the modified Chaboche model proposed by Bari and Hassan and the version of the multi-mechanism model proposed by Taleb and Cailletaud, are evaluated in terms of their simulations of the SS304L nonproportional ratcheting responses. A modeling scheme for nonproportional ratcheting responses using the kinematic hardening rule parameters in addition to the conventionally used isotropic hardening rule parameter (yield surface size change) in the modified Chaboche model is evaluated. Strengths and weaknesses of the models in simulating the nonproportional ratcheting responses are identified. Further improvements of these models needed for improving the nonproportional ratcheting simulations are suggested in the paper.

Keywords: Constitutive Modeling, Cyclic Hardening, Cyclic Plasticity, Nonproportionality, Ratcheting.

2.1. Introduction

The need for a robust low-cycle fatigue simulation model is gradually increasing in nuclear power, offshore structures, aerospace, automobile and many other industries. This is mainly because of the need of developing an improved design methodology against

conventional low-cycle fatigue and ratcheting-fatigue failures. To address this need, many efforts have been made in understanding various fatigue failure mechanisms and developing improved constitutive models around the world over the last five decades (Benham, 1960, 1965, Coffin, 1964, Dafalias and Popov, 1975, Chaboche and his coworkers, 1979, 1986, 1989, 1991, Hassan and his coworkers, 1992, 1994a,b, Ohno and his coworkers, 1990, 1993, 1997, Delobelle, et al., 1995, McDowell, 1995, Jiang and Sehitoglu, 1996a,b, Xia and Ellyin, 1997, Voyiadjis and Basuroychowdhury, 1998; Yoshida, 2000, Portier, et al., 2000, Bocher, et al., 2001, Kang and his coworkers, 2001, 2002a,b, 2004, 2005, 2006, Vincent, et al., 2002, Chen and Jiao, 2004, Taleb, et al., 2006, Sai and Cailletaud, 2007, and others). However, understanding and modeling of various ratcheting-fatigue phenomena still remain challenging.

Many of the earlier efforts demonstrated very good simulation of uniaxial ratcheting responses which included the influences of mean and amplitude stresses (Chaboche and his coworkers, 1989, 1991, Hassan and Kyriakides, 1992, 1994a, Ohno and Wang, 1993, Bari and Hassan, 2000, Kang, et al., 2002a,b, 2004, Taleb, et.al., 2006, and others). It was demonstrated that the accuracy of uniaxial ratcheting simulation primarily depended on the hysteresis loop shape simulation. Biaxial ratcheting responses, on the other hand, keep challenging the constitutive models. Many factors influence the material responses under multiaxial loading cycles, such as, degree of non-proportionality (function of loading path and history), cross-effect, loading rate, temperature, strain aging, and finally, the interactions between these factors. These factors were mostly studied under axial-shear strain-controlled, constant amplitude loading histories (Lamba and Sidebottom, 1978, Benallal and his coworkers, 1987, 1989, Tanaka, et al., 1985a, b, Ruggles and Krempl, 1989, Voyiadjis and Basuroychowdhury, 1998, McDowell, 1985, Delobelle, et al., 1995, Haupt and Kamlah, 1995, Kang, et al., 2001, and others).

In mechanical or structural components under cyclic loading, localized loading histories at fatigue critical locations could be strain-controlled, stress-controlled or combination of the

two. Hence, it is important to understand material responses under all three types of load-controlled histories for developing robust constitutive models. However, experimental data under "stress-controlled histories" are extremely limited. Most biaxial ratcheting experiments available in the literature are either conducted under constant tension and shear strain cycles (Moyar and Sinclair, 1963, Benham 1965, Freudenthal and Ronay, 1966, Yoshida, et al., 1978, Benallal, et al., 1989, Yoshida, 1995, Delobelle, et al., 1995, Bocher, et al., 2001, Portier, et al., 2000, Kang, et al., 2004, and others), or constant internal pressure and axial strain cycles (Yoshida, et al., 1978, Ruiz, 1967, Hassan, et al., 1992, Hassan and Kyrikides, 1994b, Delobelle, et al., 1995, Corona, et al., 1996, Bocher, et.al., 2001).Hassan, et al. (1992), Hassan and Kyriakides (1994b), Aubin, et al. (2003a), and Kang, et al. (2004, 2006) demonstrated the complexity in simulating ratcheting responses under biaxial stress-controlled loading histories. It was demonstrated that the deficient ratcheting simulation was related to the poor representation of the hysteresis curve shape evolution with progressive cycle (Hassan and Kyriakides, 1994b). In addition, simulation of biaxial ratcheting responses also depended on the yield surface evolution determined by the kinematic hardening rule of a model (Hassan, et al., 1992). None of the models proposed so far are robust enough on both these modeling features. Consequently, most models failed to simulate multiaxial ratcheting responses reasonably. This deficiency is anticipated to be related to inadequate nonproportional modeling for multiaxial stress-controlled histories. Hence, a new nonproportional modeling scheme in improving the simulations of ratcheting under biaxial stress-controlled histories are evaluated in this study.

One novel contribution recently made by Aubin, et al. (2003a) is the demonstration of the influence of loading nonproportionality on biaxial ratcheting responses. They have performed experiments on duplex stainless steel under four different loading paths in axial and shear stress space as shown in Fig. 2.1. Loading path and history in Fig. 2.1a represents a uniaxial stress cycle about a mean axial stress (referred by *uniaxial ratcheting experiment*), that in Fig. 2.1b represents a shearing stress cycle about a steady axial stress (referred by

shear ratcheting experiment). The third loading path is a combination of the last two paths as can be seen in Fig. 2.1c, hence referred by *cross ratcheting experiment*. The fourth loading path and related histories shown in Fig. 2.1d will be referred by *square ratcheting experiment*. In these four experiments, the mean or steady axial stress $\left(\sigma_{xm}\right)$ prescribed was 100MPa, whereas the equivalent amplitude stress, $\left(\sigma_a^{eq} = \sqrt{\left(\sigma_x - \sigma_{xm}\right)^2 + 3\tau_{x\theta}^2}\right)$, represented by the radius of the dotted circle in Fig. 2.1, was approximately 500MPa. To give an idea of the levels of these prescribed stresses, it is noted to the readers that the linear elastic range of the duplex stainless steel determined from a uniaxial hysteresis loop of 1% strain range was about 400MPa.

Axial strain ratcheting rates (mean axial strain in each cycle versus the number of cycles) recorded from the four experiments of Aubin, et al. (2003a) are shown in Fig. 2.2. It is well known that the prescribed mean or steady axial stress is the driving force in inducing axial strain ratcheting in these experiments (Yoshida, et al., 1988, Chaboche and his coworkers, 1986, 1994, Ruggles and Krempl, 1989, 1990, Delobelle, et al., 1995, Hassan and Kyriakides, 1992, 1994a,b, Hassan, et al., 1992, Jiang and Sehitoglu, 1996a,b, Kang, et al., 2004, 2006, and others). However, the rate of ratcheting is influenced by the magnitudes of the mean or steady stress and amplitude stress of the loading history. Hence, it was surprising to see in Fig. 2.2 that the rates of ratcheting from the four loading paths are so different when they have the same mean or steady stress and comparable equivalent amplitude stresses. This difference in the ratcheting rates can be attributed to the difference in the degree of nonproportionality of loading paths. Similar influence of nonproportional loading on ratcheting has also been demonstrated by Kang, et al. (2002b).

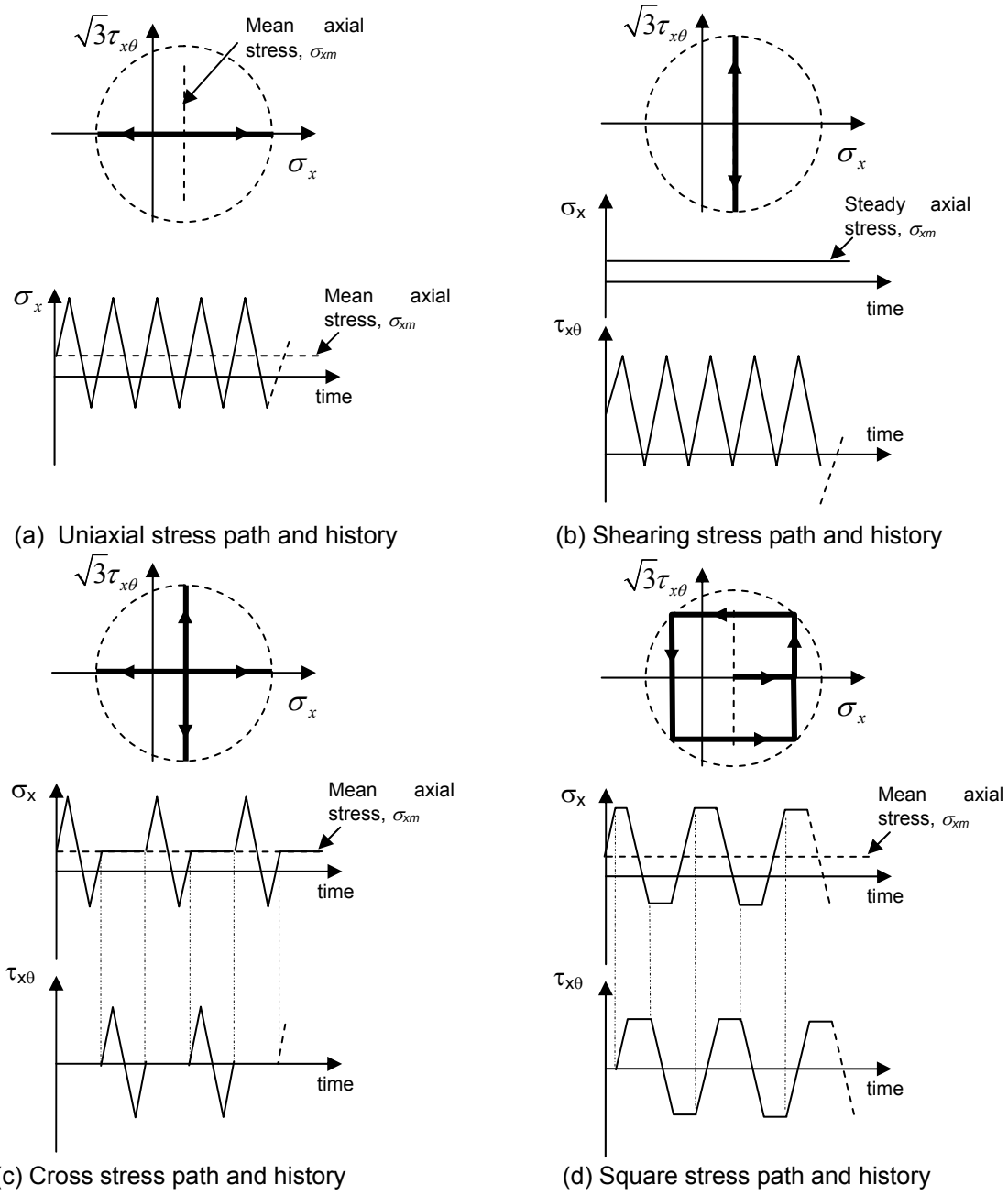

Fig. 2.1. Four loading paths and related histories in Aubin, et al. (2003a) experiments. (a) Axial stress cycle about a mean axial stress (*uniaxial ratcheting experiment*), (b) shearing stress cycle with a steady axial stress (*shear ratcheting experiment*), (c) superposition of last two loading paths: one cycle of unsymmetric axial stress followed by one cycle of shearing stress with a steady axial stress (*cross ratcheting experiment*), and (d) square path and related history (*square ratcheting experiment*).

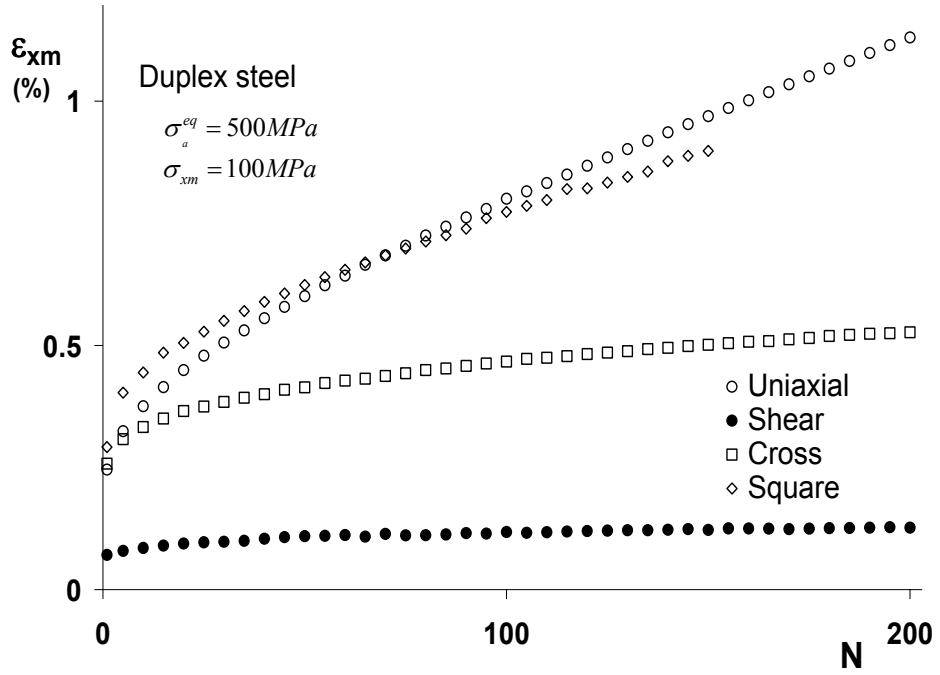

Fig. 2.2. Mean axial strain in each cycle versus the number of cycle from the axial (Fig. 2.1a), shear (Fig. 2.1b), cross (Fig. 2.1c) and square (Fig. 2.1d) ratcheting experiments (data developed by Aubin et al., 2003a).

The ratcheting responses from Aubin, et al. (2003a) are explained further in order to demonstrate the influence of non-proportionality of loading on the ratcheting response. In Fig. 2.2, the ratcheting rate in the shear ratcheting experiment is much smaller than that in the uniaxial ratcheting experiment despite the fact that the equivalent amplitude stress in the earlier experiment is somewhat larger ($\sqrt{3}(300) = 520$ MPa) than that in the latter experiment (500 MPa), and the mean or the steady axial stress in these two experiments is the same (100 MPa). This demonstrates that the shearing stress cycle is not as influencing as the axial stress cycle in inducing axial strain ratcheting. In the cross ratcheting experiment (Fig. 2.1c) each cycle is composed of one uniaxial and one shear ratcheting cycles. Hence, it is surprising to find in Fig. 2.2 that the ratcheting rate in the cross experiment is lower than that in the uniaxial experiment. In the square ratcheting experiment, the equivalent amplitude stress is 492 MPa ($\sqrt{350^2 + 3(200)^2}$) and axial mean stress is 100 MPa, and the ratcheting rate in this

experiment is comparable to that in the uniaxial ratcheting experiment as can be seen in Fig. 2.2.

Aubin, et al. (2003a) clearly demonstrated the influence of non-proportionality of stress-controlled histories on ratcheting responses. The difference between the stress-controlled histories in Aubin, et al. (2003a) and Hassan and Kyriakides (1994b) is that in the earlier paper, different loading paths with same equivalent mean and amplitude stresses were studied, whereas in the latter paper, one loading path with various mean and amplitude stresses was studied. On the other hand, Kang, et al. (2004), demonstrated the influences of various loading paths and parameters on nonproportional ratcheting responses. All these studies also demonstrated the modeling challenges in simulating nonproportional ratcheting responses. Aubin, et al. (2003a) showed that the non-linear kinematic hardening model proposed by Ohno and Wang (1993) can not simulate all four ratcheting responses in Fig. 2.2. However, they superposed only two kinematic hardening rules for simulation with the Ohno-Wang model. Ohno and Wang (1993) demonstrated reasonable simulation of uniaxial and multiaxial ratcheting responses with a minimum of four kinematic hardening rules. Rahman, et al., (2008) demonstrated for both material and structural ratcheting responses that a minimum of five kinematic hardening rules is essential for obtaining reasonable simulations with the Ohno-Wang model.

This recently observed influence of non-proportionality of stress-controlled paths on ratcheting responses made by Aubin, et al. (2003a) is explored further in this study. The material studied by Aubin, et al. (2003a, b), the duplex stainless steel, is a complex material because of its cyclically hardening response during the first few cycles followed by the cyclic softening response. Criterion and modeling features for such mixed isotropic hardening responses are not well established yet. Hence, this study developed a new set of ratcheting data on austenitic stainless steel (SS) 304L. Two recent cyclic plasticity models, the modified Chaboche model based on Bari and Hassan (2002) and the modified multi-mechanism model of Taleb, et al. (2006), are evaluated for simulating these ratcheting responses. A new

nonproportional modeling scheme using the kinematic hardening rule parameters of the modified Chaboche model, in addition to the conventional isotropic hardening rule parameter, is also evaluated. As mentioned earlier, there are many factors, such as, degree of non-proportionality, cross effect, loading rate, temperature, strain aging, and finally interactions between these factors that influence the ratcheting responses. This study explored only the influence of non-proportionality of loading cycles on the ratcheting responses. Hence, the rate and temperature independent constitutive models were considered. The loading rates in the experiments were set such that the rate effects were small and of the same order of magnitude in all the experimental responses studied.

2.2. Ratcheting Experiments on Stainless Steel 304L

Biaxial stress-controlled experiments were conducted by prescribing the uniaxial, shearing, cross, and square load paths (Fig. 2.1) similar to Aubin, et al. (2003a) on SS 304L tubular specimens at INSA de Rouen (Laboratory of Mechanics). The specimens were annealed by exposing them to 1050^{o}C for an hour followed by slow air cooling. In the experiments, the mean axial stress prescribed was 50 MPa and the equivalent amplitude stress prescribed was 200 MPa. The period for each cycle for the axial and shear load paths (Figs. 2.1a and 2.1b) was 30 seconds and that for the cross and square load paths (Figs. 2.1c and 2.1d) was 60 seconds. The detail stress-strain responses are shown in Figs. 3a, 4a, 4b, 5a, 5b, and 6a, which are important for critical evaluation of model performance. In Fig. 2.3a, the axial stress-strain hysteresis loops at intermittent cycles are shown to demonstrate the evolution of the hysteresis loops with cycles. Note in this figure for the first cycle positive stress peak that viscoplasticity is making the peak "rounded." This viscous-effect is gradually diminishing with progressive cycles and can be attributed for part of the transient ratcheting rate response observed during the initial cycles as shown in Fig. 2.8, where maximum axial strain at every 5th cycle is plotted as a function of the number of cycles (N). The transient ratcheting rate response also is mentioned to be a function of cyclic hardening (Hassan and Kyriakides, 1994a) and ratcheting hardening (Jiang and Zhang, 2008) of materials. However,

cyclic hardening indicated by thinning of the hysteresis loops or stiffening of the hysteresis curves with progressive cycles is not demonstrated by the hysteresis loops in the uniaxial ratcheting experiment in Fig. 2.3a. Conversely, a small fattening of the hysteresis loops with progressive cycles indicating cyclic softening is demonstrated in Fig. 2.3a. Such anomalous behavior of no cyclic hardening or small cyclic softening for SS304 under stress-controlled cycle has also been demonstrated by Hassan and Kyriakides (1994a). Due to the lack of data this modeling feature is not incorporated in this study.

The stress and strain responses obtained from the shear ratcheting experiment are shown in Figs. 4a and 4b, where it is observed that in addition to the axial strain the shearing strain is also ratcheting. It is surprising to observe significant cyclic softening of the shear stress-strain loops (increase in shear strain range) in Fig. 2.4a. This cyclic softening seems to be the reason for the shear strain ratcheting in the negative direction in Fig. 2.4b. The reason for this cyclic softening of SS304L, which is a cyclically hardening material, is not known. The axial and shear strain ratcheting of the cross experiment is shown in Figs. 5a and 5b. Note in Fig. 2.5a the ratcheting of axial strain at the mean axial stress level during the shear stress cycle and in 5b the ratcheting of shear strain during the axial strain cycle. Viscoplasticity effect (rounded peak) at the 1^{st} axial stress peak and small hystersis loop fattening with progressive cycles are observed in Fig. 2.5a similar to those in the uniaxial ratcheting experiment in Fig. 2.3a. The axial-shear strain response from the square experiment is shown in Fig. 2.6a, where it is observed that both the axial and shear strains are ratcheting. In the shear experiment (Figs. 4a and 4b), the shear strain ratcheting in the negative direction seems to be related to cyclic softening, whereas in the cross (Fig. 2.5b) and square (Fig. 2.6a) experiments, the shear strain ratcheting in the positive direction might be the influence of the load history.

In order to further explore the effect of loading nonproportionality on axial strain ratcheting, a fifth experiment prescribing the loading path as shown in the inset in Fig. 2.7a was conducted. This experiment is referred by *two-square ratcheting experiment* which included crossing of axial and shear stress paths in each cycle. The period for each cycle in

this experiment was set to 60 seconds. Axial-shear strain response from this experiment is shown is Fig. 2.7a, where it is interesting to note that both axial and shear strains are ratcheting at comparable rates, unlike in the earlier four experimental responses.

Axial strain ratcheting from these five experiments are compared by plotting the maximum peaks, at every 5^{th} cycle, versus the number of cycles as shown in Fig. 2.8. In this figure, it can be seen that the axial, shear and cross experimental responses reiterate the observations made for duplex steel by Aubin, et al. (2003a): the shearing stress cycle is not as influencing as the axial stress cycle in inducing axial strain ratcheting; the ratcheting rate obtained under the cross experiment is smaller than that in the uniaxial experiment. However, unlike the duplex stainless steel, the SS304L axial strain ratcheting from the square experiment is much smaller than that in the uniaxial experiment (compare Figs. 2 and 8). It is also noted in Fig. 2.8 that the axial strain ratcheting rate in the two-square experiment is higher than that in the square experiment.

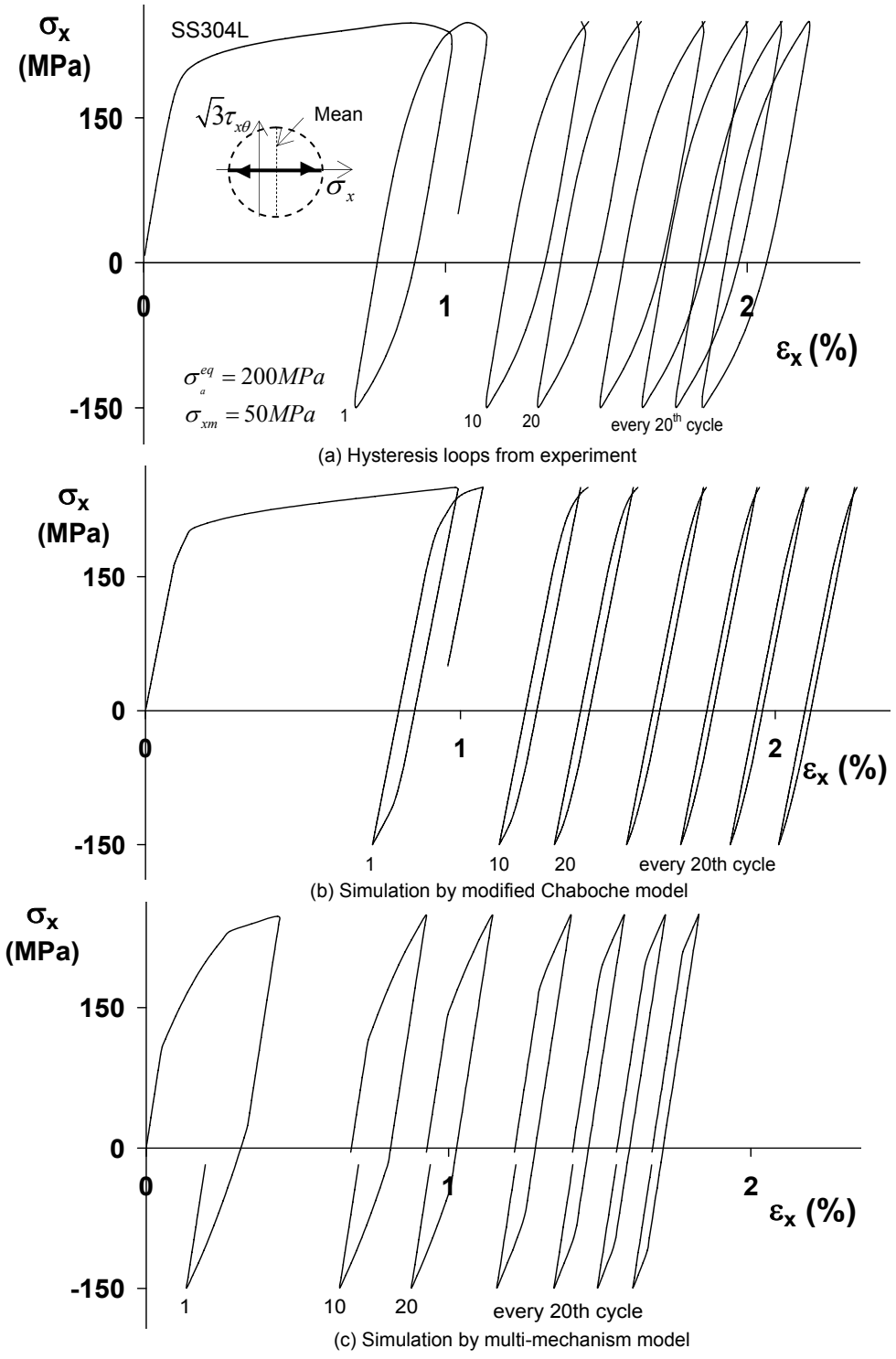

Fig. 2.3. Uniaxial ratcheting experimental response of SS304L and simulations.

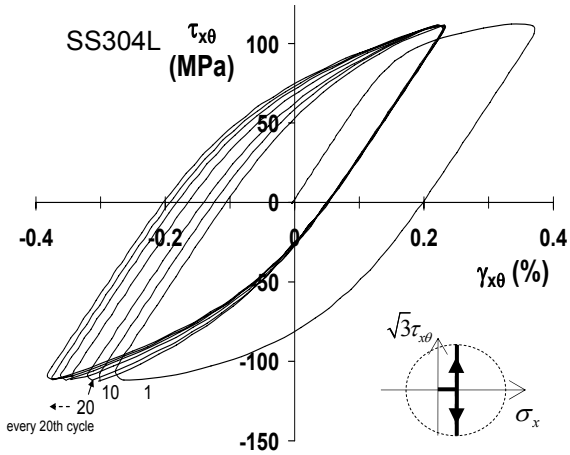

(a) Hysteresis loop from experiment

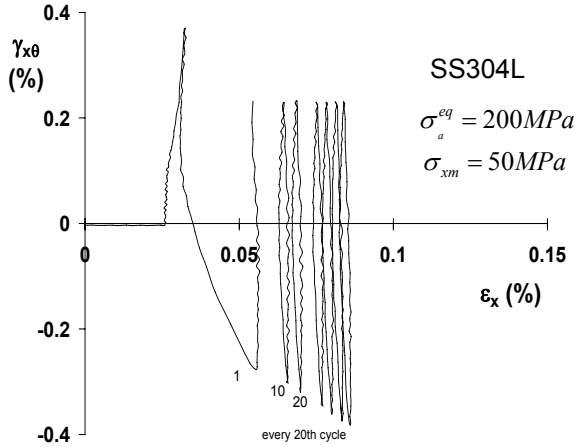

(b) Axial and shear strain ratcheting from experiment

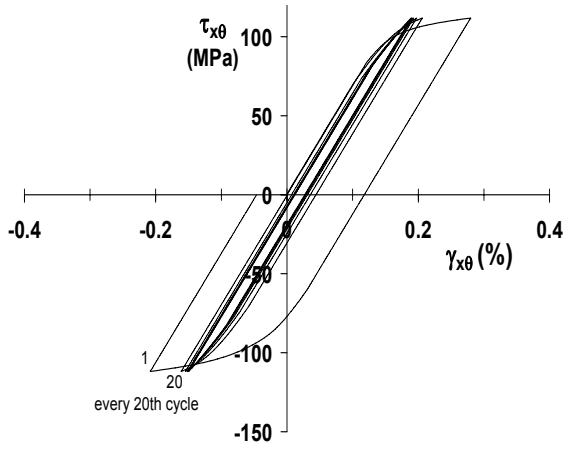

(c)Simulation by modified Chaboche model

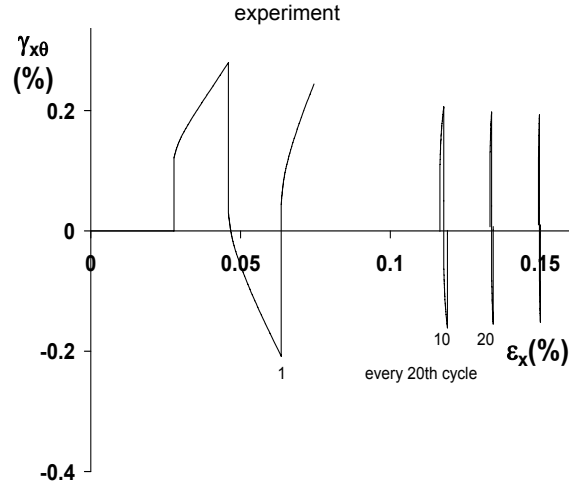

(d) Simulation by modified Chaboche model

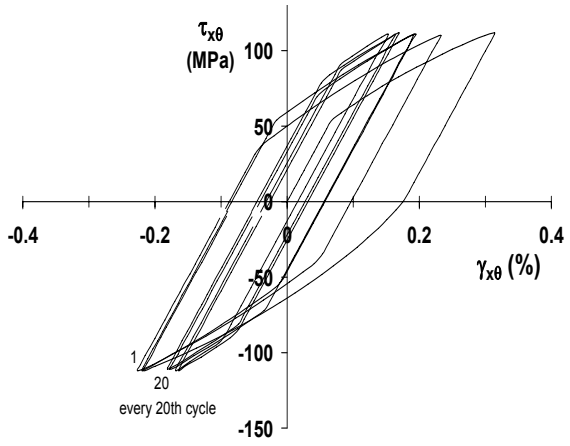

(e) Simulation by multi-mechanism model

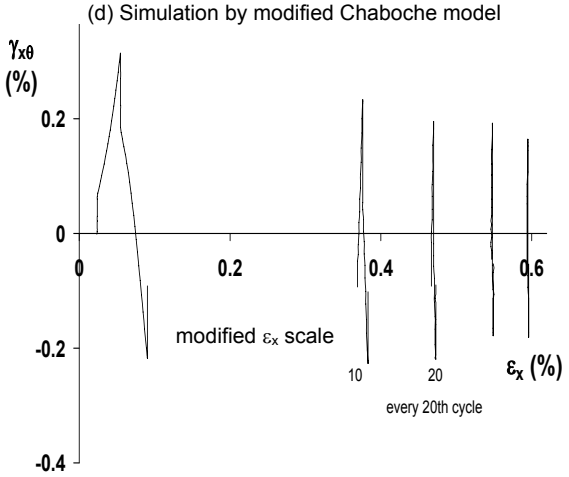

(f) Simulation by multi-mechanism model

Fig. 2.4. Shear ratcheting experimental responses of SS304L and simulations.

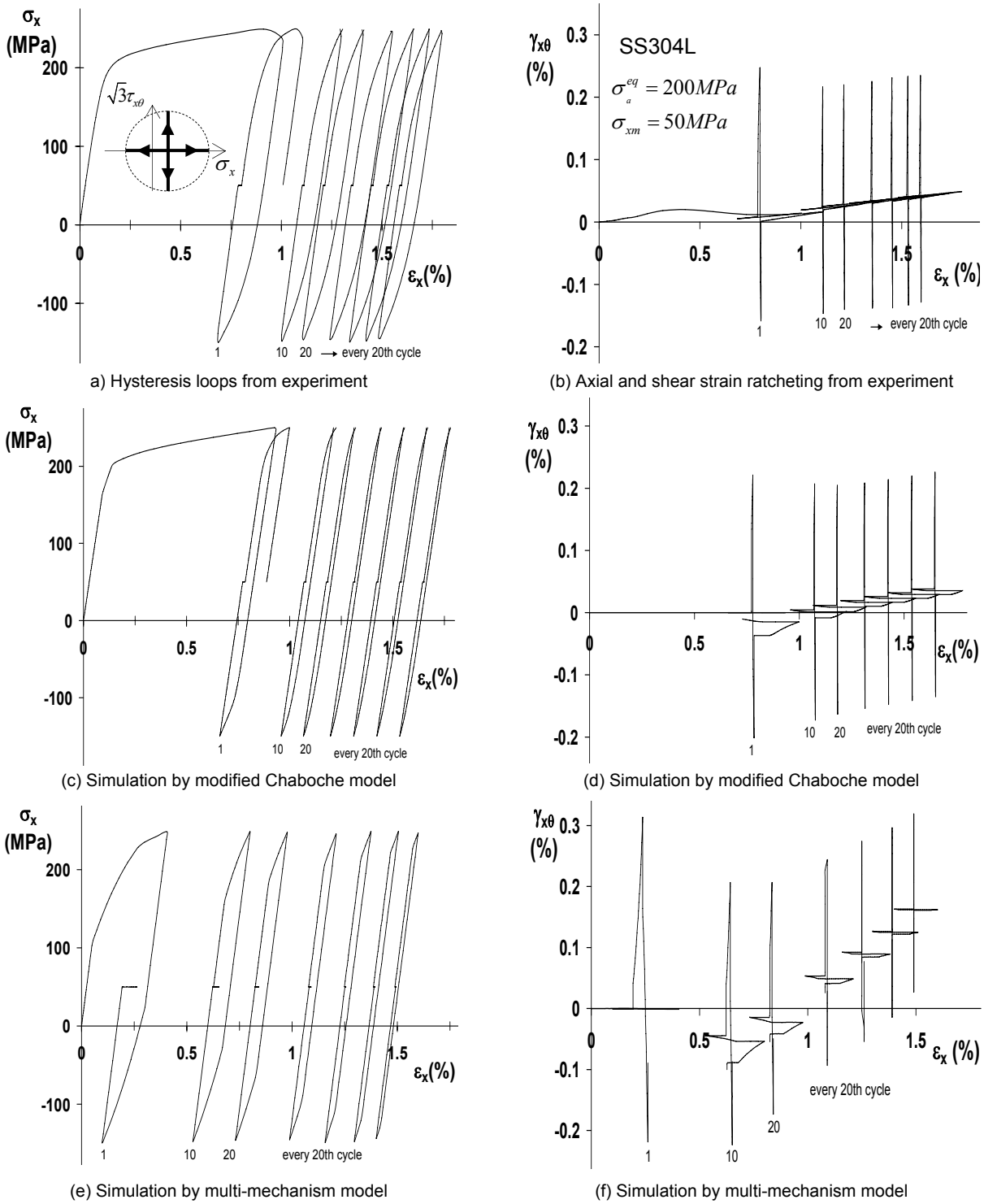

a) Hysteresis loops from experiment

(b) Axial and shear strain ratcheting from experiment

(c) Simulation by modified Chaboche model

(d) Simulation by modified Chaboche model

(e) Simulation by multi-mechanism model

(f) Simulation by multi-mechanism model

Fig. 2.5. Cross ratcheting experimental responses of SS304L and simulations.

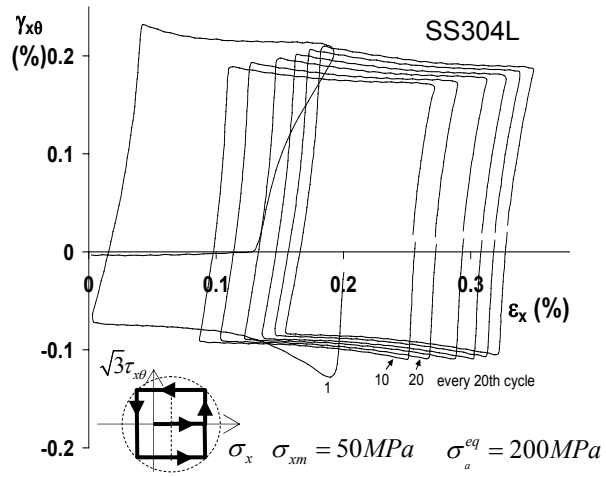

(a) Axial and shear strain ratcheting in square ratcheting experiment

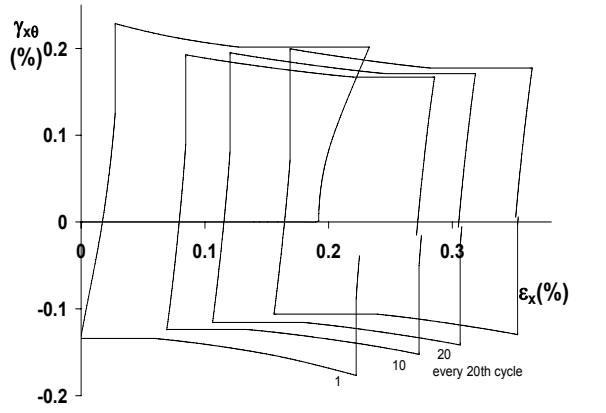

(b) Simulation by modified Chaboche model

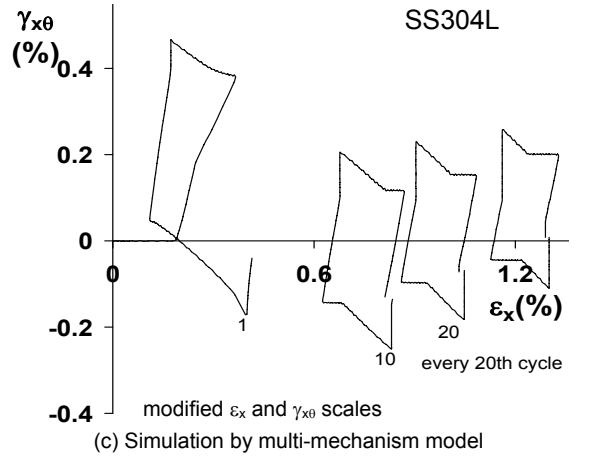

(c) Simulation by multi-mechanism model

Fig. 2.6. Square ratcheting experimental response and simulations.

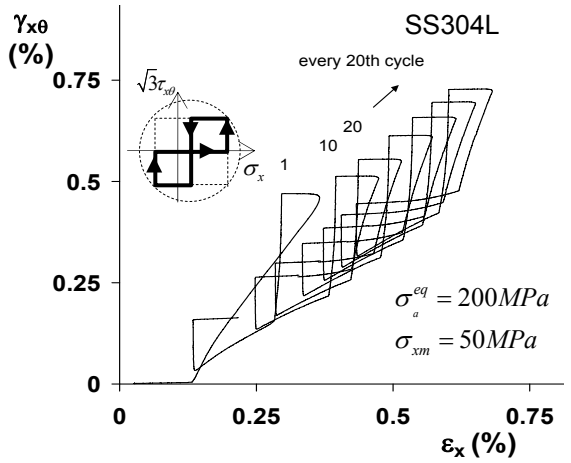

(a) Axial and shear strain ratcheting in two-square ratcheting experiment

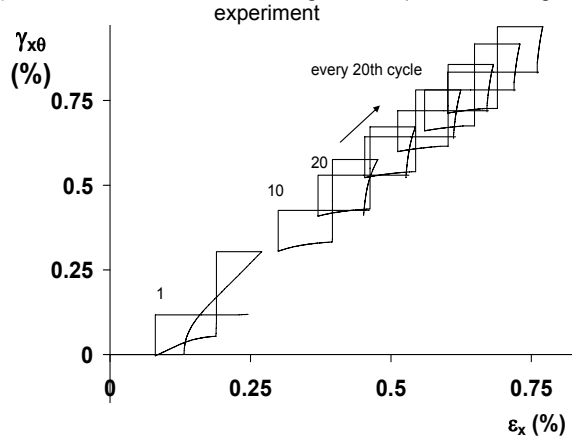

(b) Simulation by modified Chaboche model

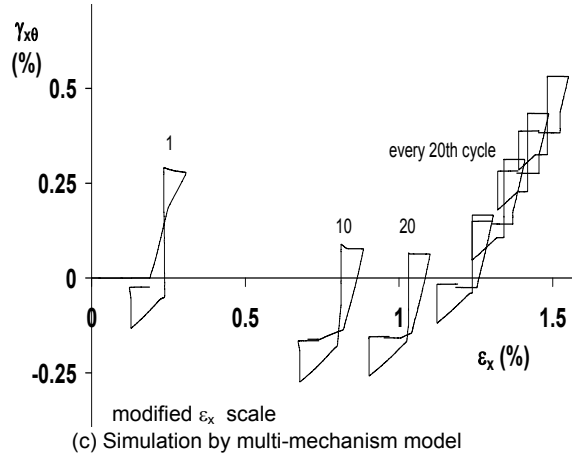

(c) Simulation by multi-mechanism model

Fig. 2.7. Two square ratcheting experimental response and simulations.

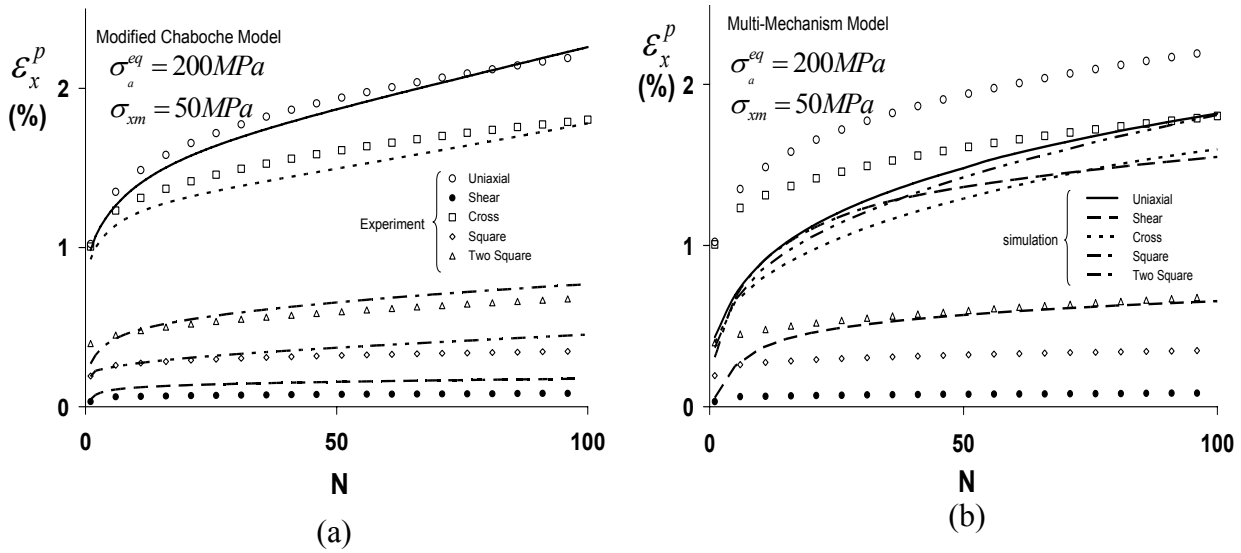

Fig. 2.8. Axial strain ratcheting from stress-controlled ratcheting experiments and simulations from (a) modified Chaboche model with Benallal and Marquis (1987) nonproportional features and (b) multi-mechanism model.

A question arises if the different rates of ratcheting in Fig. 2.8 are mainly caused by the different nonproportional cyclic hardening in these responses. As most of the cyclic hardening usually occurs during the initial cycles (Hassan and Kyriakides, 1994a), it can be argued that the different steady ratcheting rates obtained after the initial transient rates in Fig. 2.8 are not the influences of the nonproportional cyclic hardening. Instead, different rates of ratcheting could be the direct influence of loading nonproportionality itself. Moreover, not much cyclic hardening is observed in the experimental responses in Figs. 3-7; rather some cyclic softening is demonstrated by these responses. The shear experiment with the smallest axial strain ratcheting rate (Fig. 2.8), in fact, demonstrated noticeable cyclic softening (Fig. 2.4). Another reason for different rates of ratcheting under different load histories might be the influence of ratcheting hardening, which is a cyclic plasticity characteristic recently point out by Jiang and Zhang (2008) as a reason for strain rate decay.

In order to examine these hypotheses further and also to challenge the constitutive models, few more experiments were conducted on SS304L. For three of the experiments (in Fig. 2.8) second loading sequences were added as follows: 100 cycles of uniaxial path were

followed by 100 cycles of cross path (referred as *uni-cross*); 100 cycles of shear path were followed by 100 cycles of uniaxial path (referred as *shear-uni*); and finally, 100 cycles of square path were followed by 100 cycles of uniaxial path (referred as *square-uni*). The mean axial stress and the equivalent amplitude stress in the second 100 cycle sequence were kept the same, 50 MPa and 200 MPa, respectively, as the first 100 cycle sequence. The responses from these double sequence loading experiments are summarized in Fig. 2.9, where it is observed that as the experiment switches from shear to uniaxial path, an increase in axial strain ratcheting rate is obtained. In the uni-cross experiment, no reduction in the axial strain ratcheting rate is observed as the loading path is switched from uniaxial to cross path. Finally, in the square-uni experiment, almost no change in the ratcheting rate is obtained as can be seen in Fig. 2.9. The second-sequence responses in the double sequence experiment are not demonstrating the nonproportionality effect on the ratcheting rate as clearly as in the first sequence responses. This aspect needs further experimental investigation. More lights on the effect of nonproportionality on ratcheting rates will be shed later from model simulation point of view.

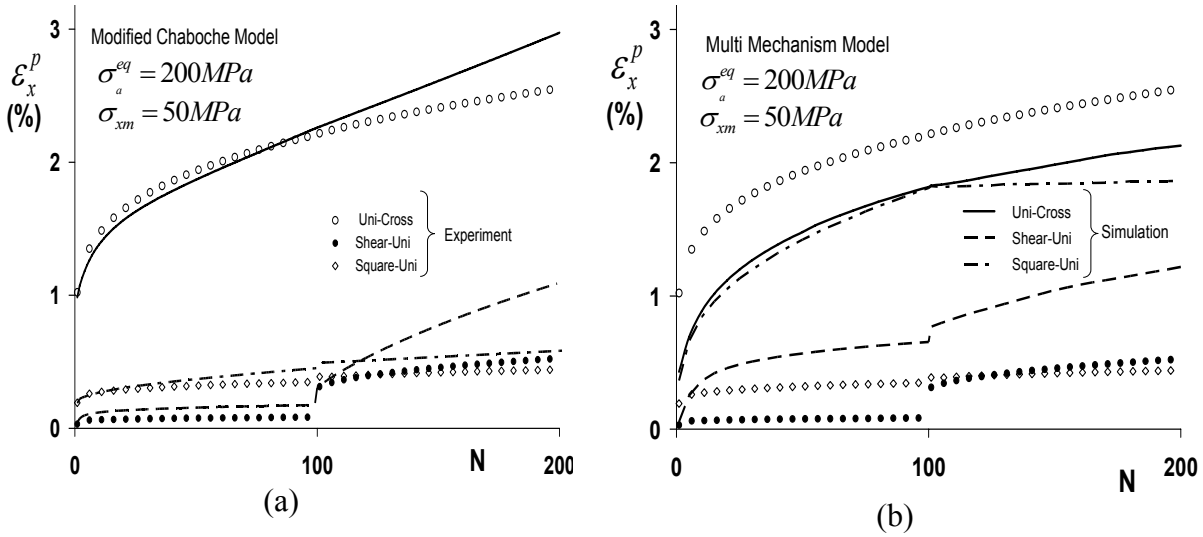

Fig. 2.9. Axial strain ratcheting from double-sequence ratcheting experiments and simulations from (a) modified Chaboche model with Benallal and Marquis (1987) nonproportional features and (b) multi-mechanism model.

In the case of the two-square ratcheting experiment, at the completion of 100 forward direction cycles (Fig. 2.7), another 100 cycles in the reverse directions were conducted (see the insets in Fig. 2.10 for these directions). Maximum axial strain peaks as a function of the number of cycles from these two steps are plotted in Fig. 2.10, where no change in strain ratcheting rate is observed as the loading path is switched. The last ratcheting experiment conducted in this study involved a triangular path in the *axial stress* and *shearing strain* space, defined by the coordinates (in MPa and %): (0,0), (250, 0), (0, 0.5), (0,0), (250,0), (0,-0.5), (0,0), for the first 100 cycles (see inset in Fig. 2.11b).

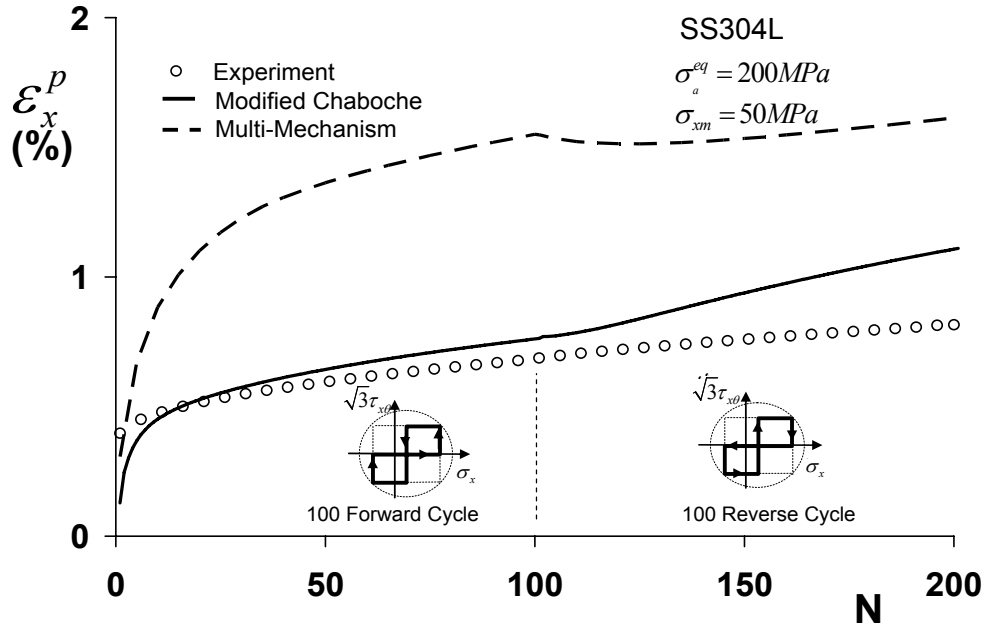

Fig. 2.10. Axial strain ratcheting from two-square path, forward and reverse directions, and simulations from the modified Chaboche and multi-mechanism models.

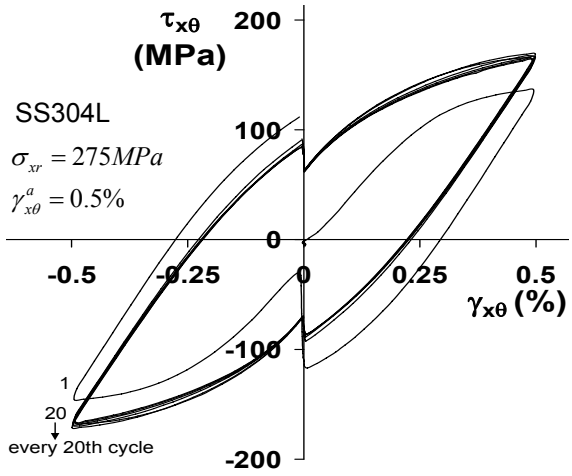

(a) Hysteresis loop from experiment

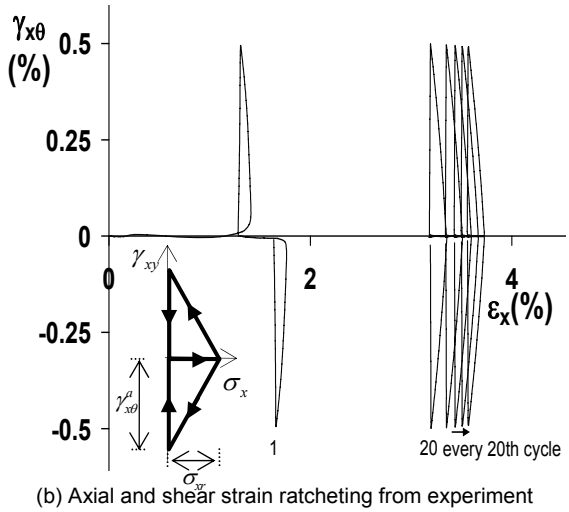

(b) Axial and shear strain ratcheting from experiment

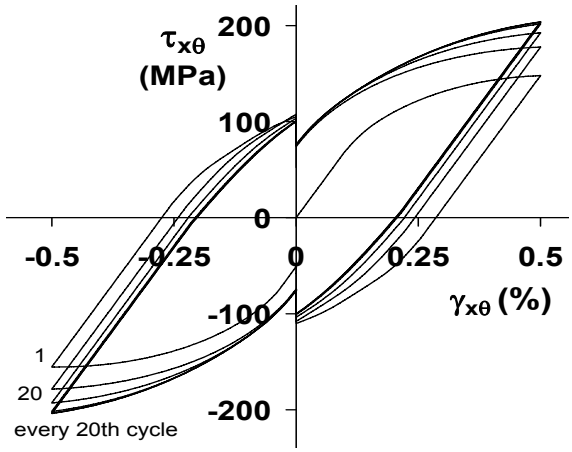

(c) Simulation by modified Chaboche model

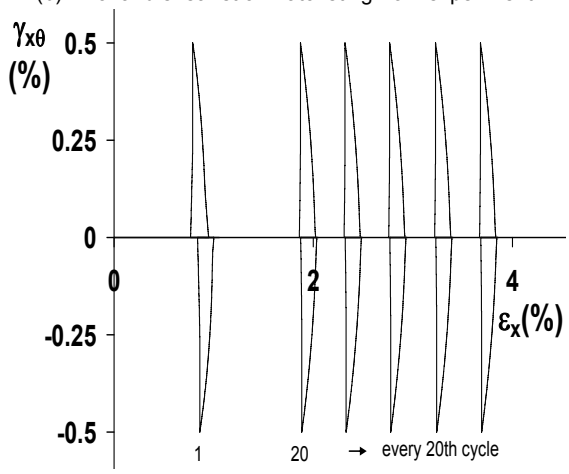

(d) Simulation by modified Chaboche model

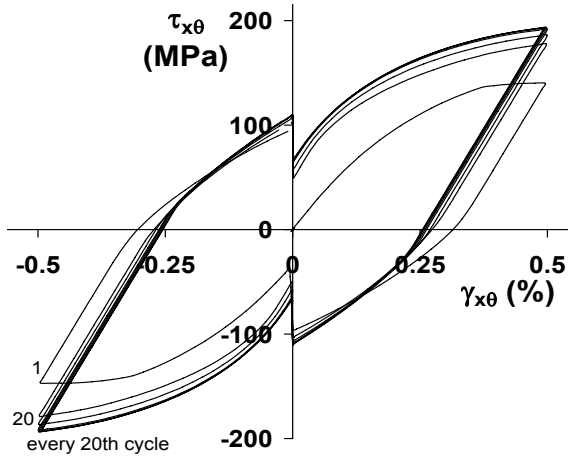

(e) Simulation by multi-mechanism model

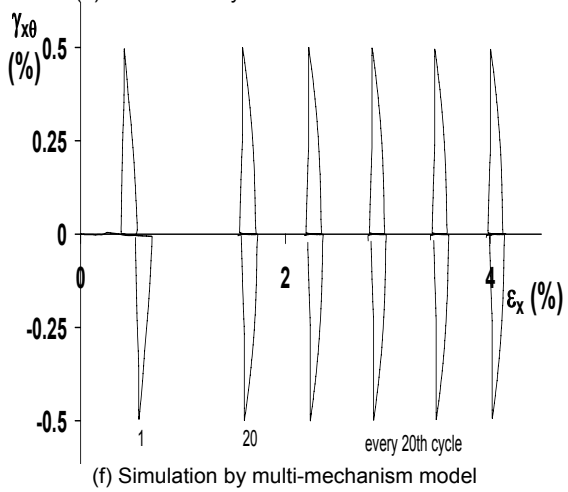

(f) Simulation by multi-mechanism model

Fig. 2.11. Triangular path ratcheting experimental responses and simulations.

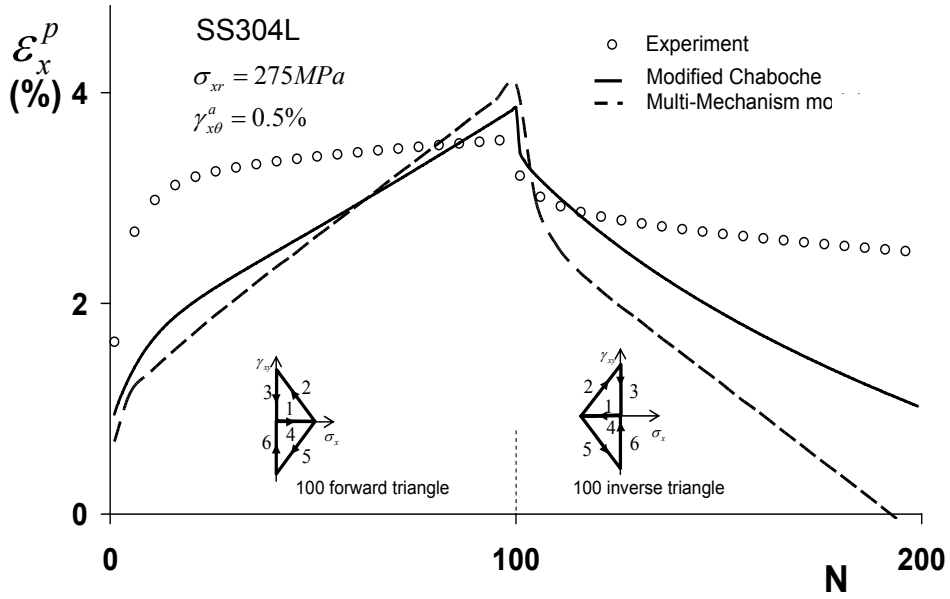

Fig. 2.12. Axial strain ratcheting rate from triangle loading experiment (positive mean axial stress during the first 100 cycles and negative mean axial stress in the next 100 cycles) and simulations from the modified Chaboche and multi-mechanism models.

The detailed stress-strain responses from the triangular path experiment are shown in Fig. 2.11, where considerable axial strain ratcheting (Fig. 2.11b) without much cyclic hardening of the hysteresis loops (Fig. 2.11a) is observed. In the triangular path experiment, first 100 cycles was followed by 100 reverse cycles as shown in the insets in Fig. 2.12. The rate of axial strain ratcheting, obtained by plotting the axial strain at every 5th cycle, at the positive axial stress peaks during the first 100 cycles and at the negative axial stress peaks during the 100 inverse cycles, is shown in Fig. 2.12. During the first 10 -15 cycles of the triangular path, the axial strain ratchets at a high rate, followed by a small and nearly stabilized rate in the subsequent cycles. It can also be observed in Fig. 2.12 that during the inverse triangular path, the axial strain ratcheting trend is reversed because of negative axial mean stress.

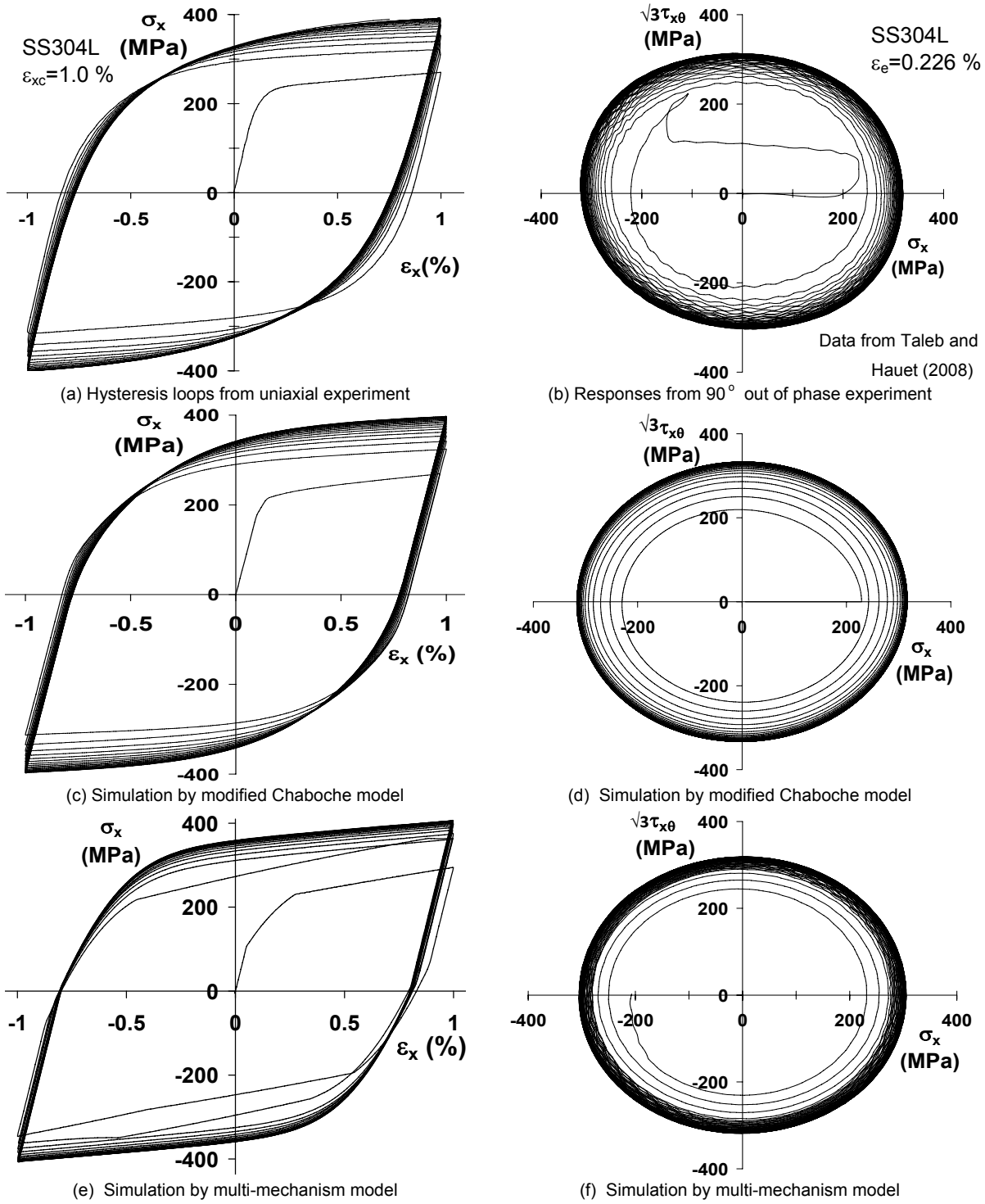

Fig. 2.13. Experimental responses for proportional and nonproportional model parameter determination and simulations.

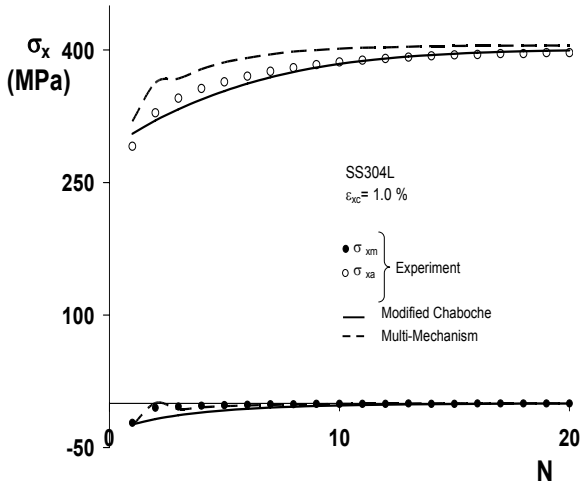

Fig. 2.14. Amplitude and mean stress responses from uniaxial strain-controlled experiment used in the parameter determination and simulations.

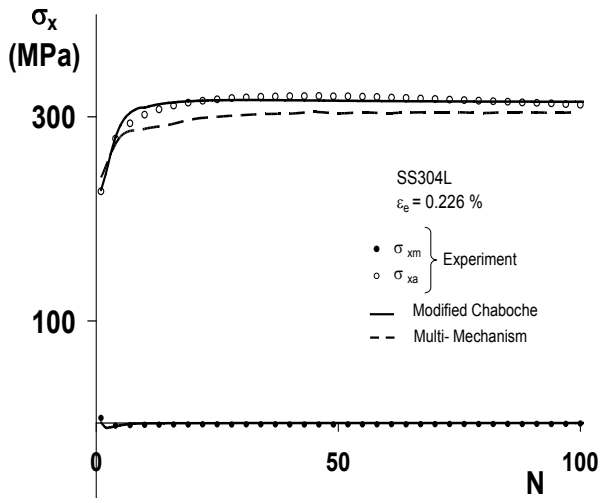

Fig. 2.15: Amplitude and mean stress response from 90-degree out-of-phase experiment used in the parameter determination and simulations.

Finally, a uniaxial strain-controlled experiment was conducted and a 90-degree out-of-phase experimental response of the same material was collected from Taleb and Hauet (2008) for model parameter determination. These responses are shown in Figs. 13a, 13b, 14 and 15. Note in Figs. 13a and 13b that SS304L demonstrates cyclic hardening under strain-controlled cycles. It is noted here that under stress-controlled loading cyclic hardening was not observed, rather small to moderate amount of cyclic softening was observed (Figs. 3a, 4a, and 5a).

Benallal and Marquis (1987), McDowell (1987), Jie and Xu (1991), Tanaka (1994), Hassan and Kyriakides (1994b), Kang, et al. (2002a,b), Aubin, et al. (2003a), and others demonstrated that for simulating nonproportional cyclic hardening and ratcheting responses model parameters are needed to be calibrated using the nonproportional responses in addition to the uniaxial loading responses. However, there are many nonproportional experimental responses (Hassan and Kyriakides, 1994b, Kang, et al., 2002a,b, 2004, 2006, Jiang and

Zhang, 2008), in addition to those presented in this paper, which are yet to be understood clearly.

Hence, experimental responses needed for determining parameters of nonproportional models are not well established yet. In this study, a 90-degree out-of-phase strain-controlled experimental response and a multiaxial ratcheting response are used for nonproportional parameter determination.

2.3. Cyclic Plasticity Models

Both successes and challenges in simulating nonproportional loading ratcheting responses have been demonstrated by Hassan and Kyriakides (1994b), Delobelle, et al. (1995), Portier, et al. (2000), Aubin, et al. (2003a), Kang, et al. (2004, 2006), and others. Simulating nonproportional ratcheting responses successfully depends on the robustness of the i) hysteresis loop simulation model, ii) cyclic hardening/softening model for proportional loading, iii) kinematic hardening rule for simulating yield surface evolution, and finally, iv) a nonproportional model for simulating the influence of multiaxiality on cyclic hardening/softening and ratcheting responses. In simulating the hysteresis loops under proportional loading, Dafalias-Popov (1976) two-surface model, nonlinear kinematic hardening models (Chaboche, 1991, Ohno and Wang, 1993, Abdel Karim and Ohno, 2000), and many modified versions of these models (Hassan and Kyriakides, 1994a,b, Delobelle, et al., 1995, Jiang and Sehitoglu, 1996a,b, Bari and Hassan, 2002, Chen and Jiao, 2004, Kang, et al., 2004, 2006, and others) demonstrated very good success.

Success of the non-linear kinematic hardening models in simulating biaxial ratcheting responses was demonstrated by Ohno and Wang (1993), Delobelle, et al., (1995), Portier, et al., (2000), Abdel Karim and Ohno (2000), Bari and Hassan (2002), Kang, et al. (2004, 2006), and others. It has been shown that for improving multiaxial loading cyclic hardening/softening and ratcheting responses, it is required to incorporate nonproportional modeling features into cyclic plasticity models (Hassan and Kyriakides, 1994b, Portier, et al.,

2000, Kang et al., 2004, 2006, and more). Most of the nonproportional hardening models, such as Benallal and Marquis (1987), Tanaka (1994), and Seyed-Ranjbari (1986), were developed and validated based on strain-controlled responses. However, to authors' knowledge, validation of these models in simulating "stress-controlled" ratcheting responses are extremely limited (Hassan and Kyriakides, 1994b and Kang, et al., 2004, 2006).

Through extensive studies on two-surface Dafalias and Popov (1976) model and non-linear kinematic hardening rule models of Chaboche (1989, 1991), Ohno and Wang (1993), and Abdel Karim and Ohno (2000), Bari and Hassan (2000, 2001, 2002) demonstrated that the non-linear kinematic hardening rule models perform satisfactorily in simulating a broad set of uniaxial and biaxial ratcheting responses. It was also demonstrated by Bari and Hassan (2002) that the ratcheting simulations from the modified Chaboche and Ohno-Wang models are comparable. This study evaluates further the modified Chaboche model (Bari and Hassan, 2002) against simulating the set of stress-controlled ratcheting responses of SS304L developed in this study. For such, the nonproportional model by Benallal and Marquis (1987) was incorporated into the modified Chaboche model. In addition to evaluate the modified Chaboche model, a different class of model known as the multi-mechanism model (Taleb, et al., 2006) also is evaluated in this study. This model is studied because it also demonstrated success in simulating the same set of the uniaxial and biaxial ratcheting responses used in validating the modified Chaboche model by Bari and Hassan (2002). Such comparative evaluations of different class of models would facilitate identification of a robust cyclic plasticity model. The rate and temperature independent modeling features are considered in this study so that the performance of these models in simulating only the nonproportional ratcheting responses can be scrutinized. Brief descriptions of the two models and their model parameter determination methodologies are presented below:

2.3.1 Modified Chaboche Model

The primary features of the rate and temperature independent Chaboche (1991) model are:

i. von-Mises Yield criterion :

$$f(\underline{\sigma}-\underline{\alpha})=\left[\frac{3}{2}\left(\underline{s}-\underline{\mathrm{a}}\right)\bullet\left(\underline{s}-\underline{\mathrm{a}}\right)\right]^{1/2}=\sigma_0+R\,, \tag{1}$$

ii. additive strain increment decomposition:

$$d\underline{\varepsilon}=d\underline{\varepsilon}^{e}+d\underline{\varepsilon}^{p}\,, \tag{2}$$

Hooke's law: $$d\underline{\varepsilon}^{e}=\frac{1+\nu}{E}d\underline{\sigma}-\frac{\nu}{E}tr(d\underline{\sigma})\underline{I}\,, \tag{2a}$$

Flow rule: $$d\varepsilon^{p}=d\lambda\frac{\partial f}{\partial\sigma}=\frac{3}{2}dp\frac{\underline{s}-\underline{\mathrm{a}}}{\sigma_0+R}\,, \tag{2b}$$

where, $\underline{\sigma}$ is the stress tensor, $\underline{\alpha}$ is the current center of the yield surface in the total stress space, $\underline{s}$ is the deviatoric stress tensor, $\underline{\mathrm{a}}$ is the current center of the yield surface in the deviatoric space, σ_0 is the initial size of the yield surface and R is the drag resistance which represents the isotropic hardening variable (initial value is zero for virgin material), $d\underline{\varepsilon}^{p}$ is the incremental plastic strain tensor, $d\underline{\varepsilon}^{e}$ is the incremental elastic strain tensor, E is elastic modulus and ν the Poisson's ratio, and $d\lambda$ is a plastic multiplier determined by the radial return method, and $dp=\left|d\underline{\varepsilon}^{p}\right|=\left[\frac{2}{3}d\underline{\varepsilon}^{p}\bullet d\underline{\varepsilon}^{p}\right]^{1/2}$.

iii. Kinematic hardening rule: Bari and Hassan (2002) modified the Chaboche model (1989, 1991) kinematic hardening rule as follows:

$$d\underline{\mathrm{a}}=\sum_{i=1}^{4}d\underline{\mathrm{a}}_i \tag{3}$$

$$d\underline{\mathrm{a}}_i=\frac{2}{3}C_i d\underline{\varepsilon}^{p}-\gamma_i\{\underline{\mathrm{a}}_i\delta^{'}+(1-\delta^{'})(\underline{\mathrm{a}}_i\bullet\underline{n})\underline{n}\}dp\,,\qquad \text{for}\qquad i=1,\,2,\,3 \tag{3a}$$

$$d\underline{a}_i = \tfrac{2}{3} C_i d\underline{\varepsilon}^p - \gamma_i \{\underline{a}_i \delta' + (1-\delta')(\underline{a}_i \bullet \underline{n})\underline{n}\} \left\langle 1 - \frac{\bar{a}_4}{f(\underline{a}_i)} \right\rangle dp \ , \quad \text{for } i = 4 \tag{3b}$$

where, $\underline{n}$ is the normal to yield surface, and C_1- C_4, γ_1-γ_4, $\bar{a}_4$ and δ' are the model parameters.

The cyclic hardening modeling feature in the Chaboche (1989, 1991) model can simulate only the proportional loading responses. Benallal and Marquis (1987) model was added to the modified Chaboche model (Bari and Hassan, 2002) to enhance its capability of simulating non-proportional loading responses. In this model, the nonproportionality parameter A is defined as:

$$A = 1 - \cos^2 \alpha \tag{4}$$

$$\text{where, } \cos\alpha = \frac{d\underline{\varepsilon}^p \cdot d\underline{s}}{\left[\frac{2}{3} d\underline{\varepsilon}^p \cdot d\underline{\varepsilon}^p\right]^{1/2} \left[\frac{3}{2} d\underline{s} \cdot d\underline{s}\right]^{1/2}} . \tag{4a}$$

Benallal and Marquis (1987) and many other non-proportional models (Tanaka, 1994 and Jiang and Sehitoglu, 1996a,b, Kang, et al., 2002a,b) included the influence of the nonproportional loading through the drag resistance, R, as follows:

$$dR = D_R(A)\left[R^{AS}(A) - R\right] dp \tag{5}$$

$$D_R(A) = (d_R - f_R) A + f_R \tag{6}$$

$$R^{AS}(A) = \frac{gAR^{\infty} + (1-A)R^0}{gA + (1-A)} \tag{7}$$

This study also included the influence of the non-proportional loading through the kinematic hardening parameters, γ_i (i =*1, 2, 4*), as follows:

$$d\gamma_i = D_{\gamma i}(A)\left[\gamma_i^{AS}(A) - \gamma_i\right] dp \tag{8}$$

$$D_{\gamma i}(A) = \left(d_{\gamma i} - f_{\gamma i}\right) A + f_{\gamma i} \tag{9}$$

$$\gamma_i^{AS}(A) = \frac{gA\gamma_i^{\infty} + (1-A)\gamma_i^{0}}{gA + (1-A)} \tag{10}$$

In the above equations, with $A = 0$, the model parameters $f_R, f_{\gamma i}, R^0, \gamma_i^0$ represent the proportional loading, and with $A = 1$, the model parameters $d_R, d_{\gamma i}, R^{\infty}, \gamma_i^{\infty}$ represent the nonproportional loading with the highest degree of nonproportionality, e.g., the 90-degree out of phase loading in the axial-shear strain space. For intermediate degree of nonproportionality A and g vary between 0 and 1 depending on the angle between $d\underline{\varepsilon}^p$ and $d\underline{S}$ (Eq. 4a).

Cyclic hardening or softening under both proportional and nonproportional loading is manifested by increase or decrease in the linear elastic range (yield surface size) and/or increase or decrease in the plastic modulus. These, in turn, result in the progressive increase or decrease in peak stress (or amplitude stress) under constant amplitude strain-controlled cycle, or progressive thinning or fattening of the hysteresis loop under constant amplitude stress-controlled cycle. Modeling of cyclic hardening or softening through progressive change of the yield surface size with cycles, know as isotropic hardening, yields very good peak stress simulations (Benallal and Marquis, 1987, Tanaka, 1994, Jiang and Kurath, 1997, Kang, et al., 2002a). However, such a method does not yield reasonable simulation of the hysteresis loop shape.

It was shown by Bari and Hassan (2000) that by calibrating the kinematic hardening rule parameters, C_i and γ_i, hysteresis loop shape can be simulated very well. This means C_i and γ_i parameters can be varied to simulate changes in the hystersis loop shape induced by cyclic hardening or softening. Such modeling approaches were reviewed by Chaboche (1989). The modeling approach of using the kinematic variable γ_i in simulating cyclic hardening or softening was originally proposed by Marquis (1979) and later validated by Haupt and

Kamlah (1995), Portier, et al. (2000), and Kang, et al. (2004). The use of the kinematic variable C_i for simulating the cyclic hardening or softening was scrutinized by Moosbrugger (1991, 1993). It is noted here that the kinematic hardening rule parameters also influence the ratcheting simulation. Hence, this paper evaluates the combined influence of the isotropic hardening parameter (R) and the kinematic hardening parameter (γ_i) in simulating both the nonproportional cyclic hardening and ratcheting responses of SS304L. Addition of C_i parameters in simulating the cyclic hardening would have added sixteen more parameters. Hence, C_i is kept constant in this study without sacrificing the simulation quality as can be seen later.

2.3.1.1 Model Parameter Determination for Modified Chaboche Model

The modified Chaboche model parameters were determined using responses from four experiments: uniaxial strain-controlled experiment (Fig. 2.13a and 14), uniaxial ratcheting experiment (Fig. 2.8), shear ratcheting experiment (Fig. 2.8) and finally, 90-degree out-of-phase strain-controlled experiment (Fig. 2.15). The elastic parameters E, ν, σ_o (Eqs. 1 and 2) are determined from the 1st hysteresis curve in Fig. 2.13a. The value of R_0 (Eq. 7) is determined from the difference between the linear elastic ranges of the 1st and stable hysteresis curves.

The systematic approach of Bari and Hassan (2000) for determining C_i, γ_i and $\bar{a}_4$ by fitting a hysteresis curve was used in this study. The parameters C_i (i = 1 to 4), which were kept constant in the simulations, were determined by fitting the uniaxial 1st hysteresis curve. The initial values of γ_i (i = 1, 2, 4) also were determined by using the uniaxial 1st hysteresis curve. As stated earlier, γ_i (i = 1, 2, 4) need to be varied (according to Eq. 8) for simulating the hysteresis loop shape change with cyclic hardening. The parameters γ_i^0 (i = 1, 2, 4) were determined from the uniaxial stable hysteresis curve (Fig. 2.13a). With progressive cyclic hardening, the values of γ_i (i = 1, 2, 4) should gradually decrease to better represent the cyclic stiffening of the hysteresis curves. The rate at which γ_i of the 1st hysteresis curve decreases

to γ_i^0 was determined by the $f_{\gamma i}$ values (in Eq. 9), which were determined by fitting the stress amplitude response in Fig. 2.14. The value of f_R (in Eq. 6) was determined based on the plot of R (not shown) of the hysteresis curves as a function of accumulated plastic strain. The value of γ_3 , which was kept constant in the simulations, was determined by fitting a uniaxial ratcheting rate. The multiaxial ratcheting parameter δ' also was kept constant in the simulations and was obtained by simulating the axial strain ratcheting rate in the shear ratcheting experiment in Fig. 2.8 (Bari and Hassan, 2002). It is noted here that Delobelle, et al. (1995) proposed a nonproportional parameter based function for δ', which would have added eight more parameters and hence was not incorporated in this study.

For simulating additional cyclic hardening induced by nonproportional loading, the proportional parameters R and γ_i are modified using Eqs. 5 to 10. In these equations, the nonproportionality parameters $R^\infty, \gamma_i^\infty, d_R, d_{\gamma i}, (i = 1, 2, 4)$ are determined using the stress amplitude response of the 90-degree out-of-phase experiment in Fig. 2.15. Methodology for determining the parameters for drag resistance, R, is given in Benallal and Marquis (1987). As indicated earlier, part of the additional cyclic hardening is obtained by decreasing γ_i (i = 1, 2, 4) values. The values of $d_{\gamma i,}$ (i = 1, 2, 4) determine the rate at which hardening (or decrease in γ_i) is achieved. The manual determination of so many nonproportional parameters from only the stress amplitudes of the 90-degree out of phase experiment is tedious. Hence, heuristic genetic algorithm (GA) software was developed for searching the initial values of parameters from a given range (Rahman, et al. 2005). Some of these GA parameters needed some manual adjustment for improved simulations. Due to the lack of an out-of-phase experiment with an intermediate degree of nonproportionality needed for determining g, its value was optimized using the axial strain ratcheting rate response in the shear ratcheting experiment in Fig. 2.8. The parameters used for simulation of the cyclic responses are listed in Table 1:

Table 2.1: Cyclic parameters of the modified Chaboche model

Elastic parameters: E=180 GPa , $\nu = 0.30$, $\sigma_0 = 153.2$ MPa	
Proportional parameters: (for $i = 1$ to 4) C_i 540224 1937 625 73251 MPa γ_i 28285 740 12.8 6084 γ_i^0 12524 340 8.78 1952 $\bar{a}_4$ 14.1 MPa, δ' 0.13, R^0 10 MPa, f_R 0.8 $f_{\gamma i}$ 16 7.7 3.45 9	Nonproportional parameters: (for $i = 1$ to 4) γ_i^∞ 9549 291 8.78 1688 $d_{\gamma i}$ 66 84 3.45 82.5 R^∞ 30 MPa d_R 5.0 g 0.9

The shape of the monotonic, axial stress-strain curve is much different from the axial hysteresis curves (see Fig. 2.13 a). The reason for such difference is pointed out by Suresh (1998, Chapter 2, Art. 2.2.1) that the strain hardening under monotonic tension occurs much faster than that under cyclic loading. Hence with the modified Chaboche model the monotonic response simulation is carried out with a different set of parameters as follows:

Table 2.2: Monotonic parameters of the modified Chaboche model

E = 180 GPa , $\nu = 0.30$, $\sigma_0 = 160.2$ MPa				
$C_{1\text{-}4}$	93401	15272	4074	75233 MPa
$\gamma_{1\text{-}4}$	11430	864	0	30870

Simulations of the parameter determination experiments with the above set of parameters are shown in Figs. 8a (uniaxial and shear ratcheting experiments), 13c, 13d, 14 and 15 (uniaxial stress-strain, out-of-phase stress, mean and amplitude responses). The fits and simulations in these figures from the modified Chaboche model are found to be quite reasonable.

2.3.2 Multi-Mechanism Model

The second model evaluated in simulating the nonproportional ratcheting responses is the multi-mechanism model which is a new class of constitutive equations where the inelastic strain is represented by more than one variable. A mechanism is defined by a set of a local stress, a kinematic variable, and a strain rate. Several versions have already been proposed in

the following references: Cailletaud and Sai (1995), Taleb, et al. (2006), Sai and Cailletaud (2007). The first version is called 2M1C (2 Mechanisms and 1 Criterion) proposed in Cailletaud and Sai (1995), where the readers may find its theoretical background. In the second version in Taleb, et al. (2006), 2M1C was modified for improving its multiaxial ratcheting simulation. In this model, used in this study, the inelastic strain is composed of two components expressing two different mechanisms of inelastic strain,

$$\underline{\varepsilon}^{in} = A_1 \underline{\varepsilon}_1^{in} + A_2 \underline{\varepsilon}_2^{in} \tag{11}$$

The relation between the macroscopic stress $\underline{\sigma}$ and the local stress $\underline{\sigma}_i$ associated to the inelastic strain is given by,

$$\underline{\sigma}_i = A_i \underline{\sigma} \tag{12}$$

The parameters A_1 and A_2 are taken equal to 1 in the present simulations. The normality flow rule is considered for each inelastic strain,

$$\dot{\underline{\varepsilon}}_i^{in} = \dot{\lambda} \underline{n}_i \tag{13}$$

$\dot{\lambda}$ is a plastic multiplier ($\dot{\lambda} \geq 0$) and is given by the relation $\dot{\lambda} = \left\langle \frac{f}{K} \right\rangle^n$, where K and n are material parameters for rate effects. For producing rate-independent effects, considered in the present study, low value for K and high value for n are used.

$\underline{n}_i = \frac{\partial f}{\partial \underline{\sigma}_i}$, f being a yield function defined below (Eq. 19), thus,

$$\underline{n}_i = \frac{3}{2} \frac{\underline{\underline{\sigma}}_i^{'} - \underline{\underline{X}}_i^{'}}{J_1} \left(\frac{J_1}{J} \right)^{N-1} \tag{14}$$

The kinematic hardening is described by two variables $\underline{\alpha}_1$ and $\underline{\alpha}_2$ which vary according to:

$$\dot{\underline{\alpha}}_i = \dot{\underline{\varepsilon}}_i - D_{ii}\{(1-\eta)\,\underline{\alpha}_i + \eta(\underline{\alpha}_i : \underline{m}_i)\underline{m}_i\}\dot{\lambda} \tag{15}$$

η is a multiaxial parameter similar to that in the modified Chaboche model and,

$$\underline{m}_i = \frac{\underline{n}_i}{\|\underline{n}_i\|} = \frac{\underline{\sigma'}_i - \underline{X'}_i}{\|\underline{\sigma'}_i - \underline{X'}_i\|} \tag{16}$$

where, $\|\underline{n}_i\|$ is the Euclidian norm of $\underline{n}_i$.

The thermodynamic associated forces $\underline{X}_1$ and $\underline{X}_2$ related to $\underline{\alpha}_1$ and $\underline{\alpha}_2$ respectively, are coupled through the material parameter C_{12},

$$\underline{X}_1 = \frac{2}{3}C_{11}\underline{\alpha}_1 + \frac{2}{3}C_{12}\underline{\alpha}_2 \tag{17}$$

$$\underline{X}_2 = \frac{2}{3}C_{12}\underline{\alpha}_1 + \frac{2}{3}C_{22}\underline{\alpha}_2 \tag{18}$$

C_{11}, C_{22} and C_{12} are material parameters.

The flow function is given by,

$$f = J - (R_0 + R) \tag{19}$$

R_0 is a function of the initial yield stress and R is the isotropic hardening variable which evolves as:

$$\dot{R} = b(Q - R)\dot{p} \tag{20}$$

Q is a material parameter while $\dot{p}$ is the accumulated plastic strain given by,

$$\dot{p} = \sqrt{\frac{2}{3}\dot{\varepsilon}_{ij}^{in}\dot{\varepsilon}_{ij}^{in}} \tag{21}$$

$$J = (J_1^N + J_2^N)^{\frac{1}{N}} \tag{22}$$

N is a material parameter and,

$$J_i = \sqrt{\frac{3}{2}(\underline{\sigma}_i' - \underline{X}_i') : (\underline{\sigma}_i' - \underline{X}_i')} \tag{23}$$

2.3.2.1 Model Parameter Determination for Multi-Mechanism Model

As mentioned earlier, the rate effects are not considered in this study, hence, the parameters n and K are set to 11 and 31, which are usual values for rate-independent conditions. R_0 and Q were estimated using the uniaxial stress-strain hysteresis loops shown in Fig. 2.13a. The remaining model parameters were identified using the optimization software included in ZeBuLoN (Besson, et al., 1998). Four experimental responses: uniaxial strain-controlled experiment (Fig. 2.13a), uniaxial ratcheting experiment (Fig. 2.3a), shearing ratcheting experiment (Figs. 4a and 4b), and finally, the 90-degree out-of-phase strain-controlled experiment (Fig. 2.13b), same as those used for the modified Chaboche model parameter determination, were used for parameter determination of the multimechanism model. Table 3 shows the values of the identified parameters:

Table 2.3: Identified Parameters of the multi-mechanism model (Units: MPa, s)

R_0	Q	b	N	C_{11}	D_1	C_{22}	D_2	C_{12}	η
200	200	20	1	481056	1513	13533	21	5458	1

This set of parameters however does not fulfill the thermodynamic consistency. Wolff and Taleb (2008) have established conditions on the multimechanism parameters in order to ensure the positivity of the free energy and the thermodynamic consistency. The free energy is positive if and only if the following condition is satisfied,

$$C_{12}^2 \le C_{11} C_{22} \tag{24}$$

A sufficient (but not necessary) condition to ensure the thermodynamic consistency is

$$(D_1 - D_2)^2 \leq 4 D_1 D_2 \frac{C_{11} C_{22} (1-\eta)^2 - C_{12}^2}{C_{12}^2} \tag{25}$$

The model parameters given in Table 3 ensure the positivity of the free energy, but they don't verify the sufficient condition of the thermodynamic consistency (Eq. 25). Hence, $\eta = 0.71$ was used in the simulations instead of 1 as shown in Table 3. Finally, note that $N = 1$ leads to a linear flow function in terms of J_1 and J_2, and Eq. 19 becomes,

$$f = (J_1 + J_2) - (R_0 + R) \tag{26}$$

The multimechanism model is incorporated into the finite element software ZeBuLoN developed at the Ecole des Mines de Paris and ONERA, France (see Besson et al., 1998). The simulations of the parameter identification experiments are performed using the ZeBuLoN and plotted in Figs. 13e, 13f, 14 and 15. In the uniaxial strain-controlled response simulation, except the first loop, all other hysteresis loops are simulated reasonably (Fig. 2.13e), which also can be observed from the stress amplitude and mean simulations in Fig. 2.14. The 90-degree out-of-phase stress response and its stress amplitude and mean responses are also simulated reasonably as can be seen in Figs. 13f and 15.

2.4. Model Simulations of the Ratcheting Responses

Simulations from the modified Chaboche and multi-mechanism models for the SS304L experimental responses presented in section 2 are evaluated in this section. The simulated and experimental responses are compared to determine the state of the modeling of nonproportional ratcheting responses and areas in the modeling that need improvement.

Simulations of the uniaxial ratcheting experiment from the two models are shown in Figs. 3 and 8. In these figures, it is observed that both models simulated the ratcheting rate well (Fig. 2.8), mainly because this rate was fitted for parameter determination. However, the simulated hysteresis loops are not comparable to the experimental loops (Fig. 2.3). The Chaboche model simulated the hysteresis curve shape better than the multi-mechanism

model, but the simulated loops from either model are thinner compared to the experiment (Fig. 2.3). The first reason for this deficiency is that the experimental loops are showing cyclic softening rather than cyclic hardening for which both model parameters are calibrated. This drawback of the model simulations can be improved by incorporating modeling features of cyclic hardening and softening that depends on strain range (Landgraf, et al., 1969, Hassan and Kyriakides, 1994a, Jiang and Zhang, 2008). In addition, incorporation of rate-dependence (visco effect) into modeling may improve the simulations of hysteresis loop under stress-controlled cycles. Note in Figs. 3 and 8 that the first peak strain simulation from the multi-mechanism model is underpredicted. This is because with this model the monotonic response was simulated by using the cyclic parameters, whereas in the Chaboche model a separate set of parameters (Table 2) was used for monotonic response simulation as discussed earlier.

The shear ratcheting experiment simulations are compared to the experimental responses in Figs. 4 and 8, where it is seen that the modified Chaboche simulated the axial strain ratcheting rate of the shear experiment reasonably and the multi-mechanism model overpredicted the ratcheting rate. The shear stress-strain loops are not simulated well by the models because significant cyclic softening is shown under shear stress cycling (Fig. 2.4a), whereas the models are calibrated for cyclic hardening (Figs. 4c and 4d). Hence, similar model improvements which are mentioned earlier for improving uniaxial ratcheting hysteresis loop simulation may also improve the shear hysteresis loop simulation. In Fig. 2.4b, the shear stain amplitudes are increasing with cycles because of cyclic softening and hence are not simulated by the models calibrated for cyclic hardening (Figs. 4d and 4f). Both models simulated the cross experiment responses reasonably as shown in Figs. 5 and 8. The modified Chaboche model simulated both the axial and shear strain ratcheting rates of the cross experiment with good accuracy (Fig. 2.5d), whereas the multi-mechanism model simulated the axial strain ratcheting reasonably, but slightly overpredicted the shear strain

ratcheting (Fig. 2.5f). Similar to the uniaxial ratcheting experiment, the axial hysteresis loop of the cross experiment are not simulated well by either model (Figs. 5c and 5e).

The modified Chaboche model simulates the axial and shear strain ratcheting rates of square and two-square paths reasonably, whereas the multi-mechanism model overpredicted the ratcheting strains of these experiments as can be seen in Figs. 6, 7 and 8. Strain responses in Figs. 6a and 7a are simulated by the modified Chaboche model better than the multi-mechanism model. Overall, the performance of the modified Chaboche model in simulating the ratcheting rates of the uniaxial, shear, cross, square and two-square paths are quite satisfactory as can be seen in Fig. 2.8.

Ratcheting rate simulations for the double-sequence experiments, uni-cross, shear-uni and square-uni, from both the modified Chaboche and multi-mechanism models are shown in Fig. 2.9. As the loading is switched from uni to cross after the 100^{th} cycle, the modified Chaboche model continue to simulate ratcheting at a steady rate, as a result, overpredicts the ratcheting in the second sequence, for which the multi-mechanism model simulates the trend better. For the shear-uni experiment, both models overpredict the ratcheting rate in the second sequence. For the second sequence in the square-uni experiment, the modified Chaboche simulates the ratcheting rate well, whereas the multi-mechanism model simulates a very low ratcheting rate. For the two-square path experiment, as the loading direction is reversed, neither model can simulate ratcheting rate or the trend reasonably as shown in Fig. 2.10. For the triangular experiment, both models fail to simulate the ratcheting rates in both sequences in an acceptable manner as can be seen in Figs. 11 and 12. The shear stress-strain loops of the triangular experiment are simulated reasonably by both models with small difference in the cyclic hardening features.

2.5. Discussion and Conclusions

Motivated by the novel experimental observation of Aubin et al. (2003a), a set of experiments were conducted on SS304L to explore further the influence of loading

nonproportionality on cyclic and ratcheting responses. In spite of the fact that the loading paths prescribed in the experiments have the same axial mean and equivalent amplitude stresses in the axial-shear space, different axial and shear strain ratcheting responses were obtained from the experiments. The observation of Aubin et al. (2003a) is reiterated in the SS304L experiments that the shearing stress cycle is not as influencing as the axial stress cycle in inducing axial strain ratcheting and the ratcheting rate obtained under the cross experiment is smaller than that in the uniaxial experiment. This phenomenon is attributed to the nonproportionality of the loading paths. Kang, et al. (2002a) demonstrated similar nonproportional ratcheting phenomenon through a different set of experiments. All these observations indicate that low-cycle fatigue analysis and design of structures based on equivalent stress may not represent the actual structural conditions.

This study illustrated several new experimental responses to further demonstrate the influences of non-proportionality on ratcheting responses. The first of these experiments is the two-square loading path (see inset in Fig. 2.7), in which in addition to the axial strain ratcheting, considerable shear strain ratcheting is also observed, even though the shear stress cycle is symmetric. For several of the above experiments a second loading sequence was prescribed to study the effect of prior history on the subsequent ratcheting responses. Different trends in regards to the influence of nonproportional loading on ratcheting responses are observed from the second sequence compare to those in the first sequence. Finally, in the axial stress-shearing strain controlled triangle load path experiment, the axial strain ratcheting started with a high rate and quickly stabilized to a slow rate, a little different rate response than observed in the axial-shear stress-controlled experiments.

Under nonproportional loading paths, the extent of cyclic hardening/softening, and plastic deformation and ratcheting might be influenced by the angle between vectors representing the stress and plastic strain, or their increments. When the angle between these two directions is large, induced plastic strain is small and vice versa. The degree of non-proportionality also influences the amount of cyclic hardening or softening during initial cycles and thus

influences the ratcheting rate during the transient. However, after the transient ratcheting state the nonproportional cyclic hardening may reach its saturation state and may not influence much the steady ratcheting rate. Hence, different steady state ratcheting rates from different nonproportional paths might be the direct influence of degree of non-proportionality itself.

An explanation of different axial strain ratcheting rates from the uniaxial and various non-proportional experiments (Figs. 3-8) might be that in the uniaxial experiment the directions of the mean and amplitude stresses are in the same direction, which is the principal stress and strain direction. Whereas, in the nonproportional experiments the principal direction continuously changes and flip-flop as the shear stress cycle reverses its direction. This explanation can also be made using slip mechanisms. During the uniaxial ratcheting cycle, the majority of the slip planes are at 45^o to the axial mean stress direction, whereas during the shear ratcheting cycle the majority of the slip planes have larger angles than 45^o to the axial mean stress direction and keep changing as the cyclic load reverses. Thus the shear ratcheting cycle has reduced influence on the axial strain ratcheting compared to the uniaxial ratcheting cycle.

This paper critically evaluates two rate-independent plasticity models, modified Chaboche (Chaboche, 1989, 1991, Bari and Hassan, 2002) and multi-mechanism (Taleb, et al., 2006), against the set of experimental responses of SS304L. The Benallal and Marquis (1987) nonproportinoality parameters were incorporated to the modified Chaboche model (Bari and Hassan, 2002) through the kinematic hardening rule parameters γ_i (i = 1, 2, 4), in addition to the classical parameter R (drag resistance). The modified Chaboche model with the added nonproportional features is able to capture the nonproportional ratcheting responses of shear, cross, square and two-square paths quite well (Fig. 2.8a). However, the performance of the multimechanism model in simulating these nonproportional ratcheting responses is not as satisfactory (Fig. 2.8b). Simulations for the two-sequence loading ratcheting responses from uni-cross, shear-uni, square-uni, and forward and reversed two-

square are not reasonable during the second sequence from either model (Figs. 9 and 10). As the second loading sequence starts, the sudden change in the degree of nonproportionality and resulting evolutions in the yield surface and plastic deformation are not represented correctly by either model. Nonproportional modeling features, such as, Tanaka (1994), Kang, et al. (2004) and others need to be studied for such simulations. However, the reasons for deficient ratcheting rate simulation for the strain-controlled triangular path, during both forward and inverse cycles, by these models are not clear.

Simulations of the hysteresis loops under stress-controlled cycles are unsatisfactory from both models. The primary reason for this deficiency is that the recorded hysteresis loops under stress-controlled cycles demonstrated cyclic softening, but the model parameters were calibrated for simulating cyclic hardening. Rate independency of the models might be another reason for the unsatisfactory hysteresis loop simulation because the stress-controlled hysteresis loops show rate dependent features during the initial cycles. Including the strain range dependent cyclic hardening/softening and the rate effect in the modeling may improve loop simulations by both models.

To demonstrate the effectiveness of the Benallal and Marquis (1987) model in simulating the nonproportional ratcheting responses a set of modified Chaboche model simulations were performed without using the nonproportional loading parameters (i.e., $A = 0$ and $g = 0$ in Eqs. 5 to 10) as summarized in Fig. 2.16. Comparison of simulations in Figs. 16a to 8a and 16b to 9a demonstrates that except for the uniaxial and cross ratcheting rate responses in the first loading sequence, all others ratcheting rates are overpredicted if the nonproportional modeling features are not used. It is noted to the readers that the simulations in Figs. 8a and 9a were obtained using the modified Chaboche model by incorporating the Benallal and Marquis nonproportional features. Comparison of Figs. 8a and 16a also demonstrates that the experimental trend of decreasing ratcheting rate with loading path changes from uniaxial to cross to two-square to square to shear is not simulated without the nonproportional modeling features.

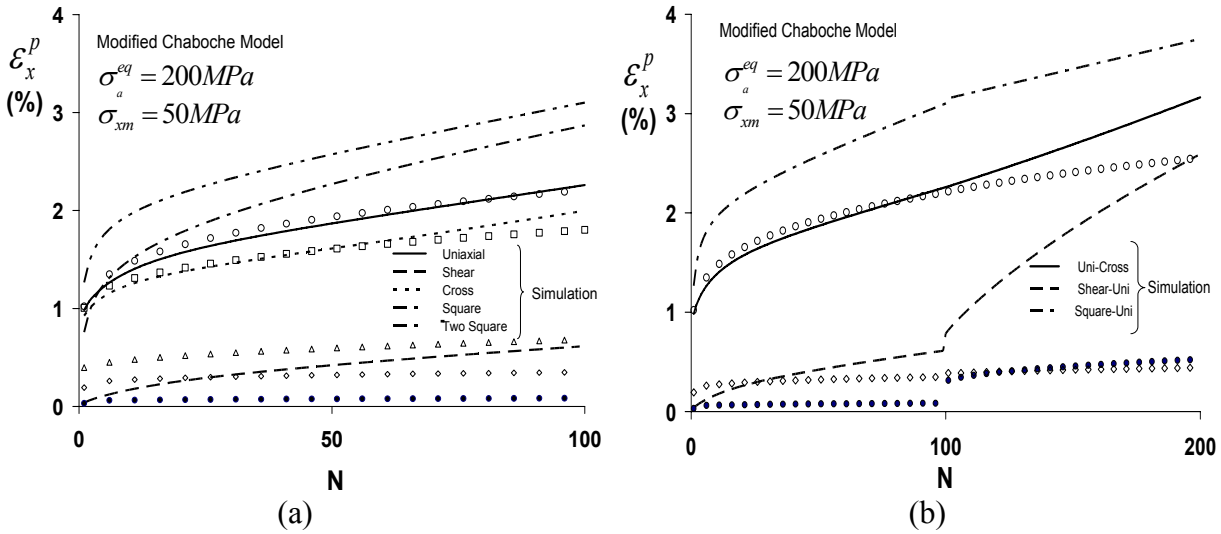

Fig. 2.16. Axial strain ratcheting from stress-controlled experiments and simulations without any nonproportional parameters. (a) Single sequence, and (b) double sequence experiments.

In order to understand the contribution of the kinematic hardening rule parameter γ_i (i = 1, 2, 4) of the modified Chaboche model in simulating the nonproportional ratcheting responses in Figs. 8a and 9a, simulations are performed with nonproportionality effect incorporated in the drag resistance R only (see Eqs. 5 to 7). Such a nonproportional modeling scheme has been proposed by Benallal and Marquis (1987), Tanaka (1994), Kang, et al. (2004), and many others. For these simulations a new set of parameters for the modified Chaboche model was determined. Most of the proportional loading parameters in Table 1 remained the same, except that R^0 changed to 70 MPa, f_R to 1.2. For nonproportional cyclic hardening, R^∞ changed to 105 MPa, d_R to 8.0, and g remained same as 0.9. For γ_i (i = 1, 2, 4), A and g were set to zero in Eqs. 8 to 10. Simulations with these parameters for the single and double sequence experimental responses are shown in Fig. 2.17, where it is observed that the simulated ratcheting rate of each case is reduced compared to the simulations in Fig. 2.16. Such reduction in ratcheting rates is mainly caused by the significant increase in R. The experimental trend of different ratcheting rate with loading path changes from uniaxial to cross to two-square to square to shear, as observed in Fig. 2.8, are not reproduced by modeling nonproportionality through R only.

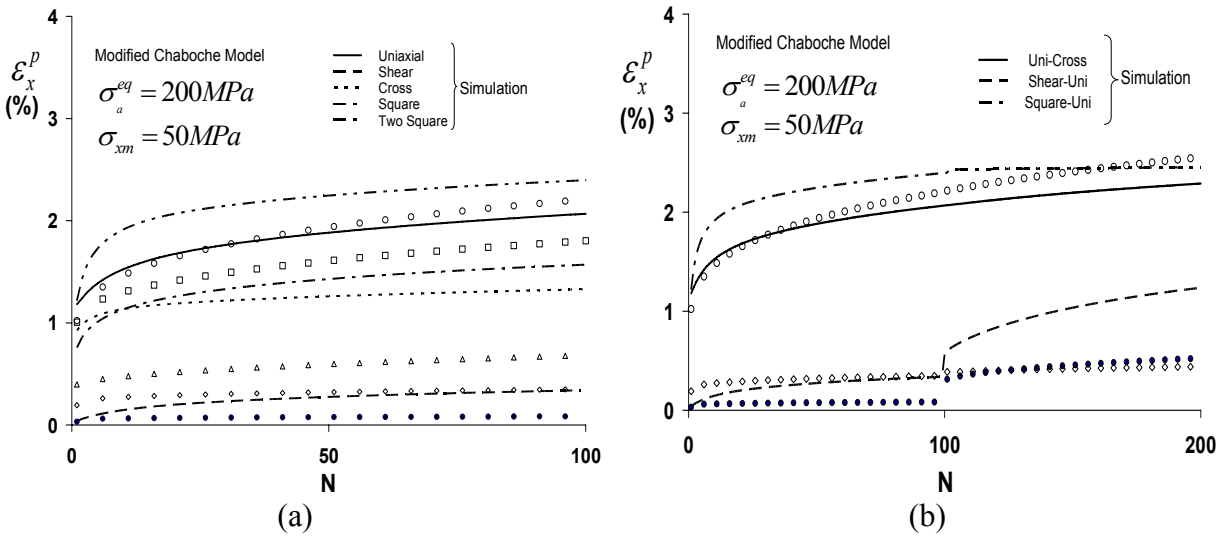

Fig. 2.17. Axial strain ratcheting from experiments and simulations with nonproportional modeling using the isotropic hardening parameter (R) only. (a) Single loading sequence ratcheting, and (b) double loading sequence ratcheting.

Overall, the performance of the modified Chaboche model with loading nonproportionality modeled using both γ_i and R parameters is reasonable in simulating nonproportional ratcheting responses from the single-sequence loading experiments (Fig. 2.8a). However, the performance of the model's ratcheting simulations need to be improved for the double-sequence loading experiments (Figs. 9a and 10) and for the strain-controlled ratcheting experiments (Figs. 11 and 12). Such improvements can be achieved by developing and incorporating models of strain range dependent cyclic hardening/softening, rate-dependence, and finally other nonproportionality parameters, such as, proposed by Tanaka et al. (1985a,b) and Kang, et al. (2004). Aubin et al. (2003a) demonstrated that by incorporating the yield surface distortion (Vincent, et al., 2002, 2004) into modeling very good simulations for the nonproportional ratcheting rates can be obtained. Such a modeling feature along with others mentioned above could be instrumental in achieving a robust model for simulating a broader set of proportional and nonproportional ratcheting responses. Finally, new modeling challenges in simulating nonproportional cyclic and ratcheting responses are demonstrated in this paper. With rate and temperature effects included in the experiments the modeling

challenges would increase several fold as demonstrated by Kang and his coworkers (2004, 2006). Hence, systematic and cooperative efforts around the world are essential for achieving a robust cyclic plasticity model.

Acknowledgements

The authors acknowledge the financial support of the "Région Haute Normandie" and the European Community, through the FEDER program, for acquisition of the equipment used in the experimental study. The experimental program of this study was developed and executed during T. Hassan's visits to INSA de Rouen. The financial support from the NSF Grant (DMR-0408910), INSA de Rouen, and the Department of Civil, Construction and Environmental Engineering at North Carolina State University are gratefully acknowledged. Experimental data provided by Dr. V. Aubin was extremely beneficial for this study.

References

Abdel Karim, M., Ohno, N., 2000. Kinematic Hardening Model Suitable for Ratcheting with Steady-state. Int. J. Plasticity, 16, 225-240.

Aubin, V., Bulthé, A.-L., Degallaix, S., Quaegebeur, P., 2003a. Ratcheting behavior of a duplex stainless steel: characterization and modeling. 9th International Conference on the Mechanical Behavior of Materials, 25-29 May 2003, Genève, Suisse.

Aubin, V., Quaegebeur, P., Degallaix, S., 2003b. Cyclic plasticity of a duplex stainless steel under non-proportional loading, Material Science and Engineering, A346, pp. 208-215.

Bari, S., Hassan, T., 2000. Anatomy of coupled constitutive models for ratchetting simulation, Int. J. Plasticity, 16, 381–409.

Bari, S., Hassan, T., 2001. Kinematic hardening rules in uncoupled modeling for multiaxial ratchetting simulation. Int. J. Plasticity, 17, 885–905.

Bari, S. , Hassan, T., 2002. An advancement in cyclic plasticity modeling for multiaxial ratcheting simulation. Int. J. Plasticity, 18, 873-894.

Benallal, A., Marquis, D., 1987. Constitutive equations for nonproportional cyclic elasto-viscoplasticity. ASME J. Eng. Mater. Tech. 109, 326–336.

Benallal, A., Le Gallo, P., Marquis, D., 1989. An experimental investigation of cyclic hardening of 316 stainless steel and of 2024 aluminum alloy under multiaxial loading, Nucl. Eng. Des. 114 (1989), 345–353.

Benham, P.P., 1960. Axial-Load and Strain-Cycling Fatigue of Copper at Low Endurance. Journal of the Institute of Metals, 89 , 328.

Benham , P.P., 1965. Some Observations on the Cyclic Strain-Induced Creep in Mild Steel at Room Temperature. International Journal of Mechanical Sciences ,7 , 81-86.

Besson, J., Leriche, R., Foerch, R., Cailletaud, G., 1998. Object-oriented programming applied to the finite element method. Part II. Application to material behaviors. Revue Européenne des Éléments Finis 7 5 , 567–588.

Bocher, L., Delobelle, P., Robinet, P., Feaugas, X., 2001. Mechanical and microstructural investigations of an austenitic stainless steel under non-proportional loadings in tension torsion internal and external pressure. Int. J. Plasticity, 17, 1491-1530.

Cailletaud, G., Sai K., 1995. Study of plastic/viscoplastic models with various inelastic mechanisms. Int. J. Plasticity, 11, 991-1005.

Chaboche, J.L., Dang-Van, K., Cordier, G.,1979. Modelization of the strain memory effect on the cyclic hardening of 316 stainless steel. Proceedings of the 5th International Conference on SMiRT, Div. L, Berlin, Germany.

Chaboche, J.L., 1986. Time-Independent Constitutive Theories For Cyclic Plasticity. Int. J. Plasticity, 2, 149-188.

Chaboche, J.L., 1989 . Constitutive equations for cyclic plasticity and cyclic viscoplasticity. Int. J. Plasticity, 5, 247–302.

Chaboche, J.L., 1991. On Some Modifications of Kinematic Hardening to Improve the Description of Ratcheting Effects. Int. J. Plasticity, 7, 661-678.

Chaboche, J.L., 1994. Modelization of ratcheting: evaluation of various approaches. Eur. J. Mech., A/Solids 13, pp. 501-518.

Chen, X., Jiao, R., 2004. Modified kinematic hardening rule for multiaxial ratchetting prediction, Int. J. Plasticity, 20, 871–898.

Coffin, L.F., 1964. The influence of mean stress on the mechanical hysteresis loop shift of 1100 aluminum. J. Basic Engg., 86, 673

Corona, E., Hassan, T., Kyriakides, S. 1996. On the Performance of Kinematic Hardening Rules in Predicting a Class of Biaxial Ratcheting Histories. Int. J. Plasticity, 12, 117-145.

Dafalias, Y.F., Popov, E.P., 1975. A model of nonlinearly hardening materials for complex loading. Acta Mech., 21, 173-192.

Dafalias, Y.F., Popov, E.P., 1976. Plastic internal variables formalism of cyclic plasticity. ASME J. Appl. Mech., 43, 645–650.

Delobelle, P., Robinet, P., Bocher, L., 1995. Experimental study and phenomenological modelization of ratcheting under uniaxial and biaxial loading on an austenitic stainless steel. Int. J. Plasticity, 11, 295-330.

Freudenthal. A.M., Ronay, M., 1966. Second Order Effects in Dissipative Media. In: Proceedings of the Royal Society A , 294 , 14-50.

Hassan, T., Kyriakides, S., 1992. Ratcheting in Cyclic Plasticity, Part I: Uniaxial Behavior. Int. J. Plasticity, 8, 91-116.

Hassan, T., Corona, E., Kyriakides, S., 1992. Ratcheting in Cyclic Plasticity, Part II: Multiaxial Behavior. Int. J. Plasticity, 8, 117-146.

Hassan, T., Kyriakides, S., 1994a. Ratcheting of Cyclically Hardening and Softening Materials, Part I: Uniaxial Behavior. Int. J. Plasticity, 10, 149-184.

Hassan, T., Kyriakides, S., 1994b. Ratcheting of Cyclically Hardening and Softening Materials, Part II: Multiaxial Behavior. Int. J. Plasticity, 10, 185-212.

Haupt, P. and Kamlah, M., 1995. Representation of cyclic hardening and softening properties using continuous variables. Int. J. Plasticity, 11, 267–291.

Jiang, Y., Sehitoglu, H., 1996a. Modeling of cyclic ratcheting plasticity, part I: development of constitutive relations. ASME J. Appl. Mech., 63, 720–725.

Jiang, Y., Sehitoglu, H., 1996b . Modeling of cyclic ratcheting plasticity, part II: comparison of model simulations with experiments. ASME J. Appl. Mech., 63, 726–733.

Jiang, Y., Kurath, P., 1997. Nonproportional cyclic deformation: critical experiments and analytical modeling. Int. J. Plasticity, 13, 743-763.

Jiang, Y., and Zhang, J., 2008. Benchmark experiments and characteristic cyclic plasticity deformation, Int. J. Plasticity, (In press).

Jie, N. and Xu, C., 1991. On the properties of plastic flow of material under nonproportional cyclic loading. Int. J. Solids Structures, 28, pp. 403-412.

Kang, G. Z., Gao, Q., Yang, X.J., Sun, Y.F., 2001. An experimental study on uniaxial and multiaxial strain cyclic characteristics and ratchetting of 316L stainless steel, J. Mater. Sci. Technol., 17, 219–223.

Kang, G.Z., Gao, Q., Cai, L.X., Yang, X.J., Sun, Y.F., 2002a. Experimental study on the uniaxial and nonproportionally multiaxial ratchetting of SS304 stainless steel at room and high temperatures. Nucl. Eng. Des., 216, 13–26.

Kang, G.Z., Gao, Q., Yang, X.J., 2002b. A visco-plastic constitutive model incorporated with cyclic hardening for uniaxial/multiaxial ratchetting of SS304 stainless steel at room temperature, Mech. Mater., 34, 521–531.

Kang, G.Z., Gao, Q., Yang, X.J., 2004. Uniaxial and nonproportional multiaxial ratchetting of SS304 stainless steel at room temperature: Experiments and simulations, Int. J. Non-linear Mech., 39, 843–857.

Kang, G.Z., Li, Y.G., Gao, Q., 2005. Non-proportionally multiaxial ratcheting of cyclic hardening materials at elevated temperatures and its constitutive modeling, Mech. Mater., 37, 1101–1118.

Kang, G.Z., Kan, Q., Zhang, J., and Sun, Y., 2006. Time-dependent ratcheting experiments of SS304 stainless steel. Int. J. Plasticity, 22, pp. 858-894.

Lamba, H.S., Sidebottom, O.M., 1978. Cyclic plasticity for nonproportional paths: Part1 and 2-comparison with predictions of three incremental plasticity models, J. of Engineering materials and tech., 100, 96-111.

Landgraf, R.W., Morrow, J-.D., and Endo, T., 1969. Determination of the cyclic stress-strain curve, Journal of Materials, JMLSA, Vol. 4, pp. 176-188.

Marquis, D., 1979. Etude théorique et vérification expérimentale d'un modèle de plasticité cyclique. Thèse Paris VI .

McDowell, D.L., 1985. A two surface model for transient nonproportional cyclic plasticity. ASME J. Appl. Mech., 52,298-308.

McDowell, D.L., 1987. An evaluation of recent developments in hardening and flow rules for rate-independent, nonproportional cyclic plasticity. ASME J. Appl. Mech. 54, pp. 323–334.

McDowell, D.L., 1995. Stress State Dependence of Cyclic Ratcheting Behavior of Two Rail Steels. Int. J. Plasticity, 11, 397- 421.

Moosbrugger, J.C., 1991. Some developments in the characterization of material hardening and rate sensitivity for cyclic viscoplasticity models. Int. J. Plasticity, 7, 405-431.

Moosbrugger, J.C., 1993. Experimental parameter estimation for nonproportional cyclic viscoplasticity: nonlinear kinematic hardening rules for two waspaloy microstructures at 650° C. Int. J. Plasticity, 9, 345-373.

Moyar, G.J., Sinclair , G.M., 1963. Cyclic Strain Accumulation Under Complex Multiaxial Loading. Proceedings of the Joint International Conference on Creep, Institution of Mechanical Engineers, London, 2–47.

Ohno, N., 1990. Recent topics in constitutive modeling of cyclic plasticity and viscoplasticity, Appl. Mech. Rev., 43, 283-295.

Ohno, N., Wang, J.D., 1993. Kinematic hardening rules with critical state of dynamic recovery, part I: formulation and basic features for ratcheting behavior. Int. J. Plasticity, 9, 375-390.

Ohno, N., 1997. Recent progress in constitutive modeling for ratchetting. Mater. Sci. Res. Int., 3,1-9.

Portier, L., Calloch, S., Marquis, D., Geyer, P., 2000. Ratchetting under tension-torsion loadings: Experiments and modelling. Int. J. Plasticity, 16, 303-335.

Rahman, S.M., Hassan, T., Ranji Ranjithan, S., 2005. Automated parameter determination of advanced constitutive models. Proceeding of the ASME Pressure Vessels Piping Conference. PVP, 2, 261-272.

Rahman, S.M., Hassan, T., Corona, E., 2008, Evaluation of cyclic plasticity models in ratcheting simulations of straight pipes under cyclic bending and steady internal pressure. Int. J. of Plasticity, (In-press).

Ruggles, M.D., Krempl, E., 1989. The influence of test temperature on the ratcheting behavior of type SS304 stainless steel. ASME J. Eng. Mater. Technol., 111 ,378-387.

Ruggles, M.D., Krempl, E., 1990. The interaction of cyclic hardening and ratcheting of AISI type 304 stainless steel at room temperature: I, Experiments. J. Mech. Phys. Solids, 38, 575-585.

Ruiz, C., 1967. High-strain fatigue of stainless-steel cylinders: experimental results and their application to pressure-vessel design. Journal of Strain Analysis, 2 , 290.

Sai, K., Cailletaud, G., 2007. Multi-mechanism models for the description of ratchetting: Effect of the scale transition rule and of the coupling between hardening variables. Int. J. Plasticity, 23, 1589.

Suresh, S., 1998. Fatigue of Materials, 2nd ed., Cambridge.

Seyed-Ranjbari, M., 1986. Further development, multiaxial formulation, and implementation of the bounding surface plasticity model for metals, PhD dissertation, University of California, Davis.

Taleb, L., Cailletaud, G., Blaj, L., 2006. Numerical simulation of complex ratcheting tests with a multi-mechanism model type. Int. J. Plasticity, 22, 724-753.

Taleb, L., Hauet, A., 2008. Multiscale Experimental Investigations about the Cyclic Behavior of the 304L SS. Submitted to Int. J. Plasticity

Tanaka, E., Murukami, S., Ooka, M., 1985a. Effect of plastic strain amplitudes on non-proportional cyclic plasticity. Acta Mech. ,57, 167-182.

Tanaka, E., Murukami, S. , Ooka, M. 1985b. Effect of strain path shapes on non-proportional cyclic plasticity. J. Mech. Phys. Solids, 33, 559-575.

Tanaka, E., 1994 . A nonproportionality parameter and a cyclic viscoplastic constitutive model taking into account amplitude dependences and memory effects of isotropic hardening. Eur. J. Mech., A/Solids, 13, 155–173.

Vincent, L., Calloch, S., Kurtyka, T., Marquis, D., 2002. An improvement of multiaxial ratcheting modeling via yield surface distortion. J. Eng. Mater. Technol., 124, 402-411.

Vincent, L., Calloch, S., Marquis, D., 2004. A general cyclic plasticity model taking into account yield surface distortion for multiaxial ratcheting. Int. J. Plasticity, 20, 1817-1850.

Voyiadjis, G.Z., Basuroychowdhury, I.N., 1998. A plasticity model for multiaxial cyclic loading and ratchetting. Acta Mech. ,126, 19–35.

Wolff, M., Taleb, L., 2008. Consistency of two multi-mechanism models in isothermal plasticity. Int. J. Plasticity, (In-press).

Xia, Z., Ellyin, F., 1997. A constitutive model with capability to simulate complex multiaxial ratcheting behavior of materials. Int. J. Plasticity,13, 127-142.

Yoshida, F., Tajima, N., Ikegami, K., Shiratori, E., 1978. Plastic theory of the mechanical ratcheting. Bulletin of the JSME., 21, 389-397.

Yoshida, F., Kondo, J., Kikuchi, Y., 1988. Visco-plastic behavior of stainless steel SUS304 under cyclic loading at room temperature. Trans. JSME, Series A ,54, 1151-1160.

Yoshida, F., 1995. Ratcheting behavior of 304 stainless steel at 650 °C under multiaxial strain-controlled and uniaxailly/multiaxially stress-controlled conditions, Eur. J. Mech. A/Solids ,14, 97–117.

Yoshida, F., 2000. A constitutive model of cyclic plasticity. Int. J. Plasticity, 16, 359-380.

CHAPTER 3
Macro versus Micro Scale Constitutive Models in Simulating Proportional and Nonproportional Cyclic and Ratcheting Responses of Stainless Steel 304

Abstract

A recent study by Hassan et al. (2008) demonstrated that some of the nonproportional ratcheting responses under stress-controlled loading histories cannot be simulated reasonably by two recent cyclic plasticity models. Two major drawbacks of the models identified were: i) the stainless steel 304 demonstrated cyclic hardening under strain-controlled loading whereas cyclic softening under stress-controlled loading, which depends on the strain-range and which the existing models cannot describe; ii) the change in biaxial ratcheting responses due to the change in the degree of nonproportionality were not simulated well by the models. Motivated by these findings, two modified cyclic plasticity models are evaluated in predicting a broad set of cyclic and ratcheting response of stainless steel 304. The experimental responses used in evaluating the modified models included both proportional (uniaxial) and nonproportional (biaxial) loading responses from Hassan and Kyriakides (1994a, b) and Hassan et al. (2008). The first model studied is a macro scale, phenomenological, constitutive model originally proposed by Chaboche et al. (1979). This model was systematically modified for incorporating strain-range dependent cyclic hardening-softening, and proportional and nonproportional loading memory parameters. The second model evaluated is a polycrystalline model originally proposed by Cailletaud (1992) based on crystalline slip mechanisms. These two models are scrutinized against simulating hysteresis loop shape, cyclic hardening-softening, cross-effect, cyclic relaxation, subsequent cyclic softening and finally a broad set of ratcheting responses under uniaxial and biaxial loading histories. The modeling features which improved simulations for these responses are

elaborated in the paper. In addition, a novel technique for simulating both the monotonic and cyclic responses with one set of model parameters is developed and validated.

Keywords: cyclic plasticity, cyclic hardening, cyclic softening, cyclic relaxation, nonproportional effects, cross hardening, ratcheting, nonlinear kinematic hardening, polycrystalline models.

3.1. Introduction

Low-cycle fatigue life computation for analysis and design of safety critical and expensive structures requires constitutive models that can reasonably describe stress–strain responses of materials under a broad set of loading histories. Towards achieving such a constitutive model an earlier study by Hassan et al. (2008) evaluated two different types of constitutive models in simulating a systematic set of stress-strain responses of stainless steel (SS) 304. The loading histories prescribed in developing these stress-strain responses included various nonproportional, stress-controlled loading paths with the same mean and amplitude stresses. These responses demonstrated the significant influence of the degree of nonproportionality of loading histories on the strain ratcheting responses which was originally demonstrated by Aubin et al. (2003) for duplex stainless steel.

Attempts were made to simulate these responses by a nonlinear kinematic hardening model originally proposed by Chaboche et al. (1979), which was modified based on Marquis (1979), Chaboche (1989, 1991), Bari and Hassan (2002) and Benallal and Marquis (1987), and a multimechanism model developed by Calilletaud and Saï (1995) and recently modified by Taleb et al. (2006) and Saï and Cailletaud (2007). The model evaluation study of Hassan et al. (2008) demonstrated that further modifications of these two models are needed towards developing a robust constitutive model. The nonlinear kinematic hardening model, however, demonstrated promise for its capability in fatigue life computation. This model simulated the single-sequence nonproportional ratcheting responses quite well when both isotropic and kinematic hardening rule parameters were used to describe the effect of loading nonproportionality on cyclic hardening and ratcheting (Hassan et al., 2008). However, they

demonstrated that the model fails to simulate the ratcheting responses of the second sequence in the double-sequence nonproportional loading experiments. Sudden change in loading nonproportionality at the start of the second sequence was not represented well by the Benallal and Marquis (1987) nonproportional parameter. This drawback of the model was pointed out as the lack of memory features in the model (Tanaka, 1994; Jiang and Kurath, 1997). Other drawbacks of the modified nonlinear kinematic hardening model identified were the lack of strain-range dependence and cross-hardening effect (Hassan et al., 2008).

After the first demonstration of "additional cyclic hardening" response of OFHC copper under the 90-degree out-of-phase nonproportional loading history by Lamba and Sidebottom (1978), this phenomenon has been extensively studied on different materials and under various loading paths (Kanazawa et al., 1979; McDowell, 1985; Krempl and Lu, 1984; Ohashi et al., 1985; Tanaka et al., 1985a; Benallal, et al., 1989 and others). It was demonstrated that the additional cyclic hardening is a function of the degree of nonproportionality and strain amplitude. The phenomenon of "cross-hardening" induced by the sudden change in the direction of loading path, "subsequent cyclic softening" induced by the reduction in the degree of nonproportionality and/or the strain amplitude are other important low-cycle fatigue phenomena (Krempl and Lu, 1984; Tanaka et al., 1985b; Benallal and Marquis, 1987; Zhang and Jiang, 2008; and others). Subsequent cyclic softening can also be observed under uniaxial or proportional loading because of the reduction in strain amplitude (Nouailhas et al., 1985; Zhang and Jiang, 2008) or prior large plastic strain excursion (Nouailhas et al., 1985).

The experimental studies mentioned above were conducted under strain-controlled loading histories. The effect of nonproportionality under stress-controlled histories has been demonstrated by Ohashi et al. (1985), Hassan et al. (1992, 2008), Hassan and Kyriakides (1994b), Aubin et al. (2003), and Kang et al. (2004, 2006). Under stress-controlled loading histories the influence of nonproportionality can be observed on the ratcheting rate (Aubin et al., 2003; Hassan et al., 2008) and the shape and size changes of hysteresis loops (Hassan and

Kyriakides, 1994b). An unexpected phenomenon observed for SS304 is that the hysteresis loop gets thinner only during the initial few cycles, as expected for a cyclic hardening material. However, in the subsequent cycles the hysteresis loop gets fatter, a characteristic of the cyclically softening material (Hassan and Kyriakides, 1994b; Hassan et al., 2008). This observation might be related to the strain-range dependent cyclic hardening-softening first demonstrated by Landgraf et al. (1969) for several materials and later by Nouailhas et al. (1985) for quenched SS316. For example, it can be seen in Nouailhas et al. (1985) that for strain amplitudes smaller than 0.3% the material shows cyclic softening, whereas for strain amplitudes larger than 0.3% the material shows cyclic hardening (see Fig. 2.1 in the reference). This feature is yet to be incorporated in any constitutive model.

For incorporating the effects of nonproportionality into constitutive modeling various measures were proposed (McDowell, 1985, 1987; Syed-Ranjbari, 1986; Benallal and Marquis, 1987; Tanaka and Okuchi, 1988; Ellyin and Xia, 1989; Doong and Socie, 1990; Tanaka, 1994, Haupt and Kamlah, 1995; Mayama, et al., 2004, and others). Ohno (1990) provided a brief description of many of these nonproportional measures and their performance in simulating nonproportional effects. Of all the measures, the Benallal and Marquis (1987) instantaneous measure or its modified version is widely being used because of its simplicity and easy implementation (McDowell, 1992; Moosbrugger, 1993; Hassan and Kyriakides, 1994b; Delobelle et al., 1995; Haupt and Kamlah, 1995; Kang et al., 2004, 2005; Hassan et al., 2008 and others). The works of Hassan and Kyriakides (1994b), Delobelle et al. (1995), Kang et al. (2004, 2005) and Hassan et al. (2008) also evaluated the performance of Benallal and Marquis (1987) in simulating various nonproportional "ratcheting" responses. Hassan et al. (2008) demonstrated that if the degree of nonproportionality during a prescribed biaxial loading history does not change, the Benallal and Marquis (1987) model can simulate the biaxial ratcheting responses for a wide variety of nonproportional loading paths quite well. However, as mentioned earlier, its simulation of the multiaxial ratcheting responses degrades as the degree of nonproportionality in a loading cycle changes abruptly.

Benallal and Marquis's (1987) measure of nonproportionality is instantaneous and lacks memory features, which may be the reason for its deficiency in simulating double-sequence nonproportional ratcheting responses of Hassan et al. (2008).

The nonproportionality measure of Tanaka and Okuchi (1988) and Tanaka (1994) yielded very good simulations of additional cyclic hardening and erasure of memory (Tanaka, 1994; Jiang and Kurath, 1997; Zhang and Jiang, 2008), cross-hardening (Zhang and Jiang, 2008) and ratcheting (Portier et al., 2000). This nonproportionality measure is based on a fourth order tensor which was developed to describe the dislocation structures of the cross-hardening process (Tanaka, 1994). The success of this nonproportional parameter lies on the fact that the components of the fourth order tensor are memory parameters (Jiang and Kurath, 1997). Another method attempted successfully by Nouailhas et al. (1985) for describing additional cyclic hardening and cross-hardening effects of nonproportional loading is the anisotropic yield surface evolution of Baltov and Sawczuk (1965). This method used the observation that the yield surface expands more along the direction perpendicular to the plastic flow direction, which is attributed to be the reason of the manifestation of cross-hardening. This cross-hardening effect is present continuously during the 90-degree out-of-phase loading cycle, resulting in the additional cyclic hardening observed experimentally. Such an anisotropic yield surface evolution also has the potential of improving the multiaxial ratcheting response simulations (Mayama, et al., 2004). Before evaluating such a complex modeling feature, this study committed to incorporating the Tanaka (1994) nonproportional parameter into the modified Chaboche model for enhancing its nonproportional cyclic and ratcheting response simulation capabilities.

Once the parameter(s) for measuring the degree of nonproportionality is defined, the next important step is to decide which variables of a constitutive model are to be influenced by the nonproportional parameter(s) in simulating experimental responses. The initial modeling approaches incorporated the nonproportional parameter(s) for influencing the isotropic hardening (yield surface size change) only (Benallal and Marquis, 1987; Tanaka and Okuchi,

1988; Krempl and Lu, 1984; Tanaka, 1994 and others). Hysteresis curve shape calculated by this method does not represent the experimental curve shape well, and consequently the simulation of ratcheting responses also get degraded (Hassan et al., 2008). McDowell (1987) and Ellyin and Xia (1989) suggested that for simulating the hysteresis curve and its hardening with progressive cycles accurately, evolutions of both the yield surface size and plastic modulus should be included in the modeling (see also Jiang and Zhang, 2008). In case of the nonlinear kinematic hardening model, the cyclic hardening/softening under both the proportional and nonproportional loading can be modeled through simultaneous evolutions of the isotropic and kinematic hardening rule variables (Marquis, 1979; Chaboche, 1989; Moosbrugger, 1991, 1993; Haupt and Kamlah, 1995; Portier et al., 2000; Kang et al., 2004; Hassan et al., 2008) and in case of the two surface model through isotropic hardening of both the yield and bounding or limit surfaces (Seyed-Ranjbari, 1986; McDowell, 1985; Hassan and Kyriakides, 1994b; and others).

This study incorporates several proportional and nonproportional loading modeling features into the modified Chaboche model (Bari and Hassan, 2002; Hassan et al., 2008) for enhancing its simulation capability for a broader range of cyclic plasticity responses. The modeling features included are strain-range dependent cyclic hardening/softening, subsequent cyclic softening, cross-hardening and memory features of nonproportional loading. First, the nonproportional parameter of Tanaka (1994) is incorporated into the modified Chaboche model to improve its simulation of the nonproportional ratcheting responses of SS304 in Hassan et al. (2008). Following that, the enhanced Chaboche model is evaluated against a systematic set of proportional and nonproportional, cyclic and ratcheting responses from Hassan and Kyriakides (1994b). In order to determine the current state-of-the-art of modeling, a polycrystalline model (Cailletaud, 1992, Cailletaud and Saï, 2008) is also evaluated concurrently to the modified Chaboche model. Note that the polycrystalline model studied here was also scrutinized against simulating many cyclic and ratcheting responses as can be found in Cailletaud and Saï (2008). In fact, Cailletaud and Saï (2008) and

Bari and Hassan (2002) simulated the same set of ratcheting responses from Hassan and Kyriakides (1992) and Hassan et al. (1992). Such a comparative study of macro and micro scale constitutive models would reveal the strengths and weaknesses of these models and thereby facilitate modelers to identify robust modeling features and users to choose a feasible model for addressing the problem at hand.

As already indicated, a broad set of uniaxial and biaxial, cyclic hardening, cyclic relaxation and ratcheting responses of SS304 from Hassan and Kyriakides (1994a, b) is used for evaluating the models in this paper. The biaxial ratcheting responses include two sets of experiments: the first set involves steady internal pressure and axial strain-controlled cycle, which demonstrates ratcheting of the circumferential strain only; the second set involves steady internal pressure and axial stress-controlled cycle, which demonstrates simultaneous ratcheting of both the axial and circumferential strains. Hassan and Kyriakides (1994a, b) with a modified Dafalias-Popov model in combination with the Benallal and Marquis (1987) nonproportional parameter simulated most of the cyclic and ratcheting responses reasonably, except the stress-controlled, biaxial ratcheting responses. A reason of the deficient simulation was identified as the poor simulation of the hysteresis curve shape, which resulted from the poor simulation of the nonproportional cyclic hardening/softening under stress-controlled loading. No other model yet demonstrated successful simulation of such a broad set of cyclic and ratcheting responses under proportional and nonproportional loading. This study made an effort to address this challenge. Finally, it has been shown by Hassan et al. (2008) that when the parameter set of a model is determined using a hysteresis curve, the simulation of the monotonic curve suffers. Based on the experimental observation of yield surface size change from monotonic to first hysteresis curve, a new technique of simulating both the monotonic and hysteresis curves using the same set of model parameters is proposed and validated in this study.

The modern constitutive plasticity models, both macro and micro scale, are complex and their parameter determination is a difficult task for the model users. This is one of the reasons

that the modern constitutive models are not widely used in finite element simulations of complex fatigue problems. Hence, a philosophy for developing constitutive models should be such that an automated parameter-determination scheme that uses specific experimental responses can be developed. Thus, the parameter determination would be a black box to the model users and modern cyclic plasticity models may gain popularity in solving complex simulation problems more accurately. The model development in this study is based on such a philosophy towards gradually increasing the popularity of modern plasticity models. Hence, the models studied in this paper are presented below in a systematic manner along with a parameter determination scheme.

3.2. Modified Chaboche model

This paper evaluates the rate and temperature independent modeling features of the modified Chaboche model. The study of simulating rate-dependent, cyclic and ratcheting responses by this model is near completion and the results will be presented in a forthcoming paper (Krishna and Hassan, 2008). The primary features of the rate-independent modified Chaboche model (Chaboche et al., 1979; Chaboche, 1989, 1991; Bari and Hassan, 2002; Hassan et al., 2008) evaluated are presented below.

3.2.1 Yield criterion and isotropic hardening rule

The yield criterion used is:

$$f(\underline{\sigma}-\underline{\alpha})=\left[\frac{3}{2}\left(\underline{s}-\underline{a}\right)\cdot\left(\underline{s}-\underline{a}\right)\right]^{1/2}-\sigma_0-R(p,q)=0\,, \tag{1}$$

where, $\underline{\sigma}$ is the stress tensor, $\underline{\alpha}$ is the current center of the yield surface in the total stress space, $\underline{s}$ is the deviatoric stress tensor, $\underline{a}$ is the current yield surface center in the deviatoric space, σ_0 is the initial size of the yield surface, and R is the drag resistance (initial value of R is zero for virgin material) which represents the isotropic hardening variable as a function of

the accumulated plastic strain p and the size of the plastic strain surface q (see later for discussions on these parameters).

As stated in section 1, this paper attempts to simulate the monotonic and subsequent cyclic responses using one set of parameters. If only the monotonic curve-fitted parameters are used the hysteresis curve simulation suffers as shown in Fig. 3.1a. On the other hand, if only the hysteresis curve-fitted parameters are used the monotonic curve simulation suffers as shown in Fig. 3.1b. As the evolution of some of the modified Chaboche model parameters is dependent on the calculated plastic strains, it is important to simulate both curve shapes as accurately as possible. This is why Hassan et al. (2008) simulated these curves using two sets of model parameters. Such a scheme is imperative when the shapes of the monotonic curve are significantly different than that of the hysteresis curve, or the monotonic curve includes a yield plateau like the mild steel. However, when the shapes of the monotonic and hysteresis curves are not much different (e.g. semi-Masing material; see Jiang and Zhang, 2008), the same set of model parameters can be used for simulating both the curves through a simple extension of the Chaboche et al. (1979) isotropic hardening formulation as presented below.

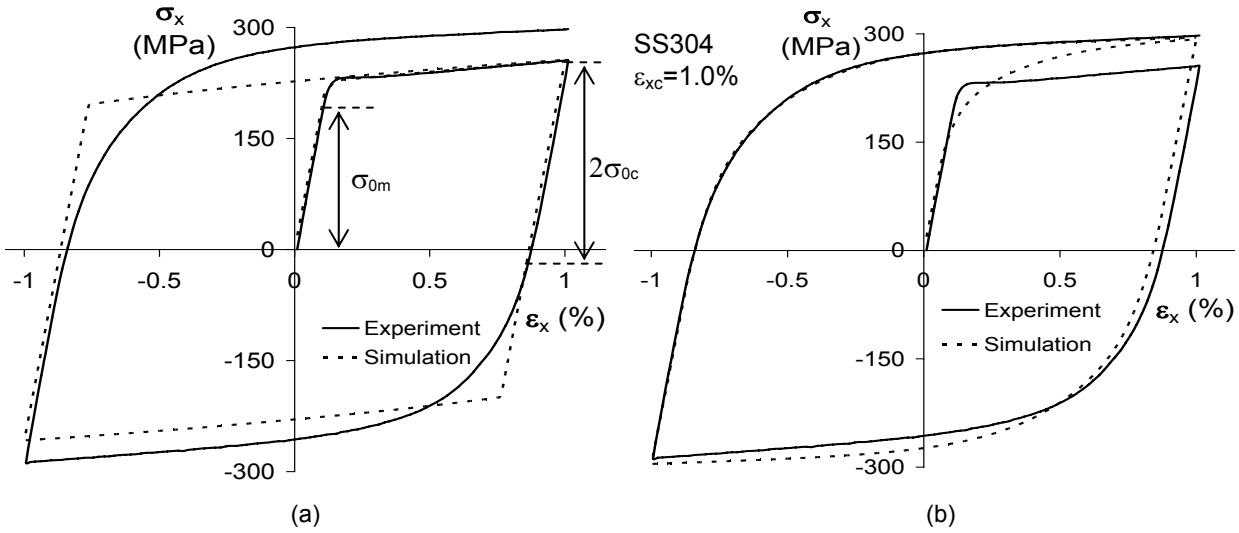

Fig. 3.1. Comparsion of the experimental (Hassan and Kyriakides, 1994a) and simulated responses of the monotonic and 1st hysteresis loop. (a) simulation using the monotonic curve fitted parameters, and (b) simulation using the hysteresis curve fitted parameters.

One of the reasons for different shapes of the monotonic and cyclic curves is that the yield stress under monotonic loading (σ_{0m}) is usually larger than that under cyclic loading (σ_{0c}) as shown in Fig.1a. Prestrain from manufacturing processes may induce such different yield stresses and thus different shapes of the two curves. One way to accommodate the yield surface size and curve shape evolution from monotonic to the first reversal is to start with the monotonic yield surface and subsequently reduce its size quickly through a softening term (2nd term) added to the isotropic hardening rule of Chaboche et al. (1979) (borrowing the approach of the polycrystalline model introduced later, see Eq. 13):

$$dR = D_R\left[R^{AS}(q) - R\right]dp + D_{Rs}\left[R^s - R\right]dp \tag{2}$$

$$R^{AS}(q) = A\left(R^{\infty}(q) - R^0(q)\right) + R^0(q) \tag{2a}$$

$$R^0(q) = a_{1R}\left(1 - e^{-b_{1R}(q - c_{1R})}\right) \tag{2b}$$

$$R^{\infty}(q) = k_R\left(R^0(q)\right) \tag{2c}$$

where, $R^{AS}(q)$ is the saturated value of the drag resistance R which evolves based on the rate constant D_R; R^s is the amount of cyclic softening during the monotonic response, and D_{Rs} determines the rate of softening. The evolution of $R^{AS}(q)$ in Eq. 2a is defined according to Tanaka (1994) as a function of the nonproportionality parameter A (discussed later in section 2.5), the maximum yield surface evolution R^{∞} obtained from a 90-degree out-of-phase strain-controlled experiment, the maximum yield surface evolution R^0 obtained from a proportional strain-controlled experiment and the size of the plastic strain surface q (discussed later in section 2.4). The modeling scheme in Eq. 2, which uses the same set of parameters for simulating both the monotonic and cyclic curves works reasonably well as demonstrated in section 4.

3.2.2 Additive strain decomposition, elastic and flow rules

Following the classical plasticity approach:

$$d\underline{\varepsilon} = d\underline{\varepsilon}^e + d\underline{\varepsilon}^p, \tag{3}$$

$$d\underline{\varepsilon}^e = \frac{1+\nu}{E} d\underline{\sigma} - \frac{\nu}{E} tr(d\underline{\sigma})\underline{I}, \tag{3a}$$

$$d\varepsilon^p = d\lambda \frac{\partial f}{\partial \sigma} = \frac{3}{2} dp \frac{\underline{s} - \underline{\mathrm{a}}}{\sigma_0 + R}, \tag{3b}$$

where, $d\underline{\varepsilon}^e$ is the incremental elastic strain tensor, $d\underline{\varepsilon}^p$ is the incremental plastic strain tensor, E is elastic modulus and ν the Poisson's ratio, and $d\lambda$ is a plastic multiplier determined by the consistency condition, and dp is the magnitude of the plastic strain increment given by $dp = \left| d\underline{\varepsilon}^p \right| = \left[\tfrac{2}{3} d\underline{\varepsilon}^p \bullet d\underline{\varepsilon}^p \right]^{1/2}$.

3.2.3 Nonlinear kinematic hardening rule

The nonlinear kinematic hardening rule of a coupled model (Bari and Hassan, 2000) is the most important feature because of its influence on the evolutions of yield criterion, cyclic hardening/softening and ratcheting responses. This study uses the kinematic hardening rule obtained by superposing four different Armstrong-Frederick type rules (Armstrong and Frederick, 1966, Chaboche, 1989, 1991, Bari and Hassan, 2002) in the following form:

$$d\underline{a} = \sum_{i=1}^{4} d\underline{a}_i, \tag{4}$$

$$d\underline{a}_i = \tfrac{2}{3} C_i d\underline{\varepsilon}^p - \gamma_i(q)\left\{\underline{a}_i \delta'(q) + \left(1 - \delta'(q)\right)(\underline{a}_i \bullet \underline{n})\underline{n}\right\} dp, \qquad \text{for } i = 1, 2, 3 \tag{4a}$$

$$d\underline{a}_i = \tfrac{2}{3} C_i d\underline{\varepsilon}^p - \gamma_i(q)\left\{\underline{a}_i \delta'(q) + \left(1 - \delta'(q)\right)(\underline{a}_i \bullet \underline{n})\underline{n}\right\} \left\langle 1 - \frac{\overline{a}_4}{f(\underline{a}_i)} \right\rangle dp, \qquad \text{for } i = 4 \tag{4b}$$

$$d\gamma_i = D_{\gamma i}\left[\gamma_i^{AS}(q) - \gamma_i\right] dp, \qquad \text{for } i = 1, 2 \text{ and } 4 \tag{4c}$$

$$\gamma_i^{AS}(q) = A\left(\gamma_i^{\infty}(q) - \gamma_i^{0}(q)\right) + \gamma_i^{0}(q), \tag{4d}$$

$$\gamma_i^{0}(q) = a_{\gamma i} + b_{\gamma i} e^{-c_{\gamma i} q}, \qquad \text{for } i = 1, 2 \text{ and } 4 \tag{4e}$$

$$\gamma_i^{\infty}(q) = k_{\gamma_i}\left(\gamma_i^{0}(q)\right), \qquad \text{for } i = 1, 2 \text{ and } 4 \tag{4f}$$

$$d\delta' = D_{\delta'}\left[\delta'^{\infty}(q) - \delta'\right] dp, \tag{4g}$$

$$\delta'^{\infty}(q) = a_{1\delta}\left(1 - e^{-b_{1\delta}q}\right), \tag{4h}$$

where, $\underline{n} = \sqrt{\frac{3}{2}}\frac{\underline{s} - \underline{a}}{\sigma_0 + R}$,

C_1-C_4, γ_1-γ_4, δ' and $\overline{a}_4$ are the kinematic hardening rule parameters (Bari and Hassan, 2002). Note in Eq. 4 that the modulus parameters C_i (i=1 to 4) and γ_3 are kept constants, whereas the parameters γ_i (i = 1, 2, and 4) evolve according to Eqs. 4c-f. In these equations, γ_i^{∞} and γ_i^{0} are the maximum values of γ_i for 90^o out-of-phase and axial strain-controlled responses, respectively, for the current plastic strain surface size q. The parameter γ_3 is kept constant (not a function of q) because this parameter influences only the ratcheting rate (Bari and Hassan, 2000 and Rahman et al., 2008) and does not influence the hysteresis loop shape.

This kinematic hardening rule in Eq. 4 was achieved through several generations of evolution over the last three decades (Chaboche et al., 1979; Burlet and Cailletaud, 1987; Chaboche, 1989, 1991, 2008; Delobelle et al., 1995; Bari and Hassan, 2002; Hassan et al., 2008). The fundamental basis of the decomposition of kinematic hardening rule into four different rules was demonstrated to be the mechanisms of material hardening at different length scales, ranging from dislocation substructures to grain boundaries or clusters of microtexture (McDowell, 2000).

As mentioned in the introduction, simulation of cyclic hardening through the isotropic hardening rule only (Chaboche et al, 1979; Chaboche, 1986; Benallal and Marquis, 1987; Tanaka, 1994, Jiang and Sehitoglu, 1996a, b, Kang et al., 2002a, b) can simulate the peak stresses very well, but failed to describe the hysteresis curve shapes reasonably. This is demonstrated in Fig. 3.2, where Fig. 3.2a shows the hysteresis loops recorded from a 1% strain-controlled experiment (Hassan and Kyriakides, 1994a) and Fig. 3.2b shows the simulation by the modified Chaboche model with the evolution of isotropic hardening parameters only according to Eq. 2, while keeping the kinematic hardening parameters C's

and γ's in Eq. 4a-b unchanged. Seemingly the differences between the two responses in Fig. 3.2 are small. However, such difference in hysteresis curve shape has a pronounced effect on the ratcheting response simulations (compare Figs. 8a to 17a and 9a to 17b in Hassan et al., 2008).

In the simulations in Fig. 3.2b, it can be observed that the hysteresis curves are mostly shifting, upward or downward, with cycles without much change in the shape. That means the plastic modulus in the simulation is not changing as observed in the experimental response (Fig. 3.2a). Moreover, if the yield surface size (linear elastic range) evolution from the experimental hysteresis curves in Fig. 3.2a is plotted as a function of the number of cycles (not shown), not much change in the yield surface size is observed for this SS304. This observation indicates that the cyclic hardening in Fig. 3.2a is mostly manifested by the increase in the plastic modulus. Hence, including this evolution in addition to the isotropic hardening would improve the hysteresis curve simulation significantly as indicated by McDowell (1987) and Ellyn and Xia (1989) (see section 4 for improved simulations). Change in the plastic modulus can be obtained through evolutions of γ_i and/or C_i in the kinematic hardening rule (Eq. 4), which in turn results in cyclic hardening or softening (Marquis, 1979; Chaboche, 1989; Haupt and Kamlah, 1995; Portier et al., 2000; Kang et al., 2003; Hassan et al., 2008).

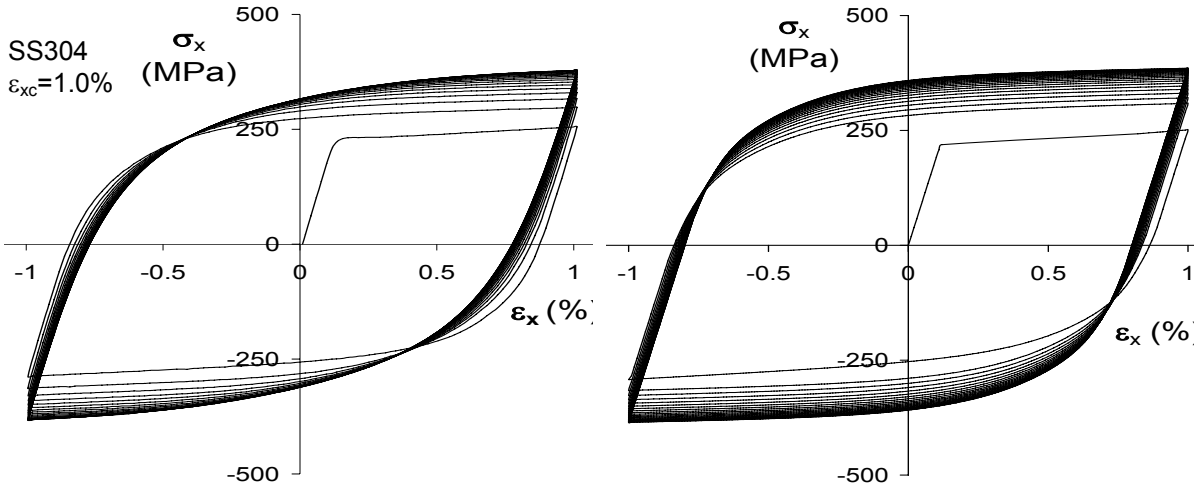

(a) Hysteresis loops from experiment (b) Modified Chaboche model simulation

Fig. 3.2 (a) Hysteresis loops from an axial, strain-controlled experiment (Hassan and Kyriakides, 1994a), and (b) simulated loops by the modified Chaboche model using only the isotropic hardening rule for representing cyclic hardening (monotonic and cyclic curves are simulated by two sets of parameters according to Hassan et al., 2008).

The cyclic hardening/softening in this study is modeled through the simultaneous evolution of both the isotropic hardening parameter R in Eq. 2 and the kinematic hardening parameter γ_i (i=1, 2 and 4) in Eq. 4. As indicated earlier, kinematic hardening rule variables C_i also can be evolved for simulating cyclic hardening/softening (Moosbrugger, 1991, 1993). However, if the initial plastic moduli C_i (i = 1 to 4) are kept constant the sacrifice in the quality of simulation is unnoticeable but the number of parameters reduce by sixteen (Hassan et al., 2008). Hence, the evolution of C_i is not included in this study (see Krishna and Hassan, 2008 for more details on this aspect).

The multiaxial ratcheting parameter δ' is a plastic strain range, q, dependent parameter and is also a function of the accumulated plastic strain, p (Chen and Jiao, 2004), as shown in Eqs. 4g-h, where δ'^{∞} is the saturated value of δ' which has an initial value of δ'_0. If the ratcheting rate in Fig. 3.3, obtained by plotting the maximum circumferential strain in each cycle from an experiment under axial strain-controlled cycle and steady internal pressure (see

Hassan and Kyriakides, 1994b for details) is analyzed, it is observed that the rate of ratcheting starts with a large value which gradually decreases towards a stable rate with progressive cycle. In a simulation with the modified Chaboche model, if the value of δ' is set constant to 0.20, the rate of ratcheting of the initial cycles is matched well but the stable rate is significantly overpredicted (see Fig. 3.3). Whereas, with δ' set to 0.005 the initial rate of ratcheting is underpredicted, but stable rate is simulated well. If $D_{\delta'}$ and δ'^{∞} in Eq. 4g are determined such that the values of δ' starts off as 0.20 and gradually decreases to 0.005, the biaxial rate of ratcheting can be simulated nicely as shown in Fig. 3.3. This indicates that in order to include the plastic strain range effect on the simulated biaxial ratcheting rate the constants of the function $\delta'^{\infty}(q)$ in Eq. 4h should be determined by at least two such biaxial strain-controlled ratcheting experiments of different axial strain range.

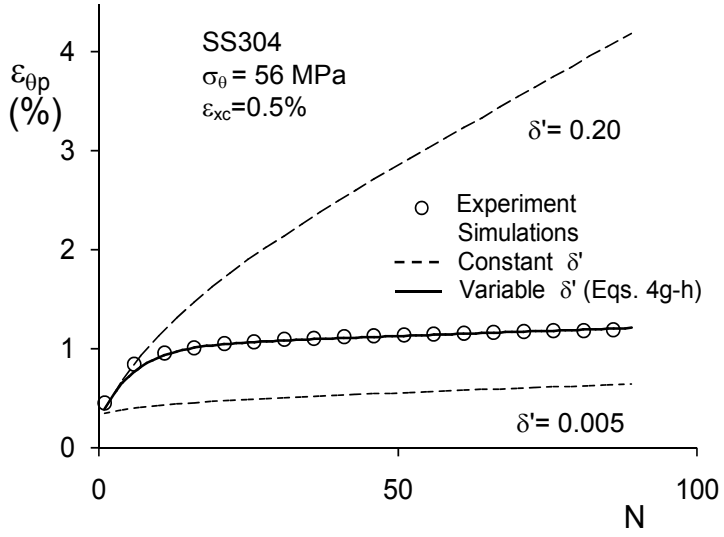

Fig. 3.3. Circumferential ratcheting rate from a biaxial experiment with strain amplitude 0.5% and steady circumferential stress of 56 MPa (Hassan and Kyriakides, 1994b) and simulations with δ' = 0.2 and 0.005, and variable δ' according to Eqs. 4g-h.

It is noted here that with a constant δ' Hassan et al. (2008) simulated the ratcheting rate responses under several stress-controlled, tension-torsion cyclic experiments reasonably well. Whereas, for the steady internal pressure and axial strain-controlled cycle a variable δ' is required to simulate the ratcheting rate response of one experiment (Fig. 3.3). The reason for

such variation of δ' in simulating the ratcheting rates under different multiaxial loading histories is not known. It is anticipated that once the yield surface shape evolution is incorporated in modeling more light on the influence of multiaxial loading and its nonproportionality on the δ' parameter can be shed.

3.2.4 Strain-range dependence

Chaboche et al. (1979) first proposed the strain-range dependent modeling for simulating cyclic hardening/softening of multiple amplitude experiments. If such an experimental response of SS304 (see Fig. 3.4a) is examined, it is observed that the amount and rate of cyclic hardening varies with strain amplitude (see also Fig. 3.4b), which was first demonstrated experimentally by Landgraf et al. (1969). The strain-amplitude dependent evolutions of isotropic hardening and plastic modulus can be clearly observed if the first and the stabilized rising hysteresis curves from each of the four strain amplitudes (Fig. 3.4a) are compared by parallel shifting of the curves to a common starting point as shown in Fig. 3.5. In this figure, except the 1st hysteresis curve from the smallest strain amplitude, all other curves are demonstrating strain-range dependent cyclic hardening, mostly due to the evolution of plastic modulus and little due to the isotropic hardening (linear elastic range). Also note in Fig. 3.4b that the extended cyclic curve (shown as dotted line) for plastic strain amplitudes lower than 0.22% is indicating cyclic softening. Such a response was first demonstrated by Landgraf et al. (1969) for different materials and later by Nouailhas et al. (1985) for quenched SS316, but is yet to be included in any model.

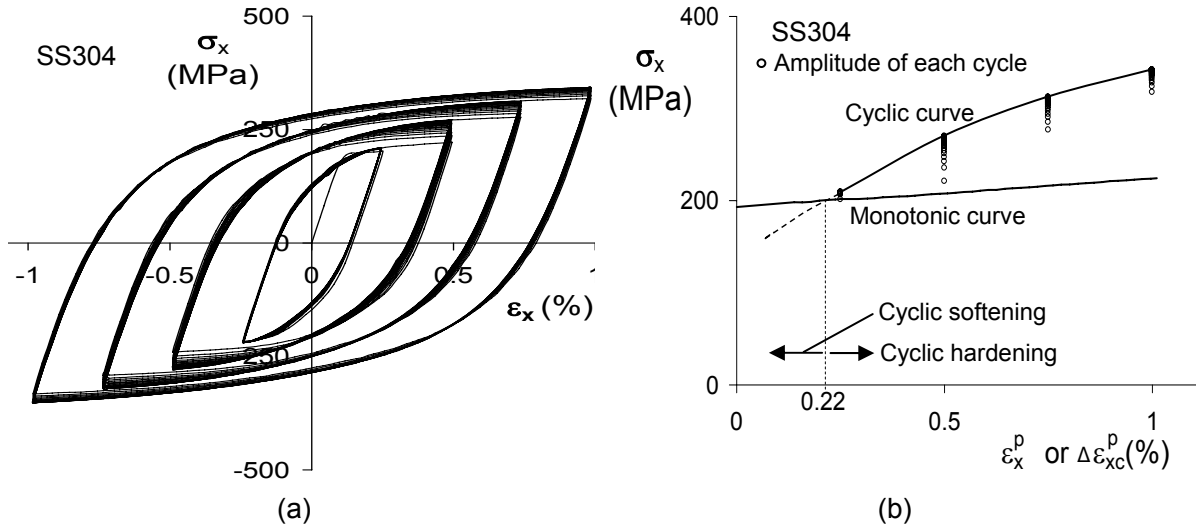

Fig. 3.4. (a) Multiple amplitude, strain-controlled experimental response (Hassan and Kyriakides, 1994a), (b) cyclic curve of saturated stress amplitudes at different strain-ranges (from Fig. 3.4a) in comparsion to the monotonic curve demonstrating the plastic strain-range dependent cyclic hardening and softening.

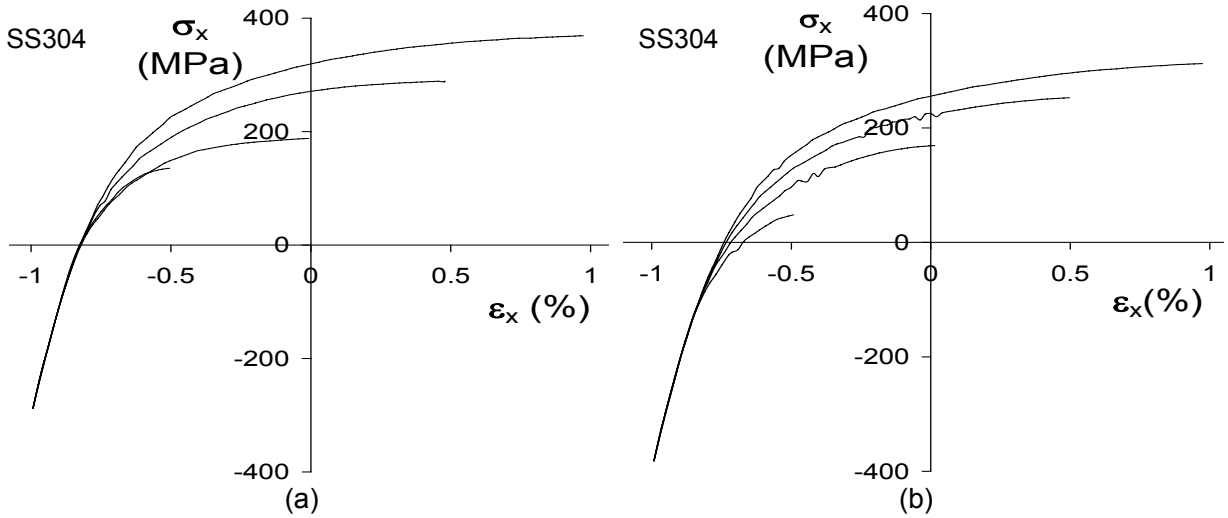

Fig. 3.5. Comparsion of the hysteresis curves from each of the four amplitudes in Fig. 3.4a. (a) First hysteresis curves and (b) stabilized hysteresis curves from each amplitude cycles demonstrating the plastic strain-range dependent cyclic hardening.

In order to include the strain-range dependence into modeling, a strain memory surface of Chaboche et al. (1979) along with the evanescent term (2nd term is Eq. 5b) for subsequent cyclic softening proposed by Nouailhas et al. (1985) are evaluated:

$$g(\underline{\varepsilon}^p - \underline{Y}) = \left[\frac{2}{3}\left(\underline{\varepsilon}^p - \underline{Y}\right) \bullet \left(\underline{\varepsilon}^p - \underline{Y}\right) \right]^{1/2} - q = 0 \tag{5a}$$

$$dq = \left[\eta H(g) \left\langle \underline{n} : \underline{n}^* \right\rangle - \xi \left(1 - H(g)\right) q^m \right] dp \tag{5b}$$

$$d\underline{Y} = \sqrt{\frac{3}{2}} \left[\left(1-\eta\right) H(g) \left\langle \underline{n} : \underline{n}^* \right\rangle \underline{n}^* - \xi (1 - H(g)) \underline{n}^* q^m \right] dp \tag{5c}$$

where, $\underline{n}^* = \dfrac{\underline{\varepsilon}^p - \underline{Y}}{q} dp$.

Eq. 5c is derived based on the strain surface consistency condition with *dq* in Eq. 5b (Delobelle, 1993). The plastic strain surface size, *q*, is incorporated into the isotropic and kinematic hardening variables as shown in Eqs. 2 and 4 (Tanaka, 1994; Jiang and Kurath, 1997; and Kang et al., 2004). It is important to note that the strain range dependence in Eq. 2c and 4f complies with the responses of multiple-step proportional and nonproportional experimental responses developed by Tanaka et al. (1985b) and Takahashi and Ogata (1991), as shown in Fig.6 and will be discussed later in section 2.6.

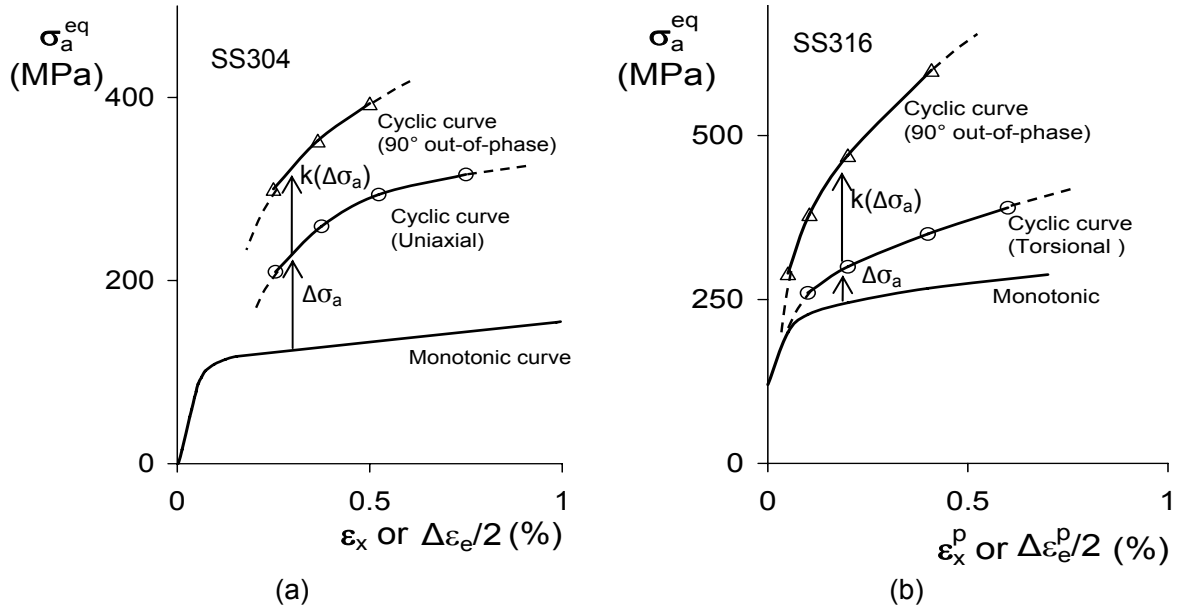

Fig. 3.6. Monotonic and cyclic curves showing the strain range dependent cyclic hardening from uniaxial and 90-degree out-of-phase experiments. (a) Respones from Takahashi and Ogata (1991) and (b) responses from Tanaka et al. (1985b).

There are several concepts of strain-memory surface proposed for describing cyclic hardening/softening responses. Tanaka (1994) modeled the strain memory surface using $q = \left[\frac{2}{3}\left(\underline{\varepsilon}^p - \underline{Y}\right)\bullet\left(\underline{\varepsilon}^p - \underline{Y}\right)\right]^{1/2}$ and $d\underline{Y} = c_y\left(\underline{\varepsilon}^p - \underline{Y}\right)dp$, where, c_y is a rate parameter. In this model, q is calculated after each load increment using the current plastic strains and hence its magnitude oscillates during loading and reverse loading cycle (indicated earlier by Jiang and Kurath, 1997) as shown in Figs. 7b,d for the uniaxial and 90-degree out-of-phase strain-controlled response simulations (Fig. 3.7a,c with c_y = 45). On the other hand, the Chaboche-Nouailhas (Nouailhas et al., 1985) strain memory surface in Eq. 5 gradually grows to a stable size within a few cycles for these response simulations (Fig. 3.7b, d). Two more strain memory surface concepts evaluated in Fig. 3.7 are the Chaboche et al. (1979) and the equivalent plastic strain surface determined from the last load reversal (recent memory parameter).

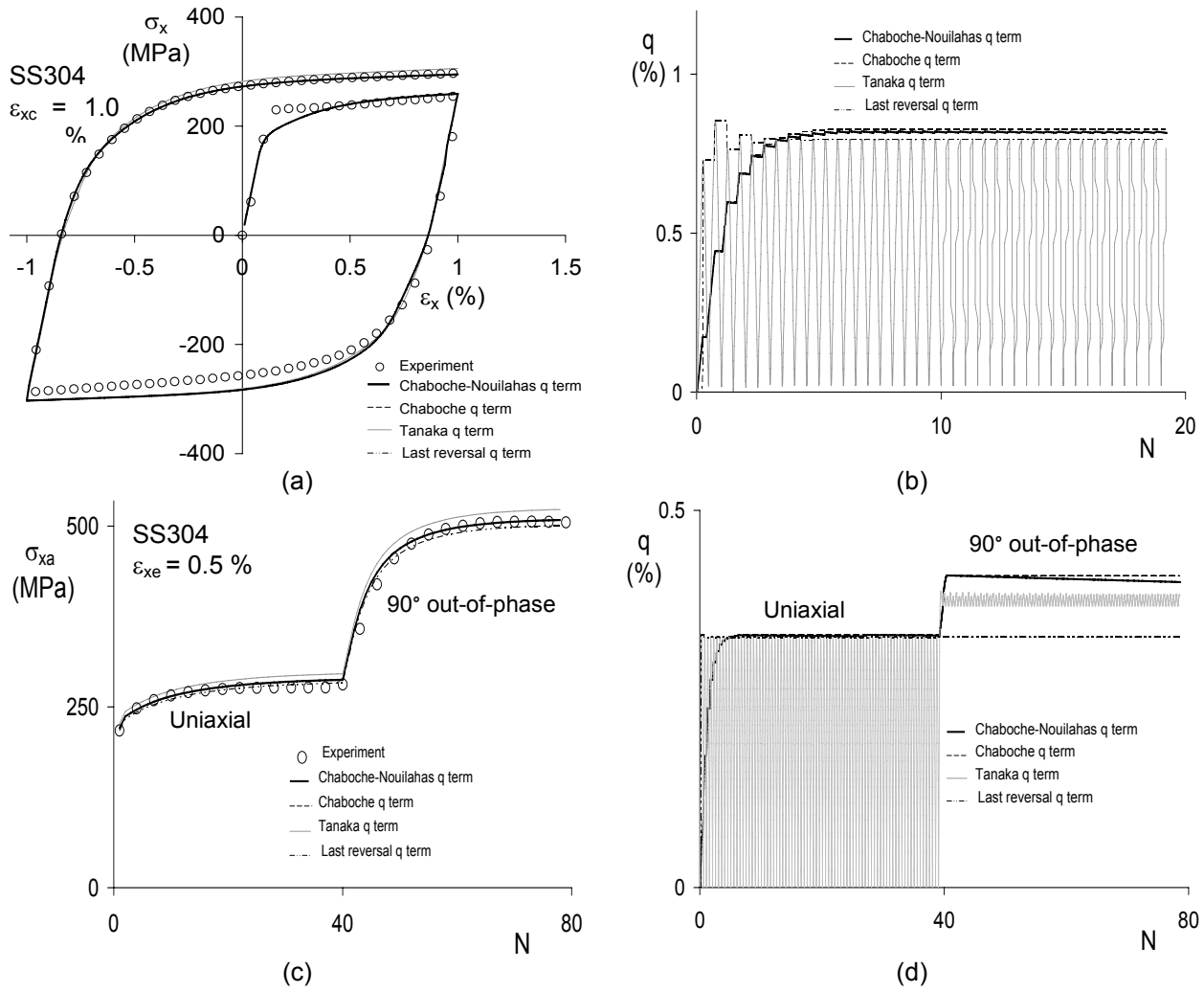

Fig. 3.7. Uniaxial and 90-degree out-of-phase strain-controlled cyclic hardening responses and modified Chaboche model simulations with four plastic strain surface models by Chaboche-Nouailhas (Nouailhas et al.,1985), Chaboche et al. (1979), Tanaka (1994) and last reversal plastic strain amplitude. (a) Experimental and simulated hysteresis loops for a 1% uniaxial strain-controlled cycle; (c) Experimental and simulated stress amplitudes showing cyclic hardening from uniaxial and 90-degree out-of-phase strain-controlled cycles with 0.5% amplitude (Experimental data from Hassan and Kyriakides, 1994a,b); (b,d) corresponding q from four plastic strain surface modeling concepts.

The strain memory surface of Chaboche et al. (1979) without the evanescent term (2nd term in Eq. 5b) evolves in a similar manner as the Chaboche-Nouailhas (Nouailhas et al., 1985) surface except for the small softening shown by the latter model because of the evanescent

term. It is interesting to note in Fig. 3.7 that despite the different q evolutions from the four strain surface concepts, the hysteresis loop and stress amplitude simulations are not much different.

For the subsequent cyclic softening response after a large prestrain, except the Chaboche et al. (1979) model, all other models describe the response qualitatively as shown in Fig. 3.8a (See Nouailhas et al.,1985 for an experimental response of SS316). Again, significant differences in the surface size q from the four strain surface models are obtained as shown in Fig. 3.8b. However, it is interesting to note in Fig. 3.8 that a small difference in the surface size q (Fig. 3.8b) calculated by the Chaboche et al. (1979) and the Chaboche-Nouailhas (Nouailhas et al., 1985) strain surface models can simulate such different cyclic softening responses (Fig. 3.8a). On the other hand, despite the significant difference in q from the Tanaka (1994), Chaboche-Nouailhas (Nouailhas et al., 1985) and the last reversal surfaces (Fig. 3.8b), the subsequent cyclic softening simulations are comparable (Fig. 3.8a).

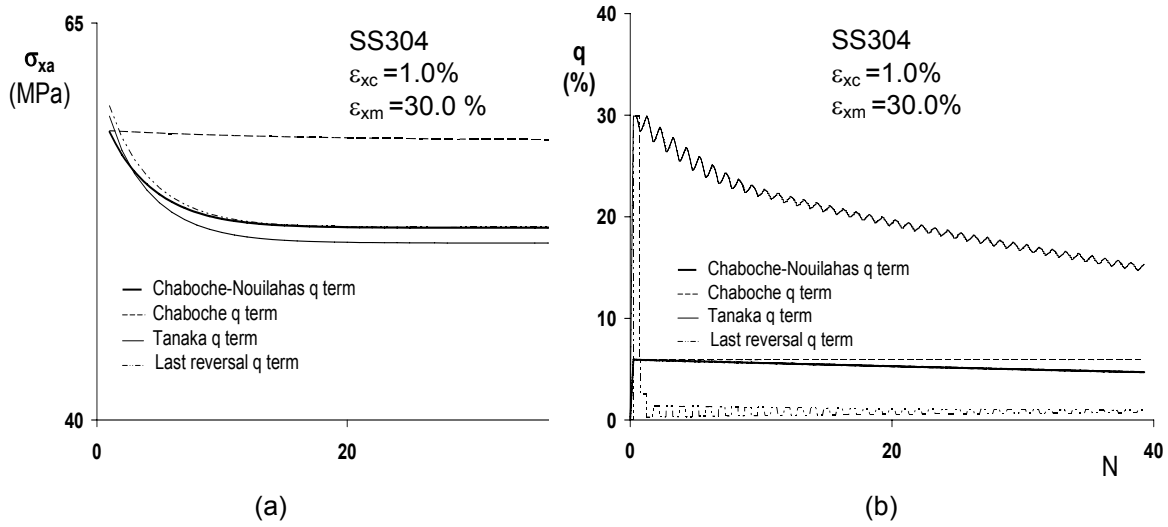

Fig. 3.8. Subsequent cyclic softening simulations by the modified Chaboche model with four plastic strain surface models by Chaboche et al. (1979), Chaboche-Nouailhas (Nouailhas et al.,1985), Tanaka (1994) and last reversal plastic strain amplitude. (a) Simulated cyclic softening of stress amplitude under 1% strain amplitude cycles after 30% prestain; (b) corresponding q from the four plastic strain surface modeling concepts.

Next, the four strain-memory surface models are evaluated against the simulations of hysteresis loop shape and size (Fig. 3.9a), axial strain ratcheting rate (Fig. 3.9b), hysteresis loop width (Fig. 3.9c) and the strain surface size q (Fig. 3.9d). Note in Figs. 9a,c that the significant difference in the 1st loop width between the simulated and experimental hysteresis loops is mainly because of the rate-dependence (rounded peaks and valleys in the experimental response) which is not included in the modified Chaboche model in this study. Strain ranges of the rounded peaks and valleys are the measure of δ_1 and δ_2 respectively. For example, axial strain range from the maximum stress to the maximum strain gives δ_1 at the peak. The rate dependence at the peaks (δ_1 and δ_2) is significant in the first few cycles and diminishes in the subsequent cycles. Hence, almost constant difference between the recorded and simulated loop widths is observed in Fig. 3.9c (more on this aspect in a forthcoming paper by Krishna and Hassan, 2008). Note also in Fig. 3.9c that the cyclic hardening (thinning of hysteresis loop) is observed only during the first couple of cycles, followed by cyclic softening (broadening of the loop). This cyclic softening response in the uniaxial ratcheting experiments is simulated by all strain surface models except the Tanaka (1994) model, which is simulating cyclic hardening (Fig. 3.9c). This cyclic hardening response is the reason that the Tanaka (1994) model cannot simulate the transient ratcheting rate in Fig. 3.9b. Note also the significant difference in the q sizes calculated by the four models (Fig. 3.9d) and the small difference in the rate of ratcheting and hysteresis loop width simulations (Figs. 9a, b, c).

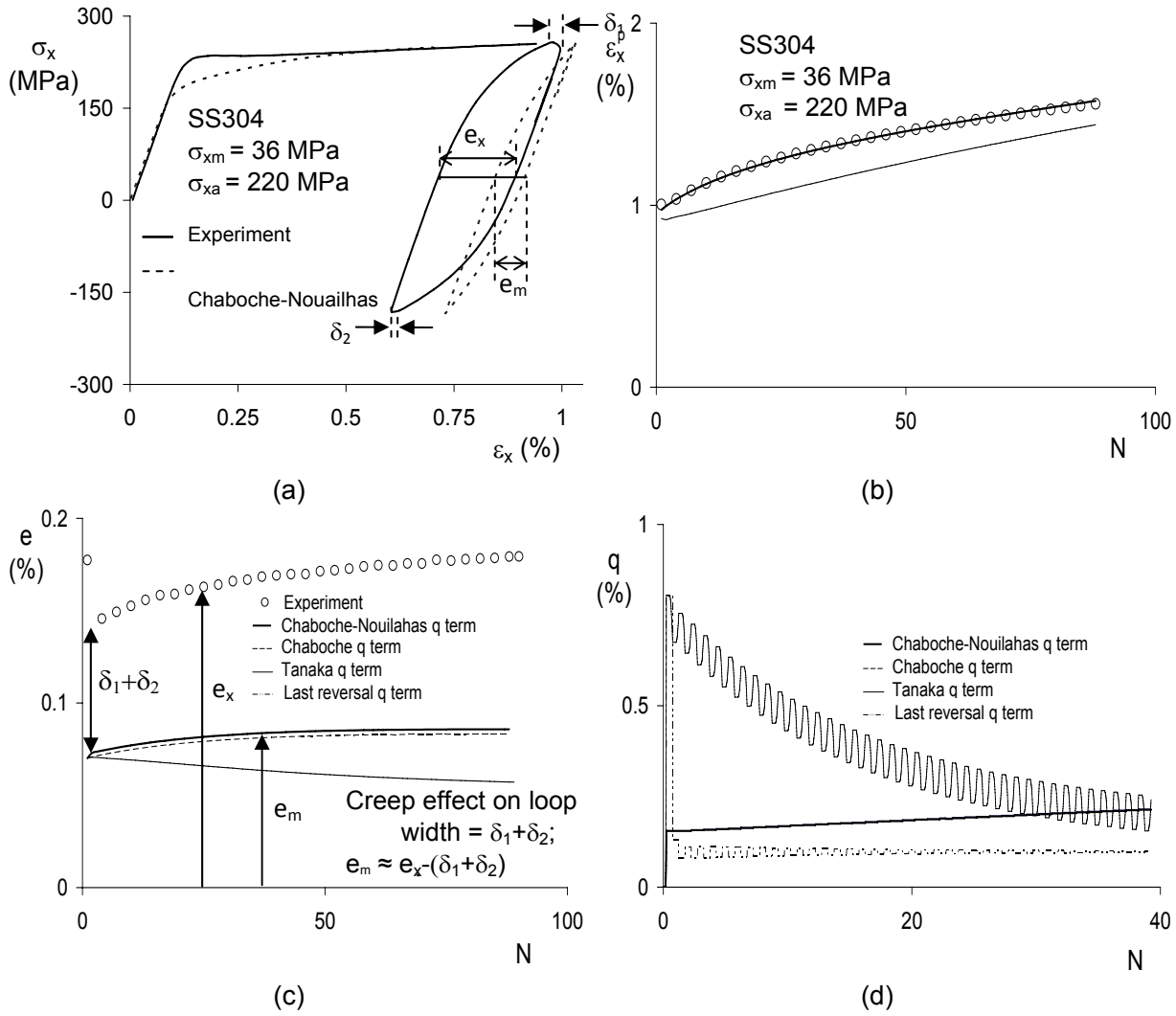

Fig.3.9. Experimental and simulated uniaxial ratcheting responses for evaluation of the four plastic strain surface models by Chaboche et al. (1979), Chaboche-Nouailhas (Nouailhas et al.,1985), Tanaka (1994) and last reversal plastic strain amplitude. (a) hysteresis loops; (b) axial strain ratcheting rates; (c) hystresis loop width, e (e_x from experiment and e_m from model simulation); (d) plastic strain surface size *q* from four modeling concepts. (Experimental data from Hassan and Kyriakides, 1994a).

Based on the responses of cyclic hardening (Fig. 3.7), subsequent cyclic softening (Fig. 3.8) and uniaxial ratcheting (Fig. 3.9) responses from the modified Chaboche model with four strain surface formulations, the Chaboche-Nouailhas (Nouailhas et al., 1985) plastic strain

surface with the evanescence term seems most promising, hence is adopted in the modified Chaboche model in this study for simulating a broad set of cyclic and ratcheting responses.

The novel feature of simulating cyclic softening for a cyclic hardening material for q smaller than the threshold q value (0.22% for SS304 from Fig. 3.4b) is achieved with the modified Chaboche model as follows. For q smaller than the threshold value, R^0 in Eq. 2b decreases (see Fig. 3.10a) and γ_i^0 (i = 1, 2, and 4) in Eq. 4e increases (see Fig. 3.10b for variation of γ_4^0) from their initial values, and the model would simulate cyclic softening. On the other hand for q larger than the threshold q the model would simulate cyclic hardening. These features of cyclic hardening and softening and corresponding R and γ_4^0 variations as a function of q are illustrated in Fig. 3.10. It is interesting to note that the initial γ_i^0 (i = 1, 2, and 4) are determined from a first rising hysteresis curve with a 2% strain range (see Art. 2.6), but these initial values are plotted near threshold q (see Fig. 3.10b for γ_4^0).

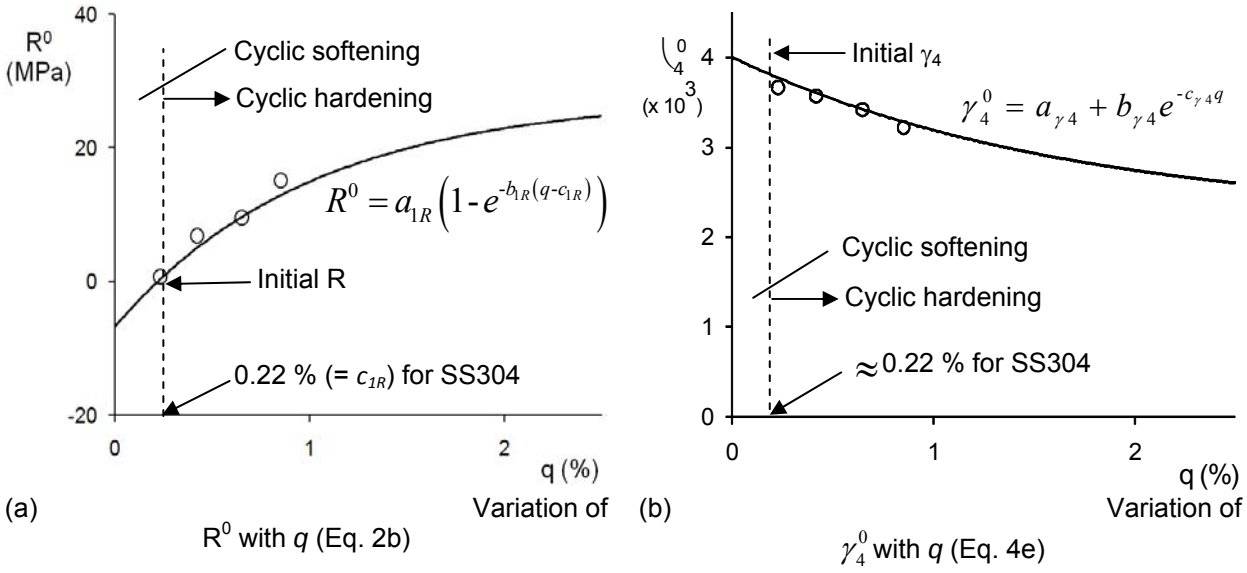

Fig. 3.10. Illustration of R^0 and γ_4^0 variations as a function of strain surface size q, and regions of cyclic softening and hardening for SS304. The R^0 and γ_4^0 data points are determined from the experimental responses in Fig. 3.4 for four strain amplitudes.

3.2.5 Modeling for nonproportionality of loading histories

To facilitate the discussion of modeling for nonproportionality of loading histories, experimental responses of SS304 from Hassan and Kyriakides (1994b) and Hassan et al. (2008) are presented first. Fig. 3.11 shows experimental responses from a strain-controlled experiment that involved 40 cycles of axial history (path I in the inset in Fig. 3.11a), followed by 40 cycles 90o out-of-phase circular history (path II), and followed by 26 cycles of axial history (path III). The readers are referred to the inset in Fig. 3.11a for the sketch of these loading paths in the axial-torsional strain space. The prescribed equivalent total strain amplitude for all the three paths was 0.5%. The equivalent, axial stress amplitude responses are shown in Fig. 3.11a, and the stable hysteresis loop from loading path I and the 1st hysteresis loop from path III are shown in Fig. 3.11b. The response in Fig. 3.11a demonstrates the uniaxial (proportional) cyclic hardening from path I, followed by additional cyclic hardening from path II due to the increase in the degree of nonproportionality, followed by cyclic softening from path III due to the decrease in the degree of nonproportionality. By comparing the stabilized (last) hysteresis loop from path I to the 1st hysteresis loop from path III in Fig. 3.11b, significant isotropic hardening (increase in the linear elastic range) before and after the 90-degree out-of-phase loading (path II) can be observed by comparing the thick lines in Fig. 3.11b.

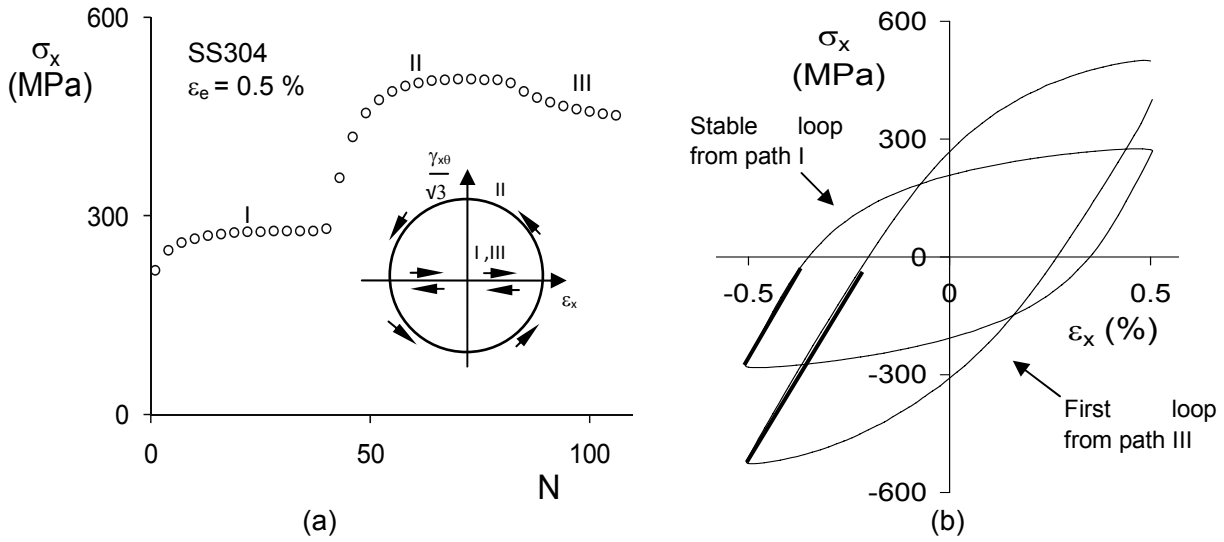

Fig. 3.11. Cyclic hardening responses of SS 304 from an experiment with three loading paths, I-axial strain-controlled cycle, II-90 degree out-of-phase cycle in axial-torional strains, III-axial strain-controlled cycle; (a) equivalent stress amplitude responses from the three loading paths, (b) comparison of the stable hysteresis loop from path I to the 1st hysteresis loop from path III (experiemntal responses from Hassan and Kyriakides, 1994b).

The influence of the degree of nonproportionality on the ratcheting rate response of SS304 was demonstrated by Hassan et al. (2008) as shown in Fig. 3.12 from single and double loading sequence experiments (see the reference for details). They also demonstrated that the Benallal and Marquis (1987) instantaneous nonproportionality measure incorporated in the modified Chaboche model can simulate the single-sequence ratcheting responses reasonably, but failed to simulate the double-sequence ratcheting responses during the second sequence (see Fig. 3.12). As mentioned earlier this drawback of the model might be caused by the lack of memory features of Benallal and Marquis (1987) and hence cannot describe the sudden change in the degree of nonproportionality during the second loading sequences.

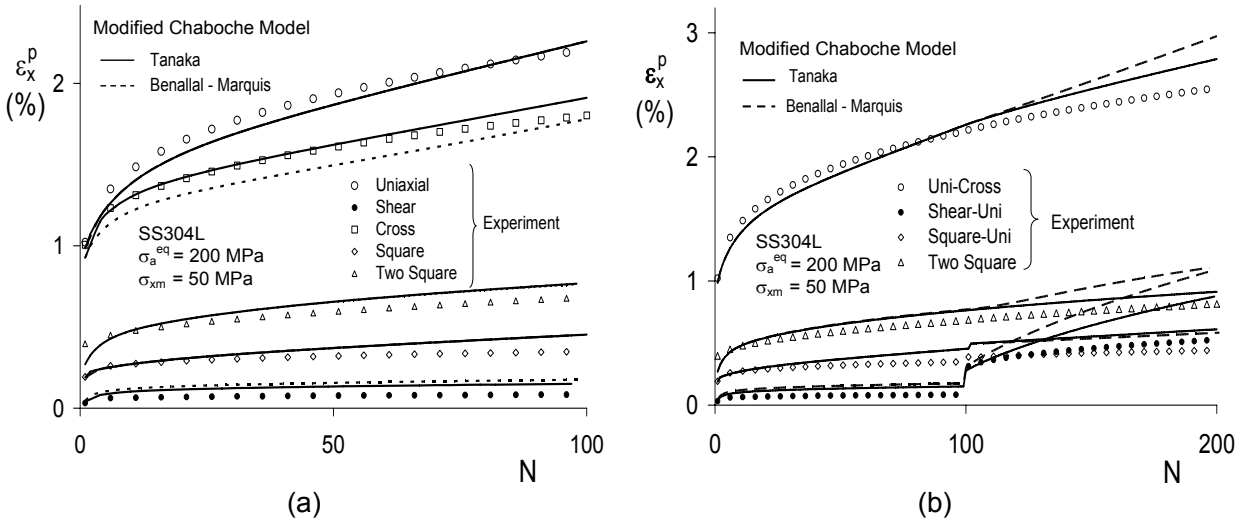

Fig. 3.12. Axial strain ratcheting responses from nonproportional stress-controlled experiments (Hassan et al., 2008) and comparison of simulations from Hassan et al. (2008) with Benallal and Marquis (1987) paramter and this study with Tanaka (1994) parameter. (a) single sequence loading, (b) double sequence loading.

In order to improve the modified Chaboche model simulation of various nonproportional cyclic and ratcheting responses, this study incorporated the nonproportional measure of Tanaka (1994) through a fourth order tensor $\underline{\underline{\underline{\underline{C}}}}$,

$$d\underline{\underline{\underline{\underline{C}}}} = c_c \left(\underline{n} \otimes \underline{n} - \underline{\underline{\underline{\underline{C}}}} \right) dp \,, \tag{6a}$$

and an associated nonproportionality parameter A,

$$A = \sqrt{\frac{Tr\left(\underline{\underline{\underline{\underline{C}}}}^T \underline{\underline{\underline{\underline{C}}}}\right) - \underline{n}\underline{\underline{\underline{\underline{C}}}}^T \underline{\underline{\underline{\underline{C}}}}\underline{n}}{Tr\left(\underline{\underline{\underline{\underline{C}}}}^T \underline{\underline{\underline{\underline{C}}}}\right)}} \,, \tag{6b}$$

where, c_c is a rate parameter. The components of the tensor $\underline{\underline{\underline{\underline{C}}}}$ have zero values for an initially isotropic material and gradually reach the target value $\left(\underline{n} \otimes \underline{n}\right)$ that depends on the plastic strain direction of the loading increment (Tanaka, 1994). As mentioned earlier, an important characteristic of these nonproportional parameters $\underline{\underline{\underline{\underline{C}}}}$ and A is that they are

memory parameters (Tanaka, 1994; Jiang and Kurath, 1997). The tensor $\underline{\underline{C}}$ describes the slow growth of the internal dislocation structure induced by the inelastic deformation process (Tanaka, 1994). If a material is loaded in tension-compression, then the dislocation substructure is formed in a particular direction. After the end of these load cycles, if the material is subjected to torsion, then the dislocation structure from the preceding cycles is destroyed and a new structure is formed. This growth sequence is incorporated in the 4th order tensor $\underline{\underline{C}}$ by Tanaka (1994). In Eq. 6b, $A = 0$ represents the proportional loading, and the maximum value of $A = 1/\sqrt{2}$ represents the highest degree of nonproportionality for the 90-degree out-of-phase loading. For an intermediate degrees of nonproportionality, A varies between 0 and$1/\sqrt{2}$.

The influence of the degree of loading nonproportionality is included in the modified Chaboche model through Eqs. 2a and 4d using the parameter A. Simulations of the Tanaka (1994) nonproportional parameter is first evaluated against the series of ratcheting rate responses from Hassan et al. (2008) as shown in Fig. 3.12. It is observed in this figure that the Tanaka (1994) parameter improved the simulations of both the single and double-loading sequence ratcheting- rate responses compared to the Benallal and Marquis (1987) parameter. Especially, the Tanaka (1994) parameter simulated the trend of the ratcheting rate in the second-sequence of the double-sequence experiments correctly. Hence, the Tanaka (1994) nonproportional parameter (Eq. 6) is implemented into the modified Chaboche model along with all other modeling features presented above (Eqs. 1 to 5) for simulating a broad set of proportional and nonproportional, cyclic and ratcheting responses from Hassan and Kyriakides (1994a,b). First, the parameter determination of the modified model is elaborated below.

3.2.6 Model parameter determination of modified Chaboche model

The modified Chaboche model presented above involves a large number of parameters in order to simulate a broad set of material responses. These parameters can be determined

following sequential and systematic steps using specific experimental responses. Manual determination of these parameters is a tedious task. Hence, a genetic algorithm-based automated parameter optimization software was developed by extending the software developed by Rahman et al. (2005) to accommodate the constitutive equations in this study, Eqs. 1 to 6. The experiment responses needed for determination of the modified Chaboche model parameters are: i) uniaxial, single-amplitude, strain-controlled cyclic response (Fig. 3.2a); ii) uniaxial, multiple-amplitude, strain-controlled cyclic response (Fig. 3.4a); iii) 90-degree out-of-phase cyclic hardening response (Fig. 3.7c); iv) uniaxial ratcheting rate response (Fig. 3.9b); and finally v) two circumferential ratcheting-rate responses from two axial strain amplitudes but same steady internal pressure (one such response is shown in Fig. 3.3). The elastic parameters E, ν, σ_o were determined from a monotonic curve as shown in Fig. 3.2a or 9a.

In the first step, the parameters of Eq. 2 are determined. In order to simulate the monotonic and the subsequent cyclic curves using the same set of model parameters, R^s is introduced in Eq. 2 as the difference between the linear elastic range of monotonic curve and that of a first hysteresis curve from a uniaxial experiment (indicated by thick lines in Fig. 3.13a). The rate term D_{Rs} in Eq. 2 is determined such that the yield surface size of the monotonic curve (σ_{0m}) reduces to the size of the first reversal (σ_{0c}) by the end of the monotonic loading. The rate D_R in Eq. 2 is determined by fitting the evolution of yield surface size R of the hysteresis curves in Fig. 3.2a as a function of accumulated plastic strain as shown in Fig. 3.13b. The equation for fit of the experimental data in Fig. 3.13b is obtained by integration of the first term in Eq. 2. The constant c_{1R} in Eq. 2b (the q threshold for cyclic hardening and softening) is determined by the q value at the intersection of the monotonic and cyclic curves in Fig. 3.4b, where c_{1R} = 0.22% for SS304. The remaining two constants of $R^0(q)$ function in Eq. 2b (a_{1R}, b_{1R}) are determined by fitting the evolution of R (change in the linear elastic range) from the initial to the stable hysteresis curve for each amplitude in Fig. 3.4a (see Fig.10a). The parameter k_R in Eq. 2c is determined by the ratio of the R evolution of

the hysteresis curves just after and before the 90-degree out-of-phase experiment as shown in Fig.11b.

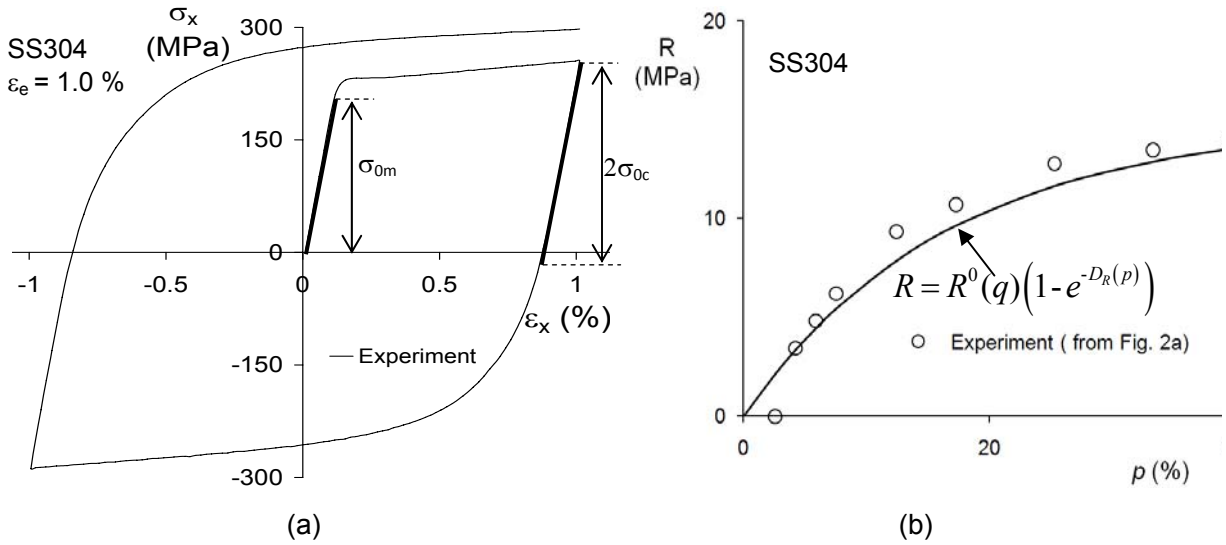

Fig. 3.13. Evolution of yield surface and determination of isotropic hardening parameter D_R. (a) Linear elastic range (yield surface size) for monotonic curve (σ_{0m}) and first cyclic reversal (σ_{0c}), (b) Evolution of yield surface (variation of R) as a function of accumulated plastic strain p.

In the second step, the kinematic hardening rule parameters, the values of C_i and initial γ_i (i = 1 to 4) are determined by fitting the first rising hysteresis curve in Fig. 3.2a. A systematic approach for determining C_i and γ_i is presented in Bari and Hassan (2000) and Rahman et al. (2005). The values of γ_i^0 (i = 1 to 4), which are the stable values of γ_i for a particular strain range, are determined from the four stable hysteresis loops in Fig. 3.5b, keeping the parameters C_i constant to the values determined above. These values are used to determine the constants $a_{\gamma i}$, $b_{\gamma i}$, $c_{\gamma i}$ (i = 1, 2 and 4) in Eq. 4e by fitting the plastic strain range dependence of γ_i^0 as shown in Fig. 3.10b. The value of γ_3, known as the ratcheting parameter, is set to zero during the above parameter determination, and subsequently its value is determined by fitting the uniaxial ratcheting rate response (Fig. 3.9b). With

progressive cyclic hardening, the values of γ_i (i = 1, 2 and 4) gradually decrease to better represent the hysteresis curve shapes. The rate at which γ_i (i = 1, 2 and 4) decreases to γ_i^0 (i = 1, 2 and 4) is determined by the rate parameters $D_{\gamma i}$ (Eq. 4c), which are determined by fitting the stress amplitudes of multiple-amplitude experimental response in Fig. 3.16d. The threshold term $\overline{a}_4$ in Eq. 4b, kept zero so far, is determined such that the fit of the 1st rising hysteresis curve in Fig. 3.2a and uniaxial ratcheting rate in Fig. 3.9b are improved. The parameters $k_{\gamma i}$ in Eq. 4f are determined by the ratio of the kinematic hardening parameters γ_i (i = 1, 2 and 4), determined by fitting the rising hysteresis curves obtained from axial cycles just after and before the 90-degree out-of-phase tension-torsion cycle (see Fig. 3.11b).

The initial value ($\delta_0^{'}$) of the multiaxial ratcheting parameter $\delta^{'}$ is determined by simulating the rate of circumferential strain ratcheting during the first few cycles in Fig.3. In order to determine the constants of the $\delta^{'\infty}$ function in Eq. 4h, at least two values of $\delta^{'\infty}$ need to be determined using the stable circumferential ratcheting rates from two biaxial ratcheting experiments with two different strain ranges but the same internal pressure. Due to the lack of such a set of experimental data, two values of $\delta^{'\infty}$ are determined by using the circumferential ratcheting rates from a biaxial strain-controlled experiment (Fig. 3.22a or Fig. 3.3) and a biaxial stress controlled experiment (Fig 26b). Based on these two values and the corresponding q, the constants $a_{1\delta}$ and $b_{1\delta}$ of Eq. 4h are determined. The rate parameter $D_{\delta'}$ in Eq. 4g is obtained by simulating the circumferential ratcheting rate in Fig. 3.3.

The value of η = 0.2 for the strain memory surface in Eqs. 5b-c yielded good simulations for the experimental responses used for parameter determination. This value falls within the bound of 0.5 suggested by Ohno (1982) for progressive growth of the strain memory surface. The values of ξ = 0.3 and m = 1.5 as suggested by Nouailhas et al. (1985) for strain memory surface (Eqs. 5b, c) also worked nicely for simulation of the parameter determination experimental responses. Finally, the parameter c_c in Eq. 6a doesn't influence the saturated

value of cyclic hardening under proportional and 90-degree out-of-phase cycles. Hence, it is determined from a biaxial stress-controlled experimental response (Fig. 3.26a, b) with an intermediate degree of nonproportionality. The parameters determined using the above procedure through the genetic algorithm software and used in the simulation of a broad set of cyclic responses are listed in Table 1 below.

Table 3.1: Parameters of the modified Chaboche model

Elastic Parameters: E = 192 GPa , ν = 0.33, σ_0 = 148 MPa	
Proportional Parameters (for i = 1 to 4) R^s , D_{Rs} , D_R = 6, -25.5 , 2125 C_i = 357670, 38396, 1310, 147775 MPa γ_i = 15946, 530, 2.75, 3700 a_{1R}, b_{1R}, c_{1R} = 27.7, 95, 0.0022 (in Eq. 2b) $a_{\gamma 1}$, $b_{\gamma 1}$, $c_{\gamma 1}$ = 9835, 8000, 110 (for γ_1 in Eq. 4e) $a_{\gamma 2}$, $b_{\gamma 2}$, $c_{\gamma 2}$ = 390 150 30 (for γ_2 in Eq. 4e) $a_{\gamma 4}$, $b_{\gamma 4}$, $c_{\gamma 4}$ = 2200 1800 60 (for γ_4 in Eq. 4e) γ_3 remains constant at 2.75, $\overline{a}_4$ = 5.2 $D_{\gamma 1}$ $D_{\gamma 2}$ $D_{\gamma 4}$ = 16 , 7.7, 6.5 (in Eq. 4c)	**Nonproportional Parameters** (for i = 1 to 4) k_R = 10.5 $k_{\gamma i}$ = 0.66, 0.63, 0.0, 0.50 Initial δ', δ'_0 = 0.2 $a_{\delta 1}$, $b_{\delta 1}$ =.01, 90 (δ'^{∞} in Eq. 4h) η = 0.2, ξ = 0.3, m = 1.5 c_c = 85

3.3. Polycrystalline plasticity model

Section 2 was devoted to discuss the different features introduced in the modified Chaboche model to account for different mechanical effects (ratcheting, strain range dependence, nonproportional loading and memory effect). A disadvantage of such an approach is the elevated number of model parameters. An alternative view is to consider model development based on fundamental mechanisms to represent a wide range of experimental responses in an acceptable way with fewer model parameters. It is expected, however, that this choice may compromise the accuracy of the simulation of some responses. With this objective, a polycrystalline plasticity model developed by Cailletaud (1992) and

modified by Cailletaud and Pilvin (1994) and Cailletaud and Saï (2008) is evaluated concurrently to the modified Chaboche model in simulating a broad set of cyclic and ratcheting responses. This polycrystalline model is presented in this section. It was pointed out in section 2.1 that the monotonic and subsequent cyclic stress-strain curves are incompatible in terms of their shapes. To account for the different shapes of the monotonic and cyclic curves, the single crystal formulation of the isotropic hardening variable is modified in this study. With this modification, the material parameters become universal in regards to simulating both monotonic and cyclic responses using one set of model parameters.

This model is based on a micro-macro transition approach (see Flowchart 1), in which two localization steps and two homogenization steps are used (macroscopic ↔ grain ↔ slip system). The transition from the macroscopic level to the stress level in each grain will be detailed in subsection 3.2. The transition from grain to the slip system level is achieved by using the resolved shear stress. The slip plasticity (Schmid's criterion) is used in sub-section 3.1 to compute the slip rates. The plastic strain rate of the grain is the result of slip processes according to the different slip systems. The additive macroscopic strain decomposition is used as in the modified Chaboche model. The elastic part is obtained by the Hooke's law. Whereas, the plastic strain is the volume average over all the grains. The above physical considerations allow reducing the number of the material parameters comparing to the unified model types. Note that the consideration of some effects of specific microstructure such as grain neighbourhood, grain size, grain shape or precipitate size are not yet incorporated in the actual phenomenological transition rule. Some modifications are being performed on the polycrystalline model; see for example the recent works of Cailletaud and Saï (2008), Abdeljaoued et al. (2008) and Hlilou et al. (2008), where some of these physical considerations are taken into account.

Flowchart 1. Illustration of localization and homogenization steps of the polycrystalline model.

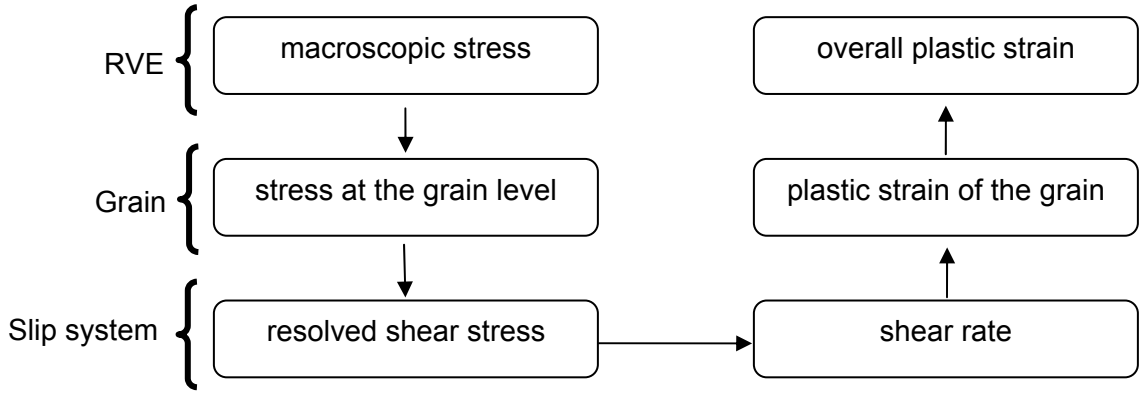

3.3.1 The single crystal formulation

The elasto-viscoplastic single crystal model (Méric et al., 1991) is briefly discussed first, followed by the development of the polycrystalline model used in this study. The model assumes the framework of small perturbation theory, an additive decomposition of the elastic and the viscoplastic strain rates. The so-called resolved shear stress τ^s acting on a particular slip system (s) is given by the relation:

$$\tau^s = \underline{\sigma}^g \bullet \underline{m}^s \tag{7}$$

where $\underline{\sigma}^g$ is the stress tensor in the grain (g) and $\underline{m}^s$ is the orientation tensor attributed to the slip system (s):

$$\underline{m}^s = \frac{1}{2}\left(\vec{l} \otimes \vec{n} + \vec{n} \otimes \vec{l}\right) \tag{8}$$

where, $\vec{n}$ and $\vec{l}$ are the "slip plane" normal vector and the "slip direction" vector on this plane, respectively. The resolved shear stress τ^s can be related to corresponding shear rate $\dot{\gamma}^s$ via a power law expression:

$$\dot{\gamma}^s = \left\langle \frac{\left|\tau^s - x^s\right| - r^s}{K} \right\rangle^n sign(\tau^s - x^s) \tag{9}$$

For each slip system, internal variables are introduced to describe the hardening of the material, such as, isotropic hardening variables r^s and kinematic hardening variables x^s. Viscoplastic flow reaches a rate-independent limit for large values of the parameters *n* or *1/K*. The non-linear evolution rule for isotropic hardening involves an interaction matrix h^{rs} which represents self hardening (diagonal terms) and latent hardening (non-diagonal terms) through:

$$r^s = r_0 + Q\sum_r h^{rs}\left(1 - e^{-bv^r}\right) \qquad \text{with} \qquad \dot{v}^r = \left|\dot{\gamma}^s\right| \tag{10}$$

where r_0 denotes the initial value of r^s. The term h^{rs} of the interaction matrix allows introducing the cross-influence of the slip system (*r*) on the hardening of all the systems, belonging to the same family or not. The quantity $r^s = r_0 + Q\sum_r h^{rs}$ is the maximum value that could be reached in a system, for a strain path that would allow all the systems to become active, for example, for the out-of-phase tension-torsion loading. In uniaxial loadings, this value remains small.

The following form of nonlinear kinematic hardening is adopted:

$$\dot{x}^s = c\dot{\gamma}^s - d\dot{v}^s x^s \tag{11}$$

where, *c* and *d* are model parameters. For the case of FCC materials, plastic strain rate in the crystal is the result of slip processes from twelve octahedral slip systems:

$$\underline{\dot{\varepsilon}}^g = \sum_{s=1}^{12} \underline{m}^s \dot{\gamma}^s \tag{12}$$

As mentioned earlier in Section 2, the polycrystalline model evaluated in this study modifies the previous single crystal formulation to account for different isotropic hardening characteristics between the monotonic and subsequent cyclic responses by introducing a new set of isotropic hardening variables. For each slip system, the isotropic hardening variable r^s in Eq. 10 is modified as follows:

$$r^s = r_0 + Q_1 \sum_r h^{rs}\left(1 - e^{-b_1 v^r}\right) + Q_2 \sum_r h^{rs}\left(1 - e^{-b_2 v^r}\right) = r_0 + \sum_r h^{rs}\left(q_1^r + q_2^r\right) \qquad (13)$$

where, the variables q_1^r and q_2^r, expressed in MPa, represent the hardening contribution and the softening contribution of the slip system (r) in the evolution of the isotropic hardening variable respectively. The experimental results show that the monotonic yield stress is higher compared to the subsequent reversal yield stresses (see Fig. 3.2a and 9a). Even though the polycrystalline behavior is not equivalent to simply adding the behavior of each individual crystallite, the two different behaviors can be taken into account in the following manner: (i) Q_1 and b_1 are chosen so that q_1^r increases slowly with the accumulated plastic strain, and (ii) Q_2 and b_2 allows q_2^r to decrease quickly with the accumulated plastic strain and thus to saturate q_2^r quickly during the monotonic loading.

To illustrate this new feature introduced in the model, the local isotropic variables q_1^r and q_2^r are investigated through a uniaxial ratcheting response. The material parameters are the same used for the simulations of the SS304 responses. Fig. 3.14a shows the competition between the two isotropic variables and their sum for the active slip systems for the uniaxial ratcheting response simulation with loading parameters σ_{xa}=220 MPa, σ_{xm} = 36 MPa. Fig 14b shows the evolution of the two isotropic hardening variables and their sum for two selected slip systems for the same ratcheting response simulation.

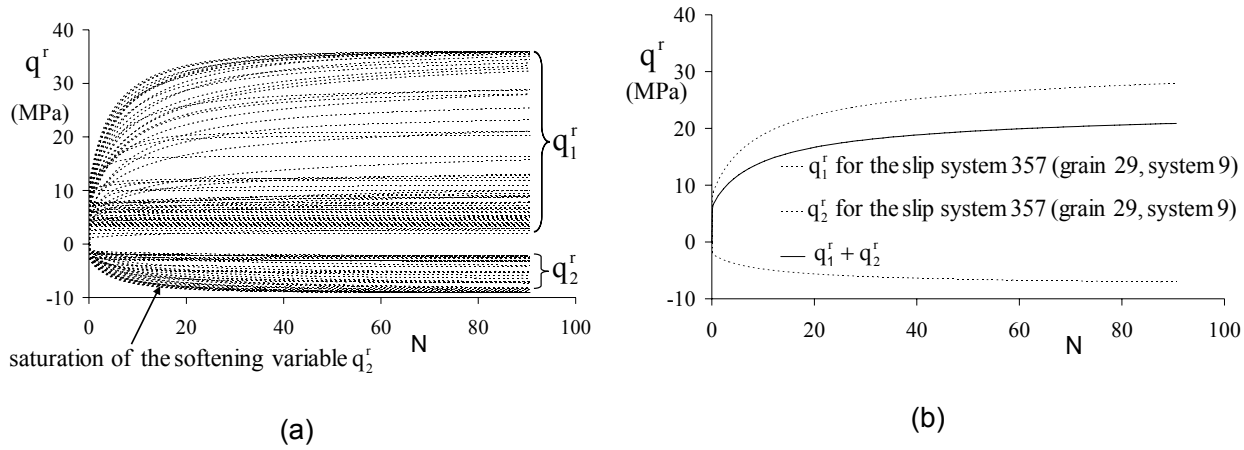

Fig. 3.14. Evolution of the two isotropic hardening variables q_1^r and q_2^r from a uniaxial ratcheting response simulation (σ_{xa} = 220 MPa, σ_{xm} = 36 MPa). (a) for all the active slip systems and (b) for a single slip system.

3.3.2 Explicit rules used for the scale transition in uniform field models

Phases in the polycrystalline aggregate are defined according to the crystal orientation; that is, all the grains falling in the class of Euler angles are in the same phase. The models used to predict polycrystalline behavior in plasticity differ essentially by their transition rule that allows obtaining local stresses and strains. Besides the simplest and most widely used models (uniform plastic strain or uniform stress), the most popular concept is the self-consistent framework proposed by Hill (1965) and revisited by others (see Molinari, 1999). In terms of rates, the local stress rate $\dot{\underline{\sigma}}^g$ is a function of the global stress rate $\dot{\underline{\sigma}}$, the global strain rate $\dot{\underline{\varepsilon}}$ and the local (grain) strain rate $\dot{\underline{\varepsilon}}^g$:

$$\dot{\underline{\sigma}}^g = \dot{\underline{\sigma}} + \underline{\underline{L}}^* \left(\dot{\underline{\varepsilon}} - \dot{\underline{\varepsilon}}^g \right) \tag{14}$$

where, the fourth order tensor $\underline{\underline{L}}^*$ takes into account the incremental behavior of the equivalent medium and the tangent behavior of each grain.

Berveiller and Zaoui (1979) deduced an explicit transition rule from the previous approach for the monotonic loading path and applied it to a globally isotropic behavior:

$$\underline{\sigma}^g = \underline{\sigma} + \mu\alpha\left(\underline{\sigma}, \underline{\varepsilon}^p\right)\left(\underline{\varepsilon}^p - \underline{\varepsilon}^g\right) \qquad \text{with} \qquad \frac{1}{\alpha} \approx 1 + \frac{3\mu p}{2\sigma_{eq}} \tag{15}$$

where, σ_{eq} and p are respectively the equivalent stress and the equivalent total plastic strain. They showed also that Eq. 15 allows plastic accommodation (shakedown) in the polycrystal. Meanwhile, Kröner's rule (obtained with α = 1; Kröner, 1961) produces only elastic accommodation and high stresses. The idea behind all these approaches is to introduce a corrective term depending on plastic strains to compute local residual stresses. Nevertheless, a linear dependency of this term with respect to plastic strains gives high stresses. The nonlinear accommodation can also be obtained by means of a phenomenological approach, where Kröner's solution with the difference of the local and global plastic strains is replaced by the difference between a local and a global nonlinear hardening variable. The concept of β–rule (Cailletaud and Pilvin, 1994) introduced a variable $\underline{\beta}^g$ and its average on the whole aggregate $\underline{\beta}$ as follows:

$$\underline{\sigma}^g = \underline{\sigma} + C\left(\underline{\beta} - \underline{\beta}^g\right) \text{ with } \underline{\beta} = \overline{\underline{\beta}^g} \tag{16}$$

where, C is a material parameter and $\overline{\underline{\beta}^g}$ denotes the volume average of $\underline{\beta}^g$ over the aggregate. The variable $\underline{\beta}^g$ gives non-linear evolution with respect to plastic strain as follows:

$$\dot{\underline{\beta}}^g = \dot{\underline{\varepsilon}}^g - D\underline{\beta}^g \left\|\dot{\underline{\varepsilon}}^g\right\| \tag{17}$$

This formulation is purely explicit; it does not need any iterative procedure like the classical self-consistent models (Molinari, 1999). The parameter D is a scale transition parameter, which should be determined by means of finite element computations on realistic polycrystalline aggregates. In addition, it was shown by Cailletaud and Saï (2008) that the

evolution rule (linear or nonlinear) of the accommodation variable has a significant effect on ratcheting behavior. The non-linear evolution of $\underline{\beta}^g$ may be written more generally as:

$$\dot{\underline{\beta}}^g = \dot{\underline{\varepsilon}}^g - D\left(\underline{\beta}^g - \delta\underline{\varepsilon}^g\right)\left\|\dot{\underline{\varepsilon}}^g\right\| \tag{18}$$

In this expression, $\delta = 0$ leads to the non-linear evolution rule of Eq. 17, whereas $\delta = 1$ leads to the Kröner (1961) rule. In the model parameter determination, the three parameters C, D and δ will be considered as free during the optimization process.

Cailletaud and Saï (2008) have shown that if only intergranular kinematic hardening is considered ($c = 0$), then high ratcheting rate is obtained. This is due to the singular character of the interaction matrix at the intergranular level. Moreover, ratcheting rate increases with the decrease of the parameter C. A shakedown behavior is obtained if only the intragranular kinematic hardening is considered ($C = 0$). The asymptotic tensile peak strain is higher for the small values of the parameter c. They also have shown that, when non-linear kinematic hardening rules of the two levels (intergranular and intragranular) are considered, noticeable ratcheting behavior occurs. Otherwise, shakedown is obtained.

3.3.3 Model Parameter Determination of Polycrystalline Model

The model parameters were determined by means of the optimization module of the software Zset/Zébulon (Besson and Foerch, 1997) which includes an optimizer routine (Besson et al. 1998). The elastic parameters E, ν and ro were determined from a monotonic curve as shown in Fig. 3.2a or 9a. With the polycrystalline model, all the parameters are optimized simultaneously for best simulation of the whole set of the experimental responses. While doing so, the following constraints are imposed so that the best fit of all the experimental responses are obtained:

• In order to control the limited amount of SS304 ratcheting, a linear kinematic variable is considered at the intragranular level ($d = 0$).

• The experimental results show that the ratcheting rate decreases at final stage of the experiments. For this reason, the evolution rule of Eq. 18 is considered ($\delta \neq 0$). That means at the intergranular level a non linear variable $\underline{\beta}^g$ is superimposed over a linear one.

• The accommodation parameter C is maintained close to the elastic shear modulus of the material.

• The latent hardening parameters, h^{rs}, influence mainly the 90-degree out-of-phase tension-torsion response and to some extent the ratcheting response. This is why they have been considered among the identified parameters with initial values equal to 1.

• To account for different shapes of the monotonic and the subsequent cyclic curves, the isotropic hardening parameters are chosen so that in Eq. 13 $Q1>0$ and $Q2<0$.

The polycrystalline model parameters optimized for best fit of the experimental responses and used in the simulations are given in Table 3 below.

Table 3.2: Model parameters of the polycrystalline model for SS304 (units MPa, s)

Elasticity		**Norton parameters**		**Isotropic Hardening**				
E	ν	K	n	r_0	Q_1	b_1	Q_2	b_2
192000	0.3	31	11	60	36	29	-9	29
Latent Hardening								
h_1	h_2	h_3	h_4	h_5	h_6			
0.7	0.8	0.3	1.9	0.2	1.77			
Kinematic Hardening								
c	d		C	D	δ			
220	0		60440	65	0.19			

3.4. Model Simulations

The modified Chaboche and polycrystalline models introduced in sections 2 and 3 are evaluated in this section against simulating a broad set of proportional and nonproportional, cyclic and ratcheting responses of SS304 from Hassan and Kyriakides (1994a, b). The modifications incorporated in the Chaboche model are the plastic strain surface with an evanescent term, Tanaka (1994) nonproportional parameter and various internal state variable functions to represent cyclic hardening and softening. The version of the polycrystalline model evaluated was proposed by Cailletaud and Pilvin (1994) and Cailletaud and Saï (2008). Both the modified Chaboche and polycrystalline models also included a modified isotropic hardening function (Eq. 2 and 13, respectively) so that the monotonic and cyclic responses can be simulated using one set of model parameters for each model. The model parameters used in the simulation are presented in sections 2.6 and 3.3. The set of the experimental responses considered for model evaluation are grouped as follows: i) strain-controlled cyclic responses, ii) uniaxial ratcheting responses, iii) biaxial strain-controlled ratcheting responses, and iv) biaxial stress-controlled ratcheting responses.

3.4.1 Simulations of strain-controlled cyclic responses

The strain-controlled cyclic responses considered for model evaluations were developed by Hassan and Kyriakides (1994a, b) by prescribing symmetric, single amplitude cycle (Fig. 3.15a, d), symmetric, multiple amplitude cycle (Fig. 3.16a, d), multiple mean, single amplitude cycle (Fig. 3.17a, d), and finally 90-degree out-of-phase axial-torsional cycle (Fig. 3.18a, d). In case of the 90-degree out-of-phase nonproportional experiment, axial strain-controlled cycles were also prescribed before and after the nonproportional cycle (Fig. 3.18d). For each of these cases, in addition to the detailed stress responses (Figs. 15a, 16a, 17a, and 18a), mean and amplitude stress responses also are plotted to study the cyclic hardening, softening and relaxation responses (Figs. 15d, 16d, 17d, and 18d).

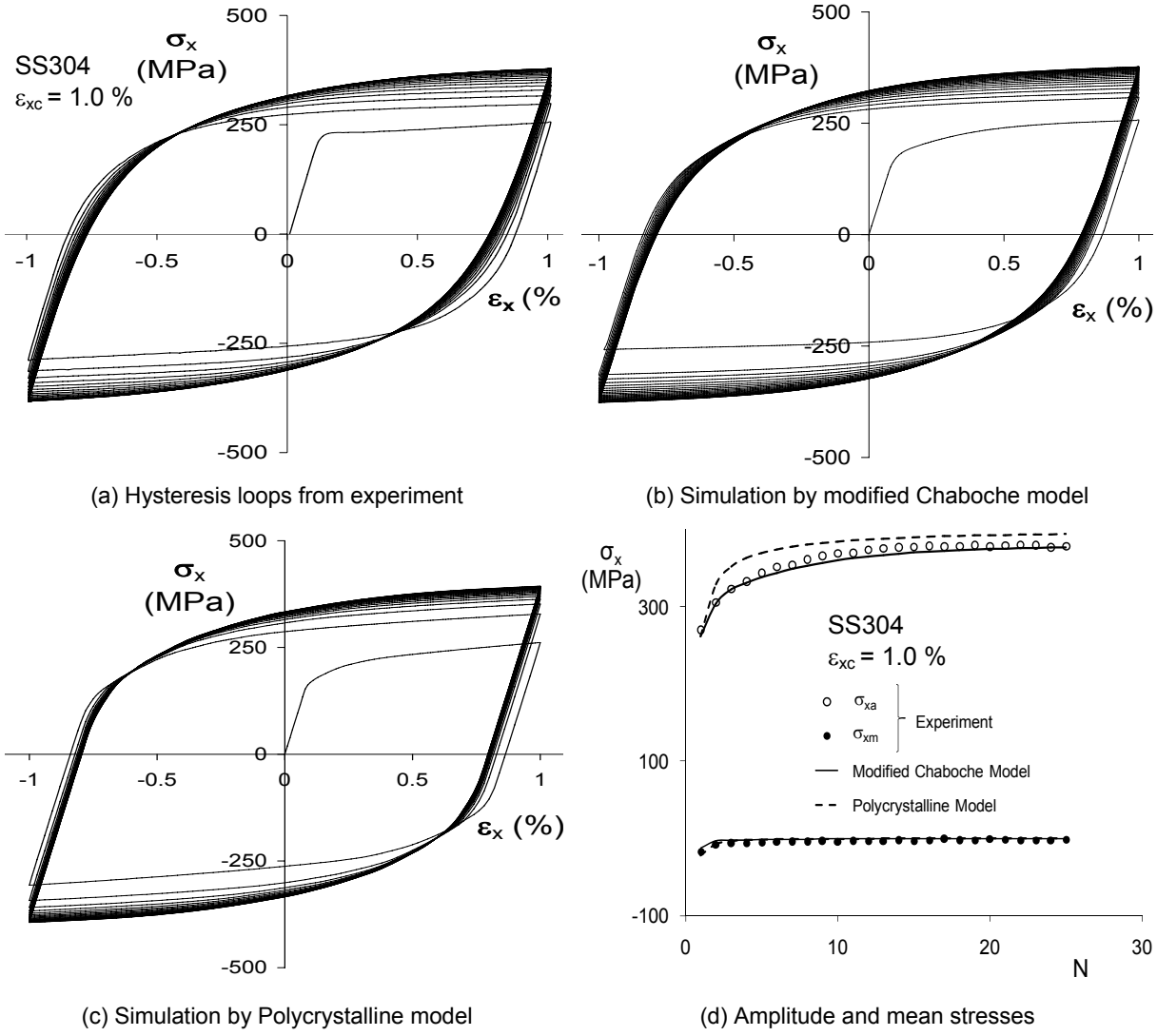

Fig. 3.15. Experimental and simulated responses under uniaxial strain-controlled cycle. (a) Experimental response, (b) simulations by the modified Chaboche model, (c) simulations by the polycrystalline model, (d) amplitude and mean axial stresses. (experimental data from Hassan and Kyriakides, 1994a)

For the symmetric, single amplitude, uniaxial strain-controlled cycle with amplitude ε_{xc} = 1%, both models simulated the cyclic hardening (increases in stress amplitude, σ_{xa}, with cycles) and the mean stresses (σ_{xm}) well (Fig. 3.15d). The modified Chaboche model simulated the hysteresis loop shape and cyclic hardening better than the polycrystalline

model (compare Figs. 15a, b, and c). This is mainly because the earlier model used both isotropic and kinematic hardening rule (Eqs. 2 and 4c), whereas the latter model used only the isotropic hardening rule for modelling cyclic hardening. Also, if the simulated hysteresis curves in Fig. 3.2b and 15b are compared to the experimental curves, the significant improvement of the hysteresis loop simulation by the modified Chaboche model (because of simulating cyclic hardening using both the isotropic and kinematic hardening rule parameters; see section 2.3) can be observed.

The experimental responses from the symmetric, multiple amplitude, uniaxial strain-controlled experiment are shown in Figs. 16a, d. The cyclic hardening response for different strain ranges can be seen in these figures. Again, the modified Chaboche model is simulating the shapes of the hysteresis curves and the cyclic hardening (stress amplitude, σ_{xa}) responses better than the polycrystalline model due to the same reason mentioned above, and in addition, due to the plastic strain memory surface and incorporation of the size of the surface, q, into the kinematic hardening variables (Eqs. 4e-f).

The experimental response from the multi-mean, single amplitude, uniaxial strain-controlled experiment is shown in Figs. 16 a, d. The increase in the mean stress (σ_{xm}) as the mean strain is increased and subsequent cyclic relaxation is observed in Fig. 3.17d for all loading steps except the first step. Another interesting phenomenon is that the cyclic hardening is observed only during the first loading step, whereas for the subsequent steps, as the mean strain gradually increases, cyclic softening is observed (see Fig. 3.17d). Both the cyclic relaxation and cyclic hardening/softening are simulated by the modified Chaboche model very well. Due to the lack of a strain surface with an evanescent term, the polycrystalline model fails to simulate these features (Figs. 17c, d).

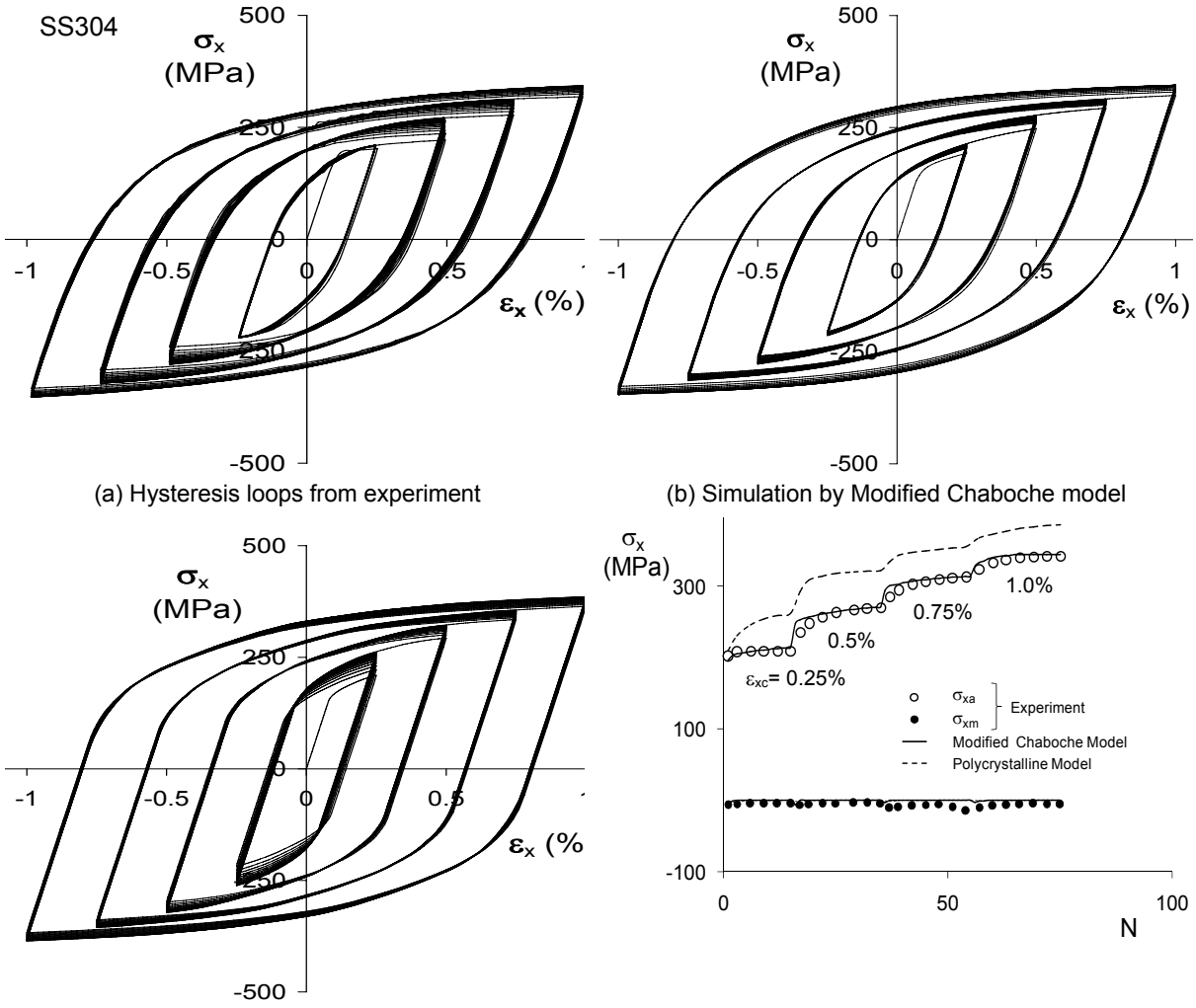

Fig. 3.16. Experimental and simulated responses under symmetric, multiple amplitude cycle. (a) Experimental response, (b) simulations by the modified Chaboche model, (c) simulations by the polycrystalline model, (d) amplitude and mean axial stresses. (Experimental data from Hassan and Kyriakides, 1994a)

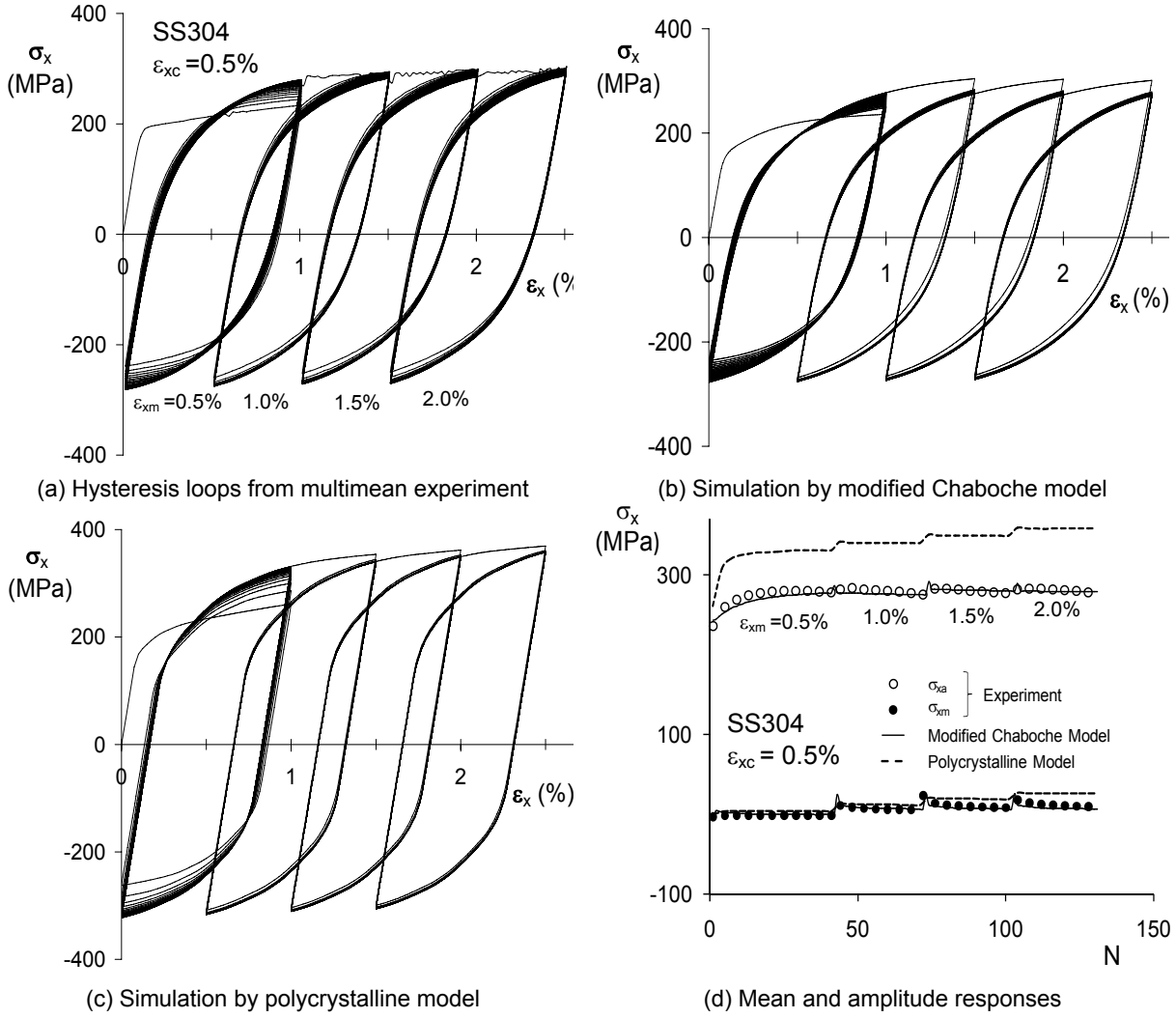

Fig. 3.17. Experimental and simulated responses under multimean, single amplitude cycle. (a) Experimental response, (b) simulations by the modified Chaboche model, (c) simulations by the polycrystalline model, (d) amplitude and mean axial stresses. (Experimental data from Hassan and Kyriakides, 1994a.)

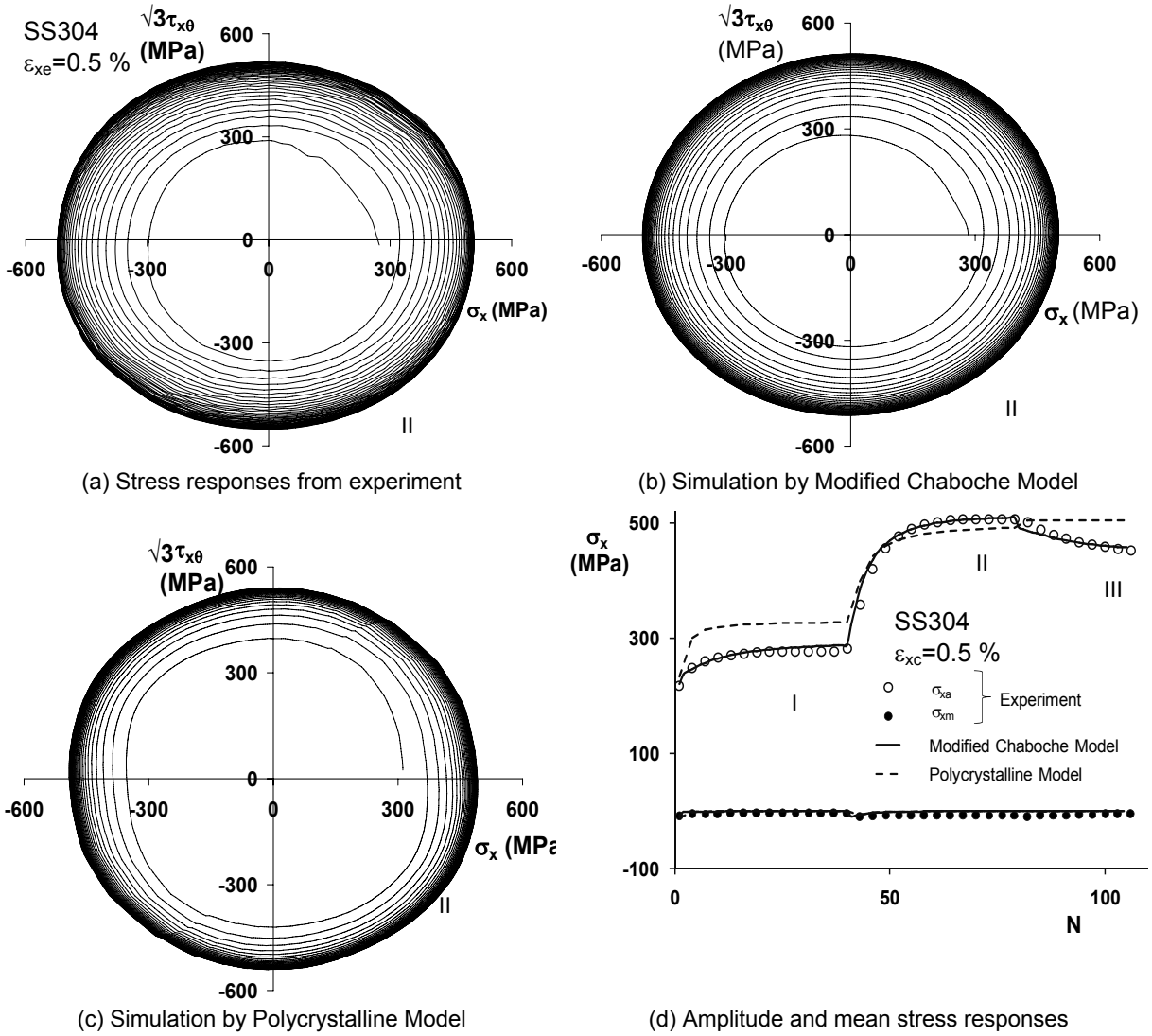

Fig. 3.18. Experimental and simulated responses under 90 degree out-of-phase strain-controlled cycle. (a) Experimental stress response, (b) simulations by the modified Chaboche model, (c) simulations by the polycrystalline model, (d) amplitude and mean axial stress responses from three step cycles: axial cycle, 90-degree out-of-phase cycle, followed by axial cycle. (Experimental data from Hassan and Kyriakides, 1994b)

The axial-shear stress response from the 90-degree out-of-phase cycle is shown in Fig. 3.18a. The additional cyclic hardening from this step compared to that from the uniaxial cycle of equal strain amplitude applied beforehand is shown in Fig. 3.18d. The cyclic softening from the axial strain-controlled cycle following the 90-degree out-of-phase cycle is

also shown in this figure. The modified Chaboche model simulated all the responses from these three loading steps very well (Fig. 3.18). Because of the Tanaka (1994) nonproportional parameter, the modified Chaboche model could simulate the cyclic softening for the uniaxial cycle after the 90-degree out-of-phase cycle (Fig. 3.18d). The polycrystalline model overpredicts the cyclic hardening in the first loading step, underpredicts the additional cyclic hardening in the second step and fails to predict the cyclic softening in the third loading step.

It is noted here that some of the strain-controlled experimental responses presented above were used in the model parameter determination as discussed in sections 2.6 and 3.3. Hence the good cyclic hardening simulations shown in Figs. 15d and 18d (Step II) are because of the direct fit for parameter determination. However, the simulations of the strain-controlled cyclic responses by the modified Chaboche model are quite good.

3.4.2 Simulation of uniaxial ratcheting response

In this section, the models are evaluated against a broad set of uniaxial ratcheting responses of SS304 from Hassan and Kyriakides (1994a). Under an unsymmetrical, axial, stress-controlled cycle the maximum axial strain in each cycle gradually increases as shown in Fig. 3.19a. The simulated axial stress-strain responses from the two models are shown in Fig. 3.19b, c. The maximum axial strain (ε_x^p) in each cycle from the experimental and simulated responses is plotted as a function of the number of cycles (N) in Fig. 3.19d. The rate of ratcheting in Fig. 3.19d was fitted for determining model parameters hence the demonstrated simulations are the best from each model.

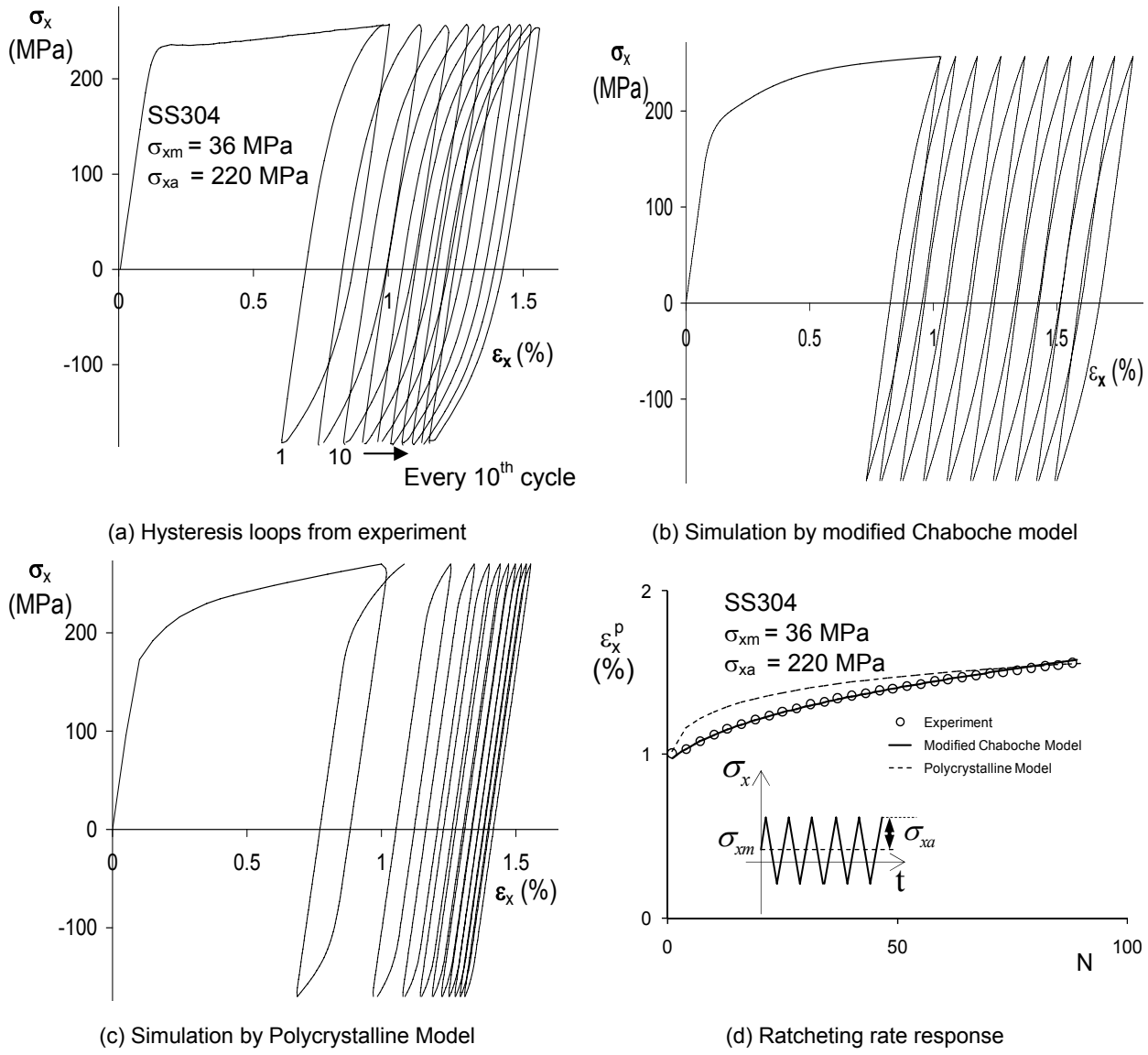

Fig. 3.19. Experimental and simulated responses under unsymmetrical, stress-controlled cycle. (a) Experimental stress response, (b) simulations by the modified Chaboche model, (c) simulations by the polycrystalline model, (d) ratcheting rate response. (Experimental data from Hassan and Kyriakides, 1994a)

The simulated hysteresis loops from either model are not comparable to the experimental loops. The Chaboche model simulated the hysteresis curve shape better than the polycrystalline model, but its simulated hysteresis loops are much thinner compared to the experimental loops. However, the Chaboche model predicted the loop broadening (see Fig.

3.9c) like the experiment, whereas the polycrystalline mode is simulating loop thinning. The novel strain-range dependent cyclic hardening-softening feature of the modified Chaboche model, as discussed earlier in section 2.4, is the primary reason for obtaining the loop broadening during uniaxial ratcheting. As mentioned earlier in section 2.4 (see discussions related to Figs. 9a, c), the loop size simulation of the modified Chaboche model can be improved by incorporating the rate-dependence into the model (Krishna and Hassan, 2008).

Both models were evaluated against simulating a series of uniaxial ratcheting rate responses as shown in Fig. 3.20. The experimental responses in Figs. 20a,b are showing the influence of amplitude stress and those in Figs. 20c, d are showing the influence of mean stress on the rate of ratcheting. As observed in these figures, ratcheting rate simulations of the modified Chaboche model match the experimental responses better than the polycrystalline model. Because of the isotropic hardening (increase in yield surface size), the polycrystalline model simulates larger transient during the initial cycles and lower stable ratcheting rate during the later cycles compared to the experimental responses. If the simulations of the modified Chaboche model in Fig. 3.20a, c are compared to the simulations of the two-surface Dafalias-Popov model in Fig. 3.9 of Hassan and Kyriakides (1994a), it is observed that the simulations of the modified Chaboche model are quite good. The uniaxial ratcheting simulation of the modified Chaboche model can be improved further by incorporating a novel backstress shift model as will be demonstrated in a forthcoming paper (Krishna and Hassan, 2008).

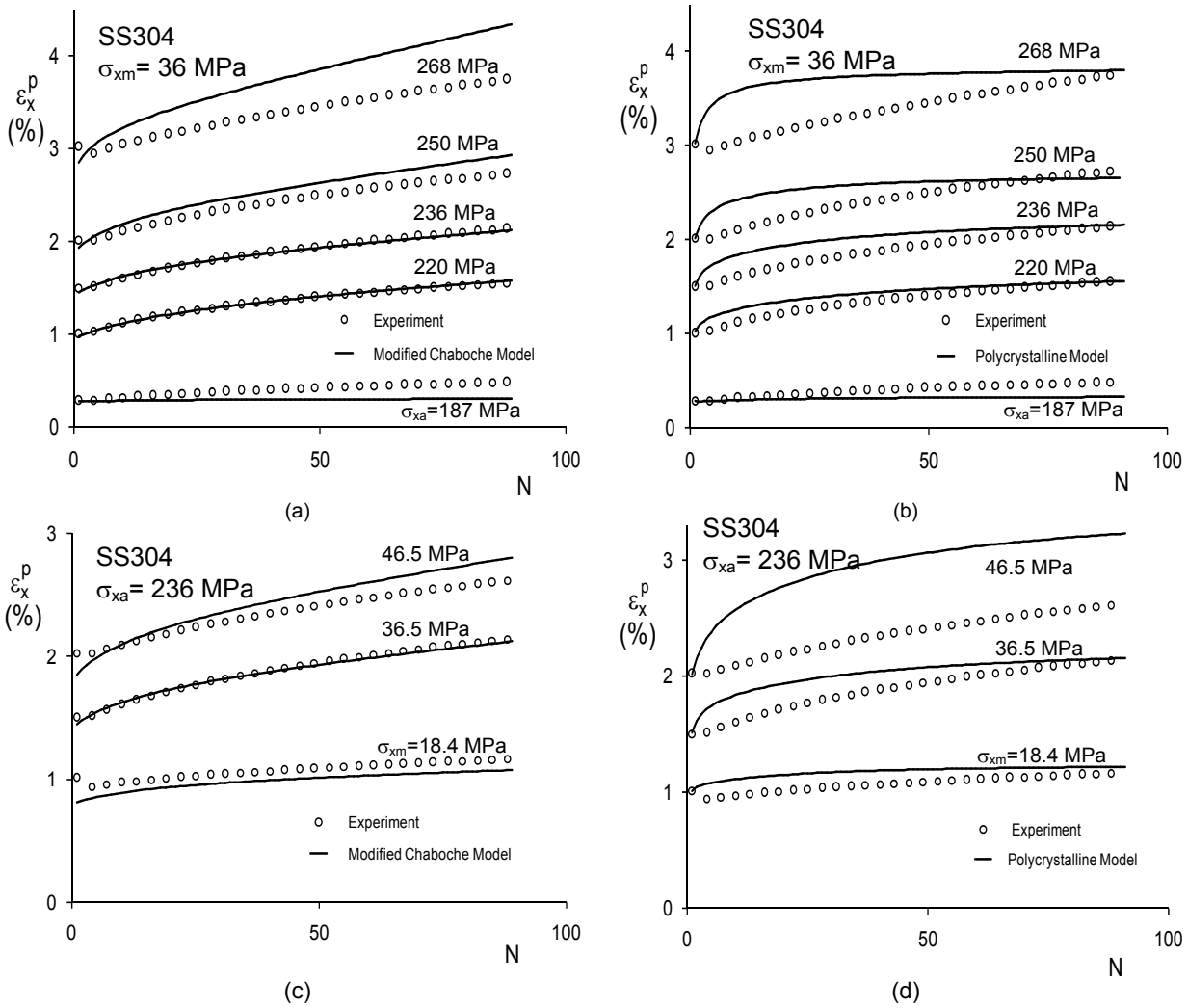

Fig. 3.20. Experimental and simulated responses of axial ratcheting rates. (a, b) influence of amplitude stress (c, d) influence of mean stress. (Experimental data from Hassan and Kyriakides, 1994a)

3.4.3 Simulation of biaxial strain-controlled ratcheting response

The biaxial loading of axial strain-controlled cycle in the presence of steady circumferential stress (steady internal pressure) induces circumferential strain ratcheting as shown in Figs. 21b (see Hassan and Kyriakides, 1994b for detail). Ratcheting rate, and axial stress amplitude and mean responses from three such experiments with different internal

pressure but the same axial strain cycle are shown in Fig. 3.22. It is noted here that the ratcheting rate of the experiment with ε_{xc} = 0.5% and σ_θ = 56 MPa was used in model parameter determination (see Fig. 3.3). The simulations of the axial stress-strain and circumferential strain ratcheting responses by both models are quite impressive as can be seen in Fig. 3.21. Also, the circumferential strain ratcheting rates for all three experiments, including the transient rate during the initial cycles and stable rates during later cycles, are simulated very well by both models (Figs. 22a, b). The increase of the axial mean stress with increasing circumferential stress is simulated well by both models; however, the axial stress amplitudes (cyclic hardening) are simulated better by the modified Chaboche model than the polycrystalline model (compare Fig. 3.22c, d). Stress amplitudes from all three experiments show cyclic softening after the initial cyclic hardening, which is not simulated by either of the two models. Compared to the simulations of Hassan and Kyriakides (1994b; see Fig. 3.4a in the reference), both models studied here perform much better in simulating the biaxial strain-controlled ratcheting responses. Presence of the strain-range dependent multiaxial parameter δ'^{∞} (Eq. 4h) in the modified Chaboche model plays a significant role in simulating the circumferential ratcheting rate so well.

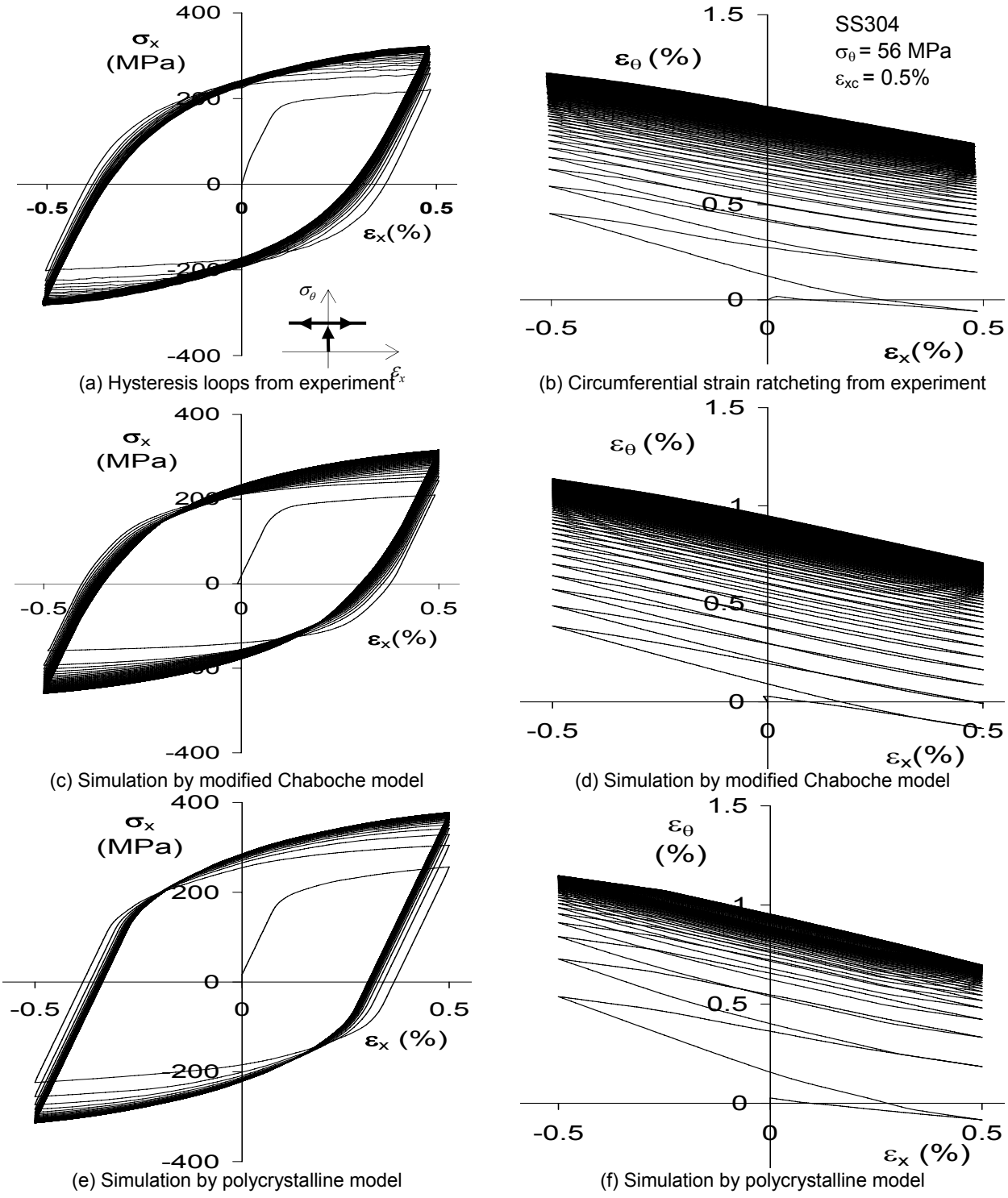

(a) Hysteresis loops from experiment

(b) Circumferential strain ratcheting from experiment

(c) Simulation by modified Chaboche model

(d) Simulation by modified Chaboche model

(e) Simulation by polycrystalline model

(f) Simulation by polycrystalline model

Fig. 3.21. Experimental and simulated responses from axial, strain-controlled cycle under steady circumferential stress. (Experimental responses from Hassan and Kyriakides, 1994b)

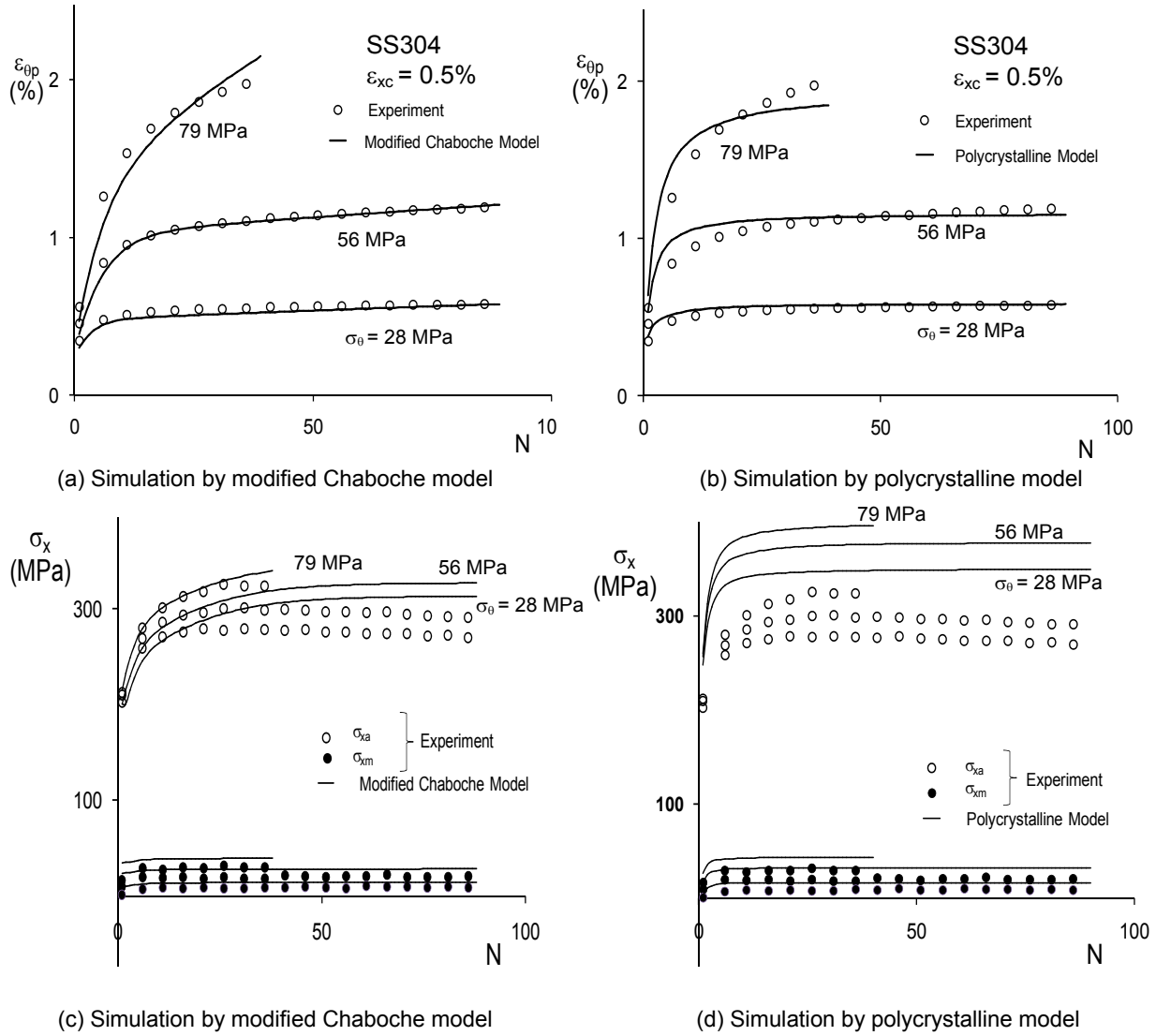

Fig. 3.22. Experimental and simulated responses under biaxial strain-controlled ratcheting cycles. (a,b) Circumferential ratcheting rates, (c,d) amplitude (σ_{xa}) and mean (σ_{xm}) stresses. (Experimental responses from Hassan and Kyriakides, 1994b)

3.4.4 Simulation of biaxial stress-controlled ratcheting response

The challenges of simulating the biaxial stress-controlled ratcheting response have been demonstrated by Hassan and Kyriakides (1994b). In this experiment, under unsymmetric, axial, stress-controlled cycle in the presence of internal pressure, both axial and circumferential strains ratchet as shown in Figs. 3.23a, b. As can be seen in this figure,

because of the high level of circumferential stress (internal pressure) the circumferential strain is ratcheting in the tensile direction at a high rate and axial strain is ratcheting in the compression direction even when the mean axial stress is positive. If the circumferential stress in an experiment is reduced to zero, keeping the axial-stress cycle parameters close to the last experiment, the axial strain ratchets in the tensile direction and circumferential strain ratchets in the compression direction (due to plastic incompressibility) as shown in Fig. 3.24a, b. If a low level of circumferential stress is prescribed, the axial strain ratcheting rate is reduced while the circumferential strain ratchets slowly in the tensile direction as shown in Fig. 3.25a, b. With further increase of the circumferential stress to a medium level or high level, the axial strain ratcheting changes its direction towards compression and the circumferential strain ratcheting-rate increases further along the tensile direction as shown in Fig. 3.26a, b and 3.23a, b.

Simulations of this complex biaxial stress-controlled ratcheting response by the modified Chaboche and polycrystalline models are shown in Fig. 3.23-26. Overall, the modified Chaboche model is simulating this set of responses better than the polycrystalline model as also can be seen in Fig. 3.27. In Fig. 3.24, for the response with no circumferential stress (uniaxial ratcheting response), the modified Chaboche model is simulating the axial strain ratcheting and its rate well, whereas the polycrystalline model is simulating a compressive ratcheting, which is opposite to the experimental response. In Figs. 23 and 26, the simulations of the rate of ratcheting and its direction from the modified Chaboche model are in better agreement with the experimental responses than those from the polycrystalline model. The simulation of the axial stress-strain hysteresis loops by the modified Chaboche model (Figs. 23c, 26c) are in better agreement with the experimental loops (Figs. 23a, 26a) than the polycrystalline model (Figs. 23e, 26e). This seems to be the reason that the modified Chaboche model is simulating the axial and circumferential strain ratcheting better than the polycrystalline model in Figs. 23 and 26. However, a discrepancy observed between the experimental and simulated hysteresis loops is that the experimental loops show cyclic

hardening (thinning) during the initial few cycles and cyclic softening (broadening) during the following cycles (see Fig. 3.14b in Hassan and Kyriakides, 1994b), whereas, simulated loops from both models show persistent cyclic hardening. This discrepancy of the simulated loops may yield a wrong ratcheting direction as observed in Fig. 3.25 for the biaxial stress-controlled cycle under a low level of circumferential stress. In other words, the rate of circumferential strain ratcheting depends on both the direction of axial strain ratcheting and hysteresis loop size. Hence, any further improvement of the biaxial stress-controlled ratcheting simulation would require improved simulation of the hysteresis loops.

This speculation of improving biaxial stress-controlled ratcheting simulation is strengthened by the observation in Fig. 3.22 where under axial strain-controlled cycle and steady circumferential stress, the circumferential strain ratcheting rates are simulated quite well. To further examine the validity of this speculation, a simulation for the experimental response in Fig. 3.25 is performed by the modified Chaboche model by inputting the recorded axial strain peaks and a steady circumferential stress. The simulated responses are shown in Fig. 3.28 along with the experimental responses. Note in this figure that as the axial strain ratcheting-rate, direction and the hysteresis loop sizes are enforced, the simulated circumferential strain response matches the experimental response quite well (compare Figs. 28b to 28d). What is inferred from this controlled simulation is that improvement in the axial stress-strain hysteresis loop simulation of the modified Chaboche model would improve the circumferential strain-ratcheting simulation of the model. That means the observation of cyclic hardening (thinning of hysteresis loops) during the initial cycles and subsequent cyclic softening (broadening of hysteresis loops) under stress-controlled cycles, as shown in Fig. 3.15 in Hassan and Kyriakides (1994b), needed to be understood in order to improve the multiaxial ratcheting simulation of the modified Chaboche model. Similar comments are valid for the polycrystalline model, since this model simulated the biaxial strain-controlled circumferential ratcheting responses quite well as shown in Fig. 3.22.

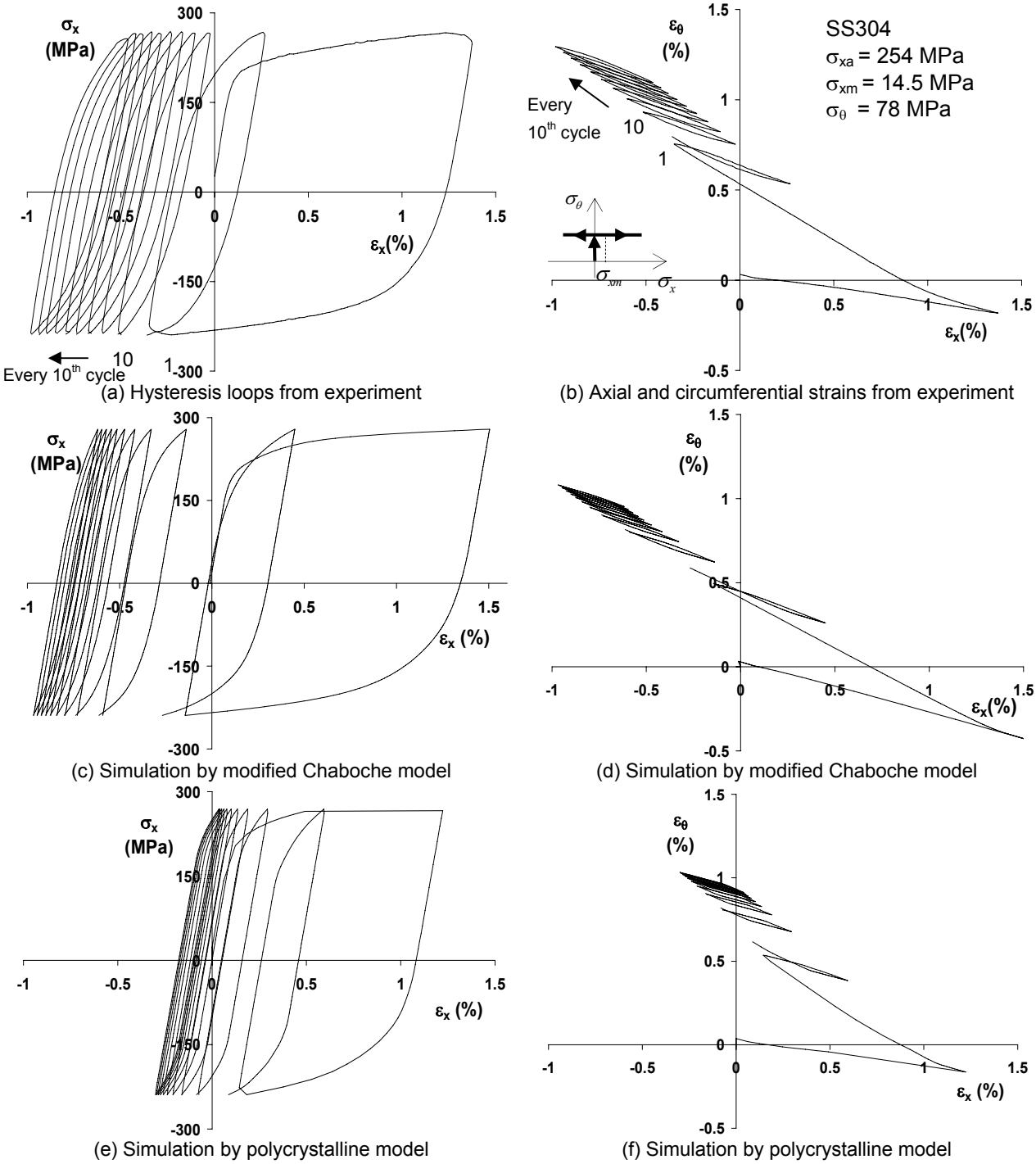

Fig. 3.23. Experimental and simulated responses for a biaxial stress-controlled cycle in the presence of a high level of circumferential stress. (Experimental responses from Hassan and Kyriakides, 1994b)

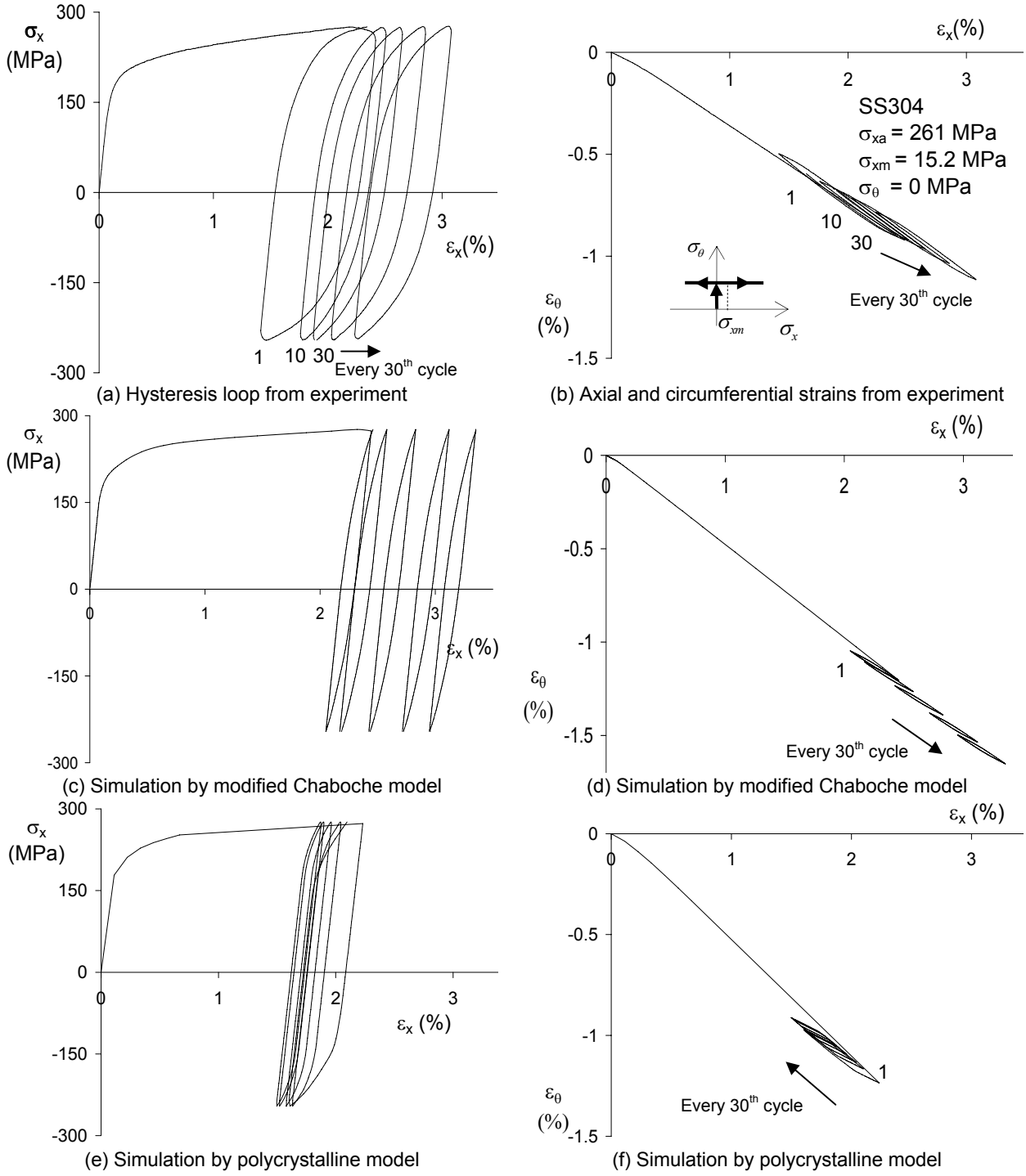

Fig. 3.24. Experimental and simulated responses under axial stress-controlled cycles with the same mean and amplitude stresses as the biaxial stress-controlled experiment in Fig. 3.23. (Experimental response from Hassan and Kyriakides, 1994b)

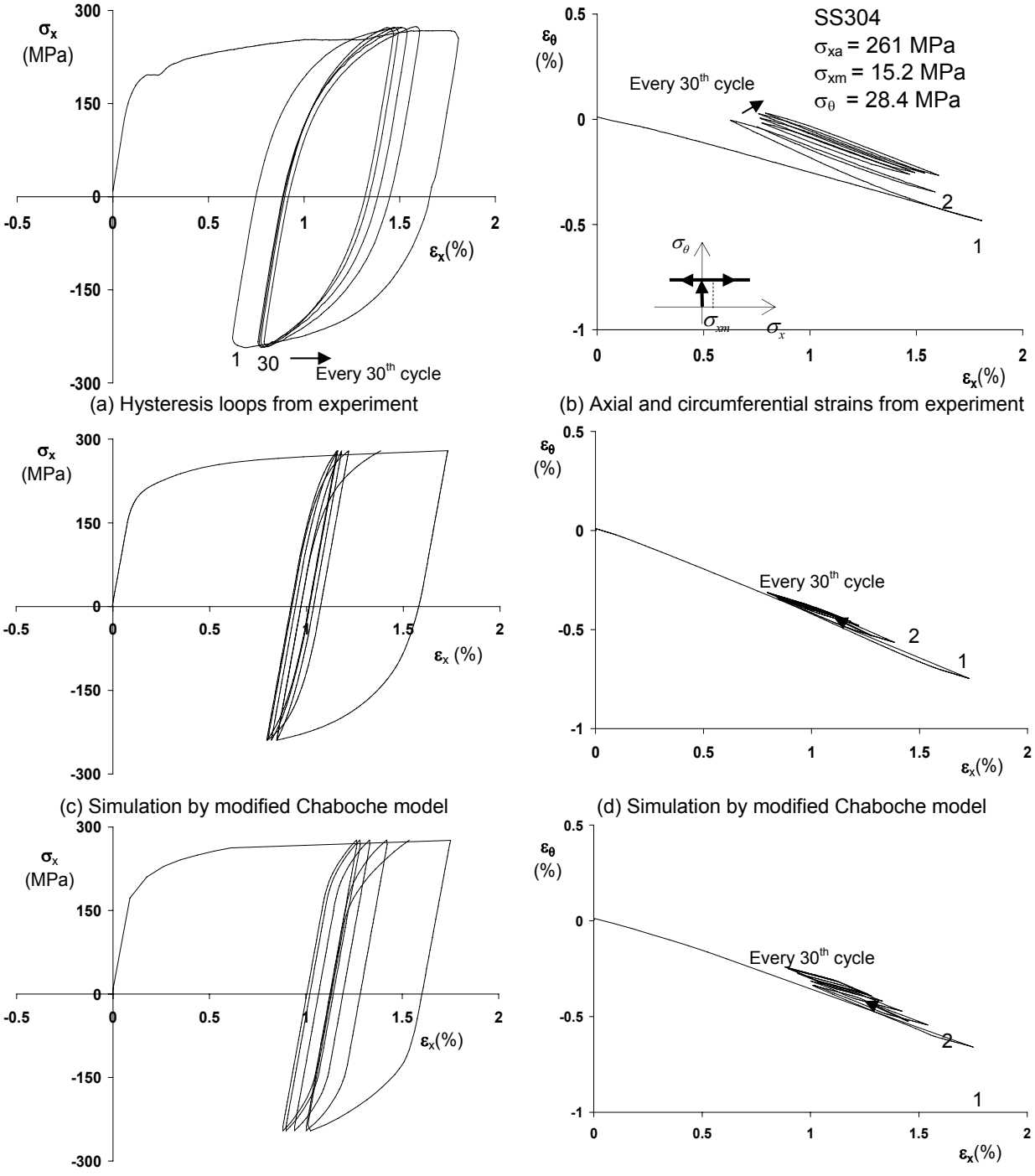

Fig. 3.25. Experimental and simulated responses for a biaxial stress-controlled cycle in the presence of a low level of circumferential stress. (Experimental response from Hassan and Kyriakides, 1994b)

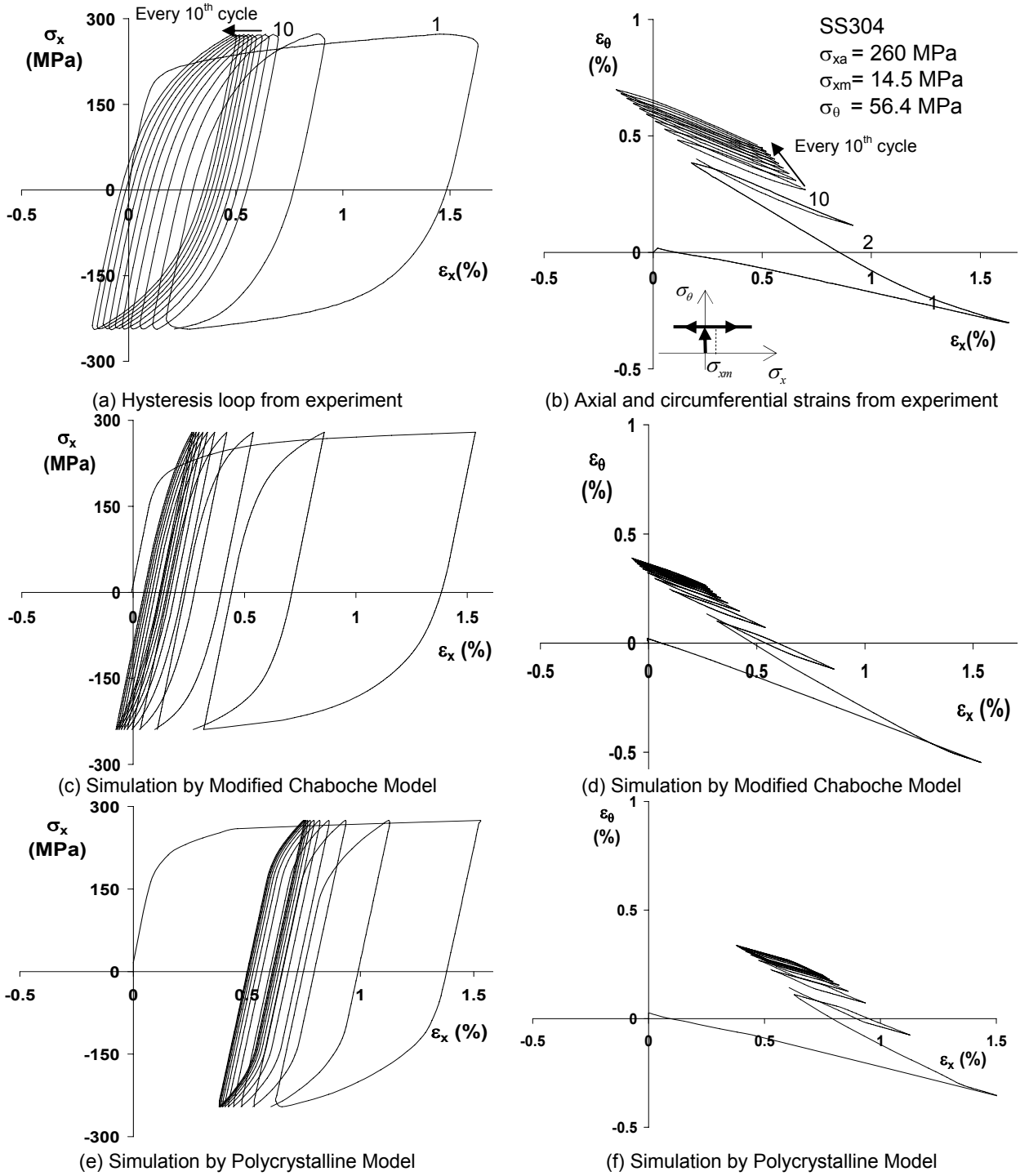

Fig. 3.26. Experimental and simulated responses for a biaxial stress-controlled cycle in the presence of a moderate level of circumferential stress. (Experimental responses from Hassan and Kyriakides, 1994b)

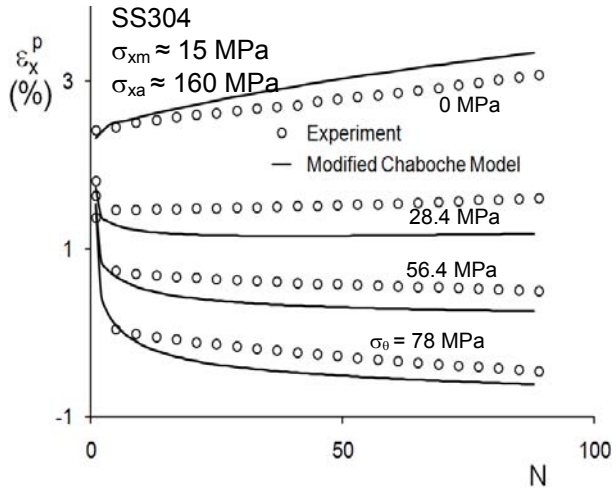

(a) Simulation by modified Chaboche model

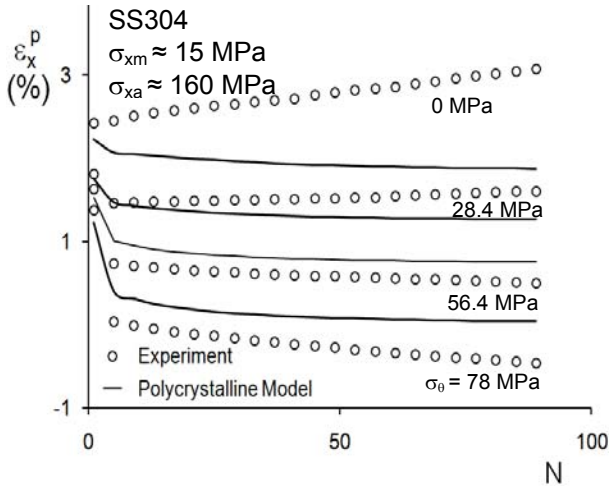

(b) Simulation by polycrystalline model

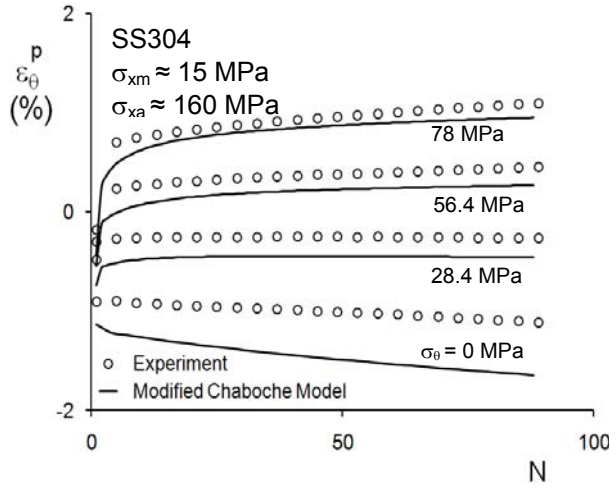

(c) Simulation by modified Chaboche model

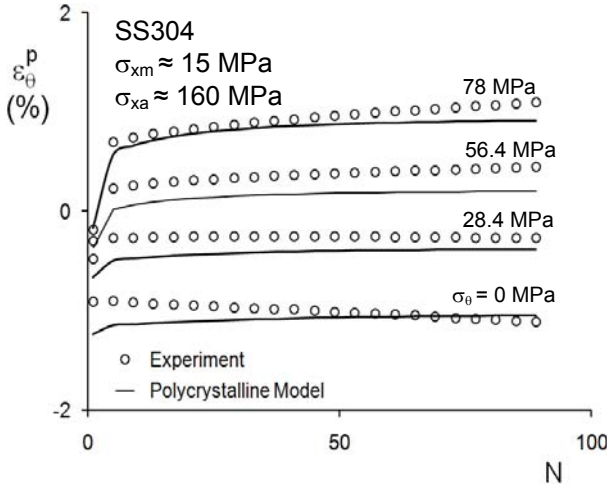

(d) Simulation by polycrystalline model

Fig. 3.27. Experimental and simulated responses under biaxial stress-controlled ratcheting cycles. (a,b) Axial ratcheting rates, (c,d) circumferential ratcheting rates. (experimental responses from Hassan and Kyriakides, 1994b)

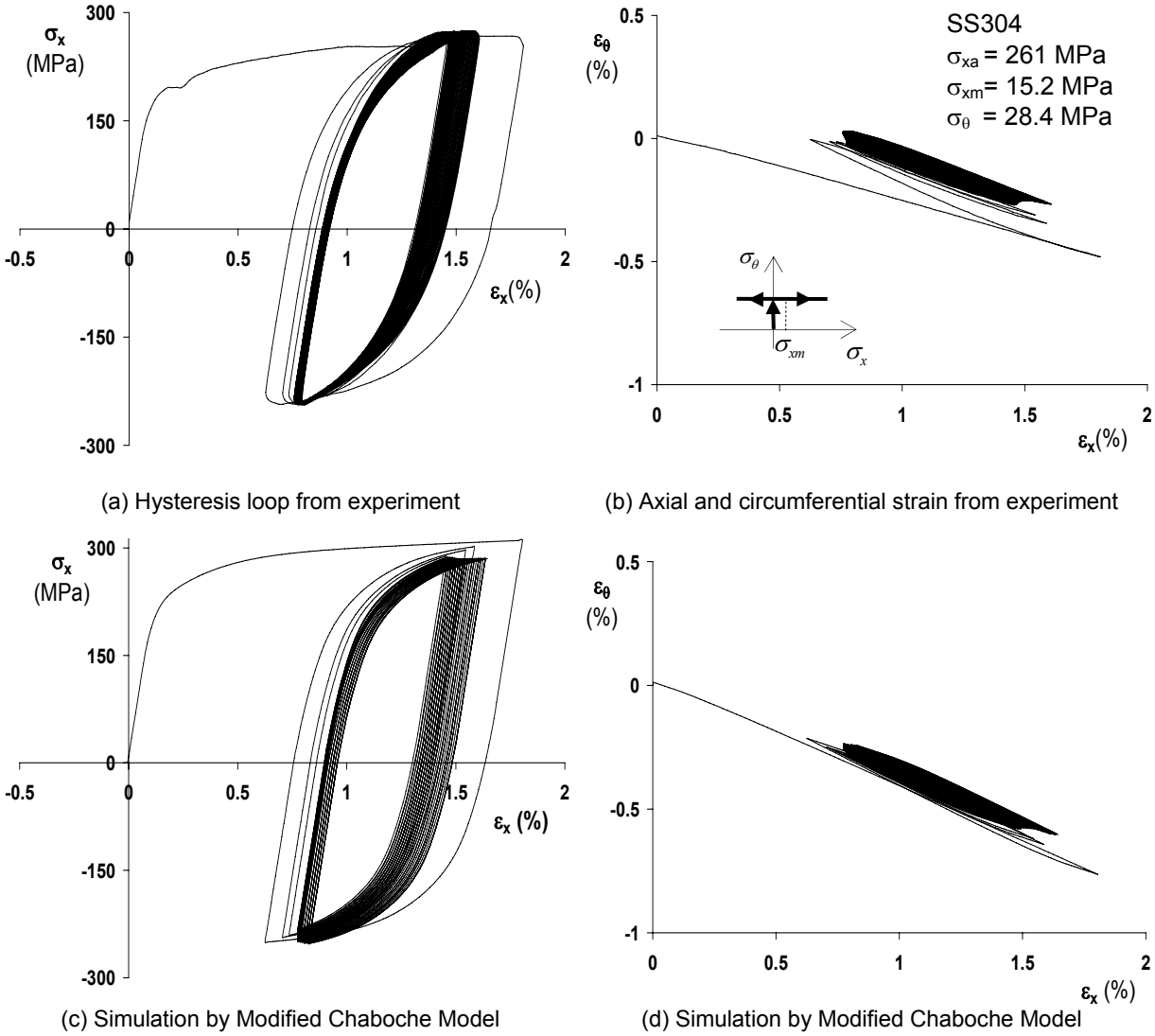

Fig. 3.28. (a, b) Experimental responses under biaxial stress-controlled cycle in the presence of low level internal pressure, and (c, d) corresponding simulations by inputting recorded strain peaks and steady circumferential stress. (experimental responses from Hassan and Kyriakides, 1994b)

3.4.5 Isotropic hardening rule for integrated simulation of monotonic and reversed hysteresis curves

Finally, a novel isotropic hardening rule (in Eqs. 2 and 13), which included a softening term to reduce the yield surface size from its initial size to the subsequent size of the first reversal, is proposed. Implementation of this isotropic hardening rule into a constitutive model allowed the use of a single set of model parameters to simulate both monotonic and cyclic responses, under uniaxial and biaxial loading cycles, with good accuracy. Validation of this novel modeling idea can be observed by comparison of the experimental and simulated responses in Fig. 3.15, 17, 19, 21, and 23-26, which show good simulations of the monotonic and reversal curves by each model. When the monotonic response involved a short yield plateau (see Fig. 3.15 and 19), the knee part of the monotonic curve is underpredicted, but the simulated curve catches up with the experimental curve quickly as the plastic strain increases.

3.5. Discussion and Conclusions

In search of a constitutive model that can simulate a broad set of cyclic and ratcheting responses of metallic materials, this paper scrutinized two recently proposed constitutive models. The ultimate goal of this search is to develop a robust constitutive model that can be implemented into finite element programs for low-cycle fatigue life analysis and design of safety-critical and expensive structures. Hence, two recent constitutive models which demonstrated success in simulating various cyclic and ratcheting responses are modified further in this study and evaluated against a broad set of uniaxial (proportional) and biaxial (nonproportional) responses of stainless steel 304 from Hassan and Kyriakides (1994a,b) and Hassan et al. (2008).

The first model evaluated is the rate-independent, macroscale (phenomenological) modified Chaboche model which was first proposed by Chaboche et al. (1979) and modified over the last three decades by Chaboche (1989, 1991), Bari and Hassan (2002), and Hassan et

al. (2008). Several novel features are developed and incorporated into the modified Chaboche model in this study. The second model evaluated is the rate-dependent crystalline (micro-scale) based model developed combining the proposed models of Cailletaud (1992), Cailletaud and Pilvin (1994) and Cailletaud and Saï (2008). For each model, the isotropic hardening rule is modified by adding a softening term in order to simulate both monotonic and reversal responses using one set of model parameters. The experimental responses used for evaluation of the models included several uniaxial strain-controlled responses, axial-torsional 90-degree out-of-phase strain-controlled response, a set of uniaxial ratcheting responses, a set of biaxial strain-controlled ratcheting responses and a set of biaxial stress-controlled ratcheting responses. Moreover, in order to evaluate the Tanaka (1994) nonproportional parameter incorporated in the modified Chaboche model, a set of nonproportional ratcheting responses from Hassan et al. (2008) is used.

The modelling features added to the Chaboche model are the isotropic hardening rule with a softening term (Eq. 2), a plastic strain surface with an evanescent term (Nouailhas et al., 1985), strain-range dependent cyclic hardening-softening using both the isotropic and kinematic hardening rule parameters, Tanaka (1994) nonproportional parameters, and finally a strain-range dependent multiaxial ratcheting parameter. The polycrystalline model, originally proposed by Cailletaud (1992) and later modified by Cailletaud and Pilvin (1994) and Cailletaud and Saï (2008), is evaluated in order to determine the simulation performance of the micro-scale model.

The uniaxial, strain-controlled responses of cyclic hardening, cyclic softening, cyclic relaxation, and hysteresis loop shapes (Figs. 15, 16 and 17) are simulated much better by the modified Chaboche model than the polycrystalline model. This success of the modified Chaboche model mainly relies on the improved simulation of the hysteresis loops because of the combined action of isotropic and kinematic hardening-rule parameters. For the nonproportional, axial-torsional 90-degree out-of-phase, strain-controlled cycles, the modified Chaboche model simulated the additional cyclic hardening very well, whereas the

polycrystalline model underpredicited the response (Fig. 3.18). The Tanaka (1994) nonproportional parameter in the modified Chaboche model is the main reason for this successful simulation. Another feature simulated well by the modified Chaboche model is the cyclic softening for the axial strain-controlled cycles prescribed immediately after the 90-degree out-of-phase cycles because of the memory feature in the Tanaka parameter (Step III in Fig. 3.18d). The Tanaka (1994) nonproportional parameter incorporated in the modified Chaboche model yielded very good ratcheting response simulations for a series of biaxial ratcheting responses (Fig. 3.12).

The Chaboche model simulated a series of uniaxial ratcheting responses reasonably well. The polycrystalline model, on the other hand, overpredicted the initial rate of ratcheting and underpredicted the stable rate of ratcheting because of its isotropic hardening feature. Both models fail to simulate the hysteresis loop shape and size of the uniaxial ratcheting experiments. For the modified Chaboche model, this drawback of the model can be improved by incorporating rate-dependence. In addition, it is noted that the threshold parameter $\overline{a}_4$ in the modified Chaboche model was added to improve its hysteresis loop shape simulation (Chaboche, 1991). This threshold parameter has no physical meaning; rather, it is an artificial approach of improving hysteresis loop shape and uniaxial ratcheting simulations (Bari and Hassan, 2000; Chaboche, 1991). Incorporation of a physically based backstress shift modeling feature into the modified Chaboche model improves the hysteresis curve and thus the uniaxial ratcheting simulations as will be demonstrated in Krishna and Hassan (2008).

The biaxial strain-controlled ratcheting responses are simulated very well by both the modified Chaboche and polycrystalline models, except that the cyclic hardening for these responses are overpredicted by the latter model. The biaxial stress-controlled ratcheting responses are also simulated reasonably by both models. However, as the modified Chaboche model simulated the axial hysteresis loops and ratcheting strain better than the polycrystalline model, the circumferential strain ratcheting simulation of the earlier model is also better than the latter model. Both models simulated cyclic hardening (thinning of the loops), whereas the

experimental loops show cyclic softening (broadening of the loops). This feature of cyclic softening (loop broadening) subsequent to cyclic hardening (loop thinning) under both the strain and stress-controlled cycles for SS304 is not well understood. Further improvement of the biaxial ratcheting simulation will require investigation of this phenomenon.

Overall, the performance of the modified Chaboche model in simulating a broad set of uniaxial and biaxial, cyclic and ratcheting responses is quite impressive. The performance of the polycrystalline model is reasonable under biaxial strain and stress-controlled cycles, but needs improvement for simulating uniaxial strain-controlled, uniaxial ratcheting and 90-degree out-of-phase cycles. The main drawback of this model seems to be the overpredcition of cyclic hardening due to the use of only isotropic hardening parameters for modeling cyclic hardening. This aspect of the model needs to be improved first in order to identify other modeling features needing improvement. For the modified Chaboche model, the feature of loop broadening (cyclic softening) under stress-controlled cycle versus loop thinning (cyclic hardening) under strain-controlled cycle needs improvement. The strain-range dependent cyclic hardening-softening improved this behavior for the uniaxial ratcheting responses, but not as much for the biaxial stress-controlled responses. In addition, the influence of the nonproportionality of loading on the multiaxial ratcheting parameter δ' needs to be understood. Further along the line, the constitutive models should be verified against experimental response for a large number of cycles (Jiang and Zhang, 2008). Finally, it is noted that the incorporation of the yield surface shape change into modeling would determine the need and influence of δ' parameter for simulating multiaxial ratcheting responses.

Acknowledgements

The financial support from the National Science Foundation (Award # DMR-0408910) and the Department of Civil, Construction and Environmental Engineering at North Carolina State University is gratefully acknowledged.

References

Abdeljaoued, D., Ben Naceur, I., Saï, K., Cailletaud, G., 2008. A new polycrystalline plasticity model to improve ratchetting strain prediction, Mechanics Research Communications, In Press, DOI: 10.1016/j.mechrescom.2008.09.012.

Armstrong, P.J., Frederick, C.O., 1966. A mathematical representation of the multiaxial bauschinger effect. CEGB Report No. RD/B/N 731, Berkely Nuclear Laboratories, Berkely,UK.

Aubin, V., Bulthé, A.-L., Degallaix, S., Quaegebeur, P., 2003. Ratchetting behavior of a duplex stainless steel: characterization and modeling. 9th International Conference on the Mechanical Behavior of Materials, 25-29 May 2003, Genève, Suisse.

Baltov, A., Sawczuk, A., 1965. A rule of anisotropic hardening. Acta. Mech., 1, 81-92

Bari, S., Hassan, T., 2000. Anatomy of coupled constitutive models for ratcheting simulation, Int. J. Plast., 16, 381-409.

Bari, S., Hassan, T., 2002. An advancement in cyclic plasticity modeling for multiaxial ratcheting simulation. Int. J. Plast., 18, 873-894.

Benallal, A., Marquis, D., 1987. Constitutive equations for nonproportional cyclic elasto-viscoplasticity. ASME J. Eng. Mater. Tech., 109, 326-336.

Benallal, A., Le Gallo, P., Marquis, D., 1989. An experimental investigation of cyclic hardening of 316 stainless steel and of 2024 aluminum alloy under multiaxial loading. Nucl. Eng. Des., 114, 345-353.

Berveiller, M., Zaoui, A., 1979. An extension of the self-consistent scheme to plastically-flowing polycrystals. J. Mech. Phys. Solids, 26, 325-344.

Besson, J., Foerch, R., 1997. Large scale object-oriented finite element code design, Comp. Meth. App. Mech. Eng., 142, 165-187.

Besson, J., Leriche, R., Foerch, R., Cailletaud, G., 1998. Object-oriented programming applied to the finite element method. Part II. Application to material behaviors. Revue Européenne des Éléments Finis 7-5, 567-588.

Burlet, H., Cailletaud, G., 1987. Modeling of cyclic plasticity in finite element codes. Proc. of 2nd Int. Conf. on Constitutive Laws for Engineering Materials: Theory and Applications, 1157-1164.

Cailletaud , G., 1992. A micromechanical approach to inelastic behavior of metals. Int. J. Plast., 8, 55-73.

Cailletaud, G., Pilvin, P., 1994. Utilisation de modèles polycristallins pour le calcul par éléments finis. Revue Européenne des Eléments Finis 3-4, 515-541.

Cailletaud, G., Saï, K., 1995. Study of plastic/viscoplastic models with various inelastic mechanisms. Int. J. Plast., 11, 991-1005.

Cailletaud, G., Saï, K., 2008. A polycrystalline model for the description of ratchetting: effect of intergranular and intragranular hardening, Mater. Sci. Eng. A, 480, 24-39.

Chaboche, J.L., Dang-Van, K., Cordier, G., 1979. Modelization of the strain memory effect on the cyclic hardening of 316 stainless steel. Proceedings of the 5th International Conference on SMiRT, Div. L, Berlin, Germany, L11/3.

Chaboche, J.L., 1986. Time-independent constitutive theories for cyclic plasticity. Int. J. Plast., 2, 149-188.

Chaboche, J.L., 1989. Constitutive equations for cyclic plasticity and cyclic viscoplasticity. Int. J. Plast., 5, 247-302.

Chaboche, J.L., 1991. On some modifications of kinematic hardening to improve the description of ratcheting effects. Int. J. Plast., 7, 661-678.

Chaboche, J.L., 2008. A review of some plasticity and viscoplasticity constitutive theories. Int. J. Plast., 24, 1642-1693.

Chen, X., Jiao, R., 2004. Modified kinematic hardening rule for multiaxial ratchetting prediction, Int. J. Plast., 20, 871-898.

Delobelle, P., 1993. Synthesis of the elastoviscoplastic behavior and modelization of an austenitic stainless steel over a large temperature range, under uniaxial and biaxial loading: Part I. Behavior. Int. J. Plast. 9, 65-85.

Delobelle, P., Robinet, P., Bocher, L., 1995. Experimental study and phenomenological modelization of ratcheting under uniaxial and biaxial loading on an austenitic stainless steel. Int. J. Plast., 11, 295-330.

Doong, S.H., Socie, D.F., 1990. Constitutive modeling of metals under nonproportional cyclic loading. J. of Engg. Matl. Tech., 113, 23-30.

Ellyin, F., Xia, Z., 1989. A rate-independent constitutive model for transient non-proportional loading. J. of the Mech. Phys of Solids, 37, 71-91.

Hassan, T., Kyriakides, S., 1992. Ratcheting in cyclic plasticity, part I: uniaxial behavior. Int. J. Plast., 8, 91-116.

Hassan, T., Corona, E., Kyriakides, S., 1992. Ratcheting in cyclic plasticity, part II: multiaxial behavior. Int. J. Plast., 8, 117-146.

Hassan, T., Kyriakides, S., 1994a. Ratcheting of cyclically hardening and softening materials, part I: uniaxial behavior. Int. J. Plast., 10, 149-184.

Hassan, T., Kyriakides, S., 1994b. Ratcheting of cyclically hardening and softening materials, part II: multiaxial behavior. Int. J. Plast., 10, 185-212.

Hassan, T., Taleb, L., Krishna, S., 2008. Influences of non-proportional loading paths on ratcheting responses and simulations by two recent cyclic plasticity models. Int. J. of Plast., 24, 1863-1889.

Haupt, P., Kamlah, M., 1995. Representation of cyclic hardening and softening properties using continuous variables. Int. J. Plast., 11, 267-291.

Hill, R., 1965. Continuum micro-mechanisms of elastoplastic polycrystals. J. Mech. Phys. Solids 13, 89-101.

Hlilou, A., Ben Naceur, I., Saï, K., Cailletaud, G., 2008. Generalization of the polycrystalline beta-model: finite element assessment and application to softening material behaviour. Submitted to Computational Materials Science.

Jiang, Y., Sehitoglu, H., 1996a. Modeling of cyclic ratcheting plasticity, part I: development of constitutive relations. ASME J. Appl. Mech., 63, 720-725.

Jiang, Y., Sehitoglu, H., 1996b . Modeling of cyclic ratcheting plasticity, part II: comparison of model simulations with experiments. ASME J. Appl. Mech., 63, 726-733.

Jiang, Y., Kurath, P., 1997. Nonproportional cyclic deformation: critical experiments and analytical modeling. Int. J. Plast., 13, 743-763.

Jiang, Y., Zhang, J., 2008. Benchmark experiments and characteristic cyclic plasticity deformation. Int. J. Plast., 24, 1481-1515.

Kanazawa, K., Miller, K.J., Brown, M.W., 1979. Cyclic deformation of 1% Cr-Mo-V steel under out-of-phase loads. Fatigue of Engg. Materials and Struct.,2, 217-222.

Kang, G. Z., Gao, Q., Cai, L.X., Yang, X.J., Sun,Y.F., 2002a. Experimental study on the uniaxial and nonproportionally multiaxial ratchetting of SS304 stainless steel at room and high temperatures. Nucl. Eng. Des., 216, 13-26.

Kang, G.Z., Gao, Q. ,Yang, X.J., 2002b. A visco-plastic constitutive model incorporated with cyclic hardening for uniaxial/multiaxial ratchetting of SS304 stainless steel at room temperature. Mech. Mater., 34, 521-531.

Kang, G.Z., Ohno, N., Akira, N., 2003. Constitutive modeling of strain range dependent cyclic hardening, Int. J. Plast., 19, 1801-1819.

Kang, G.Z., Gao, Q., Yang, X.J., 2004. Uniaxial and multiaxial ratchetting of SS304 stainless steel at room temperature: experiments and visco-plastic constitutive model, Int. J. Non-linear Mech., 39, 843-857.

Kang, G.Z., Li, Y.G., Gao, Q., 2005. Non-proportionally multiaxial ratcheting of cyclic hardening materials at elevated temperatures and its constitutive modeling, Mech. Mater.,37, 1101-1118.

Kang, G.Z., Kan, Q., Zhang, J., Sun, Y., 2006. Time-dependent ratcheting experiments of SS304 stainless steel. Int. J. Plast., 22, 858-894.

Krishna, S., Hassan, T., 2008. A novel backstress shift and time-dependence of the modified Chaboche model. In preparation.

Krempl, E., Lu, H., 1984. The hardening and rate-dependent behavior of fully annealed AISI type 304 stainless steel under biaxial in-phase and out-of-phase strain cycling at room temperature. J. of Engg. Mat. And Tech., 106, 376-382.

Kröner, E., 1961. Zur plastischen verformung des vielkristalls. Acta Metall. 9, 155-161.

Lamba, H.S., Sidebottom, O.M., 1978. Cyclic plasticity for nonproportional paths: part1 and 2-comparsion with predictions of three incremental plasticity models, J. of Engg. Mat. And Tech., 100, 96-111.

Landgraf, R.W., Morrow, J-.D., Endo, T., 1969. Determination of the cyclic stress-strain curve, Journal of Materials, JMLSA, 4, 176-188.

Marquis, D., 1979. Etude théorique et vérification expérimentale d'un modèle de plasticité cyclique. Thèse Paris VI .

Mayama, T., Sasaki, K., Ishikawa, H., 2004. Biaxial rachetting deformation of type 304 stainless steel: effect of memorization of back stress. Proc. Inst. Mech. Eng. Part C, J. Mech. Eng. Sci., 218, 901-908.

McDowell, D. L., 1985. A two surface model for transient nonproportional cyclic plasticity. ASME J. Appl. Mech., 52,298-308.

McDowell, D.L., 1987. An evaluation of recent developments in hardening and flow rules for rate-independent, nonproportional cyclic plasticity. ASME J. Appl. Mech., 54, 323-334.

McDowell, D.L., 1992. Nonlinear kinematic hardening theory for cyclic thermoplasticity and thermoviscoplasticity. Int. J. Plast., 8, 695-728.

McDowell, D.L., 2000. Modeling and experiments in plasticity. Int. J. Sol. Struct., 37, 293-309.

Méric, L., Poubanne, P., Cailletaud, G., 1991. Single crystal modeling for structural calculations. Part 1: Model presentation. J. of Engg. Mat. And Tech., 113, 162-170.

Molinari, A., 1999. Extensions of the self-consistent tangent model. Modelling Simul. Mater. Sci. Engng., 7, 683-697.

Moosbrugger, J.C., 1991. Some developments in the characterization of material hardening and rate sensitivity for cyclic viscoplasticity models. Int. J. Plast., 7, 405-431.

Moosbrugger, J.C., 1993. Experimental parameter estimation for nonproportional cyclic viscoplasticity: nonlinear kinematic hardening rules for two waspaloy microstructures at 650° C. Int. J. Plast., 9, 345-373.

Nouailhas , D., Cailletaud, G., Policella, H., Marquis, D., Dufaily, J., Lieurade, H.P., Ribes, A., Bollinger, E., 1985. On the description of cyclic hardening and initial cold working. Engg. Fracture Mech., 21,887-895.

Ohashi, Y., Kawai, M., Kaito, T., 1985. Inelastic behavior of type 316 stainless steel under multiaxial nonproportional cyclic stressings at elevated temperature. ASME J. of Eng. Mat. Tech., 107, 101-109.

Ohno, N., 1982. A constitutive model of cyclic plasticity with a nonhardening strain region. ASME J. Appl. Mech. 49, 721-727.

Ohno, N., 1990. Recent topics in constitutive modeling of cyclic plasticity and viscoplasticity. Appl. Mech. Rev., 43, 283-295.

Portier,L., Calloch, S., Marquis,D., Geyer, P., 2000. Ratchetting under tension-torsion loadings: experiments and modelling. Int. J. Plast., 16, 303-335.

Rahman, S. M., Hassan, T., Ranjithan, R. S., 2005. Automated parameter determination of advanced constitutive models. ASME Pressure Vessels Piping Div. Publ. PVP, 2,261-272.

Rahman, S.M., Hassan, T., Corona, E., 2008, Evaluation of cyclic plasticity models in ratcheting simulations of straight pipes under cyclic bending and steady internal pressure. Int. J. Plast., 24,1756-1791.

Saï, K., Cailletaud, G., 2007. Multi-mechanism models for the description of ratchetting: effect of the scale transition rule and of the coupling between hardening variables. Int. J. Plast., 23, 1589-1617.

Seyed-Ranjbari, M., 1986. Further development, multiaxial formulation, and implementation of the bounding surface plasticity model for metals, PhD dissertation, University of California, Davis.

Takahashi, Y., Ogata, T., 1991. Description of nonproportional cyclic plasticity of stainless steel by a two surface model. ASME J. of App. Mech., 58, 623-630.

Taleb, L., Cailletaud, G., Blaj, L., 2006. Numerical simulation of complex ratcheting tests with a multi-mechanism model type. Int. J. Plast., 22, 724-753.

Tanaka,E., Murukami, S., Ooka, M., 1985a. Effect of strain path shapes on non-proportional cyclic plasticity. J. Mech. Phys. Solids, 33, 559-575.

Tanaka,E., Murukami, S., Ooka, M., 1985b. Effect of plastic strain amplitudes on non-proportional cyclic plasticity. Acta Mech., 57, 167-182.

Tanaka, E., Okuchi, H., 1988. Constitutive modelling of viscoplasticity incorporating non-proportional hardening effects. Trans. of the Japan society of Mech. Engg., 54, 1588-1596.

Tanaka, E., 1994 . A nonproportionality parameter and a cyclic viscoplastic constitutive model taking into account amplitude dependences and memory effects of isotropic hardening. Eur. J. Mech., A/Solids, 13, 155-173.

Zhang, J., Jiang, Y., 2008. Constitutive modeling of cyclic plasticity deformation of a pure polycrystalline copper. Int. J. Plast., 24, 1890-1915.

CHAPTER 4
A Novel Backstress Shift and Time-Dependence of the Modified Chaboche Model

Abstract

Hassan et al. [2008] and Krishna et al. [2009] have demonstrated successes and challenges in simulating a broad set of proportional and nonproportional, strain and stress-controlled cyclic plasticity responses using the modified Chaboche model. The major drawbacks identified from these studies were that the hysteresis loop shape and width were not simulated well. The first reason identified for the simulation deficiencies was the lack of time-dependence (visco-effect) of the model. The second reason for the deficiencies was identified to be the evolution of kinematic hardening rule variables which represent cyclic hardening/softening and ratcheting responses. Detailed accounts on the influence of these variables are presented in the paper. An observation is made that the initial hysteresis loops obtained under strain and stress-controlled cycles match closely when they are shifted along the stress and strain directions to start at the same point. This observation is instrumental in improving the uniaxial hysteresis curve shape and ratcheting response simulations significantly through introducing a novel modeling concept of "backstress shift." The backstress shift modeling concept also gives a physical meaning to the threshold modeling concept of Chaboche [1991]. The evolutions of the kinematic hardening variables, the novel back-stress shift modeling concept, and finally the time-dependent modeling are discussed in detail in order to enumerate their influences on improving the cyclic and ratcheting response simulations. These modifications to the Chaboche cyclic viscoplasticity model however introduce a large number of parameters and thereby make the parameter determination complex. Hence, ideas of parameter identification steps and determining the parameters using a genetic algorithm scheme also are presented.

Keywords: Cyclic plasticity, viscoplasticity, cyclic hardening, cyclic softening, ratcheting, nonlinear kinematic hardening.

4.1 Introduction

The need for robust constitutive models is gaining importance for prediction of low cycle fatigue life of structures and components accurately. This accuracy is achieved by capturing the various features of cyclic plasticity and thereby describing the stress-strain response of materials under a broad set of experimental responses. Efforts were undertaken towards the search of an advanced constitutive model in previous papers by Hassan et al. (2008) and Krishna et al. (2009). A detailed study was carried out by incorporating several features of cyclic plasticity, namely strain-range dependent cyclic hardening/ softening, subsequent cyclic softening, cross hardening and memory features of nonproportional loading, into the modified Chaboche model (Bari and Hassan, 2002; Hassan et al., 2008; Krishna et al., 2009). Inclusion of these advanced features enhanced the simulation capability for a broader range of cyclic plasticity responses, hence increasing its robustness.

Bari and Hassan (2002) proposed the improved kinematic hardening rule by incorporating a multiaxial parameter δ' to the Chaboche model to improve the multiaxial simulation of stabilized material. The improved model simulates a broad set of cyclic plasticity responses well. However, the model performed well for a stabilized material only. Therefore, the next step was to develop the model for cyclic hardening/softening material. Efforts were undertaken in the earlier papers (Hassan et al., 2008 and Krishna et al., 2009) to model strain-range dependent cyclic hardening/softening behavior. A detailed study of nonproportionality and its effect on ratcheting was also carried out. Strain-range dependent kinematic and isotropic hardening rule parameters were incorporated along with nonproportionality parameter of Benallal and Marquis, 1987 and Tanaka, 1994 to demonstrate good simulation of stress-strain responses. A broad set of experimental responses, which include various nonproportional stress-controlled loading paths with the

same mean and equivalent amplitude stresses, as discussed in Hassan et al. (2008), was used to validate the model developed. Along with this, several uniaxial stress-controlled and biaxial strain and stress-controlled experiments from Hassan and Kyriakides (1994a, b) were also used to validate the developed model. The newly improved model has demonstrated successes in simulating a broad range of cyclic and ratcheting experimental responses with great accuracy.

These models demonstrated that the success in modeling the experimental response depends on the hysteresis loop shape simulation. However, the model developed failed to simulate the hysteresis loop shape and size well. This drawback was mainly as a result of lack of time-dependence. The strain accumulation with cycles and its rate was simulated up to a great accuracy. However, the shape of hysteresis loops suffered both for the uniaxial and biaxial stress-controlled experimental responses. Hysteresis loop width was not simulated well because of rounding nature of the loops at the stress peaks and valleys. This rounding nature is as a result of time-dependence or viscous effect (Hassan et al., 2008; Krishna et al., 2009) which was not addressed in the model. Also, other areas of improvement for the modified Chaboche model were on the features of loop broadening under stress-controlled cycles and loop thinning under strain-controlled cycles.

Addressing this major issue of improving the hysteresis loop shape and size is the main objective of the paper. Hysteresis loop shape is a function of kinematic and isotropic hardening rule parameters. Hence the paper first tries to understand the evolution of kinematic and isotropic hardening features and their effect on hysteresis loop shape. Again, cyclic hardening/softening is a manifestation of change of yield surface and the change of plastic modulus (Marquis, 1979; Chaboche 1989; Portier et al., 2000; Kang et al., 2003; Hassan et al., 2008; Krishna et al., 2009). These changes in yield surface and plastic modulus can be brought by the evolution of kinematic and isotropic hardening features. Understanding these features requires a detailed analysis of the parameters and their evolution as a function of plastic strain. Also, it is more important to note which parameters have more effect in

producing cyclic hardening and thereby assess the significance of each term. Hence the first part of the paper discusses the evolution of the kinematic and isotropic hardening rule parameters. Also, the initial modeling approach included only the evolution of isotropic hardening rule parameters (Chaboche et al., 1979; Chaboche 1986; Benallal and Marquis, 1987; Tanaka, 1994; Jiang and Sehitoglu, 1996a,b; Kang et al., 2002a,b). This approach could simulate the peak stresses very well but failed to simulate the hysteresis curve reasonably (see Krishna et al., 2009 for more details). Hence to better simulate the hysteresis curve, the evolution of kinematic hardening parameters have to be considered along with the isotropic hardening parameters. Krishna et al. (2009) demonstrated the simultaneous evolution of both the isotropic and kinematic hardening feature but didn't discuss their evolution and significance in detail. Hence, this paper elaborates the physical significance of each term and thereby their roles in modeling the hysteresis loop shape.

Next, the paper brings forth a novel idea of backstress shift parameter for simulating the stress-strain response. It was demonstrated in Krishna et al. (2009) that the modified Chaboche model simulated the uniaxial ratcheting responses well. However, the model fails to simulate the hysteresis loop shape and size well. In order to improve the hysteresis loop shape and ratcheting simulation, a threshold parameter $\overline{a}_4$ was added in the kinematic hardening rule (Chaboche, 1991). This threshold parameter has no physical significance. It is an artificial approach, undertaken to improve the uniaxial ratcheting simulations (Chaboche, 199; Bari and Hassan, 2002). Hence, this paper brings a novel idea of incorporation of physically based backstress shift modeling feature into the modified Chaboche model. It not only shows the improvement of the hysteresis curve shape but also improves the uniaxial ratcheting simulation significantly.

Finally, as noted in Hassan et al., (2008) and Krishna et al. (2009), the experimental hysteresis loop shape showed rounding at the peak stresses and valleys in the stress-controlled experimental responses. This rounding effect is as a result of time dependence or the viscous effect of stainless steel (Rugges and Krempl, 1989). Also, it was demonstrated by

Krempl (1979) that the inelastic behavior of SS304 has strong rate sensitivity even at room temperature. The influence of time-dependence on ratcheting was studied in great detail by Chaboche and Rousselier 1983; Chaboche, 1989, 2008; Ruggles and Krempl, 1990; McDowell, 1992; Moosbrugger 1991, 1993; Kang 2004, 2006 and several others over the last two decades. Under stress-controlled histories, the influence of time-dependence can be observed on ratcheting rate (Yoshida, 1990, Kang, 2006 etc.) and also on the shape and sizes of hysteresis loops (Kang, 2004). Again, the peak stress of a strain-controlled experiment depends on the rate of the loading (Chaboche, 1989), which also gives the hysteresis loops shape. The solution to all these observations can be achieved by the incorporation of time dependence in the constitutive modeling. The paper elucidates the incorporation of the time-dependence in the model by a unified approach and shows promise of improvement of hysteresis loop and thereby ratcheting simulation.

Finally, the paper brings together the several complexities involved with hysteresis loop shape, threshold incorporation and the rate dependence. It brings forth a robust unified approach of constitutive modeling of cyclic plasticity responses. Again, the paper is restricted to uniaxial strain and stress-controlled experimental responses from Hassan and Kyriakides, 1994a and b. A detailed discussion of hysteresis loop shape and size improvement is discussed in detail in the following sections. These steps of model development will lead towards the computation of low cycle fatigue life of structures and components and towards a robust constitutive model for cyclic plasticity.

4.2. Constitutive Modeling

The modified Chaboche model developed by Hassan et al. (2008) and Krishna et al. (2009) is robust in capturing various cyclic plasticity responses but fails to simulate the hysteresis loop shape and size reasonably. A loop shape and size simulation depends on the kinematic and isotropic hardening rule evolutions. Incorporation of these evolutions into the

constitutive models is carried out through either the time-independent or the time-dependent framework. Decision of which framework to implement for simulations usually depends on the rate of loading and temperature ranges. It is demonstrated in this paper that improving the simulations of SS304 hysteresis loops obtained at room-temperature under quasi-static loading require rate-dependent modeling features. Several time independent and dependent modeling features of the modified Chaboche model are presented in the paper.

4.2.1 Time-Independent Modified Chaboche Model

The primary features of the rate-independent modified Chaboche model (Chaboche et al., 1979; Chaboche, 1986, 1989, 1991; Bari and Hassan, 2002; Hassan et al., 2008 and Krishna et.al., 2009) included the yield criterion, strain decomposition, elastic and plastic incremental relations, as summarized below.

i. Yield criterion:

$$f(\underline{\sigma}-\underline{\alpha})=\left[\frac{3}{2}\left(\underline{s}-\underline{a}\right)\cdot\left(\underline{s}-\underline{a}\right)\right]^{1/2}-\sigma_0-R(p,q)=0, \tag{1}$$

ii. additive strain-increment decomposition:

$$d\underline{\varepsilon}=d\underline{\varepsilon}^{e}+d\underline{\varepsilon}^{p}, \tag{2}$$

$$d\underline{\varepsilon}^{e}=\frac{1+\nu}{E}d\underline{\sigma}-\frac{\nu}{E}tr(d\underline{\sigma})\underline{I}, \tag{2a}$$

$$d\underline{\varepsilon}^{p}=d\lambda\frac{\partial f}{\partial\underline{\sigma}}=\frac{3}{2}dp\frac{\underline{s}-\underline{\mathrm{a}}}{\sigma_0+R}, \tag{2b}$$

where, $\underline{\sigma}$ is the stress tensor, $\underline{\alpha}$ is the current center of the yield surface in the total stress space, $\underline{s}$ is the deviatoric stress tensor, $\underline{a}$ is the current yield surface center in the deviatoric space, σ_0 is the initial size of the yield surface, R is the drag resistance (initial value is zero for virgin material), which represents the isotropic hardening variable as a function of the accumulated plastic strain p and the size of the plastic strain surface q, $d\underline{\varepsilon}^{e}$ is the incremental

elastic strain tensor, $d\underline{\varepsilon}^p$ is the incremental plastic strain tensor, E is elastic modulus and ν the Poisson's ratio, $d\lambda$ is a plastic multiplier determined by the consistency condition, and dp is the magnitude of the plastic strain increment given by $dp = \left| d\underline{\varepsilon}^p \right| = \left[\frac{2}{3} d\underline{\varepsilon}^p \bullet d\underline{\varepsilon}^p \right]^{1/2}$.

The nonlinear kinematic hardening rule of a coupled model is the most important feature because of its influence on the evolutions of yield criteria, cyclic hardening/softening and ratcheting responses (Bari and Hassan, 2000, 2001, 2002; Hassan et al., 2008 and Krishna et al., 2009). The kinematic hardening rule is obtained by superposing four different Armstrong-Frederick type rules (Armstrong and Frederick, 1966, Bari and Hassan, 2002) in the following form, which simulates a broad set of cyclic responses very well:

$$d\underline{a} = \sum_{i=1}^{4} d\underline{a}_i \,, \tag{3}$$

$$d\underline{a}_i = \frac{2}{3} C_i d\underline{\varepsilon}^p - \gamma_i \left\{ \underline{a}_i \delta' + (1-\delta')(\underline{a}_i \bullet \underline{n})\underline{n} \right\} dp \,, \qquad \text{for } i = 1, 2, 3 \tag{3a}$$

$$d\underline{a}_i = \frac{2}{3} C_i d\underline{\varepsilon}^p - \gamma_i \left\{ \underline{a}_i \delta'(q) + (1-\delta')(\underline{a}_i \bullet \underline{n})\underline{n} \right\} \left\langle 1 - \frac{\overline{a}_4}{f(\underline{\alpha}_i)} \right\rangle dp \,, \qquad \text{for } i = 4 \tag{3b}$$

$C_{1\text{-}4}$, $\gamma_{1\text{-}4}$, δ', $\overline{a}_4$ are kinematic hardening rule parameters (Bari and Hassan 2002). A detailed description of these parameters and their evolution with respect to loading nonproportionality, strain-range dependence and plastic strain accumulation is discussed in Krishna et al. (2009).

4.2.2 Evolution of Kinematic and Isotropic Hardening Parameters

Hysteresis loop shape is a function of kinematic and isotropic hardening parameters and their evolution as demonstrated in Krishna et al. (2009). These parameters are a function of strain-range, nonproportionality of loading, and also rate and temperature effects (Chaboche, 1989; McDowell 1992; Tanaka, 1994). Evolution of these parameters brings the cyclic hardening or softening in the material response (see details in Krishna et al., 2009). However, a detailed study of these kinematic and isotropic hardening rule parameters and their evolution was not discussed. Therefore, a detailed study is essential to correlate the cyclic

hardening/ softening of the material with evolution of isotropic hardening and kinematic hardening rule parameters.

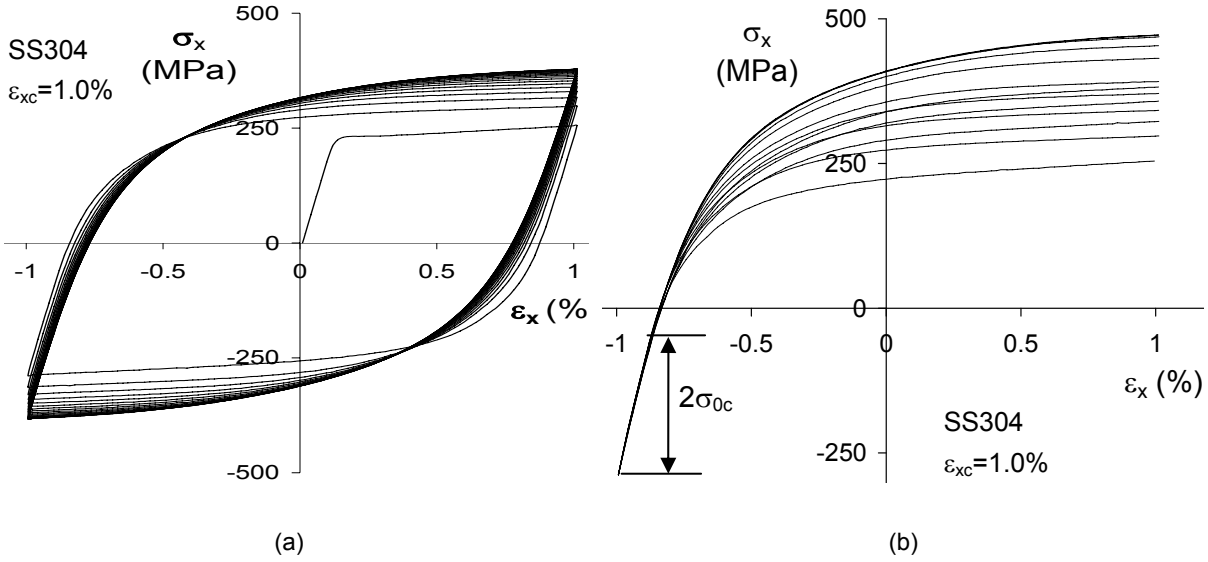

Fig. 4.1. (a) Hysteresis loops from an axial, strain-controlled experiment (Hassan and Kyriakides, 1994a), and (b) rising curves from uniaxial strain-controlled 1.0% strain-controlled loop shifted to a common starting point showing the variation of linear elastic part.

The evolution of isotropic hardening parameters can be demonstrated by change of linear elastic range of stress reversal curves. The evolution of the kinematic hardening parameters changes the plastic modulus and hence again causes the cyclic hardening and softening (see Eq.6 in Bari and Hassan, 2000). To better understand the evolution of the kinematic and isotropic hardening parameters, a cyclic hardening strain-controlled experimental response is taken. Several rising curves of 1.0% strain-controlled experiment were shifted and brought to same common point as shown in Fig. 4.1b. Several rising curves of 1.0% strain-controlled loop where brought to the starting point of the first rising curve of the experiment. The rising curves, when brought to the same reference point, show the variation of the linear elastic

range. On close observation, the change of the yield size is minimal or small for this particular strain-controlled cyclic hardening material response (data from Hassan and Kyriakides, 1994a). This also shows that modeling of cyclic hardening by the evolution of isotropic hardening parameters (i.e. change of yield surface size only) will fail to describe the hysteresis curve shapes reasonably. Hence, change of plastic modulus is essential to better simulate the hysteresis curves shape. This change of plastic modulus can be brought by the evolution of kinematic hardening parameters (C_i's and γ_i's in Eq. 3).

The exact nature of their evolution is unpredicted in the past research. Chaboche (1989) had mentioned that evolution of C_i's and/or γ_i's can be considered as function of plastic strain. Moosbrugger (1991) used the first option while Marquis (1979) and Rousselier (1985) had used the latter option. But a detailed analysis of their development is not shown. Also, their exact variation is also not clear from their analysis.

Hence, to demonstrate the evolution of kinematic hardening parameters, the rising curves of a strain-controlled experiment are plotted against plastic strain as shown in Fig. 4.2. The total plastic strain range is divided into four zones. The first zone is at 1% of the total strain range and marked as $\Delta\varepsilon^p_1$. Similarly, the second zone is at 15% of the total strain range and marked as $\Delta\varepsilon^p_2$. The strain range, $\Delta\varepsilon^p_4$ for the fourth zone is the region of constant slope at the end. The remainder is the zone three. These zones are indicated as $\Delta\varepsilon^p_1$, $\Delta\varepsilon^p_2$, $\Delta\varepsilon^p_3$, $\Delta\varepsilon^p_4$ respectively in Fig.2. The corresponding stress ranges between these zones are denoted by $\Delta\sigma_1$, $\Delta\sigma_2$, $\Delta\sigma_3$, $\Delta\sigma_4$ respectively. The slope at the beginning of three initial zones gives the value of C_1, C_4, and C_2 respectively. C_3 is calculated from the linear slope at the end of each rising curve. This gives the value of initial plastic modulus for each curve at the specified zones and hence its variation with the plastic strain accumulation. The variation of C_3 is very small as seen from the thick lines in Fig. 4.2 (i.e. the slope remains constant with the rising curves). The variation of C_2 and C_4 is significant in the rising curves. C_1 is a large value and is constant as seen in Fig. 4.2.

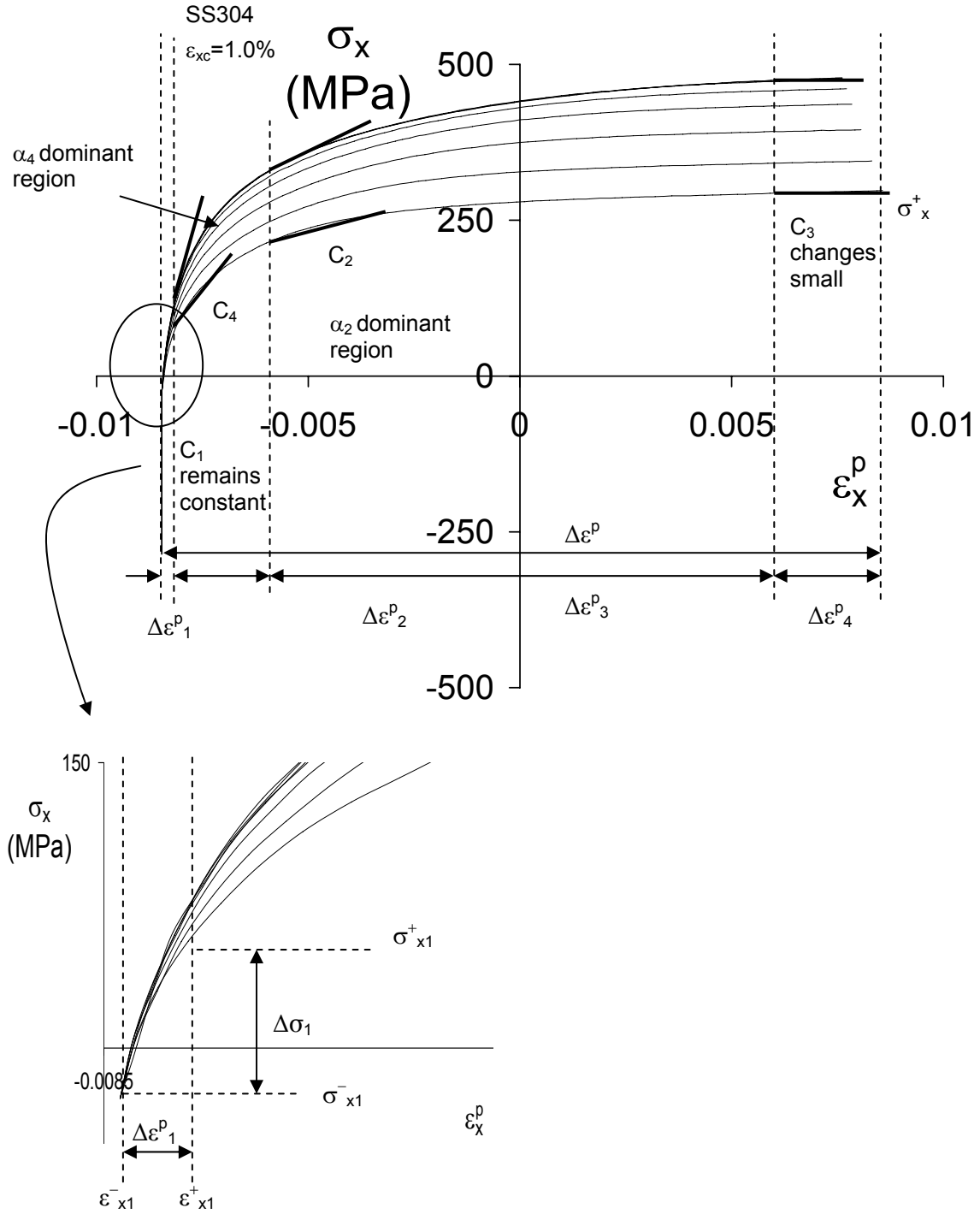

Fig. 4.2. The variation of the C's with the plastic strain and with the hystersis curve

This also shows that the value of the plastic modulus cannot be kept constant while modeling the cyclic hardening/softening. Nevertheless, not all values change with the plastic strain accumulation and it depends on the material characteristics obtained from material responses.

Similarly, the rising curves are again considered in order to understand the variation of kinematic hardening rule parameters, γ_i's. Each of the rising hysteresis curves can be written as: $\sigma_x = \sum_{i=1}^{4} \alpha_i + \sigma_0$, where α_i is the backstress component given by:

$$\alpha_i = \frac{C_i}{\gamma_i}\left[1 - 2\exp\left\{-\gamma_i\left(\varepsilon_x^p - \left(-\varepsilon_L^p\right)\right)\right\}\right].$$

These rising curves are of reasonable strain limit ($\pm\varepsilon_L^p$=0.85%) which ensures that all, except the third slightly nonlinear kinematic hardening variables get stabilized within the strain limit. In other words, the total stress range will be equal to stabilized values of backstresses and yield stress and given by:

$$\Delta\sigma = \sigma_x^+ - \sigma_x^- = 2\left\{\frac{C_1}{\gamma_1} + \frac{C_2}{\gamma_2} + \frac{C_4}{\gamma_4} + C_3\left(\varepsilon_x^p - \left(-\varepsilon_L^p\right)\right) + \sigma_0\right\}.$$

Again, the total peak to peak stress range ($\Delta\sigma_i = \sigma_{xi}^+ - \sigma_{xi}^-$) of each zone can be considered for the initial γ_1, γ_2, γ_3, γ_4 parameters, where σ_{xi}^+ and σ_{xi}^- are the positive and negative peaks of each of the zones respectively. Again, the value of γ_3 is considered zero, which gives the backstress component α_3 as linear hardening rule. Thus, the initial values of γ_1, γ_2 and γ_4 can be estimated based on the stabilization of the decomposed back stresses α_1, α_2, α_4 within the above mentioned zones of the peak stress range. The procedure is followed backward as γ_2 is obtained first and γ_4 and γ_1 at the end. Hence the kinematic variables γ_2, γ_4 and γ_1 are obtained consecutively using:

$$\frac{2C_2}{\gamma_2} = \left(\Delta\sigma_2 - C_3 * \left(\Delta\varepsilon_3^p\right)\right) \qquad (4a)$$

$$\frac{2C_4}{\gamma_4} = \left(\Delta\sigma_4 - C_3 * \left(\Delta\varepsilon_4^p \right) - \frac{C_2}{\gamma_2} * \left(1 - \exp \gamma_2 * \left(\Delta\varepsilon_4^p \right) \right) \right) \quad (4b)$$

$$\frac{2C_1}{\gamma_1} = \left(\Delta\sigma_1 - C_3 * \Delta\varepsilon_1^p - \frac{C_2}{\gamma_2} * \left(1 - \exp\left(\gamma_2 * \Delta\varepsilon_1^p \right) \right) - \frac{C_4}{\gamma_4} * \left(1 - \exp\left(\gamma_4 * \Delta\varepsilon_1^p \right) \right) \right) \quad (4c)$$

where $\Delta\sigma_i$ and $\Delta\varepsilon_i^p$ represent the values of the peak to peak stress and strain range for each zone as seen in the Fig. 4.2. Calculating the values backwards takes care of the effect of the subsequent backstresses. Choosing this form of calculation comes from the decomposed rules of the back stresses with three nonlinear kinematic and one linear kinematic hardening rules (i.e. γ_3=0) as mentioned in Bari and Hassan, 2000.

Once the parameters are obtained for each rising curve, they are plotted against the plastic strain accumulation as shown in Fig. 4.3a and b. As mentioned before, the terms C_1 and C_3 are kept constant and γ_3 is kept zero. Observing the trends of the kinematic variables in Fig. 4.3b, the parameters γ_2 and γ_4 can also be kept constant. Hence, the cyclic hardening can be modeled for this experimental response by considering just the variation of C_2 and C_4 and γ_1. The experimental trends for C_2 and C_4 and γ_1 can be modeled by a concave exponential curve and a convex exponential curve respectively to best fit the experimental results. This gives the evolution rules of the kinematic hardening variables C_2, C_4 and γ_1 as follows:

$$dC_i = D_{C_i}\left[C_i^{AS}(q) - C_i \right] dp, \qquad \text{for } i = 2 \text{ and } 4 \quad (5a)$$

$$d\gamma_i = D_{\gamma i}\left[\gamma_i^{AS}(q) - \gamma_i \right] dp, \qquad \text{for } i = 1 \quad (5b)$$

Additionally, the isotropic evolution of the parameter (i.e. change in the linear elastic part of each upgoing curve) is given by

$$dR = D_R\left[R^S(q) - R_i \right] dp, \quad (5c)$$

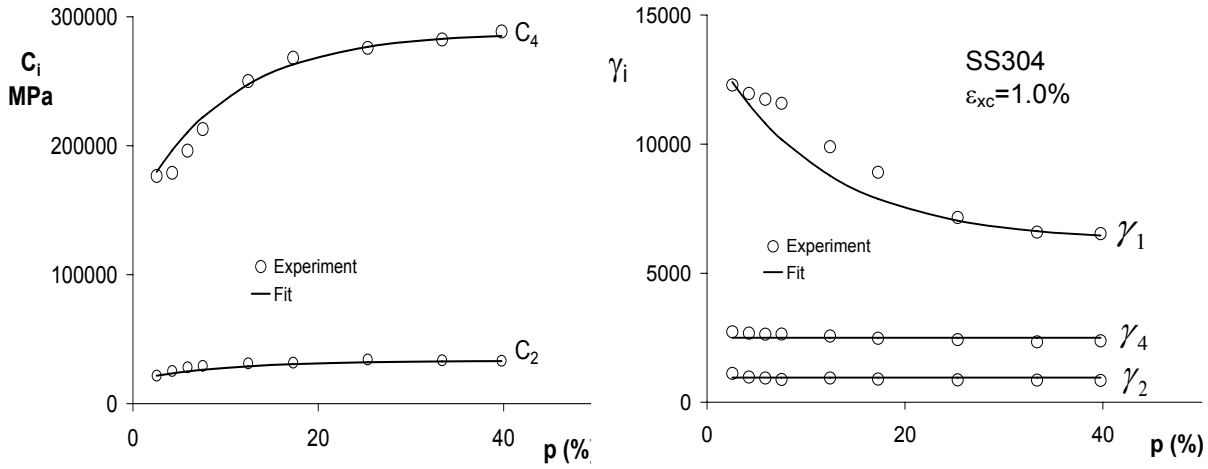

(a) Variation of Ci's with *p*

(b) Variation of γ_i's with *p*

Fig. 4.3. Illustration of the C_i and γ_i variations as a function of strain accumulation *p* and their fit

This gives the evolution of the kinematic and isotropic hardening rule parameters. The philosophy can be used for any experimental response, showing the necessity of considering the evolution of the kinematic hardening rule parameters. This also shows the importance of specific kinematic variables over others and their evolution in particular. For instance, it is seen that the kinematic variable C_4 changes substantially for the uniaxial strain-controlled response, the evolution of which gives most of cyclic hardening of the material. It can also be stated that the fourth backstress component has the most significant effect on cyclic hardening and softening.

Based on these evolution rules, the uniaxial 1.0 % strain-controlled experiment was simulated by considering only the isotropic evolution (parameters discussed in Krishna et al., 2009), evolution of R and γ_i's (parameters discussed in Krishna et al., 2009), and evolution of R, C_4, C_2 and γ_1 as obtained above. The hysteresis loops comparison with respect to all the three different models is shown in Fig. 4.4. The simulations show that peaks can be matched well by all the three different ways of modeling. However, modeling only by isotropic hardening parameter evolution does not give the hysteresis loop shape well (see Hassan et al., 2008 and Krishna et al., 2009 for details). Modeling by γ_i's introduces a large number of

parameters, but gives the loop shape well. Hence, the new modeling step by the above analysis predicts the cyclic hardening very reasonably along with the hysteresis loop shape. Besides, it has fewer parameters and is more reasonable for practical applications. Again, the rule is not generalized for any material responses. Hence, cyclic hardening response of a material has to be considered in the method explained above to know the variation of kinematic and isotropic hardening rule parameters for a specific material.

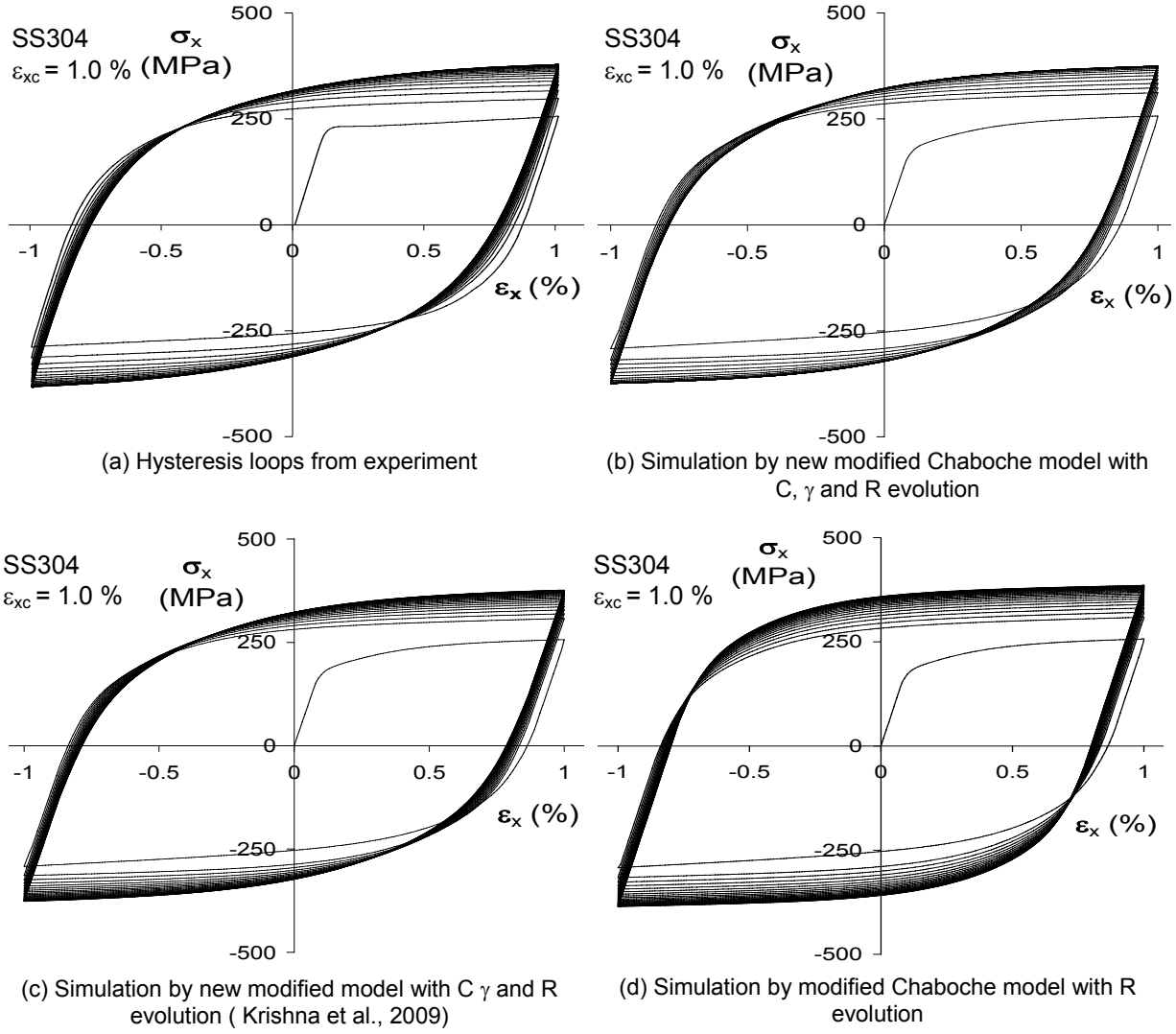

(a) Hysteresis loops from experiment

(b) Simulation by new modified Chaboche model with C, γ and R evolution

(c) Simulation by new modified model with C γ and R evolution (Krishna et al., 2009)

(d) Simulation by modified Chaboche model with R evolution

Fig. 4.4. Experimental and simulated responses under symmetric, strain-controlled uniaxial cycles. (Experimental data from Hassan and Kyriakides, 1994a)

4.2.3 Threshold Modeling

In the framework of time-independent plasticity, the kinematic hardening is described by the superposition of four different Armstrong-Frederick type rules (Armstrong and Frederick, 1966) as stated above in Eq. 2. Chaboche (1991) introduced the concept of the threshold in the nonlinear kinematic hardening rule, to improve the ratcheting simulations. A modified dynamic recovery term with a threshold as shown in Eq. 3b was introduced in fourth kinematic hardening rule.

$$d\underline{a}_i = \tfrac{2}{3} C_i d\underline{\varepsilon}^p - \gamma_i \left\{ \underline{a}_i \delta'(q) + (1-\delta')(\underline{a}_i \bullet \underline{n})\underline{n} \right\} \left\langle 1 - \frac{\overline{a}_4}{f(\underline{\alpha}_4)} \right\rangle dp \qquad (3b)$$

This modified recovery term gives an additional hardening in the loop as shown in the schematic in Fig. 4.5. As seen in the schematic, the kinematic hardening grows linearly to a certain threshold stress level and subsequently hardens according to the Armstrong and Frederick rule. Due to this incorporation, the strain accumulation with cycles is reduced for unsymmetric stress-controlled cycles without affecting the shape of cyclic stress-strain of strain-controlled experiments. In addition, this reduction depends on the value of the threshold. As a result, the fourth kinematic hardening has a linear hardening with a slope of C_4 within the threshold $\pm\overline{a}_4$ and becomes nonlinear outside the threshold (see the schematic in Fig. 4.5). The modified kinematic hardening rule is harder than the kinematic hardening rule without threshold. This, in addition to the other three decomposed kinematic hardening rules, produces a reduced rate of ratcheting (Chaboche, 1991; Bari and Hassan, 2000) for initial cycles without affecting the shape of cyclic stress-strain loops.

However, the modification is introduced in only the fourth kinematic hardening rule. One of the reasons for this introduction is it changes the value of the plastic modulus at the beginning of hysteresis curve. This makes the loop stiffer and hence reduces the ratcheting rate significantly. In addition to that, change of C_4 brings maximum change in the cyclic

hardening as seen in Fig. 4.3a and discussed earlier. This is one other reason for its incorporation in the fourth kinematic hardening rule.

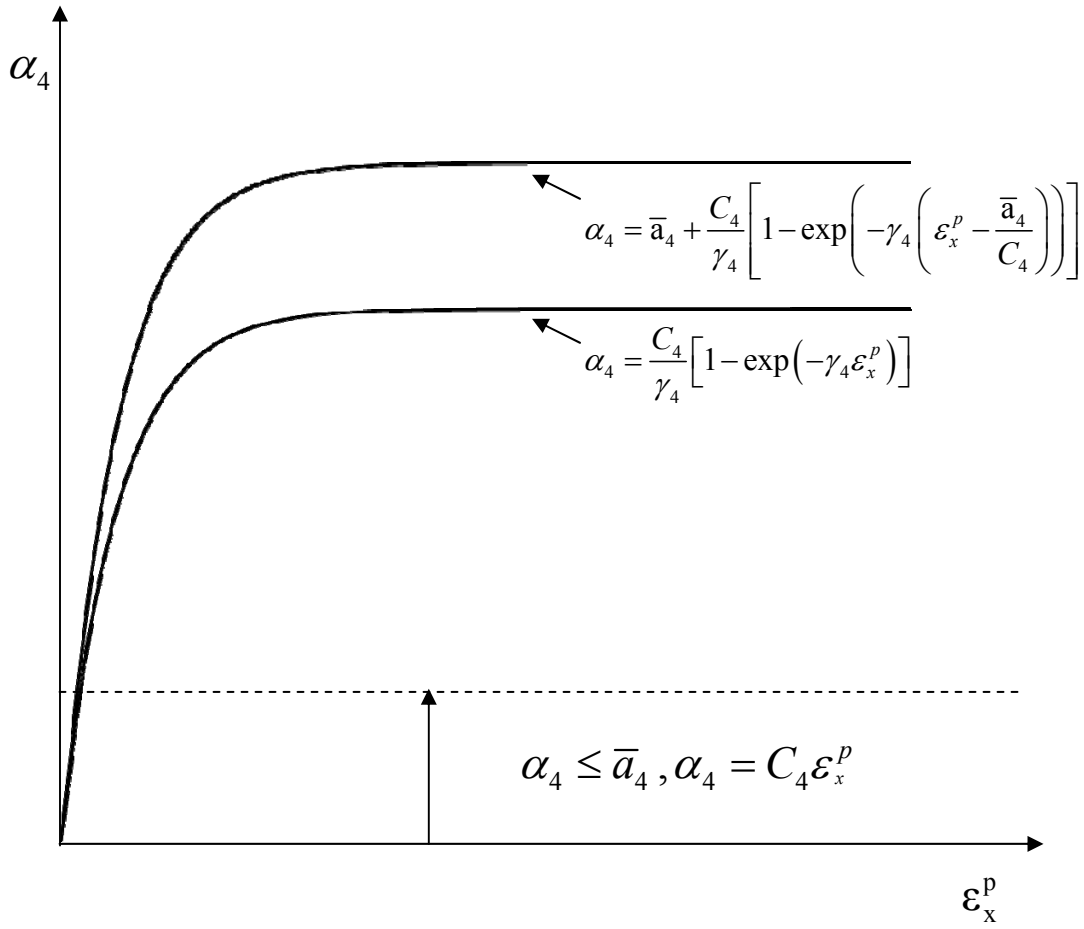

Fig. 4.5: Illustration of stiffening of the hysteresis curve with and without the threshold in the Armstrong-Frederick nonlinear kinematic hardening rule (Chaboche, 91).

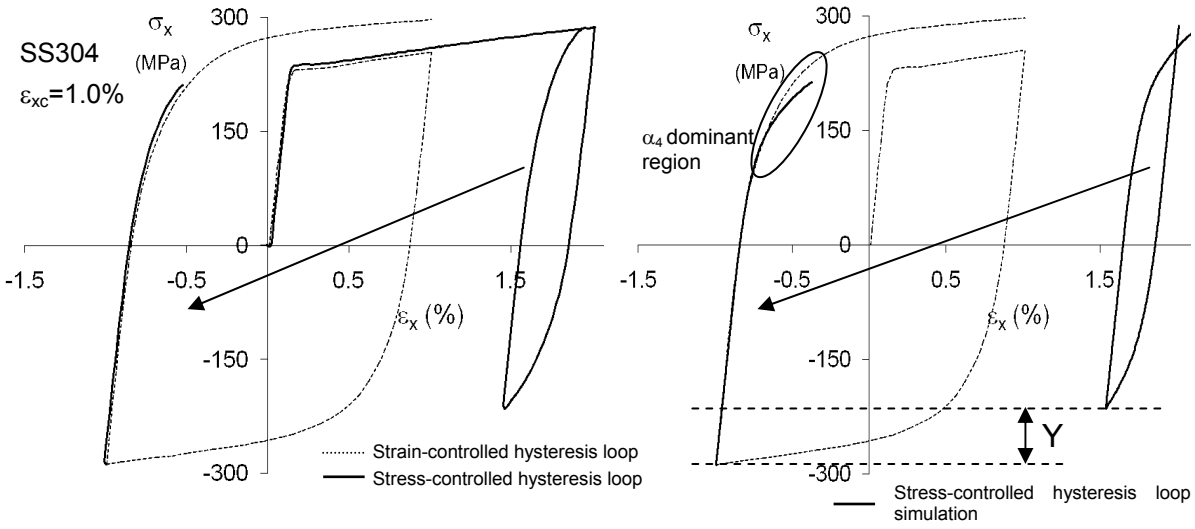

(a) Hysteresis loops from experiments

(b) Hysteresis loop from simulation and experiment

Fig. 4.6. Comparison of the upgoing curves of the strain-controlled and stress-controlled by shifting the hysteresis curves from experiment and simulation (a) the comparison with strain and stress-controlled experiment (b) the comparison with strain-controlled experiment and stress-controlled simulation with threshold.

Incorporation of the threshold has improved the ratcheting simulation as shown in Bari and Hassan (2000, 2002). However, as mentioned in Krishna et al. (2009) the hysteresis loops of stress-controlled experiment were not simulated well by the threshold (see Fig. 4.6b). Threshold incorporation improved the ratcheting peak simulation for the fitted experiment. But again, when the same threshold was used to simulate experiment with different stress-amplitude and mean, it either overpredicts or underpredicts as seen in Fig. 4.10a and b. Hence, the threshold was an arbitrary fix and did not explain the physical significance in terms of its calculation and effect. In order to understand the physical significance, the rising hysteresis loop of stress-controlled was compared with the rising strain-controlled loop by bringing it to the same starting point as shown in Fig. 4.6a. It is seen that the rising stress-controlled curve matches very closely with the rising strain-controlled curve (i.e. master curve). Not only this, but the first rising curves of several stress-controlled

experiment of constant stress-mean and stress-amplitude also were compared with the same upgoing strain-controlled curve, or the master curve as shown in Fig. 4.7. All of them match well with a slight difference due to rate effects in loading. On the other hand, when the rising curve of the stress-controlled simulation was compared, it is found to be softer than the master curve (i.e. the rising hysteresis curve of strain-controlled experiment from which the parameters are obtained), as shown in Fig. 4.6b. Again, the upgoing stress-controlled curve simulation can be made harder by increasing the value of $\overline{a}_4$, but it will affect the simulation of other sets of experiments. Besides it will also reduce the ratcheting rate for all the other stress-controlled experiments. Hence, a constant value of $\overline{a}_4$ was chosen to improve the simulation of the set of experiments collectively (Bari and Hassan 2000, Hassan et al., 2008, Krishna et al., 2009).

This observation is similar to a prior observation of Jhansale (1975), where the rising curve of several strain-controlled experiments of different range matches with the rising curve of stable cyclic stress-strain response. Also Jhansale (1975) had shown that upgoing curves of different strain-ranges match by suitable upward translation of these curves either in the strain or stress direction (see Fig. 4.3 and 5 in the reference). This further increased the curiosity for modeling this cyclic behavior and also laid the reasoning to model this behavior. It also motivates the necessity of understanding the difference of the experimental and simulation characteristics.

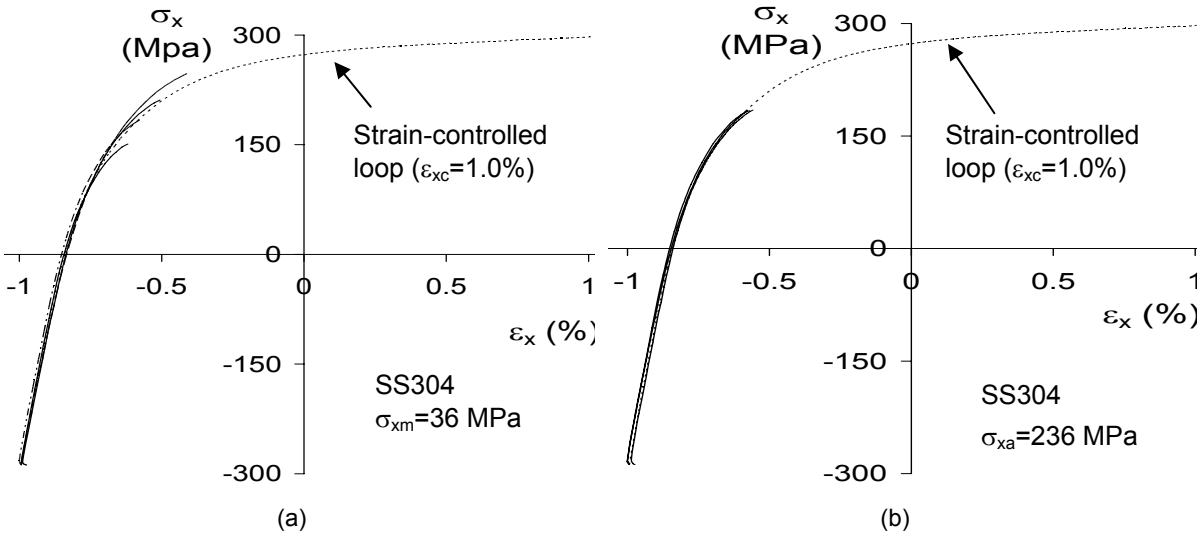

Fig. 4.7. Comparision of several rising curves of stress-controlled experiments with the rising curve of strain-controlled experiments. (a) Effect of constant amplitude stress , (b) Effect of constant mean stress (Experimental data from Hassan and Kyriakides, 1994a)

4.2.4 Backstress Shift Model

As mentioned in the earlier section, the rising stress-controlled curve simulation is softer than the rising curves of experiment. This difference in the behavior of simulation and experimental curve is due to the different starting point of the two upgoing loops. The upgoing strain-controlled loop or the master curve, which is used for the parameter determination, has a different starting point as compared to the upgoing hysteresis loop of the stress-controlled loops. Besides, the starting point of the different stress-controlled experiment also varies with the mean and amplitude of loading. As a result of this difference, the kinematic hardening term has a value which is softer than the required value and thereby makes the loop softer in nature. Hence, it is quite obvious that the threshold term of Chaboche (1991) and Bari and Hassan (2000) is a constant term obtained by fitting a uniaxial stress-controlled experiment. It can also be said that this constant can't be used for simulating other stress-controlled experiments with different stress-amplitude and mean.

Based on these observations, the hysteresis loop shape improvement can be modeled by shifting the backstress to the starting value of the strain-controlled curve or the master curve from which the parameters are obtained. The difference in the starting value of the rising strain-controlled curve and the rising stress-controlled curve is the value of the backstress shift parameter. This shift value is shown in Fig. 4.6b and referred to as "***Y***". Again, the incorporation of this shift term is carried out in the fourth backstress component α_4 and is shown in Eq. 6.

$$d\underline{\mathrm{a}}_4 = \tfrac{2}{3} C_4 d\underline{\varepsilon}^p - \gamma_4 \{\underline{\mathrm{a}}_4 \delta' + (1-\delta')(\underline{\mathrm{a}}_4 \bullet \underline{n})\underline{n}\}\left(1 - \frac{Y}{f(\underline{\alpha}_4)}\right) dp \tag{6}$$

Eq. 6 is similar to Eq. 3b accept there is a backstress shift term *'Y'* instead of the regular threshold term $\overline{a}_4$. Also, it is not in the form of a Macaulay bracket, as it was in Eq. 3b, since the backstress shift term depends on the starting value of the rising hysteresis curve and so is no more a constant. It is an internal variable that depends on the difference in the backstress at the starting point of stress reversal of strain-controlled and stress-controlled curves and also is shown in Fig. 4.6b. However, the starting point of strain-controlled loop is not constant for the cyclic hardening material. It constantly changes with the strain accumulation and with loading cycle. For instance, in Fig. 4.8, the value of the backstress changes considerably from the first rising curve to the stable rising hysteresis curve of a 1.0% strain-controlled uniaxial experiment (shown by black dots in Fig.8).

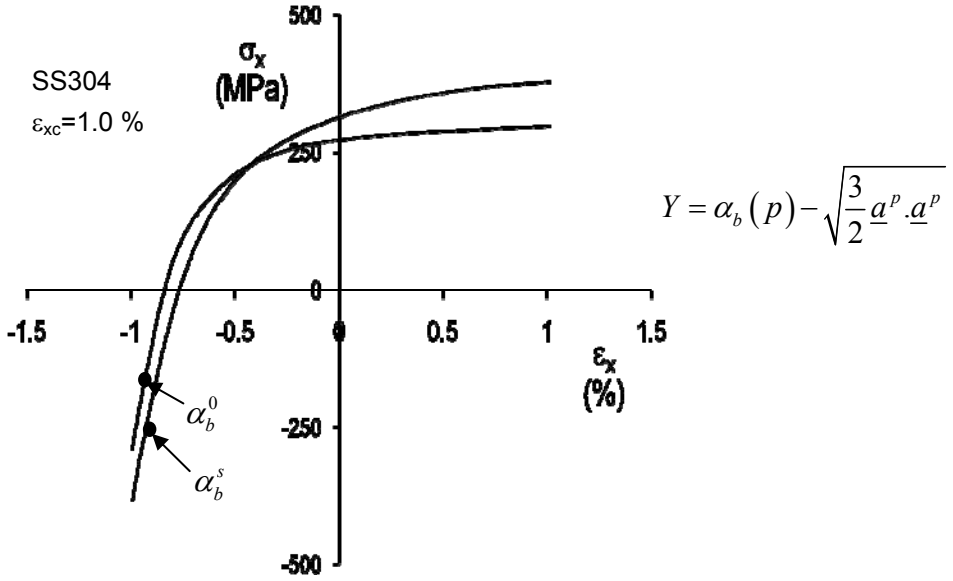

Fig. 4.8 Variation of the peak backstress and its change in the first and stable stress reversal curves.

Similarly the backstress of the rising or down going stress-controlled curves are different. In other words, the value of backstress for stress-controlled curve is different at the starting point of rising or down-going hysteresis curve. Hence, the shift term is calculated based on peak value for each hysteresis curve either of the rising or downgoing curve and continued for the path. Once, the path is changed, the value is calculated again and used. The difference between these two backstresses defines our new variable known as backstress shift parameter (BSP) as given by:

$$Y = \alpha_b(p) - \sqrt{\frac{3}{2}\underline{\mathrm{a}}^p.\underline{\mathrm{a}}^p}\ , \tag{7a}$$

$$\alpha_b(p) = \alpha_b^s\left(1 - \exp\left(-b_s p\right)\right) \tag{7b}$$

where *'α_b'* is the backstress at the start of the rising master curve or the strain-controlled hysteresis curve. The peak stresses are equal to the sum of back stresses components and the yield stress. Hence, the peak backstress *'α_b'* is obtained by subtracting yield stress from the

peak stress obtained with cycles as shown in Fig. 4.9. It also shows that the peak backstress is varying with the accumulated plastic strain. Similarly, $\underline{a}^{p}$ is the peak deviatoric backstress obtained at the starting of each rising and downgoing hysteresis curve of any experiment (i.e. stress-controlled or strain-controlled). In other words, α_b is a parameter varying with the strain accumulation and the other term depends on the experiment and loading parameters. Introduction of these parameters serves two major purposes.

1.) The backstress shift is not present in the 1.0% strain-controlled simulation as the difference goes to zero for the uniaxial strain-controlled experiment. Both the experimental hysteresis curve and the master curve explained above start from the same point and also cyclically harden to give the difference as zero and therefore do not affect the strain-controlled simulation.

2.) The backstress shift has a variable magnitude for different stress-controlled experiments with varying stress mean or stress amplitude. As a result, it stiffens or softens the curve depending on the difference and hence further improves the ratcheting simulation.

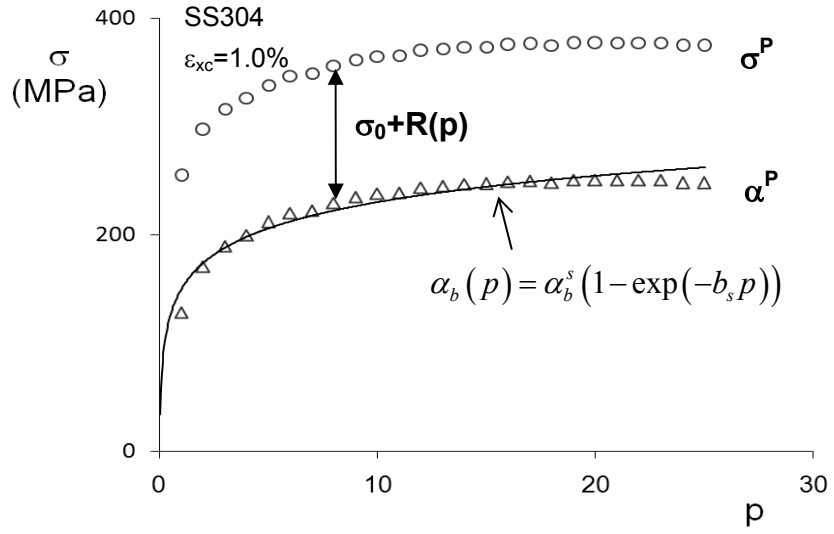

Fig. 4.9 Variation of the peak backstress with plastic strain accumulation.

The reason for incorporating *Y* only in the backstress term α_4 is mainly because of the observation shown in Fig. 4.6b. It can be seen from the Fig. 4.6b that the region of maximum discrepancy is the α_4 region (see α_4 dominant region in Fig. 4.2b). It can also be observed that the stress-controlled simulation under predicts in the α_4 dominant region as shown by a circle. In other words, this region is mainly influenced by the α_4 term (see Bari and Hassan 2000 for more details) and hence by introducing this shift term in the fourth kinematic hardening rule it can harden the backstress component significantly. One more reason of its incorporation in the fourth term is based on the observation of C_4 variation as mentioned in Section 2.2. It was seen that C_4 varies considerably and thereby influences cyclic hardening and softening. Or in other words, the fourth kinematic hardening rule plays a significant role in producing cyclic hardening or softening. This serves as one more reason to incorporate the shift term *"Y"* in the fourth kinematic hardening rule.

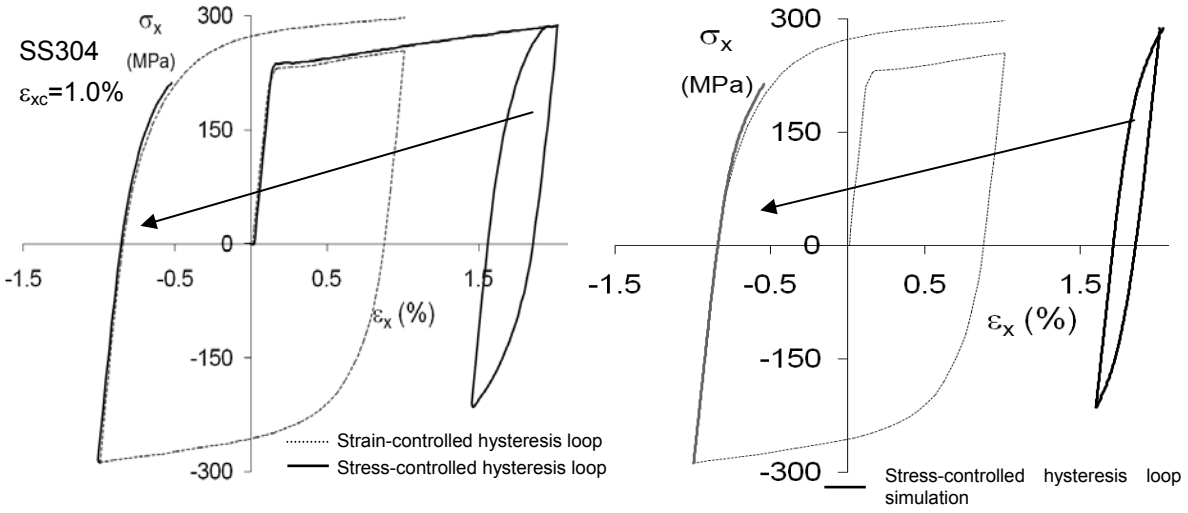

(a) Hysteresis loops from experiment (b) Hysteresis loop from simulation and experiment

Fig. 4.10. Comparison of the upgoing curves of the strain-controlled and stress-controlled, experiment and simulation. (a) The comparison with strain and stress- controlled experiment, (b) the comparison with strain-controlled experiment and stress-controlled simulation with BSP.

4.2.5 Simulations with Backstress Shift Model

This new modeling concept gives a physical meaning to the threshold modeling concept of Chaboche (Chaboche, 1991; Bari and Hassan 2000, 2002). The backstress shift concept introduced in the fourth kinematic hardening rule makes the rising curve stiffer and hence improves the shape significantly. The comparison of the stress-controlled rising curve simulation with the rising strain-controlled curve replicates the experimental observation as shown in Fig. 4.10. The rising curves obtained by modified Chaboche model with backstress shift parameter matches well with the experimental curves. Introduction of this new parameter produces a significant improvement in the ratcheting peak and rate response of all the stress-controlled experiments. Stress-controlled experiments with varying amplitude and constant mean ratcheting peak comparison are shown in Fig. 4.11a and experiments with varying mean and constant amplitude ratcheting peak comparison are shown in Fig. 4.11b (data obtained from the work of Hassan and Kyriakides, 1994a). The simulation validates that the new modeling concept of backstress shift has improved the uniaxial ratcheting simulation considerably. It also shows that the ratcheting rate is improved significantly with the backstress shift parameter.

The model was further validated with the biaxial stress-controlled experiments (data obtained from the work of Hassan and Kyriakides, 1994b). However, the peak comparison does not show any improvement. The main reason was axial and circumferential ratcheting peaks depend considerably on the hysteresis loop shape and width. Again, the loop width is a function of visco-effect and hence remains unsolved with the time-independent modeling as discussed above. Hence, to further resolve this visco-effect and loop width issue, the time-dependence is considered in the present modified Chaboche model and as discussed in next section.

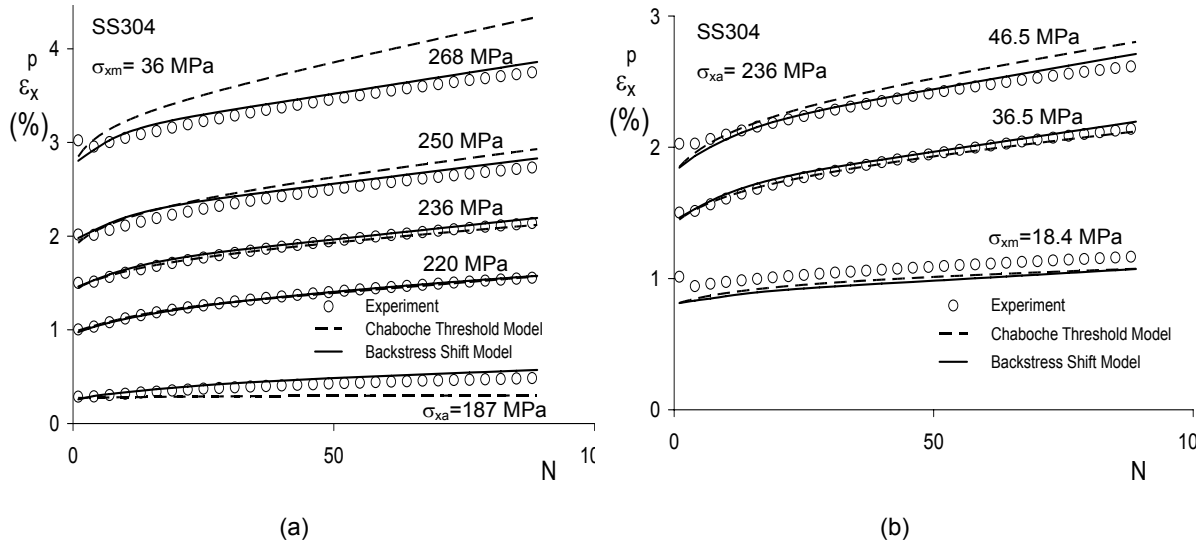

Fig. 4.11. Experimental and simulated response of axial ratcheting rates (a) influence of amplitude stress (b) influence of mean stress. (Experimental data from Hassan and Kyriakides, 1994a)

4.3. Time-Dependent Modified Chaboche Model

The finding observed in the previous section and in the earlier works of Hassan et al. (2008) and Krishna et al. (2009) motivates the need for hysteresis loop shape and width improvement. Also, the main flaw observed in the simulation is hysteresis loop shape and width. It is also noted that loop shape was poor because of rounding of loops or viscous-effect. As mentioned in Hassan et al. (2008) and Krishna et al. (2009), the rounding nature at the stress peaks was due to the creep and change of loading at the stress peaks. Thus, apart from the cyclic hardening/softening, nonproportionality of loading, and strain-range effect, rate of loading plays an important role for the hysteresis curve shape and the loop width. Hence, this improvement can be carried out by incorporation of time-dependence in the constitutive model.

The major difference between a time-dependent and time-independent loading is that the stress state is admissible in excess of yield condition. The stress in addition to yield condition

is called "overstress" or viscous stress, $\sigma_v = J(\sigma-\alpha) - R(p) - \sigma_0$, where $J(\sigma-\alpha)$ is equal to $\left(\frac{3}{2}(s-a):(s-a)\right)^{1/2}$ and $R(p)$ is the drag resistance term as a function of strain accumulation (Chaboche, 1989). This viscous stress forms the basic quantity to define the viscoplastic potential. Just like the plastic potential, a viscoplastic potential is required to obtain the viscoplastic strain-rate. Several variations of viscoplastic potential are present in the literature (see the review paper by Chaboche, 2008). The most preferred and used viscoplastic potential was proposed by Malinin and Khadjinsky (1972) with the simple power relationship:

$$\Omega = \frac{K}{n+1}\left\langle \frac{\left(\frac{3}{2}(s-a):(s-a)\right)^{1/2} - R(p) - \sigma_0}{K} \right\rangle^{n+1} \tag{8}$$

The strain-rate decomposition relation can be written as:

$$\underline{\dot{\varepsilon}} = \underline{\dot{\varepsilon}}^{e} + \underline{\dot{\varepsilon}}^{vp}, \tag{9}$$

Modified Hooke's law: $\underline{\dot{\varepsilon}}^{e} = \frac{1+\nu}{E}\underline{\dot{\sigma}} - \frac{\nu}{E} tr\left(\underline{\dot{\sigma}}\right)\underline{I}$, (9a)

Flow rule: $$\underline{\dot{\varepsilon}}^{vp} = \frac{\partial \Omega}{\partial \sigma} = \frac{3}{2}\dot{p}\frac{s-a}{J(\sigma-\alpha)}, \tag{9b}$$

where $\dot{p} = \left\langle \frac{\left(\frac{3}{2}(s-a):(s-a)\right)^{1/2} - R(p) - \sigma_0}{K} \right\rangle^{n} = \left\langle \frac{J(\sigma-\alpha) - R(p) - \sigma_0}{K} \right\rangle^{n}$

or $\dot{p} = \left\langle \frac{\sigma_v}{K} \right\rangle^{n}$

where K and n are time-dependent parameters representing the viscosity of the material; R and σ_0 are the drag resistance and yield stress respectively; $\dot{\underline{\varepsilon}}, \dot{\underline{\varepsilon}}^{vp}, \dot{\underline{\varepsilon}}^{e}$ and $\dot{\underline{\sigma}}$ are the total strain rate, viscoplastic strain rate, elastic strain rate and stress rates respectively; $\dot{p}$ is the accumulated strain-rate calculated by $\dot{p} = \left[\frac{2}{3}\dot{\varepsilon}^{vp} \bullet \dot{\varepsilon}^{vp}\right]^{1/2}$ .The above strain-rate decomposition takes into account an elastic strain-rate increment and a viscoplastic strain-rate increment. However, the effect of plastic strain and creep strain is collectively incorporated in the viscoplastic strain increment, making it a unified approach to obtain total strain-rate (Chaboche, 1989).

Considering the above relation in Eq. 9b and expanding it, the viscous stress can be expressed by:

$$\sigma_v = K\dot{p}^{1/n} \tag{9c}$$

The above relation in Eq. 9b when expanded for a uniaxial case can be written as:

$$\sigma = \alpha + R(p) + \sigma_0 + K\dot{p}^{1/n} \tag{9d}$$

The above equation shows the difference between the stress state for a time dependent and time-independent formulation. The additional viscous term accounts for the rate-dependent loading. Hence, the rate-independent model can be considered as the limiting case of rate-dependent model by using $n \to \infty$ ($K \to 0$). Thus K and n also account for different rates of loading.

4.3.1 Kinematic and Isotropic Hardening rule

Based on the time-dependent framework, the kinematic and isotropic hardening rule has a static recovery term to take into consideration the effect of the very low and high strain rates. Incorporation of the terms as given in Chaboche (1989) and Chaboche (2008) is as follows:

$$\dot{\underline{a}} = \sum_{i=1}^{4} \dot{\underline{a}}_i \ , \tag{10}$$

$$\dot{\underline{a}}_i = \tfrac{2}{3} C_i \dot{\underline{\varepsilon}}^p - \gamma_i(q)\left\{\underline{a}_i \delta'(q) + \left(1-\delta'(q)\right)(\underline{a}_i \bullet \underline{n})\underline{n}\right\} \dot{p} - b_i \left(J\left(\underline{a}_i\right)\right)^{r-1} \underline{a}_i \text{ , for } i = 1, 2, 3 \tag{10a}$$

$$\dot{\underline{a}}_i = \tfrac{2}{3} C_i \dot{\underline{\varepsilon}}^p - \gamma_i(q)\left\{\underline{a}_i \delta'(q) + \left(1-\delta'(q)\right)(\underline{a}_i \bullet \underline{n})\underline{n}\right\} \left\langle 1 - \frac{Y}{f(\underline{\alpha}_i)} \right\rangle \dot{p} - b_i \left(J\left(\underline{a}_i\right)\right)^{r-1} \underline{a}_i \text{ , for } i = 4 \tag{10b}$$

The general form of the kinematic hardening rule has a strain hardening term, a dynamic recovery term and a static recovery term, as given by the three parts above in Eqs. 10a and b (Chaboche, 2008). The backstress shift term as studied before is again introduced here. Similarly, concepts of strain range dependent cyclic-hardening and nonproportionality as developed in Chapter 3 are introduced in the model to give unified constitutive equations.

The first term gives an (increasing) evolution of kinematic hardening term a_i with the plastic strain. The second term gives a recall or evanescent memory effect which is again evolving with the plastic strain and hence called the dynamic term. The third term is called the static recovery term or time recovery, since it is independent of the plastic strain (Chaboche, 2008). It takes care of thermal recovery or the very low rate effects. In all other time, the influence of static term is negligible.

The above kinematic hardening rule if considered in simplified form (δ'= 1, r = 1) can be written for a uniaxial case as:

$$\dot{a}_i = \tfrac{2}{3} C_i \dot{p} - \gamma_i a_i \dot{p} - b_i a_i \tag{11a}$$

With the assumption of accumulated plastic strain-rate as constant, the above backstress rate term on integration can be written as

$$\alpha_i = \frac{C_i \dot{p}}{\gamma_i \dot{p} + b_i}\left\{1 - \exp\left(-\left(\gamma_i \dot{p} + b_i\right)t\right)\right\} \tag{11b}$$

By the expression above, the significance of static terms can be well justified. The backstress value goes to zero at very low strain rate and goes to C_i/γ_i at high strain rate,

which is similar to that of the time-independent case (Bari and Hassan 2000, Yang and Nassar, 2005). Also the saturated value depends on the strain rate as seen from the expression (11b). Hence, this static term is essentially required only under very low strain rates. It takes care of thermal recovery or the very low rate effects (Chaboche, 2008). In all other time scales, influence of the static term is negligible.

In the present scope of study, the strain rate is not low in the experimental responses and also, the responses are not considered for varying temperature. Success was observed in simulating the experimental response from the works of Hassan and Kyriakides (1994a,b) without the static term as explained above. Therefore, the static term is ignored and only the first two terms are considered as given by Eq. 12a and b below.

$$\underline{\dot{a}}_i = \tfrac{2}{3} C_i \underline{\dot{\varepsilon}}^p - \gamma_i(q)\left\{\underline{a}_i \delta'(q) + \left(1-\delta'(q)\right)(\underline{a}_i \bullet \underline{n})\underline{n}\right\}\dot{p}\,, \qquad \text{for } i = 1, 2, 3 \text{ (12a)}$$

$$\underline{\dot{a}}_i = \tfrac{2}{3} C_i \underline{\dot{\varepsilon}}^p - \gamma_i(q)\left\{\underline{a}_i \delta'(q) + \left(1-\delta'(q)\right)(\underline{a}_i \bullet \underline{n})\underline{n}\right\}\left(1-\frac{Y}{f(\underline{\alpha}_i)}\right)\dot{p}\,, \qquad \text{for } i = 4 \text{ (12b)}$$

However the success, by any means, does not again imply that kinematic hardening rule without the static term can be considered for simulation. Again, the other equations related to cyclic hardening and softening, nonproportionality of loading, and strain range effects remain the same as used in the time-independent case. A detailed description of the equations can be obtained from prior papers of the authors (Hassan et al, 2008 and Krishna et al., 2009).

4.3.2 Time-Dependent and Time-Independent Comparison

As mentioned earlier, the time-dependent and time-independent cases are different in terms of stress states. The isotropic and kinematic hardening rule and the yield surface are same for both the time dependent and time-independent framework as seen from the equations above. Only the flow rule for the plastic and viscoplastic strain calculation is different, which gives a difference in the total strain calculated.

The flow rule for viscoplastic strain-rate increment

$$\dot{\underline{\varepsilon}}^{vp} = \frac{\partial \Omega}{\partial \sigma} = \frac{3}{2}\dot{p}\frac{s-a}{J(\sigma-\alpha)}. \tag{9b}$$

The flow rule for the time-independent modeling framework is

$$d\underline{\varepsilon}^{p} = d\lambda\frac{\partial f}{\partial \underline{\sigma}} = \frac{3}{2}dp\frac{\underline{s}-\underline{\mathrm{a}}}{\sigma_0 + R}, \tag{2b}$$

Hence the basic difference between the flow rules comes from the difference in admissible stress states.

For a time-dependent case (from Eq. 9b): $J(\sigma-\alpha) = R(p) + \sigma_0 + \sigma_v$ while for the time-independent case (from Eq.2b): $J(\sigma-\alpha) = R(p) + \sigma_0$.

Hence, the flow rule is different with the presence of overstress term $\sigma_v = K\dot{p}^{1/n}$. This defines the difference between the flow rule of a time-dependent and time-independent formulation. The additional viscous term or the overstress term accounts for the rate-dependent loading. In order to further validate the similarity between the time dependent and time-independent models, a high value of n = 500 and K = 0.1 are assumed. The strain-controlled hysteresis loop and the stress-controlled loop were simulated as shown in Fig.12. The hysteresis curves were found to be exactly identical to the curves obtained from time-independent simulation, keeping all the kinematic and isotropic hardening rule parameters as constant.

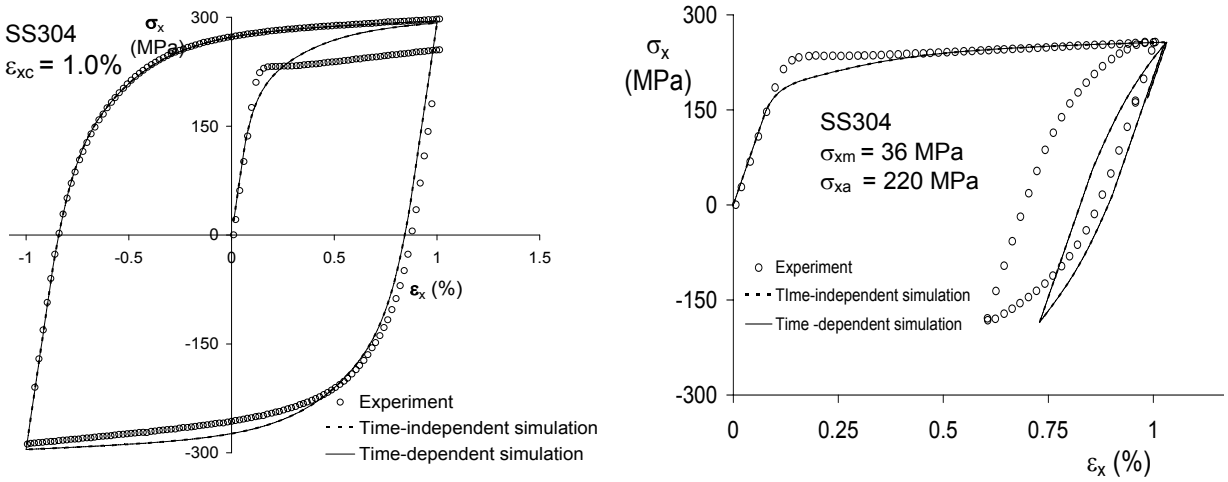

(a) (b)

Fig. 4.12. Hysteresis curve comparison with time-dependent and time-independent simulation (a) comparison of the rising and down going strain-controlled hysteresis curve (b) comparison of the stress-controlled hysteresis loop with the K = 0.1 and n = 500.

4.3.3 K and n Parameter Determination

As discussed in the earlier section, the difference in the time-independent and time dependent models is as a result of an overstress term (see Eq.9c). This overstress term, $\sigma_v = K\dot{p}^{1/n}$ is also the part in excess of yield surface at any stress state. As a result, the difference between a time-independent and a time-dependent rising hysteresis curve will be the overstress curve given by $\sigma_v = K\dot{p}^{1/n}$, provided all the other kinematic and isotropic hardening parameters are the same. As a result, if unloading takes places at any particular point beyond the yield-surface, it will introduce a rounding effect. This is because the stress state is in addition to the yield stress and while unloading it will have a plastic and elastic part depending on the K and n values, and also the increment of loading as shown in Fig. 4.13a below. As seen from Fig. 4.13a, the stress state for a time-dependent model is different from the yield surface at any particular loading point. A small unloading from the stress state σ to σ^* will have an elastic and plastic part unlike the time-independent modeling, shown in Fig. 4.13b, where the unloading has only elastic part.

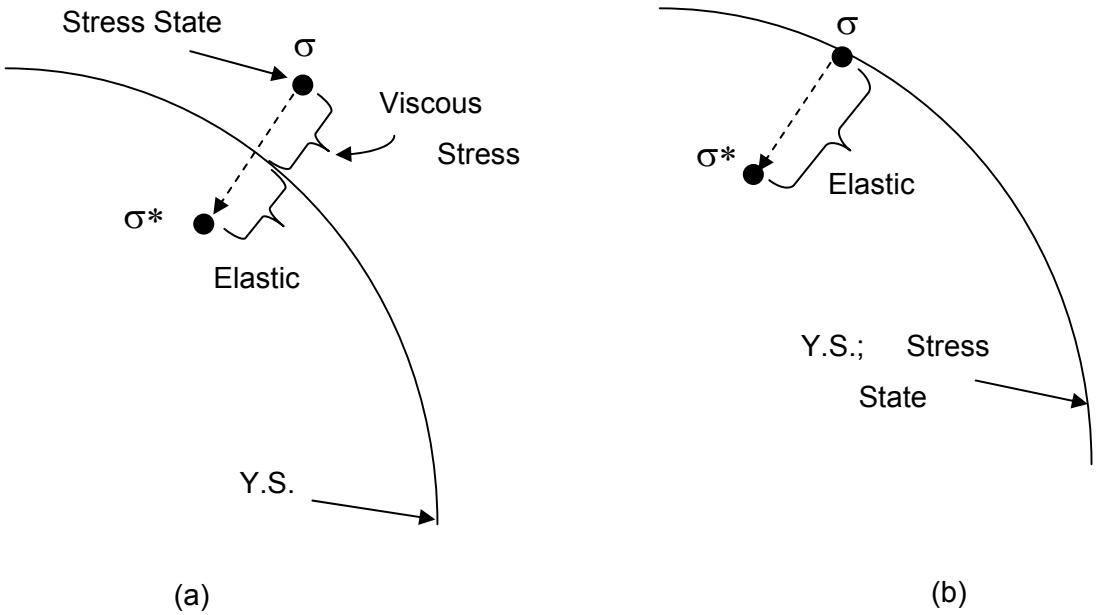

(a) (b)

Fig. 4.13. Schematic of unloading at a stress state for (a) time-dependent, (b) time-independent modeling beyond the yield stress.

In the time-independent loading the yield surface expands or translates such that the stress state for additional plastic straining is always on the yield surface. Therefore, an unloading in a time-independent case will always be elastic. Based on these discussions, there is a plastic strain in the rate-dependent unloading that gives a rounding as represented in Fig. 4.14a. This rounding is related to K and n value and the stress state in addition to the yield surface. Again, the interaction of the kinematic and isotropic hardening parameters (C_i's, γ_i's and R) with the time-dependent overstress parameter K and n is quite complex. Hence, the first step would be to determine the parameters K and n and then understand their significance in producing the rounding and other hysteresis loop shape effects (e.g. stiffening or softening of the curve).

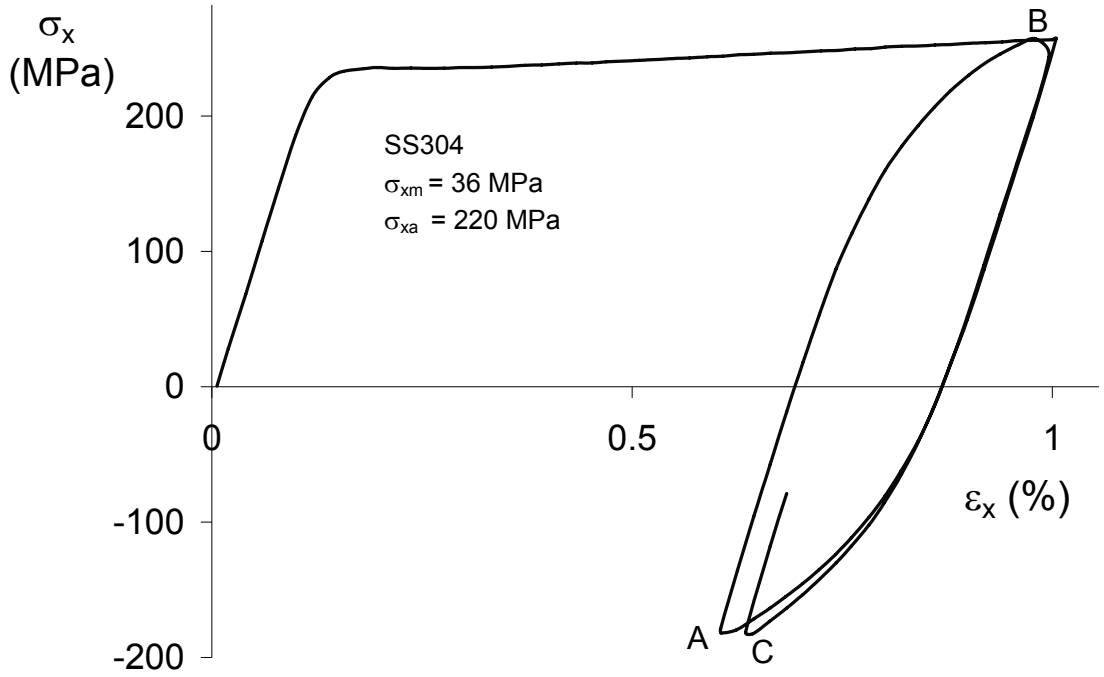

Fig. 4.14. First hysteresis curve of stress-controlled experiment

To understand the effect of viscous parameters and their values, the first hysteresis curve of the stress-controlled experiment is considered. The stress peaks and valleys clearly show the rounding nature which was explained earlier and is also an effect of K and n and stress states. Again, the rising hysteresis curve AB and the first stress reversal curve BC shown in Fig. 4.13 are compared by bringing them to the same point (i.e. invert BC and shift to stress and strain point A). Both the curves are shown in Fig. 4.15a. The curves' comparison shows that the down-going curve is softer than the rising curve. Again, if we clearly observe the strain range of the two curves in Fig. 4.15a, (i.e. as shown by $\Delta\varepsilon_1$ and $\Delta\varepsilon_2$), it can be stated that the strain range of the downgoing curve is smaller than the rising hysteresis curve. Also the time for upward and downward traversal is the same. This shows that the downward going curve has a slower strain rate compared to rising hysteresis curve. With the above strain-rate obtained, if the curves are adjusted with the overstress effect ($\sigma_{adjust} = \sigma - K\dot{p}^{1/n}$), they can be closely matched and thus also gives the values of K and n. The parameters are K= 42 and n =6. Again, it is verified with other stress controlled experiments for better

simulation of hysteresis curves. Parameters obtained through this method along with the C_i's and γ_i's give the rounding of the loop as seen from Fig. 4.16 and a close fit of the first hysteresis curve of stress-controlled experiment. Once the K and n are determined, the next step is to determine all the rest of the kinematic and isotropic hardening rule paramaters. As discussed, the time-dependent modified Chaboche model involves a large number of paramaters to simulate a broad set of experimental responses. These parameters are determined by following a sequential methodology as outlined in Krishna et al. (2009). A genetic algorithm program was developed to accommodate the consitutive equations in this study (see Appenedix A for details). The other parameters related to strain-range dependent kinematic hardening paramaters evolution are determined based on the steps discussed in Krishna et al. (2009).

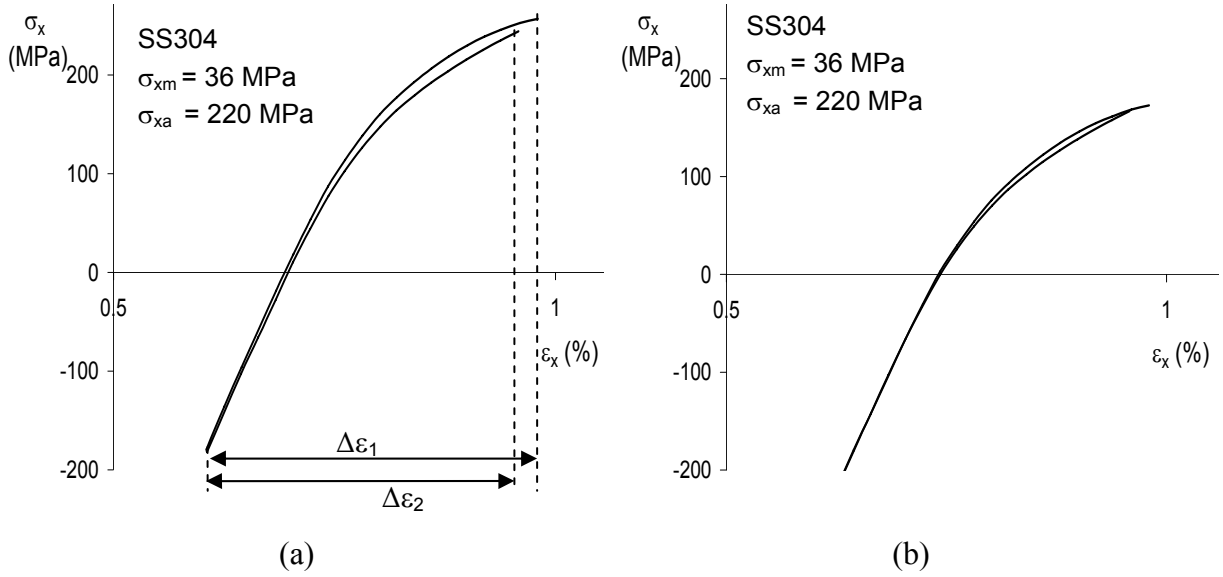

Fig. 4.15. Hysteresis curve comparison (a) comparison of the rising and down going hysteresis curve (b) comparison of the same curves with the K and n adjustment.

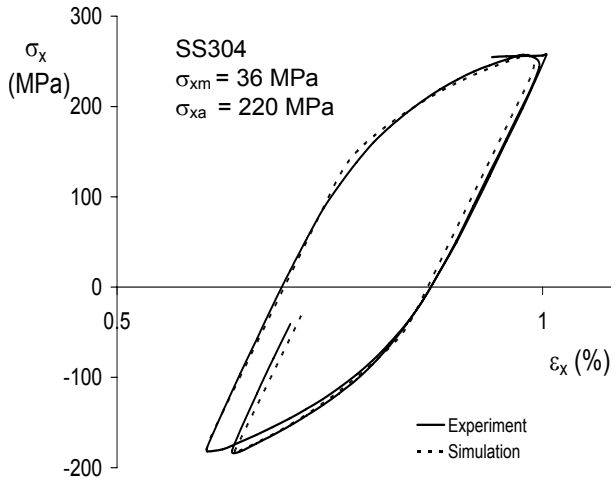

Fig. 4.16. Comparsion of first hystersis curve of experiment and simulation with time-dependent modeling.

4.4 Simulations

The time-dependent modified Chaboche model is evaulated against a set of uniaxial stress-controlled ratcheting responses. It will be further validated against a set of biaxial and other multiaxial stress and strain controlled experiments. Based on these paramaters, all the uniaxial stress-controlled histories with constant mean stress and varying amplitude and with constant amplitude and varying mean (data from Hassan and Kyriakides 1994a) were simulated as shown in the Fig. 4.18. As seen from the simulations of Fig. 4.17, the hystersis loop shape has improved considerably. Also, the loop width is sumulated well with the incorporation of time-dependence in the constituive model. Although the loop width simulation in Fig. 4.17d shows improvement, cyclic softening is not simulated well and needs further improvement. One of the reasons for lack of significant cyclic softening may be due to underprediction of rounding at stress peaks.

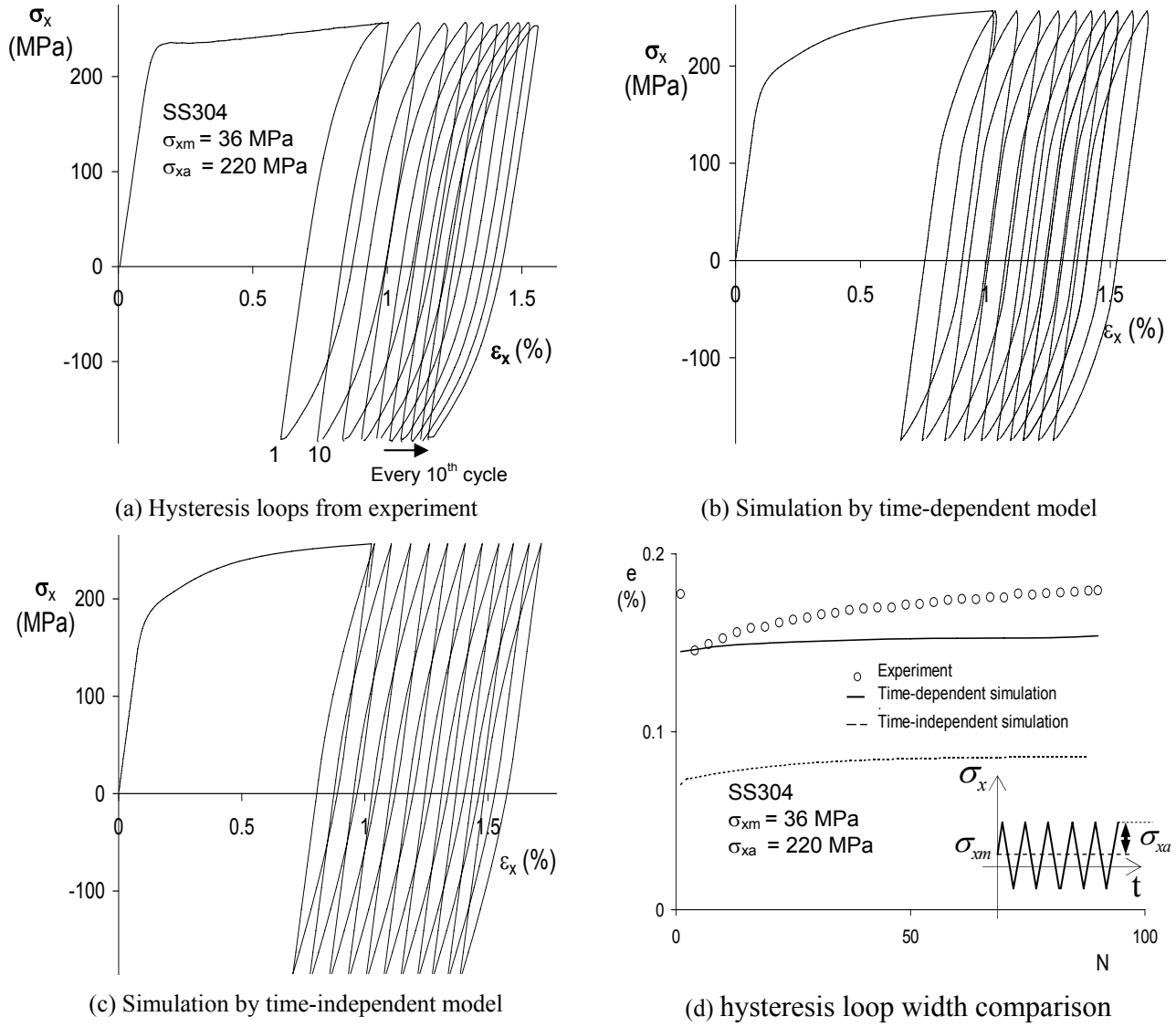

Fig. 4.17. Experimental and simulated responses under unsymmetrical, stress-controlled cycle. (a) Experimental stress response, (b) simulations by the modified Chaboche time-dependent model, (c) simulations by the modified Chaboche time-independent model, (d) hysteresis loop width comparison. (Experimental data from Hassan and Kyriakides, 1994a)

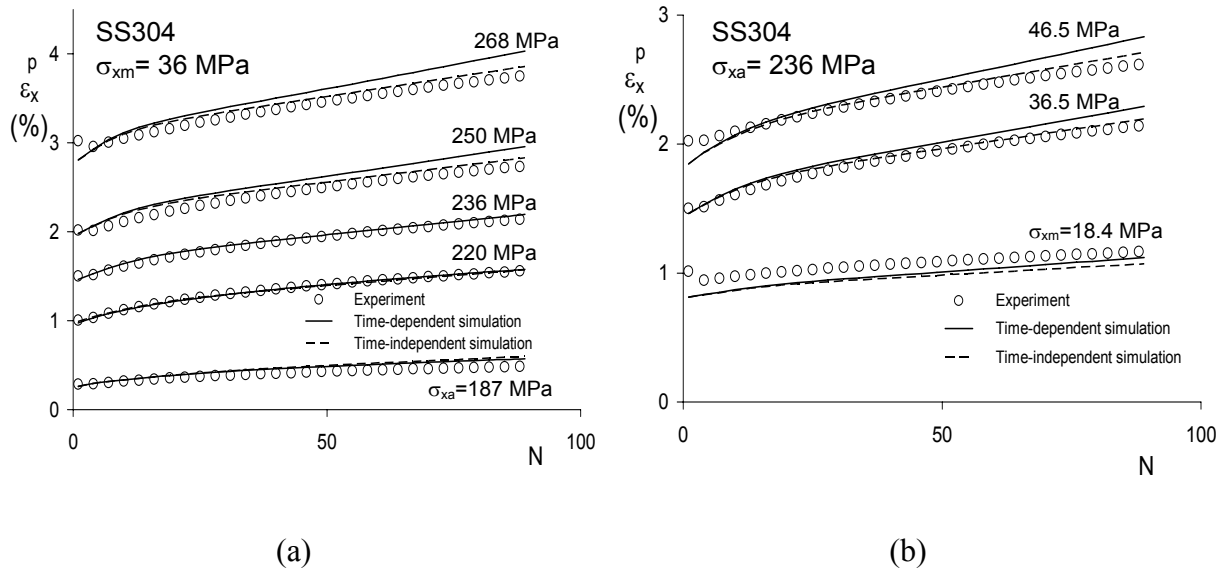

(a) (b)

Fig. 4.18. Experimental and simulated response of axial ratcheting rates with time-dependent and time-independent modified Chaboche model: (a) influence of amplitude stress; (b) influence of mean stress. (Experimental data from Hassan and Kyriakides, 1994a)

The model developed was used to simulate all the stress-controlled simulations and the simulations show significant improvement. The strain accumulation with cycles for unsymmetrical, axial, stress-controlled experiments are shown in Fig. 4.18. The maximum axial strain (ε_x^p) in each cycle from the experimental and simulated responses is plotted as a function of number of cycles (N) in Fig. 4.18a and b. The rate of ratcheting as shown in Fig. 4.17 was used to determine the model parameters. The simulated responses from the time-dependent modified Chaboche model shows considerable hysteresis loop-shape improvement. The parameters obtained have to be further modified to obtain the broadening of the loops under stress-controlled loading.

4.5. Conclusions

The paper presents several modeling features which improved the hysteresis curve shape and size simulations significantly when implemented into the modified Chaboche model (Hassan et al., 2008 and Krishna et al., 2009). The modified Chaboche model has

demonstrated successes and challenges in simulating a broad set of proportional and nonproportional, strain and stress-controlled cyclic plasticity responses. The major drawbacks of the modified Chaboche model identified were that the hysteresis loop shape and size were not simulated well. A detailed study on the evolution of the kinematic hardening rule parameters (Cs and γs) in representing cyclic hardening/softening responses was conducted. It is demonstrated that only C_2, C_4, and γ_1 need to evolve with plastic strain (others remain constant) in order to produce the same quality simulations as obtained by Hassan et al. (2008) and Krishna et al. (2009), but with fewer parameters.

A novel modeling concept of backstress shift is developed and shown to improve uniaxial ratcheting simulation significantly. This modeling concept is an alternative to the Chaboche threshold modeling concept, which was a fix to improve the fit of a specific hysteresis loop. Hence, the Chaboche threshold concept is unable to simulate a broad set of uniaxial ratcheting responses with reasonable accuracy (Krishna et al., 2009). The backstress shift concept added only one additional parameter but improved the hysteresis curve shape and ratcheting rate simulations significantly. The backstress shift modeling concept also gives a physical meaning to the threshold modeling concept of Chaboche (1991).

Finally, the initial, rounded positive stress peaks obtained in the uniaxial ratcheting experiments are simulated well by incorporating time-dependent modeling features into the modified Chaboche model. The time-dependent modified Chaboche model also simulated the hysteresis loop shape and size quite well. The modified time-dependent Chaboche model needs to be validated against the non-proportional ratcheting responses (see Hassan et al., 2008 and Krishna et al., 2009). In order to achieve a unified constitutive model, temperature dependence needs to be included in the modified Chaboche model. Finally, to achieve a robust model for cyclic plasticity, incorporation of the yield surface shape change into the modeling scheme would be essential.

Acknowledgements

The financial support from the National Science Foundation (Award # DMR-0408910) and the Department of Civil, Construction and Environmental Engineering at North Carolina State University is gratefully acknowledged.

References

Armstrong, P.J., Frederick, C.O., 1966. A mathematical representation of the multiaxial bauschinger effect. CEGB Report No. RD/B/N 731, Berkely Nuclear Laboratories, Berkely,UK.

Bari, S., Hassan, T., 2000. Anatomy of coupled constitutive models for ratcheting simulation, Int. J. Plast., 16, 381-409.

Bari, S., Hassan, T., 2002. An advancement in cyclic plasticity modeling for multiaxial ratcheting simulation. Int. J. Plast., 18, 873-894.

Benallal, A., Marquis, D., 1987. Constitutive equations for nonproportional cyclic elasto-viscoplasticity. ASME J. Eng. Mater. Tech., 109, 326-336.

Chaboche, J.L., Dang-Van, K., Cordier, G., 1979. Modelization of the strain memory effect on the cyclic hardening of 316 stainless steel. Proceedings of the 5th International Conference on SMiRT, Div. L, Berlin, Germany, L11/3.

Chaboche, J.L., Rousselier, G., 1983. On the plastic and viscoplastic constitutive equations-part 1: rules developed with internal variable concept, part 2: application of internal variable concepts to the 316 stainless steel. J. Pressure Vessels Piping, 105, 153-164.

Chaboche, J.L., 1986. Time-independent constitutive theories for cyclic plasticity. Int. J. Plast., 2, 149-188.

Chaboche, J.L., 1989. Constitutive equations for cyclic plasticity and cyclic viscoplasticity. Int. J. Plast., 5, 247-302.

Chaboche, J.L., Nouailhas, D., 1989. Constitutive modeling of ratcheting effects-part1: experimental facts and properties of the classical models, part 2: possibilities of some additional kinematic rules. ASME J. Eng. Mater. Tech., 111, 384-416.

Chaboche, J.L., 1991. On some modifications of kinematic hardening to improve the description of ratcheting effects. Int. J. Plast., 7, 661-678.

Chaboche, J.L., 2008. A review of some plasticity and viscoplasticity constitutive theories. Int. J. Plast., 24, 1642-1693.

Delobelle, P., 1993. Synthesis of the elastoviscoplastic behavior and modelization of an austenitic stainless steel over a large temperature range, under uniaxial and biaxial loading: Part I. Behavior. Int. J. Plast. 9, 65-85.

Delobelle, P., Robinet, P., Bocher, L., 1995. Experimental study and phenomenological modelization of ratcheting under uniaxial and biaxial loading on an austenitic stainless steel. Int. J. Plast., 11, 295-330.

Ellyin, F., Xia, Z., 1989. A rate-independent constitutive model for transient non-proportional loading. J. of the Mech. Phys of Solids, 37, 71-91.

Hassan, T., Kyriakides, S., 1994a. Ratcheting of cyclically hardening and softening materials, part I: uniaxial behavior. Int. J. Plast., 10, 149-184.

Hassan, T., Kyriakides, S., 1994b. Ratcheting of cyclically hardening and softening materials, part II: multiaxial behavior. Int. J. Plast., 10, 185-212.

Hassan, T., Taleb, L., Krishna, S., 2008. Influences of non-proportional loading paths on ratcheting responses and simulations by two recent cyclic plasticity models. Int. J. of Plast., 24, 1863-1889.

Jhansale, H. R., 1975. A new parameter for the hysteretic stress-strain behavior of metals. Trans. ASME, H, J. Eng. Mater. Technol., 97, 33-38.

Kang, G. Z., Gao, Q., Cai, L.X., Yang, X.J., Sun,Y.F., 2002a. Experimental study on the uniaxial and nonproportionally multiaxial ratchetting of SS304 stainless steel at room and high temperatures. Nucl. Eng. Des., 216, 13-26.

Kang, G.Z., Gao, Q. ,Yang, X.J., 2002b. A visco-plastic constitutive model incorporated with cyclic hardening for uniaxial/multiaxial ratchetting of SS304 stainless steel at room temperature. Mech. Mater., 34, 521-531.

Kang, G.Z., Ohno, N., Akira, N., 2003. Constitutive modeling of strain range dependent cyclic hardening, Int. J. Plast., 19, 1801-1819.

Kang, G.Z., Gao, Q., Yang, X.J., 2004. Uniaxial and multiaxial ratchetting of SS304 stainless steel at room temperature: experiments and visco-plastic constitutive model, Int. J. Non-linear Mech., 39, 843-857.

Kang, G.Z., 2004. A visco-plastic constitutive model for ratcheting of cyclically stable materials and its finite element implementation. Mech. Mater., 36, 299-312.

Kang, G.Z., Li, Y.G., Gao, Q., 2005. Non-proportionally multiaxial ratcheting of cyclic hardening materials at elevated temperatures and its constitutive modeling, Mech. Mater.,37, 1101-1118.

Kang, G.Z., Kan, Q., Zhang, J., Sun, Y., 2006. Time-dependent ratcheting experiments of SS304 stainless steel. Int. J. Plast., 22, 858-894.

Krempl, E., Lu, H., 1984. The hardening and rate-dependent behavior of fully annealed AISI type 304 stainless steel under biaxial in-phase and out-of-phase strain cycling at room temperature. J. of Engg. Mat. And Tech., 106, 376-382.

Krishna, S., Hassan,T., Naceur,I.B., Saï, K., Cailletaud G., 2009. Macro versus micro-scale constitutive models in simulating proportional and nonproportional cyclic and ratcheting responses of stainless steel 304. Int. J. Plast., doi:10.1016/j.ijplas.2008.12.009.

Marquis, D., 1979. Etude théorique et vérification expérimentale d'un modèle de plasticité cyclique. Thèse Paris VI .

McDowell, D.L., 1985. A two surface model for transient nonproportional cyclic plasticity. ASME J. Appl. Mech., 52,298-308.

McDowell, D.L., 1987. An evaluation of recent developments in hardening and flow rules for rate-independent, nonproportional cyclic plasticity. ASME J. Appl. Mech., 54, 323-334.

McDowell, D.L., 1992. Nonlinear kinematic hardening theory for cyclic thermoplasticity and thermoviscoplasticity. Int. J. Plast., 8, 695-728.

McDowell, D. L., 2000. Modeling and experiments in plasticity. Int. J. Sol. Struct., 37, 293-309.

Moosbrugger, J.C., 1991. Some developments in the characterization of material hardening and rate sensitivity for cyclic viscoplasticity models. Int. J. Plast., 7, 405-431.

Moosbrugger, J.C., 1993. Experimental parameter estimation for nonproportional cyclic viscoplasticity: nonlinear kinematic hardening rules for two waspaloy microstructures at 650° C. Int. J. Plast., 9, 345-373.

Nouailhas , D., Cailletaud, G., Policella, H., Marquis, D., Dufaily, J., Lieurade, H.P., Ribes, A., Bollinger, E., 1985. On the description of cyclic hardening and initial cold working. Engg. Fracture Mech., 21,887-895.

Nouailhas, D., 1989. Unified modeling of cyclic viscoplasticity: application to austenitic stainless steel. Int. J. Plast., 5, 501-520.

Ohno, N., 1982. A constitutive model of cyclic plasticity with a nonhardening strain region. ASME J. Appl. Mech. 49, 721-727.

Ohno, N., 1990. Recent topics in constitutive modeling of cyclic plasticity and viscoplasticity. Appl. Mech. Rev., 43, 283-295.

Portier,L., Calloch, S., Marquis,D., Geyer, P., 2000. Ratchetting under tension-torsion loadings: experiments and modelling. Int. J. Plast., 16, 303-335.

Rahman, S.M., Hassan, T., Ranjithan, R. S., 2005. Automated parameter determination of advanced constitutive models. ASME Pressure Vessels Piping Div. Publ. PVP, 2,261-272.

Rahman, S. M., Hassan, T., Corona, E., 2008, Evaluation of cyclic plasticity models in ratcheting simulations of straight pipes under cyclic bending and steady internal pressure. Int. J. Plast., 24,1756-1791.

Rousselier, G., 1985, Etude comparative de modeles de comportement pour la simulation d'essais en traction-pression sur tubes en acier inoxydable. Document Edf., Annexe du rapport no. 8 du GIS, rupture a chaud.

Tanaka, E., 1994 . A nonproportionality parameter and a cyclic viscoplastic constitutive model taking into account amplitude dependences and memory effects of isotropic hardening. Eur. J. Mech., A/Solids, 13, 155-173.

Yang, X., Nassar, S., 2005. Constitutive modeling of time-dependent cyclic straining for solder alloy 63Sn-37Pb**.** Mech. Mater., 37, 801-814.

Yoshida, F., 1990. Uniaxial and biaxial creep ratcheting behavior of SUS304 stainless steel at room temperature. Int. J. Pressure Vessels Piping. 44, 207-223.

Yoshida, F., 2000. A constitutive model of cyclic plasticity. Int. J. Plast., 16, 359-380.

Zhang, J., Jiang, Y., 2008. Constitutive modeling of cyclic plasticity deformation of a pure polycrystalline copper. Int. J. Plast., 24, 1890-1915.

CHAPTER 5
Conclusions and Recommendations

5.1 Conclusions

All the enclosed journal papers (chapter 2, 3, and 4) written from this study contain conclusions from the corresponding parts of the study. A summary of each set of conclusions is presented below:

5.1.1 Nonproportional Loading and its Constitutive Modeling (Paper 1, Chapter 2)

The paper demonstrates the influence of nonproportionality of loading history on cyclic responses. A novel set of experiments were conducted on SS304 under various uniaxial and biaxial stress-controlled nonproportional histories. The study demonstrates the influence of nonproportional loading on ratcheting responses. A detailed description of these experiments is discussed in chapter 2. Different trends in regard to the influence of nonproportional loading on ratcheting responses are observed from the second sequence as compared to those in the first sequence.

The Chaboche model was modified for simulating cyclic hardening/softening response through the kinematic hardening rule parameters, in addition to the conventional isotropic hardening rule parameters. The Benallal-Marquis nonproportionality parameter is incorporated in the modified Chaboche model through the kinematic hardening rule parameters γ_i in addition to the classical parameter (R). The modified Chaboche model with the added nonproportional features is able to capture the nonproportional ratcheting responses of shear; cross, square and two square paths well (see Fig. 4.8 in Chapter 2). However, the current model failed in simulating the two sequence loading ratcheting responses from uni-cross, shear-uni and forward and reversed two-square reasonably.

Improvement and development can be carried out by incorporating features of strain range dependent cyclic hardening/softening, rate dependence and finally other nonproportionality parameters such as proposed by Tanaka et al., 1994.These steps are discussed in chapter 3.

Also, simulations of the hysteresis loops under stress-controlled cycles are unsatisfactory from the modified Chaboche model. The primary reason for this deficiency is that the recorded hysteresis loops under stress-controlled cycles demonstrated cyclic softening, but the model parameters were calibrated for simulating cyclic hardening. The hysteresis loop is also not simulated well because of time-independency of the model. Hence these drawbacks are addressed in the next chapters. Finally, new modeling challenges in simulating nonproportional cyclic and ratcheting responses are demonstrated in this paper.

5.1.2 Time-independent constitutive modeling (paper 2, chapter 3)

The main goal of this paper is to develop a robust constitutive model that can be implemented in the finite element program for low cycle fatigue life analysis. The chapter addresses many of the features of cyclic plasticity: for instance, strain-range dependent cyclic hardening/softening, ratcheting, relaxation, loading nonproportionality, and their interactions in a detailed and systematic approach. Again, a methodical approach to model all these features is explained. The developed model then tries to address the drawbacks mentioned in the earlier paper. Finally, it evaluates the modified Chaboche model against a broad set of experimental responses of SS304 under uniaxial and multiaxial cyclic loading. The model was analyzed by simulating hysteresis loop shape, cyclic hardening-softening, cross effect, cyclic relaxation, subsequent cyclic softening, and a series of ratcheting responses under uniaxial and biaxial loading responses. The performance of the modified Chaboche model in simulating a broad set of uniaxial and biaxial, cyclic and ratcheting responses is impressive. The success of modified Chaboche model mainly relies on the improved simulation of the hysteresis loops because of the combined action of isotropic and kinematic hardening rule parameters. The improved model simulates the additional cyclic hardening for the 90 degree out-of-phase nonproportional experiment as well as subsequent cyclic softening for the axial

strain-controlled cycles prescribed immediately after the 90 degree out-of-phase cycles because of a memory feature in the Tanaka parameter. Also, the Tanaka (1994) nonproportional parameter incorporated in the modified Chaboche model yielded very good ratcheting response simulation for a series of biaxial ratcheting responses. Finally, a novel technique for simulating both the monotonic and cyclic response with one set of model parameters is developed and validated in this paper.

The main drawbacks identified are the hysteresis loop shape and width improvement, which is poor due to lack of rate-dependency in the model. These issues of hysteresis shape improvement, kinematic hardening rule parameters, and threshold modeling are discussed in the next chapter.

5.1.3 Improved unified constitutive model (paper3, chapter 4)

The paper presents several modeling features which improved the hysteresis curve shape and size simulations significantly when implemented into the modified Chaboche model. The major drawbacks of the modified Chaboche model identified were that the hysteresis loop shape and size were not simulated well. A detailed study on the evolution of the kinematic hardening rule parameters (Cs and γs) in representing cyclic hardening/softening responses was conducted. It is demonstrated that only C_2, C_4, and γ_1 need to evolve with plastic strain (others remaining constant) in order to produce same quality simulations as obtained in earlier papers but with less number of parameters.

Again, a novel modeling concept of backstress shift is developed and shown to improve uniaxial ratcheting simulation significantly. This modeling concept is an alternative to the Chaboche threshold modeling concept, which was a fix to improve the fit of a specific hysteresis loop. This backstress shift concept added only one additional parameter but improved the hysteresis curve shape and ratcheting rate simulations significantly.

Finally, the initial rounded positive stress peaks obtained in the uniaxial ratcheting experiments are simulated well by incorporating time-dependent modeling features into the modified Chaboche model. Incorporation of these futures has improved the hysteresis loop shape and size significantly. However, further validation with respect to multiaxial and other nonproportional experiments is required.

5.2 Recommendations for Future Research

The present study has opened new realms of constitutive modeling and the need of an even more detailed study of the material behavior to predict the stress-strain cyclic proportional and nonproportional responses, low cycle structural fatigue, and local and global deformation. From the knowledge gained in this study, the following recommendations are made for future studies.

5.2.1 Incorporation of temperature-dependence

Incorporation of temperature and related rate dependence has to be included in the modified Chaboche model developed in the study in order to achieve the unified model. The temperature-dependence needs additional thermal strain term $\dot{\underline{\varepsilon}}^T$ as follows:

Additive strain-rate decomposition: $\dot{\underline{\varepsilon}} = \dot{\underline{\varepsilon}}^e + \dot{\underline{\varepsilon}}^p + \dot{\underline{\varepsilon}}^T$,

where $\dot{\underline{\varepsilon}}^T$ is the thermal strain rate as a result of thermal expansion. In addition the cyclic responses are influenced by temperature and hence the kinematic hardening and isotropic hardening variables (i.e. C's, γ's, R) are also temperature-dependent.

5.2.2 Incorporation of the Yield-surface shape change

One of the drawbacks of the present constitutive model is that the shape of the yield surface is kept unchanged from the von-Mises yield surface. But it was observed by several researchers (Philips and his coworkers, 1972, 1979, 1984, Yoshida et al., 1978, Shriatori et al., 1979) that the yield surface continuously changes its shape with inelastic loading. This in a way effects the plastic strain increment direction and the estimation of plastic strain

directions. Hence, this anisotropy of yield surface and its evolution with progressive loading should be included in the model to improve its cyclic stress-strain response simulation.

5.2.3 Multiscale constitutive modeling

Experimental studies have shown that microstructural defects and inclusions affect the constitutive behavior of materials and failure properties. A multiscale modeling approach hence is essential to model the microstructural features and then link the micro to the macroscale behavior using the homogenization technique. Such study is imperative to understand various material complexities. Such a study will also predict the low cycle fatigue more accurately and should be carried out.

REFERENCES

(For Chapter 1 and 5.)

Armstrong, P.J., Frederick, C.O., 1966. A mathematical representation of the multiaxial bauscinger effect. CEGB Report No. RD/B/N 731, Berkeley Nuclear Laboratories, Berkely,UK.

Aubin V., Bulthé A.-L., Degallaix S., Quaegebeur, P., 2003. Ratcheting behavior of a duplex stainless steel: characterization and modeling. 9th International Conference on the Mechanical Behavior of Materials, 25-29 May 2003, Genève, Suisse.

Bari, S., Hassan, T., 2000. Anatomy of coupled constitutive models for ratcheting simulation, Int. J. Plast., 16 , 381–409.

Bari, S., Hassan, T., 2001. Kinematic hardening rules in uncoupled modeling for multiaxial ratchetting simulation. Int. J. Plast., 17, 885–905.

Bari, S., Hassan, T., 2002. An advancement in cyclic plasticity modeling for multiaxial ratcheting simulation. Int. J. Plast., 18, 873-894.

Benallal, A., Marquis, D.,1987. Constitutive equations for nonproportional cyclic elasto-viscoplasticity. ASME J. Eng. Mater. Tech. 109, 326–336.

Castiglioni, C. A., 2005. Effects of the loading history on the local buckling behavior and failure mode of welded beam-to-column joints in moment-resisting steel frames. J. Eng. Mech., 131, 568-585.

Chaboche, J.L., Dang-Van, K., Cordier, G.,1979. Modelization of the strain memory effect on the cyclic hardening of 316 stainless steel. Proceedings of the 5th International Conference on SMiRT, Div. L, Berlin, Germany.

Hassan, T., Kyriakides, S., 1994a. Ratcheting of cyclically hardening and softening materials, part I: uniaxial behavior. Int. J. Plast., 10, 149-184.

Hassan, T., Kyriakides, S., 1994b. Ratcheting of cyclically hardening and softening materials, part II: multiaxial behavior. Int. J. Plast., 10, 185-212.

Ohno, N., 1982. A constitutive model of cyclic plasticity with a nonhardening strain region. ASME J. Appl. Mech. 49, 721–727.

Phillips, A., Tang, J.-L., (1972) The effect of loading path on the yield surface at elevated temperatures. International Journal of Solids and Structures, Vol 8, pp. 463-474.

Phillips, A., Lee, C.W., (1979) Yield surfaces and loading surfaces: experiments and recommendations. International Journal of Solids and Structures, Vol 15, pp. 715- 729.

Phillips, A. and Lu, W.-Y. (1984) An experimental investigation of yield surfaces and loading surfaces of pure aluminum with stress-controlled and strain-controlled paths of loading. J. Engg. Mat. Techno., Trans. ASME, Vol 106, pp. 349-354.

Ruggles,M.D., Krempl,E., 1989. The influence of test temperature on the ratcheting behavior of type SS304 stainless steel. ASME J. Eng. Mater. Technol., 111 ,378-387.

Rugges,M.D., Krempl, E., 1990. The interaction of cyclic hardening and ratcheting of AISI type 304 stainless steel at room temperature: I, Experiments. J.Mech. Phys. Solids,38,575-585.

Rahman, S.M., 2006. Finite element analysis and related numerical schemes for ratcheting simulation, PhD dissertation, North Carolina State University, Raleigh, NC.

Shiratori, E., Ikegami, K. and Yoshida, F., 1979. Analysis of stress-strain relations by use of an anisotropic hardening plastic potential. Journal of the Mechanics and Physics of Solids, Vol 27, pp. 213-229.

Yoshida, F., Tajima, N., Ikegami, K., Shiratori, E.,1978. Plastic theory of the mechanical ratcheting. Bulletin of the JSME., 21, 389-397.

Yoshida, F., Murakami, T., Kaneko, K., Ikegami, K. and Shiratori, E. (1977) Plastic behaviour in the combined loading along straight stress paths with a bend. Bulletin of the JSME, Vol 20, pp. 1549-1556.

APPENDIX

Appendix A: Genetic Algorithm Parameter Determination

A.1 Introduction

The modified Chaboche model has a number of parameters that are interdependent. Manual determination of these parameters is tedious, because this requires many trial and error iterations. Determining a good set of parameters manually also requires detailed knowledge of the constitutive model and extensive parameter determination experience. In order to solve these problems, an automated parameter optimization system using heuristic search technique can be used. One such optimization method is through genetic algorithm. Genetic algorithm (GA) is a systematic stochastic search procedure that uses random search as a tool to guide a highly exploitative search in parameter space. GA first generates a series of initial parameter sets randomly and subsequently generates better sets of parameters using the initial sets through a systematic search technique. This iterative search technique gradually evolves towards better and better parameter sets and finally yields the best parameter set for given fitness criteria. Parameters determined from a stable hysteresis loop also influence the ratcheting simulation and improvement in one step will degrade the simulation of the others. Genetic algorithm can determine all model parameters through sequential search, which also improves the model simulation. Following the guideline of Bari and Hassan (2002) from stress-strain and uniaxial and biaxial ratcheting responses, a GA based optimization algorithm was developed by Rahman (2006) for automated parameter determination. Cyclic hardening of the material through evolution of kinematic hardening-rule parameters is implemented into the algorithm for better simulation of material responses of cyclic hardening/softening material.

A.2 Genetic Algorithms

Genetic algorithms (GA) are robust stochastic search procedures that explore for solutions from a broad and promising region. GA randomly generates an initial population

which is composed of several sets of parameters. Each parameter set is known as an individual in the population. In the population, each individual set is assigned a fitness based on how well it fits to the observed response. Then, GA operates with the Darwinian principle of "survival of the fittest". Basic operators of GA are selection, crossover, reproduction, mutation, and elitism and these are used for producing better generation. Crossover is a GA operator with the idea that two better parents might produce a better offspring for the next generation. During crossover two parents exchange information or knowledge related to the problem between two parents and generates new offspring. Reproduction is an operator that allows a better individual to pass in the next generation.

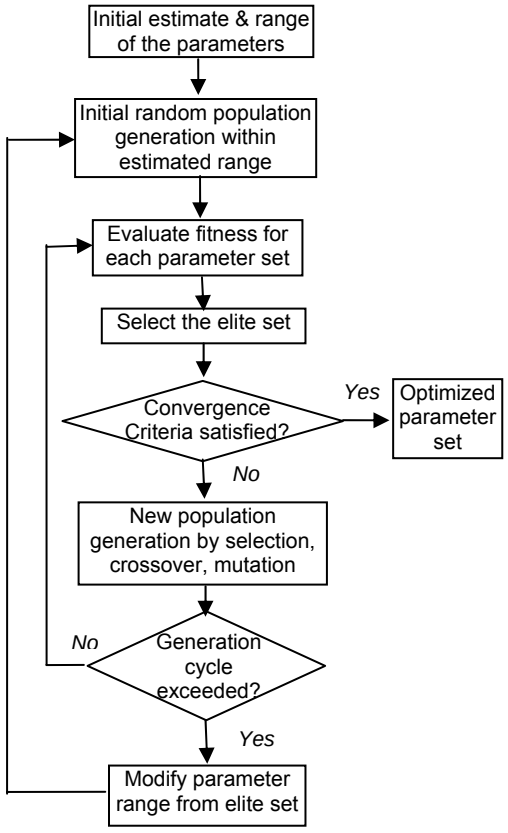

Fig. A.1. Flow chart for simultaneous genetic algorithm

Mutation randomly changes the property of an offspring to make the search global in the search space. Elitism is a selection mechanism to ensure the survival of the best individual through generations. In elitism, when the best individual in new generation is inferior to best solution of the previous generation, the worst individual in the generation is always replaced by the best individual of the previous generation. With the operators of selection, crossover, and mutation, a new generation is created. Fitness of each offspring is assigned for the new generation. The system of selection, crossover and mutation is repeated. Thus, the system evolves towards the system of better and better parameter space with each new generation. The process is repeated until a well-fit individual is obtained. A genetic algorithm procedure can be visualized from the flow diagram in Fig. A.1.

A.3 Generation of Initial Set of Parameters

The model parameters (i.e. the kinematic hardening rule parameter Cs and γs) are dependent upon the hysteresis curve. A detailed description of their physical significance is described in Bari and Hassan (2000, 2002), who presented a systematic step by step approach for determining the parameters of modified Chaboche model. Rahman (2006) implemented the steps in a GA program and outlined the steps of obtaining the initial parameter set through an automated system. The automated system generates the $\sigma_x - \varepsilon_x^P$ data from the $\sigma_x - \varepsilon_x$ responses of the first rising hysteresis curve of a 1.0 % strain-controlled experiment (or a sufficiently large strain-controlled experiment). As the parameters C_1 and C_3 can be measured more specifically, these two parameters are allowed to vary ±5% of the initial estimate. The parameter γ_3 is initially kept zero as it influences the uniaxial ratcheting rate only. The parameters C_2, C_4, γ_1, γ_2, γ_3, γ_4, $\bar{a}_4$ are varied within ±10% of the initial estimate. The range for parameter δ' is given as between 0.0 and 1.0. In this parameter determination scheme, the range is kept adaptable with generation which allows moving freely towards natural evolution. From the estimated range, a number of parameter sets are generated as

initial population. Each individual parameter set is assigned fitness based on how it fits to the experimental observation. Size of the population is taken proportional to number of the parameters to be optimized. In the first step, all uniaxial parameters $(C_{1\text{-}4}, \gamma_{1\text{-}2}, \gamma_4, \bar{a}_4)$ are determined from the loading part of the first rising stress-strain curve from a strain-controlled experiment (see Rahman, 2006 for details). Since a large number of parameters are determined from this step, a higher population size of 100 is preferred. In the second step, mostly two parameters $(\gamma_3, \bar{a}_4)$ are varied in a larger range, and others are varied within a small margin. A comparatively smaller population size of 20 is selected. The program has the flexibility of changing the population size. The aforesaid population sizes have been found to be optimum in terms of accuracy and solution time. The procedure was followed by taking the first hysteresis curve of a 1.0% strain controlled experiment. Similarly, the stable loop of a multistep strain-controlled experiment was taken (as described in Chapter 3) and was used to obtain the stable values of γs by keeping the Cs as constant. The values of Cs are the same as obtained by the procedure explained above for all the hysteresis loops. Similarly the initial values of the rate of change of γs, denoted by $D_{\gamma i}$s (see Eq. 4 in Chapter 3), are taken from 0 to 50.

A.4 Fitness Evaluation

Material parameters are selected to obtain a best fit by minimizing the difference between the experimental data and model simulation. In first loop simulation, it is necessary to match the end stress values for higher strain range. In parameter optimization, this is considered as a constraint in simulation. In GA constraint handling is done by introducing a penalty to the fitness function. Individuals that violate the constraint are subjected to penalties depending on the violation of the constraint. The parameter optimization problem can be described as reducing the fitness value with a constraint satisfying Eq.A.1. Details of this equation can be obtained from Bari and Hassan (2000).

$$\alpha_s = 2*\left(\frac{C_1}{\gamma_1}\right) + 2*\left(\frac{C_2}{\gamma_2}\right) + 2*\left(\frac{C_4}{\gamma_4} + a_4\right) = (\sigma_x^+ - \sigma_x^-) - 2*\sigma_0 - 2*C_3\varepsilon_L^p \qquad \text{(A.1)}$$

Such constraint related optimization is done with penalty function. When the parameter set violates the constraint (Eq.A.1.), the fitness value calculated based on distance measure is penalized. In this case a linear penalty is added to the fitness function (increasing the fitness value) based on the violation of the constraint. Again, in ratcheting simulation, it is imperative to minimize the distance function and to simulate the stabilized ratcheting rate. The final objective for ratcheting simulation is satisfying both criteria. The deviation measures in each objective are normalized with respect to experimental values. Then multiple objectives are satisfied by minimizing the maximum deviation. The fitness evaluation can be defined mathematically as follows:

Distance Function

Deviation measure, $f_{dist} = \sqrt{\frac{\sum_{i=1}^{N} (Y_{\exp,\,i} - Y_{m,i})^2}{N}}$. (A.2)

Normalized value, $\bar{f}_{dist} = \frac{f_{dist}}{\sqrt{\sum_{i=1}^{n} (Y^2_{\exp,\,i}/N)}}$ (A.3)

where $Y_{\exp}$ and Y_m are experimental and model predicted responses.

Slope Function

For matching the stabilized ratcheting rate in experimental and simulated results, the last 10 to 15 data points are selected. Again experimental data are not perfectly stable, some deviation is always there. With the idea of avoiding local deviation, experimental slopes are considered with respect to a number of points (e.g. 4) to get an average slope. The automated system contains two options to calculate the stabilized ratcheting rate. The first one is based on well known linear regression theory and the system takes the last few numbers of points (e.g. 10) to calculate the average slope of a best fit line. Another option is selecting 4 or 5 end points and calculating an average slope in between a few points (4 or 5). The process is repeated for the last 10 or 15 data points for experimental and model prediction. Similar

slope calculation is also made with model simulation to match with experimental data. The first option simply matches the ratcheting rate (slope) as a straight line whereas the latter method not only matches the slope but also the curvature if any at those end points. The following functions are used for ratcheting rate (slope) fitness:

Slope, $m_i = \dfrac{Y_{i+n} - Y_i}{x_{i+n} - x_i}$; n can be 4 or 10. (A.4)

Slope deviation, $f_{slope} = \sqrt{\dfrac{\sum_{i=1}^{N} (m_{\exp,i} - m_i)^2}{N}}$ (A.5)

Normalized slope value, $\overline{f}_{slope} = \dfrac{f_{slope}}{\sqrt{\sum_{i=i}^{N} (m_i^2 / N)}}$ (A.6)

The error measure for a parameter set is calculated from the objective function $f = \max(\bar{f}_{slope}, \bar{f}_{dist})$. Objective functions are defined for simulation of the loading part of stabilized hysteresis curve (f_1), uniaxial ratcheting (f_2) and multiaxial ratcheting (f_3). In parameter optimization, when simultaneous simulation is necessary for the hysteresis curve (loading part), uniaxial ratcheting and biaxial ratcheting, the parameter set is optimized minimizing the maximum fitness value. In such a situation, the objective function $f_{ult} = \max(f_1, f_2, f_3)$ is to be minimized, where f_1, f_2, f_3 are fitness for stabilized hysteresis data, uniaxial ratcheting and biaxial ratcheting respectively.

A.5 Operator

The developed optimization algorithm (GA based) in this study is equipped with selection, crossover, mutation and elitism and works with real coded parameters. In the selection step, *binary tournament selection* strategy is used. Binary selection is picking the better parameter set from randomly chosen two individual sets from the population. The process is repeated until all the parameters have gone through such selection for once and the

better-half population is selected. The selection process is repeated to get another set of the better-half population. Thus, each set has twice the probability to undergo selection criteria. Such selection strategy clearly makes individuals having better fitness more likely to be copied in the next generation. Thus, a better generation is selected from the old population. *Arithmetic crossover operator* is employed to produce a new offspring. Randomly two parameter sets are selected, and with some random probability the crossover operation is done to generate two offsprings between these two parents. With some random probability, parameters are also generated outside these two parents, within the parameter range. In *mutation*, the parameter sets are randomly selected and parameters are randomly changed within the range. In this process, all the parameters are arranged in a long string which contains all the parameters for all sets. Randomly different locations are selected on the string and the parameters are changed within the range. This mutation makes the search global within the range and helps to get rid of local optima. A mutation rate of 10% is selected in this study. A higher mutation rate initially gives better convergence but later is not likely to have a good convergence effect, whereas a smaller mutation rate works better for convergence to the ultimate value from beginning to end. *Elitism* is an operator that ensures that the best parameter set always survives with generation. This operator stores the best parameters so far obtained with the generations and replaces the worst population in the new generation through evolution.

A.6 Optimization strategy

The optimization scheme in this program locates a good approximate parameter set from the information available from the first and stabilized hysteresis curves and uniaxial and multiaxial ratcheting data. Each of the sets of experiments plays a significant role in obtaining the best set of parameters. In this optimization scheme, parameters are found with the genetic algorithm, where the residual (least squares distance) between the experimental data and model simulations becomes the objective function to be minimized. In genetic

algorithm, when parameters are optimized using multiple responses of similar and different type, optimization is carried out simultaneously simulating all responses. In this operation, the objective function is minimizing the maximum deviation between the experimental and observed responses.

Rahman (2006) developed two schemes to implement the GA for the determination of parameters. There was a sequential approach and the other was simultaneous approach of obtaining the best parameters. Simultaneous approach takes a longer time to obtain the best parameters; hence the sequential approach is better suited to obtain the parameters. A detailed description of these approaches is discussed in Rahman (2006). The sequential stepped approach has been further modified in the present research. It is implemented in four steps. At first, GA is used for parameter optimization from the first uniaxial rising hysteresis curve for the hysteresis loop parameters (C_1, C_2, C_3, C_4, γ_1, γ_2, γ_4, $\bar{a}_4$) where γ_3 is assumed as zero. In the second step, parameters determined from the first step are taken as initial estimates and uniaxial parameters C_1, C_2, C_3, C_4, γ_1, γ_2, γ_3, γ_4, $\bar{a}_4$ are optimized. In this case, the hysteresis loop parameters are varied within a narrow range (±3%) but γ_3 and $\bar{a}_4$ are varied within a range of ±10%. In the third step, the Cs obtained above are kept constant and γs are varied to obtain the best fit for the final or stabilized hysteresis curves. This step also gives the rate of variation of the γs with the plastic strain accumulation. The stabilized stress-strain and uniaxial ratcheting simulations are done simultaneously to determine all uniaxial parameters. In this parameter-determination approach, hysteresis rising-curve loop data can be isolated to eight uniaxial model parameters, whereas stable loop and uniaxial ratcheting data correspond to nine uniaxial parameters including γ_3. The tenth parameter δ' does not have any influence on uniaxial simulation. The initial estimate in the former step acts as a guiding tool to estimate the model parameters in the new step. The new step also verifies the initial estimation of the former step when simulation is carried out for the first loop, stable loop and uniaxial ratcheting simultaneously. Similarly, at the fourth step, along with other

parameters, the biaxial ratcheting parameter δ' is also optimized. In this step, the first and stabilized stress strain, and the uniaxial and biaxial ratcheting simulations are done simultaneously. Optimization achieved through this stepped sequential genetic algorithm approach works with less time consumption and also gives a better set of parameters for the complete set of experiments.

References

Bari, S., Hassan, T., 2000. Anatomy of coupled constitutive models for ratcheting simulation, Int. J. Plast., 16 , 381–409.

Bari, S., Hassan, T., 2002. An advancement in cyclic plasticity modeling for multiaxial ratcheting simulation. Int. J. Plast., 18, 873-894.

Rahman, S. M., Hassan, T., Ranjithan, R. S., 2005. Automated parameter determination of advanced constitutive models. ASME Pressure Vessels Piping Div. Publ. PVP, 2, 261-272.

Rahman, S.M., 2006. Finite element analysis and related numerical schemes for ratcheting simulation, PhD dissertation, North Carolina State University, Raleigh, NC.